THE LAPLACIAN OF THE ELECTRONIC CHARGE DISTRIBUTION

By

PRESTON JOHN MacDOUGALL, B.Sc.

A Thesis

Submitted to the School of Graduate Studies

in Partial Fulfilment of the Requirements

for the Degree

Doctor of Philosophy

McMaster University

ISBN 0-315-50268-1

THE LAPLACIAN OF THE ELECTRONIC CHARGE DISTRIBUTION

DOCTOR OF PHILOSOPHY (1989)
(Chemistry)

McMASTER UNIVERSITY
Hamilton, Ontario, Canada

TITLE: The Laplacian of the Electronic Charge Distribution

AUTHOR: Preston John MacDougall, B.Sc. (McMaster University)

SUPERVISOR: Professor R. F. W. Bader

NUMBER OF PAGES: xi, 218

ABSTRACT

The physical bases of chemical concepts are the focal points of this thesis. The chemical concepts of atoms and bonds are equated to real pieces of a molecule and the topology of the electronic charge density which defines their connectivity, respectively. Bader *et al*'s quantum theory of atoms in molecules and topological theory of molecular structure are the theories that justify the above identifications. These theories are reviewed.

The physical basis of the electron pair concept proposed by Lewis is the subject of the original work presented in this thesis. It is reiterated that, in general, the charge distributions of atoms and molecules can not be realistically described as a superposition of the separately localized charge distributions of electron pairs. The physical basis of the electron pair concept is instead argued to be the topological properties of the Laplacian of the total electronic charge distribution, specifically the local concentrations of charge found in the valence shell charge concentrations of atoms in molecules.

The postulates of Gillespie's VSEPR model of molecular geometry describe the spatial and interactive properties of valence shell electron pairs. All of these postulates are shown to be a prescription of the corresponding properties of the aforementioned local charge concentrations. The observed number, types, locations and shapes of valence shell charge concentrations are in accord with the corresponding elements of Lewis' and Gillespie's models. The interactive properties of these charge concentrations are related to the effect of Fermi correlation on the electron pair distribution function. A pair of electrons with opposite spin is found to be partially

localized and maximally separated from other electron pairs when one of the electrons is located at a position of maximum charge concentration. The properties of the charge concentrations as well as the Fermi correlation of reference electrons located at their positions, are shown to be in consonance with the primary postulate of the VSEPR model. This postulate states that molecular geometries minimizing interpair repulsions within the valence shell of the central atom are the most stable.

The relationships between the Laplacian of the electronic charge distribution and the frontier orbital theory of chemical reactivity, as well as the ligand field theory of transition metal complexes, are briefly discussed.

ACKNOWLEDGMENTS

I arrived at McMaster in August of 1979 as a recruited quarterback. I expect to receive my Ph.D. degree in May of 1989. Nearly a decade will have elapsed between these time end–points. Meanwhile, many wondrous and not so wondrous things have happened. Among the wondrous, and ultimately responsible for this thesis, I was taught by and collaborated with Professors Richard Bader and Ron Gillespie. This thesis is a natural result of being an inquisitive student of theirs. I am grateful for the knowledge and skills that they have taught me.

Tara, my partner in life and love for longer than I've been at McMaster, is fully able to read my mind. It is no loss then, that I am unable to adequately express my gratitude to her with words.

My education and the opportunity to do scientific research have been made possible through the generosity of many people and institutions. These patrons are: my wife, my parents, my grandmother Mazur, N.S.E.R.C. of Canada, McMaster University, the Xerox Research Centre of Canada and the Ontario Ministry of Colleges and Universities. I am grateful for their support.

I thank Ms. Linda Horridge–Palmer for her assistance during the hectic preparation of this manuscript.

This thesis, written in the fall semester of 1988, is dedicated to my *alma mater* in honour of its centennial.

TABLE OF CONTENTS

TABLE OF CONTENTS (Continued).

Chapter 2

Lewis Revisited: In Search of the Physical Basis of Electron Pair Models

Chapter 3

Conclusions and Additional Work

LIST OF FIGURES

LIST OF FIGURES (Continued)

LIST OF TABLES

INTRODUCTION

The evolution of science occurs in cycles. Each cycle has three distinct phases. First, there is discovery of new observations that can not be classified according to existing laws or standards of measurement. Second, the observations are modelled empirically until an ultimate and unified model reveals the underlying structure of the subject. To complete this second stage, new laws and standards of measurement are drafted that reflect the newly found principles, without violating uncontested ones. Third, the new laws and standards of measurement are used to predict and classify outcomes of subsequent experiments. Presumably, this sequence repeats itself *ad infinitum*.

As a subdiscipline of science, modern chemistry is near completion of the second phase of its evolution. The crucibles and cucurbits of eighteenth century chemists spawned observations that belied the various mystical and animated theories of the previous centuries. Model building and further experimental efforts have served one another in the ensuing era. This symbiosis has resulted in an unfolding of a unified conceptual model of the underlying structure of chemistry, that of atoms, molecular structure and electron pairs. This theoretical development has, however, stopped short of constructing a unified physical theory that embodies all of these principles and simultaneously enables one to unambiguously classify and predict chemical observations. Progress towards this end is being made steadily, particularly as the quantum theory of atoms in molecules develops.

The quantum theory of atoms in molecules establishes a theoretical basis for two of the underpinning structural elements of chemistry, atoms and the chemical

bonds that unite them to give a molecular structure. This has been accomplished with dutiful attention paid to the limitations imposed by quantum mechanics, the principal theory used to classify and predict the physics of atomic and molecular processes. Further, given that chemistry is concerned with the collective behaviour of nuclei and electrons, it is clear that the ultimate theory of chemistry must likewise be rooted in quantum mechanics.

The purpose of this dissertation is to present an account of the cumulative results from quantum mechanical studies aimed at establishing a physical basis for the electron pair model of the atom proposed by Lewis, as well as selected models of molecular geometry and chemical reactivity that have at their origin a pair–wise decomposition of the electron distribution of molecules. In particular the VSEPR model of molecular geometry. The relationship between the properties of the Laplacian and the frontier molecular orbital theory of chemical reactivity and the ligand field theory of transition metal complexes are briefly discussed. The distinguishing feature of this research is that it originally utilizes the topological and energetic properties of the Laplacian of atomic and molecular electronic charge distributions for the stated purpose above. The Laplacian is a mathematical measure of the "lumpiness" of any scalar function, it is analogous to the curvature of a line. It will be shown here that there is a physical basis for the Lewis model and its descendants, as all chemists who successfully employ these models in their daily work have surmised, but that the entity which these models mimic is generally not a localized pair of electrons, nor is it a localized molecular orbital. The truth of the models is rather their mimicry of the salient topological features of the aforementioned Laplacian distributions, in particular, the charge concentrations found in the valence shells of atoms in molecules. A quantum mechanical relationship between these topological features and the geometry and reactivity of a molecule is discussed, although it is only at a preliminary stage.

Since the quantum theory of atoms in molecules is utilized throughout this work, and because the Laplacian plays a crucial role therein, this theory and its background are discussed in the first chapter. The second chapter contains the original work of this dissertation concerning the electron pair concept and the final chapter draws conclusions and discusses additional work.

CHAPTER 1

THE CONCEPTUAL FRAMEWORK OF CHEMISTRY

> BARBERINI: *My dear Galilei, you are bent on making the universe simple. But are you sure you are not merely trying to make it more manageable? You think in ellipses, circles, equal velocities, simple movements your brain can cope with. But what if it pleased God to make his stars move like this?* (*With his finger he draws an extremely complicated orbit at irregular speeds in the air*). *What of your calculations then?*
>
> GALILEO: *Eminence, if God made the world like that,* (*He repeats Barberini's orbit*), *then he would have made our brains like that.* (*He repeats the same orbit*). *So we would see such movements as wholly simple. I believe in reason.* (Brecht 1940).

1.1 THE TRIPODAL FOUNDATION OF CHEMISTRY

Chemistry is an empirical science. Inside the chemist's tool box, beside the vast array of instruments is a personal set of simple but powerful concepts that are the essence of chemistry. Among these, the cardinal concept is undoubtedly the atomic hypothesis originally formulated by Dalton (1808). He believed, as had many scientists for a very long time, that:

> "all bodies of sensible magnitude, whether liquid or solid, are constituted of a vast number of extremely small particles, or atoms of matter bound together by a force of attraction" (Dalton 1808, p.141).

However, he advanced the atomistic philosophy by specifically postulating that:

> "Chemical analysis and synthesis go no farther than to the separation of particles (atoms) one from another, and to their reunion." (Dalton 1808, p. 211).

Section 3 of this chapter will be concerned with evidence in support of the atomic

hypothesis and will review the quantum theory of atoms in molecules (Bader and Nguyen–Dang 1981a), a theory which derives the identity of atoms and all of their observable properties from an axiom of physics.

The second most common concept shared by chemists is that of molecular structure. The proposals of a tetrahedral arrangement of bonds to a carbon atom in organic molecules (van't Hoff 1874, le Bel 1874) and octahedral ligation of a metal atom in inorganic complexes (Werner 1893), were crucial leaps forward from the earlier formless ideas of molecular structure and valence originated by Frankland (1852), Kekulé (1857), Couper (1858) and Butlerov (1861). The molecular structure hypothesis provided the language that allowed chemists to classify chemical reactions in a manner consistent with the three–dimensional nature of the physical world. Section 4 of this chapter will be concerned with evidence in support of the molecular structure hypothesis and will review a topological theory of molecular structure (Bader, Nguyen–Dang and Tal 1981b). This theory is a unification of the topological component of the quantum theory of atoms in molecules with the mathematical theory of structural stability of Palis and Smale (1970) and Thom's catastrophe theory (1975).

The concept that forms the remaining leg in the foundation of chemistry is that of the electron pair (Lewis 1916). Lewis' initial model of the atom was that of a cube with a valence electron at each of its corners. Almost as an afterthought, Lewis described organic molecules in particular as a collection of atoms which possessed four pairs of valence electrons (hydrogen and helium excepted) situated at the vertices of a tetrahedron. These tetrahedra were in turn held together by the sharing of one or more pairs of electrons, or equivalently, one or more vertices. A non–coulombic force which allowed a pair of electrons to approach one another favourably, was assumed in his latter model. Despite this unjustified assumption, Lewis' model has survived to this day as the most common conceptual tool used to classify the structure and reactivity of a molecule.

Chemists, of course, use many more than three concepts to design, rationalize and utilize chemical reactions. These additional concepts are, however, unique to a subset of chemists or are refinements of one of the above three. For instance, in Mulliken's first detailed presentation of what is now called molecular orbital theory (Mulliken 1932a), he states:

> The best chemical theory of valence covering all types of compounds is generally agreed to be that developed principally by G. N. Lewis. To a large extent, the essential features of this theory still stand, although their meaning has been made clearer and more specific by interpreting them in the light of the quantum theory".

Today, it could be argued that almost all chemists would agree with Mulliken's first remark but the second statement would be accepted less unanimously. Chapter 2 is another attempt to restate Lewis' model "in the light of quantum theory".

1.2 AN INSPECTION OF THE FOUNDATIONS

A close look at the foundations of chemistry, a vast science that classifies countless substances and predicts much of their behaviour reasonably well, reveals that the structure is self–supporting. Chemical observations are rationalized in terms of chemical concepts which are not clearly tied to any external principles. Discrete atoms that possess a characteristic set of properties that are transferable between different molecules in limiting situations, molecular structures that obey the valencies of the constituent atoms, pairs of electrons that constitute bonds and are the actors in most chemical processes, are all unanimously assumed to be indelible entities. Yet none of the above, until recently, had been defined by a physical expression that lacked a subjective element. For chemistry to become an exact science the basic tools that are used (and consequently the intrinsic language that chemists communicate with) must be expressed, or if necessary reconstructed, in terms of the physical laws that govern

the atomic domain. Quantum mechanics, as expounded by Heisenberg (1925), Schrödinger (1926) and Dirac (1928), is accepted as the aforementioned constitution.[1]

The following sections will separately review the quantum theory of atoms in molecules and the topological theory of molecular structure. It will be shown that both the atomic and molecular structure hypotheses have evolved into precise theories, thereby elevating chemistry closer to the status of an exact science.

1.3 THE PHYSICAL BASIS OF THE ATOMIC HYPOTHESIS: THE QUANTUM THEORY OF ATOMS IN MOLECULES

CLASSICAL AND QUANTUM MECHANICAL EVIDENCE OF ATOMS IN MOLECULES

Dalton's classical theory of atoms in molecules immediately followed the experimental observations of Proust. Proust initially showed that the composition of copper carbonate was fixed, regardless of the method of synthesis (Proust 1799). For nine years he continued to show that this principle held for pure substances (Leicester 1956). His observations became known as the Law of Constant Composition. Thus the contemporary evidence in support of Dalton's theory was this Law of Constant Composition. Application of his theory depended on his assuming whether a compound was binary, ternary, etc... (based on intuitive reasoning). Classical experiments continue to provide physical evidence in support of the atomic hypothesis. Notable among these are molar volume measurements and calorimetric measurements of heats of atomization. Notable, because when applied to a homologous series of molecules they yielded physical properties of atoms (or groupings of atoms) that were

[1] In order to exactly predict the magnetic moment of an electron (the current discrepancy between theory and experiment is equivalent to erring in the measurement of the distance from New York to Los Angeles by the thickness of a human hair) an ammendment was necessary to take into account the quantal nature of the electromagnetic field.

more or less transferable between different molecules (Kopp 1855, Franklin 1949, Prosen *et al.* 1946).

Experiments that probe individual atoms or molecules require a quantum mechanical interpretation. Even though numerous models of a molecule and its constituent atoms that were based on classical mechanics were shattered during a revolutionary era of transition into the quantum age, the notion of fragments of a molecule with a characteristic set of chemical properties remained wholly intact. It was not just the incontrovertibility of the physical evidence from classical experiments that held the atomic hypothesis in good stead. Ultraviolet spectroscopic measurements of electronic transitions in conjugated molecules yielded a new transferable property unique to functional groupings of atoms. Woodward assigned functional group equivalents (in nanometers) which when added to the λ_{max} characteristic value for 1,3–butadiene predicted the corresponding observed value for the so–conjugated diene (Woodward 1952). This additive behaviour has been extended to other systems and many more substituents (Fieser and Fieser 1959).

Similarly, in NMR spectroscopy the frequencies (or magnetic field strengths, depending upon which type of spectrometer is used) at which different nuclei resonate exhibit limited ranges characteristic of each active nucleus. These nuclear resonances translate into characteristic atomic properties that are routinely measured and applied to a large variety of areas of chemical research (Pople *et al.* 1959). The frequency range over which nuclei in a common immediate environment are found to resonate, often exhibits an extremely high degree of transferability.

As a further example of quantum mechanical evidence in support of the atomic hypothesis and a prelude to the quantum theory of atoms in molecules, reference is made to the pioneering efforts of partitioning calculated molecular charge distributions into discrete atomic–like fragments by Bader, Beddall *et al.* (1971a, 1971b, 1972, and 1973b). The charge density, $\rho(\mathbf{r})$, is the probability of finding an electron at a

given point in space. For a system with N electrons in a stationary state, the charge density is given by equation 1.1, where $d\tau'$ indicates the integration over all spins and the cartesian coordinates of N–1 electrons. The state function Ψ is an antisymmetrized solution to the Schrödinger equation, and is a function of the space and spin coordinates of all the electrons.

(1.1) $$\rho(\mathbf{r}) = N\int d\tau' \Psi^*\Psi$$

The earliest efforts prematurely coined the phrase "natural partitioning" to indicate a partitioning of the total molecular charge distribution in linear molecules by planes orthogonal to and intersecting the internuclear axis at its points of maximum (nuclei) and minimum (saddle) charge density values. This scheme led to two components (separated by the planes containing a nucleus) for each atomic population (bounded by planes containing the saddle points) when spatial integrations were performed within the cylindrical regions defined by these planes of demarkation. Internal atoms had two bonded population components, while terminal atoms had one bonded and one nonbonded portion. The nonbonded and the sum of the bonded populations for a variety of AB and BC systems were compared to the corresponding populations in the triatomics ABC (e.g. F–C, C–N —> F–C–N). Nearly perfect transferability of the individual nonbonded and total A–B and B–C bonded populations was observed in every case studied. This occured in spite of the gross differences in the chemical environments of the diatomics and the triatomics, witnessed by significant changes in the total atomic populations and the individual bonded components (Bader, Beddall and Cade 1971). To further explore the transferability question Bader and Beddall (1971) undertook a comparative study of fragment population and energy transferability employing the "natural partitioning" scheme above, a high degree of constancy was observed in both these properties when simple substitutions were made (e.g. S–C–S, O–C–O —> S–C–O).

In the above work the assignment of fragment energies was based on an observed virial relationship[2] that was approximately obeyed by these cylindrical fragments such that $E_{AB}(ABC) \approx -T_{AB}(ABC)$ (the vertical bar indicates the position of the partitioning plane, in this case through nucleus B). The Heisenberg uncertainty principle imposes ambiguity in the definition of a kinetic energy density in real space thru the noncommuting relationship of the position and momentum operators, an electron's position and momentum can not be measured simultaneously. Nevertheless two expressions for the kinetic energy density have been given (Bader and Preston 1969), both yield the total kinetic energy when integrated over all space yet they have drastically different distributions. Expressed in terms of the natural orbitals of a system, ϕ_i (Löwdin 1955), the kinetic energy densities are given by equations (1.2a) and (1.2b), (λ_i are the occupation numbers of the orbitals, m is the non–relativistic mass of an electron). Locally, these two functions differ by an amount proportional

(1.2a) $$K(r) = -(\frac{\hbar^2}{2m}) \sum_i \lambda_i \phi_i(r) \nabla^2 \phi_i(r)$$

(1.2b) $$G(r) = (\frac{\hbar^2}{2m}) \sum_i \lambda_i \nabla \phi_i(r) \cdot \nabla \phi_i(r)$$

to the Laplacian of the charge distribution, an observable property of the system, by equation (1.3). The Laplacian, the quantity $\nabla^2\rho(r)$, is just the sum of the curvatures in the electron density along any three orthogonal coordinate axes at the point r (equation 1.4). It is invariant to the choice of axes since it is the trace of a real symmetric matrix.

(1.3) $$K(r) - G(r) = -(\frac{\hbar^2}{4m}) \nabla^2\rho(r)$$

(1.4) $$\nabla^2\rho(r) = \partial^2\rho(r)/\partial x^2 + \partial^2\rho(r)/\partial y^2 + \partial^2\rho(r)/\partial z^2$$

The properties of the Laplacian of the charge distribution will be discussed in detail in Chapter 2. If equation (1.3) is integrated over some fragment of the total system, such

[2]For an isolated, stationary system with a coulombic potential the virial theorem states that the total energy of the system, E, is equal and opposite in sign to the total kinetic energy, T.

as the cylindrical segments above, then the discrepancy in the kinetic energy of the fragment vanishes only when the integrated value of the Laplacian does. This observation leads to a redefinition of "natural" partitioning surfaces as those for which the flux of the vector $\nabla\rho(\mathbf{r})$ across them is everywhere zero (Bader and Beddall 1972). Such surfaces are called zero–flux surfaces. They are defined by equation 1.5 where n is a unit vector normal to the surface (S) at r.

(1.5) $$\nabla\rho(\mathbf{r})\cdot\mathbf{n}(\mathbf{r}) = 0 \quad \forall\, \mathbf{r} \in S$$

The gradient vector $\nabla\rho(\mathbf{r})$ points in the direction of steepest ascent in the charge density. It is defined in terms of the first derivatives of the charge density along three orthogonal coordinate axes at the point r. Since it is a vector quantity the individual components depend on the choice of axes but its direction and magnitude do not. Gauss' theorem, by equation 1.6, allows for an infinite number of possible surfaces, S, through which the total flux is zero and each partitioned volume, Ω, has a unique total kinetic energy by equation 1.3.

(1.6) $$\oint \nabla\rho(\mathbf{r})\cdot\mathbf{n}(\mathbf{r})\,dS = \int_{\Omega} \nabla^2\rho(\mathbf{r})\,d\tau = 0$$

However, the natural partitioning surface, or zero–flux surface, is uniquely made visible by the gradient vector field of the charge density (Figure 1.1).

In the latter two of the four pioneering efforts referred to above, the zero–flux partitioning scheme was employed to provide quantum mechanical evidence of transferable atomic–like pieces of molecules as well as numerical evidence in support of a regional virial theorem. For instance, Bader and Beddall (1972) found that the integrated electron population, $N(\Omega)$, for the fragments containing a lithium nucleus in the molecules LiF, LiO and LiH were 2.063, 2.068 and 2.089 e, respectively. The near constancy of the populations is carried over into a similar transferability of the fragment kinetic energies via almost superimposable distributions of the electronic charge within the fragment boundaries. For a complete system this result is anticipated on the basis of the theorem of Hohenberg and Kohn (1964) which states

Figure 1.1

The top figure is a relief diagram of the total charge density for carbon monoxide in a plane containing the nuclei. The charge density is cut off at +2.0 au (1 au = 1 e/a_0^3). The middle figure is a contour diagram of the density plotted in the top figure. The contour values are +0.002 (outermost), +0.004, +0.008, +0.02, +0.04, +0.08, +0.2, +0.4, +0.8, +2.0, +4.0, +8.0, +20.0 au. These contour values are used in subsequent contour diagrams of the charge density. The lower figure displays the gradient vector field of the charge density. The bold gradient paths linking the carbon and oxygen nuclei originate at the bond critical point (solid circle) and trace out the bond path. The bold gradient paths perpendicular to the bond path terminate at the bond critical point and denote the intersection of the interatomic surface with the plane shown. The remaining gradient paths (70) originate at infinity and terminate at either the carbon or the oxygen nucleus. The region of space traced out by paths terminating at a given nucleus defines the atom associated with that nucleus. The angles at which the gradient paths approach each nucleus are evenly spaced 10^0 apart. The same spacing of gradient paths is used in subsequent gradient vector field illustrations. These plots were derived from a 3–21G RHF calculation.

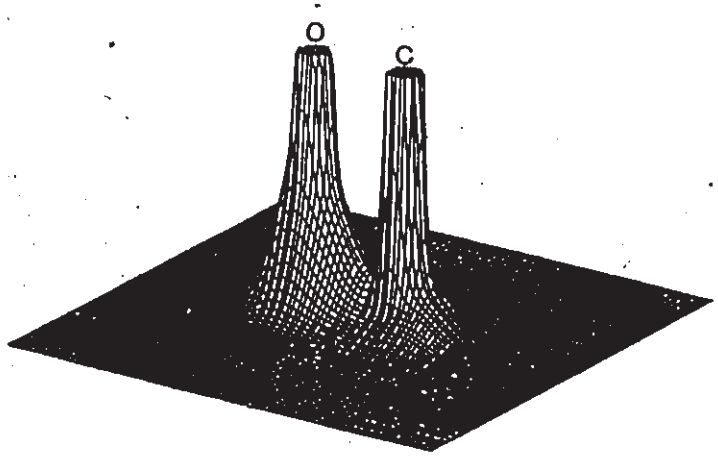
O
C

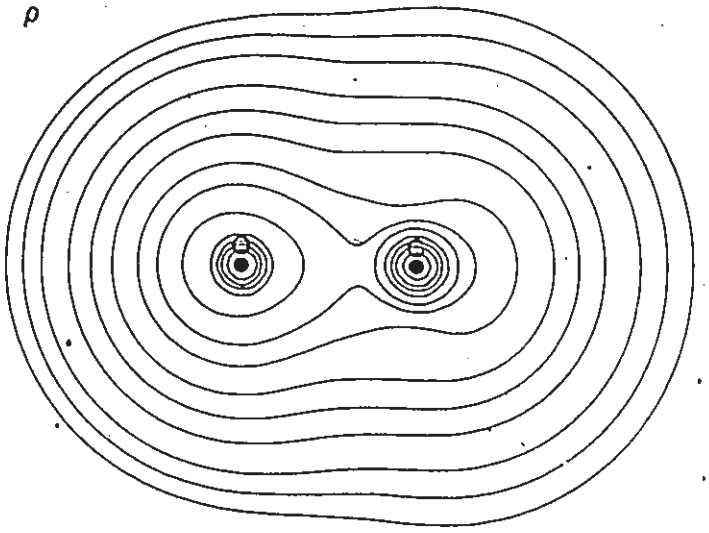
ρ

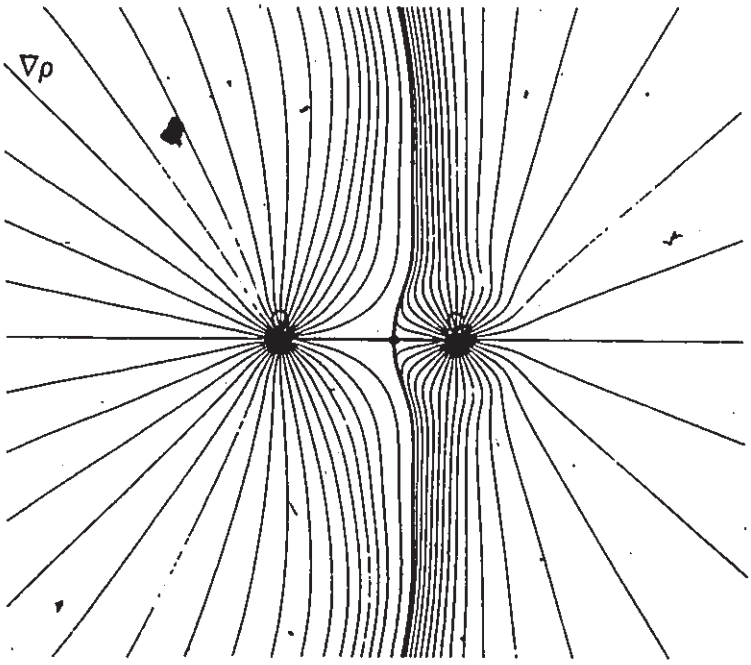
∇ρ

that the ground state energy is a unique functional, albeit unknown, of its charge distribution. Perhaps more impressive than the observed transferability of a relatively unpolarizable lithium core, Bader *et al.* observed similar superimposability of the size, shape and population of the very polarizable hydridic fragments of BeH and BeH_2 (1973b).

The partitioning of the quantum mechanical electron distribution described above complemented the interpretation of molecular spectra as a composition of characteristic signals from the constituent functional groups. Together they established a basis of quantum mechanical observations that gave clear evidence for the survival of Dalton's atomic hypothesis in the quantum age. The following subsection will outline the quantum theory of atoms in molecules.

THE QUANTUM THEORY OF ATOMS IN MOLECULES

Variational principles are axiomatic in all of physics, particularly those involving variation in the action integral, W_{12}, of a system. The classical equation of motion for a system, that which yields the path of least action, is determined by satisfying Hamilton's variational principle,

$$\delta W_{12} = \delta \int_{t_1}^{t_2} L(q_i, \dot{q}_i) dt = 0 \tag{1.7}$$

In this case the Lagrangian, $L = T - V$, is simply the difference between the kinetic energy and the potential energy of the total system and does not depend explicitly on time. Similarly, Maxwell's equations for the charge and current densities of a classical electromagnetic field can be derived via the variational principle utilizing the corresponding Lagrangian (Goldstein 1951).

In the application of the variational principal to a time–dependent quantum mechanical system, one varies the total Lagrangian, $\mathscr{L}(\Psi,t)$, defined in terms of the many–particle Lagrangian density, $L(\Psi,\nabla\Psi,\dot{\Psi},t)$. At the point of variation where the action integral is minimized, one obtains Schrödinger's equations (1.8). It is interesting

to note that at the point of variation where Schrödinger's equations (1.8) are satisfied, the total Lagrangian reduces to a function of the Laplacian of the charge density (equation 1.9).

(1.8) $$i\hbar\dot{\Psi} = \hat{\mathscr{H}}\Psi \text{ and } -i\hbar\dot{\Psi}^* = \hat{\mathscr{H}}\Psi^*$$

(1.9) $$L(r,t) = (-\hbar^2/4mN)\nabla^2\rho(r,t)$$

From equations (1.6) and (1.9), one can see that the criterion for partitioning a molecule into its most transferable pieces yields fragments for which the Lagrangian integral (equation 1.10) vanishes for any instant or interval of time.

(1.10) $$\mathscr{L}(r,t) = (-\hbar^2/4m)\int dr\nabla^2\rho(r,t)$$

In his demonstration of the principle of stationary action, Schwinger (1951) generalized the variational principle by releasing the constraints that $\delta t = 0$ at t_1 and t_2 and that $\delta\Psi(t_1) = \delta\Psi(t_2) = 0$. This added flexibility makes possible a complete variational development of quantum mechanics. By equating an atom in a molecule with a region of space bounded by surfaces of zero–flux in $\nabla\rho(r)$ (Figure 1.1) a *complete* quantum mechanical description of an atom in chemical combination has been made possible through a further extension of the quantum action principle. The atomic statement of the principle of stationary action (Srebrenik *et al.* 1978, Bader *et al.* 1978) differs from the corresponding statement for an entire system only in that it applies to open subsystems which evolve with time so as to obey the constraint given in equation (1.6). Such subsystems of the isolated carbon monoxide molecule, a closed system, are illustrated in Figure 1.1. Indeed, since most closed systems consist of two or more open systems, the atomic statement is the more general one.

Within the variational formalism invented by Schwinger the observables of a system are identified as the changes induced in the state function by generators of infinitesimal (denoted by ϵ) unitary transformations, as in equation 1.11.

(1.11) $$\delta\Psi = (-i/\hbar)\epsilon\hat{\mathscr{F}}\Psi$$

The physical interpretation of the effect of a given generator, $\hat{\mathscr{F}}$, is manifested in the

resulting modifications in the systems Langrangian, $\mathscr{L}$. The changes in the physical state are determined by the commutator of $\hat{\mathscr{F}}$ with the Hamiltonian for the total system, $\hat{\mathscr{H}}$, as shown in equation 1.12.

(1.12) $$\delta\mathscr{L}[\Psi,t] = (i\epsilon/\hbar)<[\hat{\mathscr{H}},\hat{\mathscr{F}}]>$$

By means of the action principle equation 1.12 leads to the equation of motion for the average value of the property associated with the generator $\hat{\mathscr{F}}$. The average properties of an atom in a molecule are derived in an analogous manner, in fact they are the projections of the property of the total system onto the space of the atom (Bader *et al.* 1978). Specifically, the atomic action principle yields the result that the variation in the atomic Lagrangian, as generated by the same infinitesimal unitary transformation that produced a change in the total system, is given by equation 1.13.

(1.13) $$\delta\mathscr{L}[\Psi,\Omega,t] = (\epsilon/2)\{(i/\hbar)<[\hat{\mathscr{H}},\hat{\mathscr{F}}]>_\Omega + \text{comp. conj.}\}$$

The notation $< >_\Omega$ indicates an evaluation of the average value of the commutator over the finite space of atom Ω. As a result of the existence of an atomic action principle the average value of any property of the total system associated with a generator $\hat{\mathscr{F}}$ can be expressed as a sum of atomic average values of the same property (equation 1.14).

(1.14) $$<\hat{\mathscr{F}}> = \sum_\Omega <\hat{\mathscr{F}}>_\Omega$$

For a system in a stationary state equation 1.15 is the atomic statement of the hypervirial theorem (Epstein 1974, Srebrenik and Bader 1974) which relates the atomic average of the commutator in equation 1.13 to an integral over the surface of the atom of the vector current density associated with property F (equation 1.16).

(1.15) $$\{<[\hat{\mathscr{H}},\hat{\mathscr{F}}]>_\Omega + \text{c.c.}\} = \hbar/2\oint dS\{iJ_F + \text{c.c.}\}\cdot\mathbf{n}$$

(1.16) $$J_F(r) = (N\hbar/2mi)\int d\tau'\{\Psi^*\nabla(\hat{\mathscr{F}}\Psi) - (\nabla\Psi^*)(\hat{\mathscr{F}}\Psi)\}$$

In equation 1.16 the notation $d\tau'$ indicates the integration over the coordinates of all the electrons but one. The atomic hypervirial theorem may be used to derive useful relationships which the average atomic properties must obey (Bader 1980). Bader and

Nguyen–Dang (1981a) have furnished the details of this formalism and the derivation of key quantum mechanical properties of an atom in a molecule, namely, the atomic virial theorem and the atomic force law.

ARE THE ATOMS OF THEORY THE ATOMS OF CHEMISTRY?

For one–hundred and eighty years synthetic chemistry has relied on the atomic hypothesis, as an *ipse dixit*, to organise its ever increasing body of knowledge. Likewise, physical chemistry (old and new) dogmatically interprets physical properties of a compound in terms of atomic or group equivalents. The theoretical advances described above have established that quantum mechanics permits and prescribes the partitioning of a molecule into fragments with well–defined atomic–like properties. What is truly aesthetic, is the extent to which the quantum mechanically predicted atomic or group properties (Wiberg, Bader and Lau 1987, Bader *et al.* 1987a, Bader *et al.* 1987b) agree with the experimentally determined equivalents (Franklin 1949, Prosen *et al.* 1946, Kopp 1855). Table 1.1 (reproduced from Bader *et al.* 1987b) tabulates some of the group properties calculated for a representative series of homologous hydrocarbons. A necessary condition for equating the quantum mechanical atoms with the atoms of chemistry is that the atoms of theory possess characteristic sets of properties that parallel those observed for the chemical atoms and that in limiting situations they should be transferable from one molecule to another. A sufficient condition for the above identification is the equivalence of the respective properties of the quantum and chemical atoms. The transferability of group properties is evident in each column of the table. That the data listed in Table 1.1 are the properties of the atoms of chemistry is supported by the observation that the energies (adjusted for correlation and zero–point energies) of the central methylene group in pentane, and the two such groups in hexane, are equal to the incremental value for methylene groups used to predict the experimental heats of atomization of aliphatic hydrocarbons (Wiberg, Bader and Lau 1987).

Table 1.1. Group Properties in Hydrocarbons ($6\text{-}31G^{**}/6\text{-}31G^{*}$).

	Methyl group properties[a]					Methylene group properties[b]								
Molecule	$\Delta N(CH_3)$[c] (e)	$\Delta E(CH_3)$[d] (kcal/mol)	$\lvert\mu CH_3\rvert$[e] (au)	ϵ[f] (au)	molar volume g (cm^3)	$\Delta N(CH_2)$[c] (e)		$\Delta E(CH_2)$[d] (kcal/mol)		$\lvert\mu(CH_2)\rvert$[e] (au)		ϵ[f] (au)		molar volume g (cm^3)	
Ethane	0.000	0.0	0.253	-0.3456	19.77										
Propane	-0.017	-10.9	0.244	-0.3484	19.73	0.037		+21.7		0.307		-0.3180		14.18	
Butane	-0.018	-10.8	0.243	-0.3486	19.70	0.019		+10.8		0.305		-0.3208		14.12	
Pentane	-0.017	-9.9	0.249	-0.3486	19.71	0.019	0.001	+10.9	0.0	0.310	0.304	-0.3210	-0.3238	14.08	13.98
Hexane	-0.018	-9.9	0.245	-0.3485	19.74	0.020	0.000	+10.6	-1.1	0.306	0.300	-0.3208	-0.3237	14.09	14.03

[a]Differences are relative to methyl group in ethane.

[b]Differences are relative to standard methylene group. The entries beginning with propane are for CH_2 groups bonded to one methyl group. The set beginning with pentane are for CH_2 groups bonded only to other CH_2 groups.

[c]The group population is defined as the sum of atomic populations $N(\Omega) = \int_\Omega \rho(r)dr$, the net atomic charge is simply $q(\Omega) = Z(\Omega) - N(\Omega)$.

[d]The group energy is defined as the sum of atomic energies, $E(\Omega) = \gamma K(\Omega)$. $K(\Omega)$ is the atomic kinetic energy and $\gamma = ((V/T)+1)$ is the correction factor to ensure that the sum of atomic energies over the entire molecule is the Hartree-Fock energy.

[e]Calculated with carbon nucleus as origin, $\mu = \Sigma_\Omega[q(\Omega)X_\Omega + \mu(\Omega)]$ and $\mu(\Omega) = -\int_\Omega r_\Omega \rho(r)dr$, $r_\Omega = r - X_\Omega$ and X_Ω is the position vector of the nucleus of atom Ω.

[f]Correlation energy calculated using a density functional, Langreth, D.C. and Mehl, M.J. (1983) *Phys. Rev. B*, 28, 1809.

[g]The volume of a group is that contained by the zero-flux surfaces and the 0.001 au envelope of the total density.

This section has reviewed the physical basis of the atomic hypothesis. The nonpareil ability of the quantum theory of atoms in molecules to classify and predict from first principles the mechanical properties of the pieces of either a molecule or extended system (which are labeled as the atoms of chemistry *within* this theory) is in stark contrast to more frequently applied empirical relationships and the atomic parameters unique to each of them. The most obvious difference being that the atomic hypothesis and transferability of atomic properties is output of the former philosophy, while input to the latter. Nevertheless, there certainly exists a correspondence between these two philosophies (Slee 1986a, 1986b, Slee and MacDougall 1988) which requires further elaboration before chemistry can become "bilingual".

1.4 THE PHYSICAL BASIS OF THE MOLECULAR STRUCTURE HYPOTHESIS: THE TOPOLOGICAL THEORY OF MOLECULAR STRUCTURE.

CLASSICAL AND QUANTUM MECHANICAL EVIDENCE OF MOLECULAR STRUCTURE

"*La chimie dans l'espace*" was the title of J. H. van't Hoff's paper (1874) in which he proposed that a molecule composed of a carbon atom bearing four different groups could exist in two different isomers, if the chemical bonds holding the molecule together were rigidly arranged about the central carbon atom to form a tetrahedron in real space. J. A. le Bel simultaneously proposed an hypothesis of molecular structure that espoused a geometrical arrangement of chemical bonds linking the constituent atoms of a molecule (1874). Initially, the physical evidence in support of the molecular structure hypothesis, as modified by van't Hoff and le Bel, was the existence of optical isomers, or enantiomers, of organic compounds consisting of carbon centres that were asymetrically substituted, such as salts of tartaric acid (Pasteur 1848). The realization

of the stereochemical nature of organic molecules led to advances such as Baeyer's strain theory (1885) and Meyer's theory of steric hindrance (1894). The classical experiments that led to these still actively employed ideas of stereochemistry constitute a vast amount of physical evidence bolstering the molecular structure hypothesis. Werner found hexa–coordinated complexes of cobalt and other elements that also exhibited optical isomerism. He successfully attributed this to different relative arrangements of octahedrally bonded ligands (1893). This result had the all important effect of establishing molecular structure as a universal concept.

The father and son team of William and Lawrence Bragg interpreted the intricacies of the newly discovered diffraction of X–rays by single crystals in terms of the molecular geometry of the ions making up the regular lattice of ionic crystals. One of the earliest examples is the younger Bragg's determination of the trigonal planar geometry of the carbonate ion in crystals of calcite (Bragg 1914). In the ensuing decades X–ray crystallography became, and still is, one of the most widely used tools of "molecular structure determination" (Pauling 1960). The method of electron diffraction developed by R. Wierl is similarly capable of determining the geometry of a molecule, *e.g.* the tetrahedral geometry of silicon tetrachloride was established by this technique (Wierl 1931). It is complimentary to X–ray diffraction in that it examines molecular geometry in the gas phase. Standard diffraction experiments provide direct physical evidence of the geometrical component of the molecular structure hypothesis, they generate a set of atomic coordinates (more precisely, the coordinates of the maxima in p(r) associated with each nucleus) of a crystal or volatile molecule. However, currently they provide only indirect and subjective evidence of the chemical component (which atoms are bonded to one another) of the molecular structure hypothesis systematized by Kekulé and his contemporaries. Recently, Lau *et al.* (1986) have determined the molecular structure of α–glycine from experimental measurements of the electron density. The definition of molecular structure determined in this way will be described in greater detail in the following subsection.

A phenomenal amount of quantum mechanical justification of the molecular structure hypothesis is found in the interpretations of infrared and microwave absorption and emission spectra (Herzberg 1945, Townes and Schawlow (1955). From these widely applicable techniques spectroscopists glean various pieces of structural information, both geometrical (bond lengths, bond angles, torsional angles) and chemical (bond stretching, bending and twisting force constants).

Nuclear magnetic resonance spectroscopy was mentioned earlier as a means of characterizing atoms in molecular environments. Its ability to assist in the characterization of molecular structure is another forte of this popular analytical technique. A gamut of structural data can be inferred from spin–spin coupling constants, temperature dependency of spectra, modelling of anisotropic effects *et cetera* (Jackman and Cotton 1975).

Spectroscopic characterizations of molecular structure continually strengthen belief in the molecular structure hypothesis. Nevertheless they do not provide any insight into the physical basis of this principle, since the existence of a molecular structure is argued *a posteriori*. Nor do they serve to explicitly define a chemical bond, the basic component of a molecular structure. An extreme position is held by Woolley, he denies any quantum basis for the molecular structure hypothesis (1977). To illustrate his argument he poses the rhetorical question: "can a molecular structure be associated consistently with all the observable quantum states of a molecule, as seems to be implied by the central dogma, or only with a particular subset of the experimentally accessible states?". Therein lies the crux of his failure to reconcile the "atoms and bonds" model of classical chemistry with the "electrons and nuclei" quantum model of a molecule. The molecular structure hypothesis was forged via classical methods, limited to the study of molecules in their ground states. To insist that a quantum theory of molecular structure consistently be in harmony with the classical model, even in "nonclassical" energy regimes commonly explored by

high–intensity lasers, simply precludes its formulation. Modern chemists routinely alter molecular structures photochemically, presumably generating highly excited intermediates with unknown structures *en route*. This regime of nonclassical structures is surely regarded by chemists as a challenge requiring generalization of the molecular structure hypothesis, and not justification of mutiny. A quantum mechanical theory of molecular structure should concur with the classical model in its own well–established domain. However, the quantum theory must be completely autonomous in order to predict where the classical model breaks down, yet continue to classify molecular structures with undaunted ability beyond this frontier. The starting point of a quantum theory of molecular structure ought to be a quantum mechanical definition of a chemical bond, presupposing there exists a correspondence with the classical model.

In the century following the publication of "*La chimie dans l'espace*" there were numerous attempts to define a chemical bond. Here we are concerned with those that give physical meaning to the original intuition of two atoms joined by mutual "affinity". Foremost among these is Lewis' reverberating proposal that a single bond is the result of two atoms sharing one pair of valence electrons and that multiple bonds result from sharing two or more pairs (Lewis 1916). The electron–pair bond predates quantum mechanics, yet it still dictates the way in which bonds are either put into (valence bond structures) or recovered from (localized molecular orbitals) the majority of quantum mechanical calculations. In pursuit of recovering chemical concepts from properties of the observable charge distribution, Runtz *et al.* (1977) observed that "bond paths" which were consistent with chemical expectations could be recovered from quantum mechanical calculations without recourse to the Lewis model. Their definition of a bond path stemmed from the observed pattern in which a molecule was quantum mechanically partitioned into atomic–like fragments by surfaces of zero–flux in the gradient of the charge density (Figure 1.2). Two atoms are consistently found to be separated by a single common surface when the classical model of molecular

structure assigns a bond of any type between them. The interatomic surfaces are defined in terms of the gradient vector field of the charge density. The topology of a scalar field is concisely summarized by the number and types of stationary points, or critical points, in its gradient vector field. The gradient of the charge density vanishes at a critical point and gradient paths can either originate or terminate there. The different types of critical points and their relationship to the components of a molecular structure will be discussed in the next subsection. Zero–flux surfaces possess the topological property of containing a single critical point at the point of maximum charge density in the interatomic surface. Figure 1.2 illustrates that two gradient paths originate from each of these critical points and terminate at the nuclei which separated by the corresponding interatomic surface. This pair of gradient paths, unique to each interatomic surface, traces out a bond path linking neighbouring nuclei along which the charge density is a maximum with respect to any lateral displacement. Utilizing this definition of a bond path, Bader *et al.* (1979a, 1979b and 1980) amply demonstrated a one–to–one mapping of the network of bond paths found to exist in a given molecule with its classically derived molecular structure.

The discovery of a "quantum topology" that concurred with classical means of assigning molecular structures had two important consequences. First, it provided physical evidence that directly verified the tenets of the molecular structure hypothesis. Bonds through space with definite geometrical arrangements are manifested in the observable topology of the electronic charge distribution. This theoretically demonstrated corroboration has recently been backed up by a topological analysis of the experimentally determined (X–ray crystallography) charge distribution in α–glycine crystals (Lau *et al.* 1986). Second, it provided the basis upon which a predictive theory of molecular structure and structural change could be built.

Figure 1.2

(a) A relief map of the total charge density of S_2N_2 shown in a plane containing all four nuclei. The density is cut off at $\pm$1.0 au.

(b) The gradient vector field of the charge density depicted in (a). The arrows indicate the directions of steepest ascent. The bold gradient paths and solid circles represent the same features as in Figure 1.1.

(c) A contour diagram of the charge density for the same plane as above. The bond paths and intersections of the interatomic surfaces are overlayed. The solid triangle indicates the position of a ring critical point. These plots were derived from a 6–21G* RHF calculation.

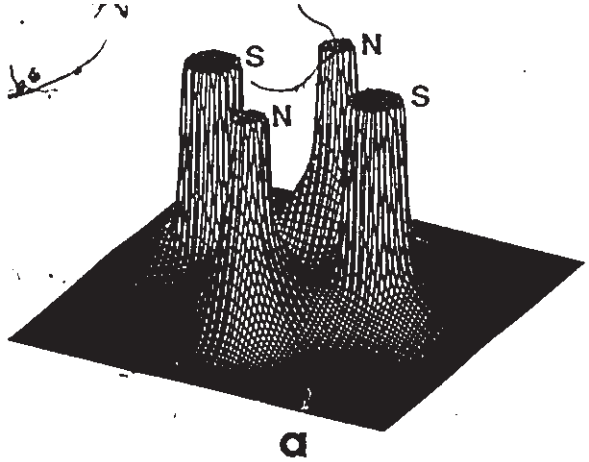

a

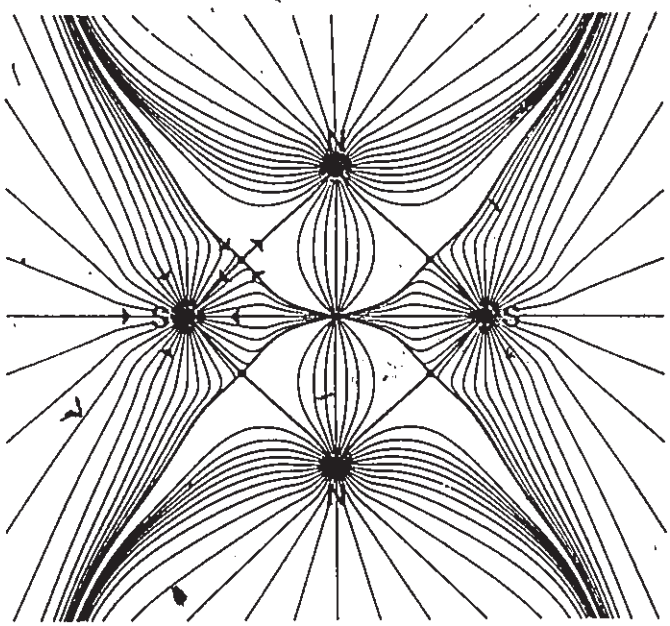

b

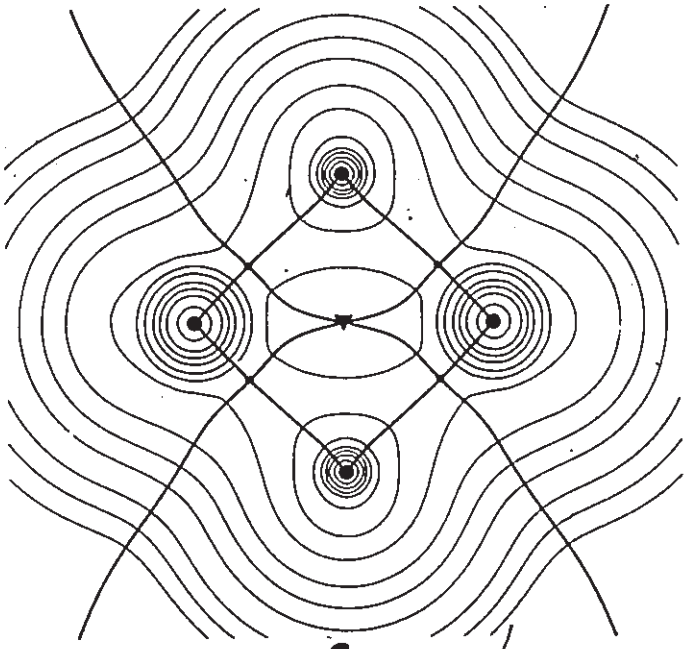

c

THE TOPOLOGICAL THEORY OF MOLECULAR STRUCTURE

The complete network of bond paths for a molecule in a given nuclear configuration (molecular geometry) is called the molecular graph (Bader *et al.* 1979a). The existence of a bond path linking a pair of nuclei is by definition a consequence of the corresponding atoms sharing a common surface. It is through these surfaces that atoms directly exert forces on one another by virtue of the atomic force law (Bader and Nguyen–Dang 1981a).[3] Therefore, a molecular graph succinctly illustrates the dominant atomic interactions for a given configuration of the nuclei. A theory of molecular structure would not capture the essence of the molecular structure hypothesis if it were burdened with the redundant task of assigning each point in nuclear configuration space a unique molecular structure, this is tantamount to equating molecular structure with molecular geometry. Within the topological theory of molecular structure, nuclearconfiguration space is partitioned into a finite number of structural regions (Bader, Nguyen–Dang and Tal 1981b). Each structural region represents an equivalence class of molecular graphs, the connectivity of the atoms is the same for any geometry within a given structural region. Molecular structure is a generic property, it is invariant to molecular vibrations that sample points in nuclear configuration space within the boundaries of a given structural region. The fixed–nucleus or Born–Oppenheimer approximation is implicit in the above discussion, i.e. molecular graphs associated with fixed points in nuclear configuration space. Beyond the Born–Oppenheimer approximation the coordinates (in nuclear

[3]The atomic force law, obtained from the atomic variational principle, relates the total force acting on the electronic charge of an atom to the time derivative of the atom's own electronic momentum density. This is the atomic equivalent of Ehrenfest's force theorem for a complete quantum system (Ehrenfest 1927). For a molecule in a stationary state, the total force acting on the nuclei is zero, however, the electronic charge of an atom experiences a constant average force, $\mathbf{F}(\Omega) = -\oint dS(\mathbf{r})\vec{\sigma}(\mathbf{r})\cdot\mathbf{n}(\mathbf{r})$. Where $\vec{\sigma}(\mathbf{r})$ is the quantum mechanical stress tensor and $\mathbf{n}(\mathbf{r})$ is a unit vector normal to the surface $S(\mathbf{r})$. Simply stated, the effect of the molecular environment on the properties of an atom is entirely determined by the net flux in the forces across its boundary. An atom's boundary consists of one zero–flux surface for each bonded neighbour, therefore atoms only directly interact with other atoms they are bonded to.

configuration space) of the boundaries of structural regions would vary with nuclear motion to a degree determined by the strength of the coupling between the nuclear and electronic coordinates. However, this is only a limited discussion of the theory of molecular structure and such approximations are invoked here solely for the purpose of illustrating the concepts introduced by this theory and to emphasize the difference between **structure** and **geometry**. All of the means of classification and prediction belonging to the topological theory of molecular structure are preserved beyond the removal of any approximation.

Molecular structures can be dissected into chains, rings and cages. Topologically, these architectural units are identified by the presence of characteristic critical points in the scalar field of the charge density. Critical points in $\rho(\mathbf{r})$, defined as positions where the gradient of ρ is zero, are classified by the notation (λ,σ) according to their rank (λ) and signature (σ) (Collard and Hall 1977, Smith *et al.* 1977). This classification requires knowledge of the three second derivatives of the charge density along the principal axes at the coordinates of the critical point. The principal axes system is that which diagonalizes the Hessian matrix of partial second derivatives, $\mathrm{H}(\mathbf{r})$. The number of diagonal elements of $\mathrm{H}(\mathbf{r})$, or the eigenvalues, that are nonzero is the rank of the critical point, (λ= 0, 1, 2 or 3). The unit vectors originating at the point r and parallel to the principal axes are called the eigenvectors of $\mathrm{H}(\mathbf{r})$. The signature of a critical point is the number of positive second derivatives minus the number of negative ones, $-3 \leq \sigma \leq +3$. At the coordinates of a nucleus, the exact non–relativistic charge density exhibits a cusp (Kato 1957), or discontinuity in its first derivative. Since $\nabla\rho$ is undefined at nuclei, their coordinates are not *bona fide* critical points. Topologically however, they behave as do (3,–3) critical points and it is more convenient to refer to them as such. This side–stepping is usually not necessary since the vast majority of charge density calculations employ infinitely differentiable

gaussian functions in their basis set. These densities do exhibit (3,–3) critical points, or local maxima, at the positions of nuclei.[4]

Open chain fragments of a molecular structure exhibit a single (3,–1) critical point for each bond, hence they are termed bond critical points. The principal axis associated with the single positive eigenvalue of the Hessian matrix (the charge density is a minimum at the bond critical point in this direction) is collinear with the bond path that connects the nuclei of bonded atoms. There is no formal restriction on the number of bond paths that can connect a pair of nuclei. However, with only a few exceptions in a multitude of calculated molecular structures there is a maximum of one bond path linking a given pair of nuclei (Bader, Nguyen–Dang and Tal 1981b, Cao *et al.* 1987)

Ring fragments of a molecular structure are identified by the presence of a (3,+1) critical point in $\rho(\mathbf{r})$. The diagonalized Hessian matrix at such a critical point has two positive eigenvalues, and the principal axes (eigenvectors) associated with them are tangential to the ring surface. The ring surface is a sheet over which the charge density is a maximum with respect to vertical displacement. The perimeter of the ring surface is defined by a closed chain of bond paths. There is no restriction on the number of ring surfaces that can share a given perimeter, although no example has yet been reported of such a multiplicity.

Bond paths and ring surfaces are free to contort into any shape that does not intersect itself, and when distortions from linearity or planarity are observed they provide a quantitative analysis of qualitative expectations. A thorough study of the molecular structures of strained and unstrained hydrocarbons examines the correlation between bond path bending and strain (Wiberg, Bader and Lau 1987). An investigation

[4]To be precise, when small gaussian basis sets are used in molecular orbital calculations the (3,–3) critical points in $\rho(\mathbf{r})$ associated with the nuclei are slightly displaced from the positions of the nuclei. This displacement is largest for hydrogen nuclei ($\approx$ 0.01 Å) and rapidly decreases as the nuclear charge increases.

of substituent effects on the tautomeric equilibrium between norcaradiene and 10–annulene included as one of its parameters the height of the ring surfaces above their respective perimeters (Gatti *et al.* 1985).

A cage, the remaining element of molecular structure, is identified by the presence of a (3,+3) critical point in $\rho(r)$. All three eigenvalues of the Hessian matrix are positive, i.e. the charge density is a local minimum at a cage critical point. No gradient paths that originate at a cage critical point can escape the volume of that cage due to its enclosure by ring surfaces. For a system consisting of a finite number of nuclei the total number of each type of critical point must obey the Poincaré–Hopf relationship,

$$n - b + r - c = 1 \tag{1.17}$$

where n, b, r and c are the number of (3,–3), (3,–1), (3,+1) and (3,+3) critical points, respectively.

Ferrocene possesses all of the above elements of molecular structure, as defined by the gradient vector field of its total charge density.[5] Using this molecule as an example, figure 1.3 graphically demonstrates the topological characteristics of each type of critical point. The skeleton of the molecular structure of ferrocene, determined from theory, is depicted in the molecular graph shown in figure 1.4. A molecular graph does not explicitly portray the presence of rings or cages. For instance, if there were no ring surfaces suspended by the five C–C bond paths of each $C_5H_5^-$ fragment, then the structure would not possess the two cages that are shown to exist in Figure 1.3. The following subsection will describe how such structural changes occur. The eqilibrium geometry of ferrocene belongs to the D_{5d} point group. The molecular graph shown has D_{5h} symmetry, it illustrates the structure of the very slightly higher energy transition state to rotation about the five–fold axis. The structure is the same

[5]The charge density is calculated from a single–determinantal SCF wave function optimized under D_{5h} symmetry constraints (Williamson and Hall 1987). The atomic basis functions are split as follows: Fe(9s7p4d/3s2p2d), C(6s3p/3s2p) and H(3s/2s).

Figure 1.3

The gradient vector field of the charge density displayed for a σ_v plane of symmetry of the ferrocene molecule (in a D_{5h} geometry). The locations of in–plane nuclei are denoted by large solid circles and labelled, while the projected positions of out–of–plane nuclei are indicated by open circles. The positions of bond critical points are denoted by small solid circles. The positions of ring critical points are denoted by solid triangles. The positions of the two cage critical points are indicated by stars. Note how the gradient vectors within the domain of the iron atom are diverted out of the equatorial plane and away from the C_5 axis in a pronounced manner.

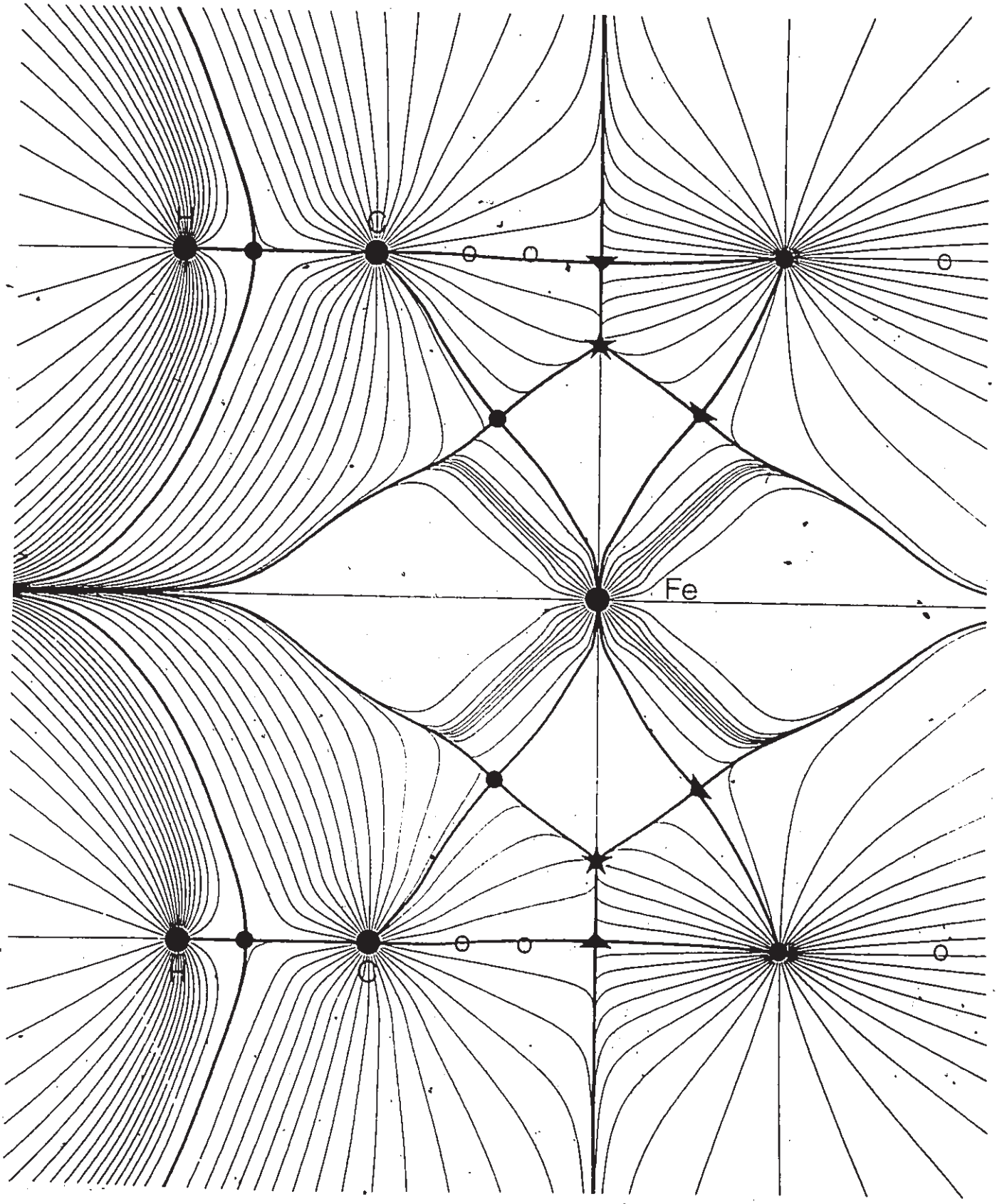
Fe

Figure 1.4

The molecular graph of the ferrocene molecule displays the projections of all the bond paths present in the molecule in its D_{5h} geometry. The solid circles denote the same features as in figure 1.3. Note how the five Fe–C bond paths on either side of the iron atom nearly coalesce.

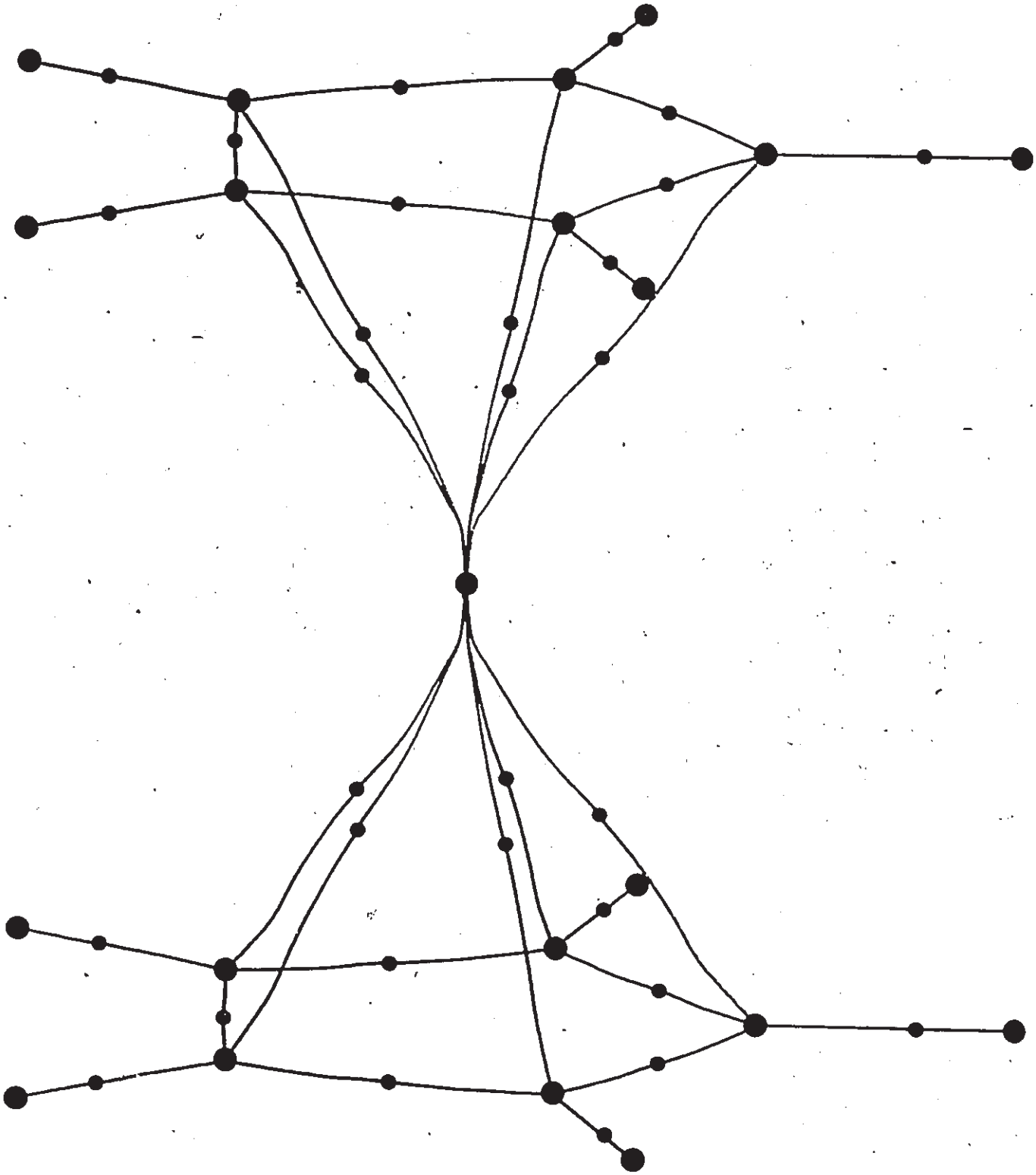

for these two different geometries. The hourglass shape of the molecular graph is consistent with both η^5 coordination of the $C_5H_5^-$ ring (an Fe—C bond is assigned to each carbon atom of the ring) and a di–coordinated Fe^{2+} ion that one might expect on the basis of the rapid rotation of the rings.

Atoms and bonds are defined by the same property of a molecule, the gradient vector field of its total charge distribution. quantum mechanics predicts the average properties of the atoms so defined, does it correspondingly predict bond properties? The atomic statement of the hypervirial theorem (equation 1.15) provides the formalism for equating the average properties of atoms to a surface integral over the surface of the atom in question. Since the surface of a given atom is comprised of one interatomic surface per bond linking that atom, any average property of an atom can be related to a sum of bond properties. It has been proposed that a bond energy may be a property that can be evaluated as a surface integral and summed overall bonds in the molecule to yield the total dissociation energy (Bader *et al.* 1982, Bader and Wiberg 1987). The possibility exists of defining a quantum mechanical bond property associated with every physical property of a molecule.

Properties of the charge density at the bond critical point have also been related empirically to chemically defined bond properties. For instance the concept of carbon–carbon bond order can related quantitatively to the value of $\rho(r)$ at the bond critical point (Bader *et al.* 1982). The ellipticity of a bond, ϵ, is a measure of the elliptical distortion, from axial symmetry, of the charge distribution in the interatomic surface. This property can be used to discuss the π character of bonds in unsaturated molecules (Bader *et al.* 1983, Cremer *et al.* 1983).

CHANGES IN MOLECULAR STRUCTURE

The predictive power of the topological theory of molecular structure also encompasses mechanisms of structural change. In the same way one draws a phase

diagram in thermodynamics, one can draw a **structure diagram** for a given collection of atoms. The control parameters in a phase diagram are the pressure, volume and temperature. In a structure diagram the control parameters define the molecular geometry. There are a finite number of molecular structures that any given system can adopt, each structure has its own structural region. Within the interior of a structural region the corresponding molecular structure is left unchanged by any nuclear displacement. The structure is said to be **stable**. Trajectories in nuclear configuration space that begin in one structural region and end in another, represent a continuous change in molecular geometry and a discontinuous change in molecular structure. The point of crossing from one structural region into another is called a **catastrophe point**, since there has been a sudden and discontinuous change in the molecular structure. The molecular structure associated with a catastrophe point is termed **unstable**, since there is at least one less degree of freedom and an infinitesimal motion along this coordinate will generate a new molecular structure. There are only two types of catastrophe points (Palis and Smale 1970). Thus the reaction mechanism by which one molecular structure changes into any other can be described as a sequence of only two types of elementary operations (Bader, Nguyen–Dang and Tal 1981b).

Chemists speak of "making and breaking chemical bonds" when they discuss a reaction mechanism. The basic mechanism of structural change that sequentially breaks one bond and forms another, occurs via a conflict catastrophe point, whereat the molecule possesses a **conflict structure**. These structures are characterized by the presence of a gradient path that originates at a critical point and terminates at one other than at a nucleus. There are only three conflict structures with one such intersection, they are 1, 2 and 3 below. In these schematics a solid circle represents a bond critical point ($\sigma = -1$) and a solid triangle represents a ring critical point ($\sigma = +1$).

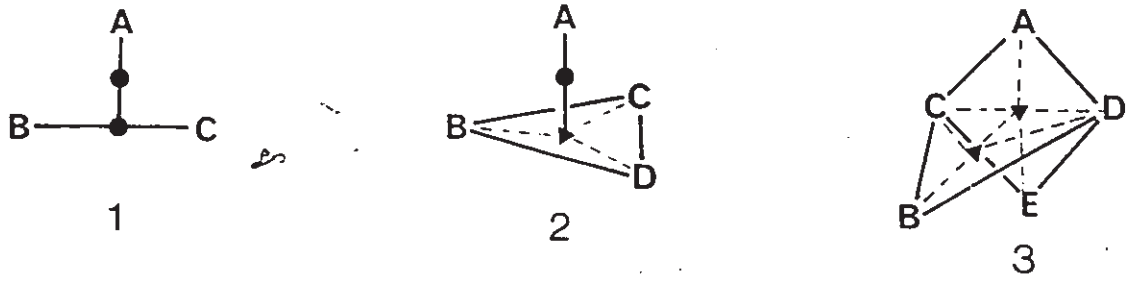

If the nuclear configurations above are jiggled in an unsymmetrical way, a stable structure will result in each case. In 1 and 2 the bond paths linking nucleus A to saddle points will instantaneously switch from their respective saddle points to one of the other nuclei. In structure 3 any unsymmetrical motion of the nuclei will transform the $\overline{\text{B–C–D}}$ ring surface into either a $\overline{\text{B–A–C–D}}$ or a $\overline{\text{B–E–C–D}}$ ring surface. The mechanism of the isomerism HCN —> CNH proceeds via the conflict structure 1. This process is illustrated in figure 1.5, taken from (Tal *et al.* 1981).

The second type of unstable structure found at catastrophe points is a bifurcation structure. These structures are identified by the presence of one or more singularities in the charge density, a point at which both the gradient and one or more of the eigenvalues of the Hessian matrix vanish. For a one dimensional function this corresponds to a point of inflection, where both the first and second derivatives are zero (figure 1.6). The mechanism of scissor–like opening (closing) of a three–membered ring involves a bifurcation structure at the moment which the bond breaks (forms). This mode of structural change is schematically illustrated in figure 1.6. Calculations of the bifurcative reaction mechanisms such as that found in methyl migration in 1–propyllium cation (Bader, Nguyen–Dang and Tal 1981b) and cyclopropane ring opening (Bader *et al.* 1983) have been previously reported. Thom's theory of elementary catastrophes (1975) provides a mathematical description of the dynamics of structural change occuring via a bifurcation point. Essentially, Thom's theory allows one to predict the behaviour of the charge density in the immediate

Figure 1.5 (taken from Tal *et al.* 1981)

The gradient vector fields of the charge density are displayed for six geometries of the triatomic system HCN. The angle formed by the H–N and C–N internuclear axes, subtended at the nitrogen nucleus, is indicated below each figure. The bond paths are denoted by bold lines. For all angles between 0.0^0 and 72.1^0, the hydrogen atom is bonded to the carbon atom. For all angles between 72.4^0 and 180.0^0, the hydrogen atom is bonded to the nitrogen atom. At some point between 72.1^0 and 72.4^0 there exists an unstable molecular structure of the conflict catastrophe type. At this particular angle the hydrogen atom is not bonded to either the carbon or to the nitrogen atom. Instead there exists a bond path linking the hydrogen nucleus to the C–N bond critical point.

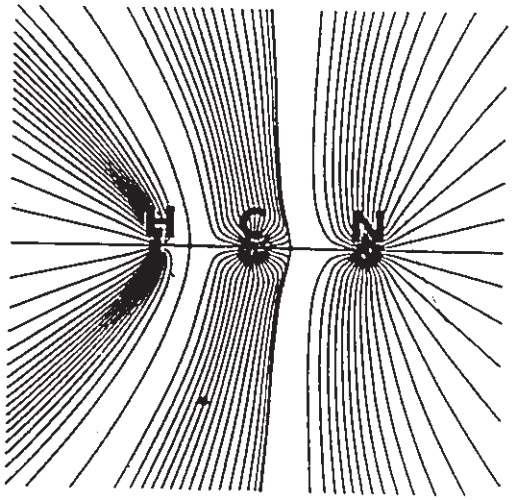

0.0

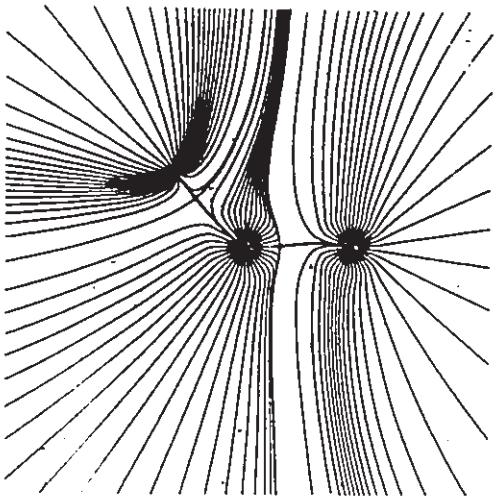

30.0

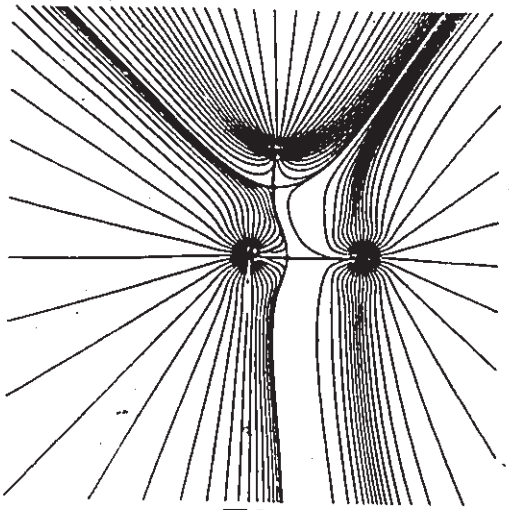

72.1

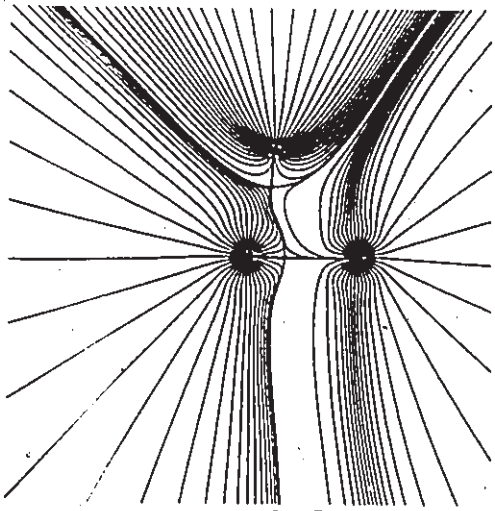

72.4

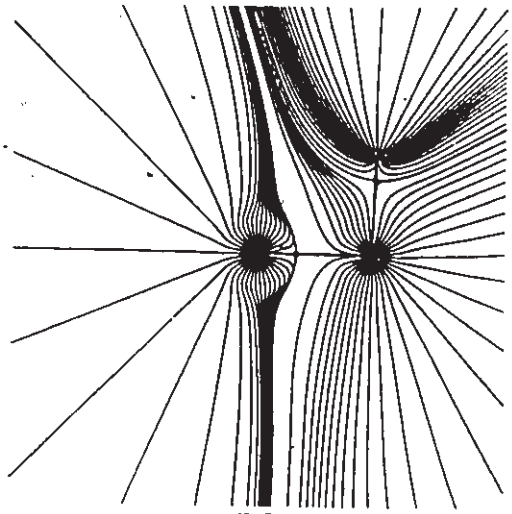

120.0

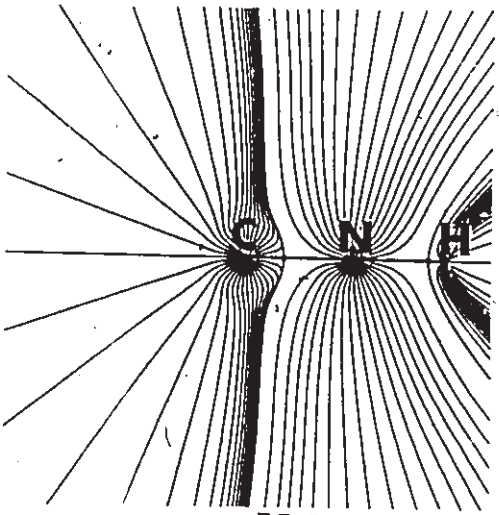

180.0

Figure 1.6

The upper set of figures schematically illustrate the profile of the charge density along the dashed lines in the lower set of figures. In the pair of figures labelled A the solid circles denote the position of a bond critical point, while the solid triangles denote the positions of a ring critical point. The pair of figures labelled B correspond to a geometry in which the angle bisected by the dashed line has been widened to the point at which the bond and ring critical points marked in A have coalesced. The point in real space at which these critical points meet is a singularity in the charge density since the gradient and one of the eigenvalues of the Hessian matrix of ρ vanish there. The point in nuclear configuration space at which the charge density exhibits a singularity is the bifurcation catastrophe point. When the angle of interest is widened further, an open structure is created. This is shown in the pair of figures labelled C.

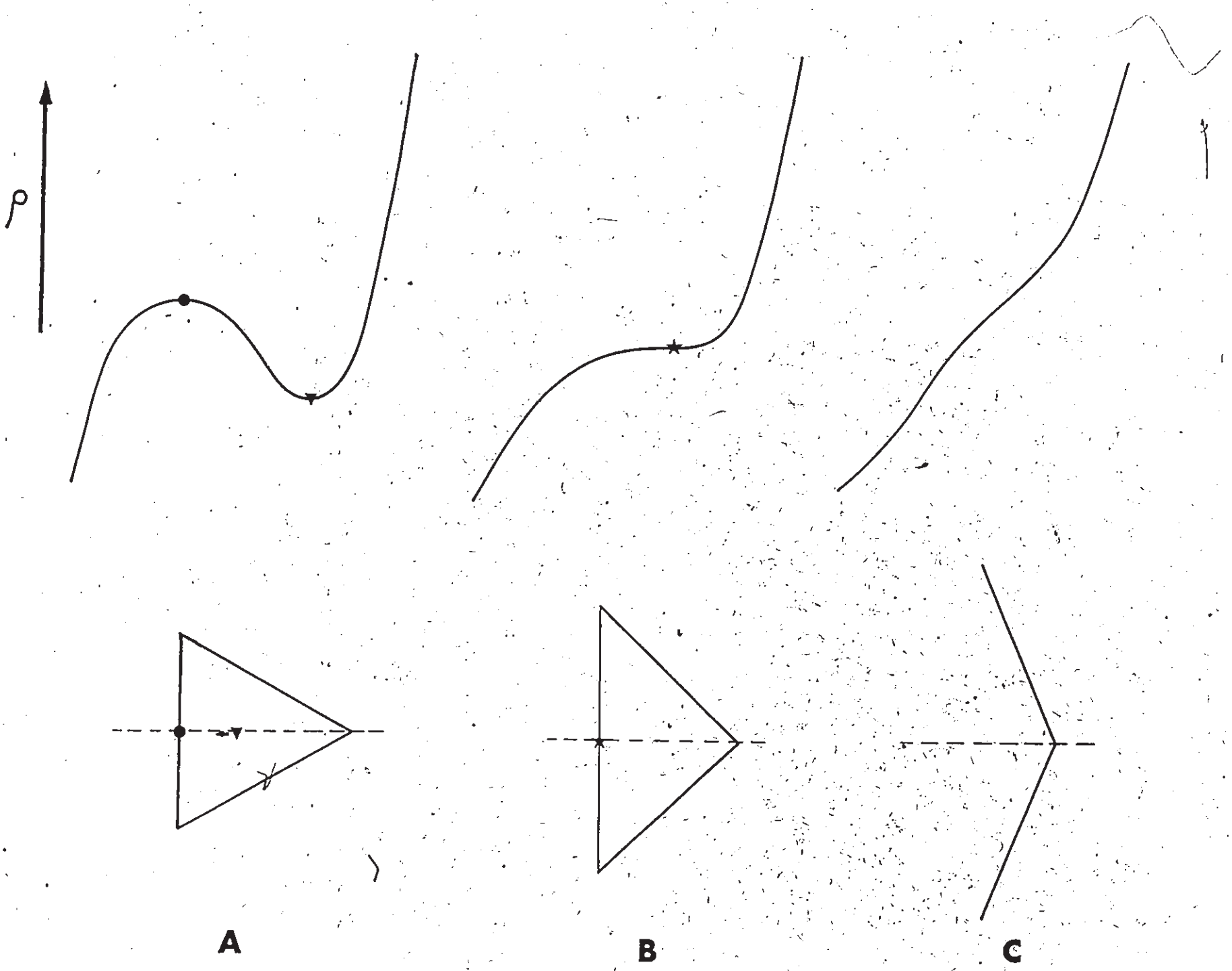
ρ
A
B
C

vicinity of the singularity in response to infinitesimal changes in nuclear configuration. This knowledge is then translated into a prediction of the resulting stable structure. Collard and Hall (1977) suggested that this theory might be used in the description of changes in molecular structure. Shortly thereafter Bader *et al.* incorporated Thom's theory into the topological theory of molecular structure and demonstrated its quantitative modelling of those parts of the structure diagrams predicting the mechanisms of ring opening and closing in the triatomic systems H_3^+ (1979b) and H_2O (1981b). An example of a catastrophic change in structure of greater complexity is suggested by preliminary results of an ongoing application of the topological theory of molecular structure in a study of the structures of binuclear metal carbonyl complexes (MacDougall *et al.* 1987). Chapter 3 will present these results and directions of future research applying and extending the theories reviewed in this chapter and the analysis of the Laplacian presented in chapter 2.

CHAPTER 2

LEWIS REVISITED: IN SEARCH OF THE PHYSICAL BASIS OF ELECTRON PAIR MODELS

2.1 PAST ATTEMPTS TO INTEGRATE THE LEWIS MODEL AND QUANTUM MECHANICS

There has been no shortage of manipulations of quantum mechanical calculations with the stated purpose of recovering the simple but powerful description of the electronic structure of a molecule as a set of spatially localized electron pairs. Unfortunately, there is no consensus on how this should be done. Since this discussion is concerned with the physical basis of the electron pair model, we are necessarily restricted to *ab initio* methods of electron structure calculation. Admittedly, no chemically significant calculation is free of short–cuts. However, the approximations that make *ab initio* calculations tractable, such as the Born–Oppenheimer and mean–field approximations of Hartree–Fock theory, can be gradually removed to gauge the robustness of insights gained at this level of theory. Whereas short–cuts to obtaining predictions of chemical interest that bypass explicit electron interactions altogether, such as the parametrization of the one–electron Hamiltonian in extended Hückel theory (Wolfsberg and Helmholtz 1952, Hoffmann 1963), forgo at the onset much of the information that is sought here.

The oscillations of molecular quantum mechanics from localized valence bond (VB) theories inspired by Lewis' model (*e.g.* Heitler and London 1927, Pauling 1931 and 1932, Slater 1931a and 1931b, Ladner and Goddard 1969) to delocalized molecular orbital (MO) theories inspired by spectroscopic classification of electronic states (*e.g.*

Hund 1928 to 1937, Mulliken 1928 to 1939, Roothaan 1951) have made the interpretation of electronic structure calculations somewhat of a rivalry (Messmer and Schultz 1986, Hay *et al.* 1972). The operational differences between the MO and VB methods give each its own character, but should not lead to any contradictions in the prediction of physical properties of a molecule since both methods are merely computational means to a common end: an approximate state function. It is the approximate state function which is deserving of investigative attention, not the intermediates calculated *en route*. Nevertheless, single–particle molecular orbitals have become the focus of the majority of studies aimed at understanding the fine details of the system. In particular, by performing a unitary transformation of the delocalized, or canonical, orbitals of MO theory one can generate a new set of orbitals according to one's own personal criteria, without affecting the physical properties of the system that are determined from the total state function. The most commonly employed transformations are those that yield orbitals relatively localized in the region of each electron–pair bond or lone pair anticipated on the basis of Lewis' model. For a molecule of high symmetry an "equivalent" set of molecular orbitals can be generated from the canonical set without extensive calculation (Lennard–Jones 1949). For molecules with low symmetry, different localization criteria have been proposed that allow a variational derivation of a set of orbitals for which some orbital–based property is extremized (Boys and Foster 1960, Edmiston and Ruedenberg 1963, McWeeny and Del Re 1968). These localization schemes sometimes yield multiple solutions, each solution representing a local extreme in the localization criterion. The impetus for these manipulations is unclear, since when considered individually the spatial form of a molecular orbital of any kind does not describe the spatial distribution or any other physical property of the electrons in a molecule.

Recall from the previous chapter that the total electron density distribution, $\rho(\mathbf{r})$, generally exhibits peaks only at the positions of nuclei. This observation was

crucial in the development of a quantum mechanical theory of atoms in molecules due to the topological constraints that were imposed on the partitioning of a molecule into quantum subsystems.[6] However, this very same observation does not permit a literal interpretation of Lewis' model of the atom. Such an interpretation of the Lewis model would require the existence of local maxima in the charge distribution centred on each two–electron bond as well as the corresponding number of maxima in the nonbonding regions. The widespread appeal of localized orbitals is undoubtedly their artificial resurrection of this picture. The following subsections describe the first orbital independent attempts at establishing a physical basis for the Lewis model.

LINNETT'S DOUBLE QUARTET

Lewis's model of the atom was based on a static description of its electronic configuration. The quantum mechanical analogue of this is Linnett's double quartet model (1964) in which the static arrangement of the N electrons of an atom is such that the square of the 4N–dimensional state function Ψ is maximized. The probability of simultaneously locating particle 1 at r_1 with spin s_1, particle 2 at r_2 with spin s_2, *et cetera*, is given by equation 2.1 where the notation $\{x_i\} = \{r_i,s_i\}$ is used.

(2.1) $\Psi^*\{x_i\}\Psi\{x_i\}dx_1dx_2...dx_N$

Linnett and Pöe (1951) have shown that for an isolated carbon atom the square of the state function is maximized when the set of coordinates $\{x_i\}$ denote a ^5S state with an α,β pair of electrons at the nucleus and four electrons of identical spin each located 2.35 au from the nucleus at the corners of a tetrahedron. As more electrons are added to this system, with either a corresponding increase in nuclear charge or hydrogen atom coordination, the extent of electron pairing is determined within this model by the alignment of the separately correlated tetrahedra of like–spin electrons. There is

[6] It has recently been observed that the local maxima in $\rho(r)$, that are contained in each fragment of a molecule that is partitioned by a zero–flux surface, are not always at (or very near) the positions of nuclei (Gatti *et al.* 1987, Cao *et al.* 1987). So far these non–nuclear atoms are found only in clusters of alkali metals.

predicted to be no pairing of electrons in the neon atom while the localization of a pair of electrons to the same region of space increases as the potential energy in the internuclear binding region decreases. The drawbacks of this model are that it does not allow for a study of the extent of electron pairing in the average distribution of electrons, nor does it allow an evaluation of the relative extents of intra– versus inter–pair coupling of electron motion (Stephens 1975).

PROPERTIES OF DENSITY DIFFERENCE MAPS

The pedestrian appearance of the total charge distribution of a molecule is not easily interpreted by visual inspection. Any perturbations to the total density in the valence region of an atom in a molecule are especially difficult to discern since the overall appearance of the charge distribution is dominated by the core electrons. Roux, Besnainou and Daudel (1956, 1958) introduced the method of subtracting from the molecular charge density, the superimposed spherical densities of the isolated atoms, α.

$$\Delta\rho(\mathbf{r}) = \rho(\mathbf{r})_{\text{molecule}} - \Sigma_{\alpha}\rho(\mathbf{r} - \mathbf{r}_{\alpha}) \tag{2.2}$$

The coordinates of the nuclei, $\mathbf{r}_{\alpha}$, in this superimposed "promolecule" are set at those found for the molecule. This method served as a useful tool for qualitatively observing how the charge density of an isolated atom changes during the procees of molecule formation. It also stimulated both theoretical and experimental investigations into the role of the electronic charge distribution in chemical bonding (Bader 1975, Coppens 1967). However, the original recipe for the construction of the promolecule has been the subject of proposed revisions, such as using nonspherical atoms in the promolecule (Bader 1969) or subtracting fragment densities instead of atomic densities (Heijser *et al.* 1980). The features of the density difference map depend explicitly on the arbitrarily chosen method of constructing the promolecule density. Consequently, the interpretations resulting from such an analysis must be viewed as subjective and not

indicative of any physical property of the molecule (Ransil and Sinai 1967, Kunze and Hall 1986). Nevertheless, the patterns observed in many density difference maps, i.e. the number and location of maxima in the function $\Delta\rho(r)$, frequently reflect the distribution anticipated on the basis of the Lewis model (Coppens 1967). While this method does not provide a physical basis for the Lewis model, it does suggest that the form of the total density is qualitatively distorted in accordance with this model.

LES DOUBLETS ELECTRONIQUES DANS DES LOGES

Daudel and coworkers (1953, 1955) proposed that the fundamental importance of the electron pair in chemistry should be evident in a relatively high probability of localizing pairs of electrons in separate regions of space. This is in contrast to Linnett's model in which the single most probable configuration is determined. The nonoverlapping regions of space are termed "loges". The task of implementing loge theory in a study of all of the event probabilities for a many electron system is prohibitive. Knowledge and use of the diagonal elements (equation 2.3) of the full spinless N–particle density matrix, $\Gamma^{(N)}$, is necessary for the prediction of the probability of a given event. Most of the calculations discussed in this thesis are of the Hartree–Fock type. Hartree–Fock calculations express the state function as a linear combination of spin–orbitals, ϕ_i, that are functions of the space and spin coordinates of a single electron. Within this approximation the density matrix of all N electrons is written as a determinantal expansion of the first–order density matrix, $\rho(x_1,x_1')$ defined in equation 2.4 (McWeeny and Sutcliffe 1969).

(2.3) $$\Gamma^{(N)}(r_1,r_2,\ldots r_N) = \int ds_1 \ldots ds_N \Psi^*(x_1,\ldots x_N)\Psi(x_1,\ldots x_N)$$

(2.4) $$\rho(x_1,x_1') = \sum_i^{occ} \phi_i(x_1)\phi_i^*(x_1')$$

In the simple case of a two–loge system the probability, $P_n(\Omega)$, of finding n electrons in region Ω while the remaining $(N - n)$ electrons are contained in the

remainder of the system Ω' is given by equation 2.5. The probabilities of all events sum to unity for a normalized state function.

$$(2.5) \qquad P_n(\Omega) = N!/[n!(N-n)!]\int_{\Omega} dr_1 \cdots \int_{\Omega} dr_n \int_{\Omega'} dr_{n+1} \cdots \int_{\Omega'} dr_N \Gamma^{(N)}(r_1 \cdots r_N)$$

Equation 2.5 gets considerably more complicated when more than two loges are considered. If one wishes to further optimize the partitioning of space into the best loges, then the probabilities defined by equation 2.5 must be evaluated for each proposed partitioning. One is still left with the task of choosing the criterion on which to evaluate the proposed partitioning. The cumbersomeness of loge theory is alleviated somewhat by the infusion of information theory (Aslangul 1971, Aslangul *et al.* 1972, Shannon 1948). Within this theory, the knowledge of a given system is greatest when the missing information function $I(P,\Omega)$ (defined in equation 2.6) is minimized with respect to variation of the loge boundaries. The system is known best when the probability of a given event, the leading event, is much higher than any other possible event. This is evident in equation 2.6 where the missing information goes to zero as the probability of the leading event approaches unity.

$$(2.6) \qquad I(P_n,\Omega) = -\sum_n P_n(\Omega) ln P_n(\Omega)$$

This methodology still requires knowledge of the diagonal elements of the full N–particle density matrix, but satisfactorily provides a unique criterion for determining the "best" loges.

Daudel *et al.* (1974) undertook the considerable task of applying the theory of loges to Hartree–Fock calculations of the hydrides LiH^+, LiH, BeH^+, BeH, BH and BeH_2. The best core loges for each of these systems were evaluated by determining the probabilities of localizing all possible numbers of electrons in a spherical core loge with a radius varied from 0.0 – 5.0 au. In each case studied the leading nontrivial event was that which localized a pair of electrons in the core loge. The best loge partitioning (minimum missing information) was found to occur at the same radius that $P_2(\Omega)$ was maximized. Figure 2.1 illustrates, from first principles, that the leading event which

localizes n electrons in the core region of BH is decisively that where n = 2. This same result was obtained for the core loge partitioning of every system studied. Furthermore, Lewis' model of the physical separation of the "kernel" of an atom (core electrons and nucleus) from the valence electrons (Lewis 1916) is shown in figure 2.1b to be the best description possible, as this description maximizes our knowledge of the electronic structure of the system. Daudel *et al.* went on to determine the best three–loge partitionings of BeH, BH. Starting from the best core loges obtained from the two–loge partitioning, the valence region was partitioned into bonding and nonbonding loges. The bonding and nonbonding loges were partitioned by a conical surface extending outward from the spherical core loge surface of radius r_c and forming an angle α with the internuclear axis. Both r_c and α were varied and the probabilities of the possible events were evaluated. The value of r_c did not change from its two–loge value. In harmony with the Lewis model the events which localized a pair of electrons in each of the core and bonding loges and the remaining electron(s) in the nonbonding loge of BeH (BH) were the leading events. The probability of the "Lewis event" was 77% in BeH and 69% in BH. The next most probable events, or satellite events, were insignificant enough that the missing information function was again minimized at precisely the r_c and α values that yielded the greatest probability of the "Lewis event". Thus the Lewis model of the electronic structure of these systems, including the electron pair bond, is truly the best. That the probabilities of the "Lewis events" are not 100% does not imply the failure of the Lewis model. Lewis himself suggested the probable existence of "tautomeric" electronic structures in certain molecules (1916). Still, the probabilities of the events which correspond to Lewis' model of BeH and BH are remarkable given the total lack of bias in the calculations.

In the triatomic system BeH_2 considered in the above study, the three–loge partitioning results were less supportive of the traditional Lewis structure. The maximum probability of the "Lewis event" placing pairs of electrons in the core and

Figure 2.1 (taken from Daudel *et al.* 1974)

For the singlet ground state of BH, this figure illustrates the variation in event probabilties $P_n(\Omega)$, the missing information function $I(P,\Omega)$ and the fluctuation $\Lambda(N,\Omega)$ for a spherical core loge of variable radius, r in au. The positions of the maximum probabilities in the figure on the left are marked by crosses on the figure illustrating $I(P,\Omega)$ and $\Lambda(N,\Omega)$. Note that the only nontrivial minimum in both $I(P,\Omega)$ and $\Lambda(N,\Omega)$ occurs at the radius where the probability of event localizing a pair of electrons in the loge is maximized.

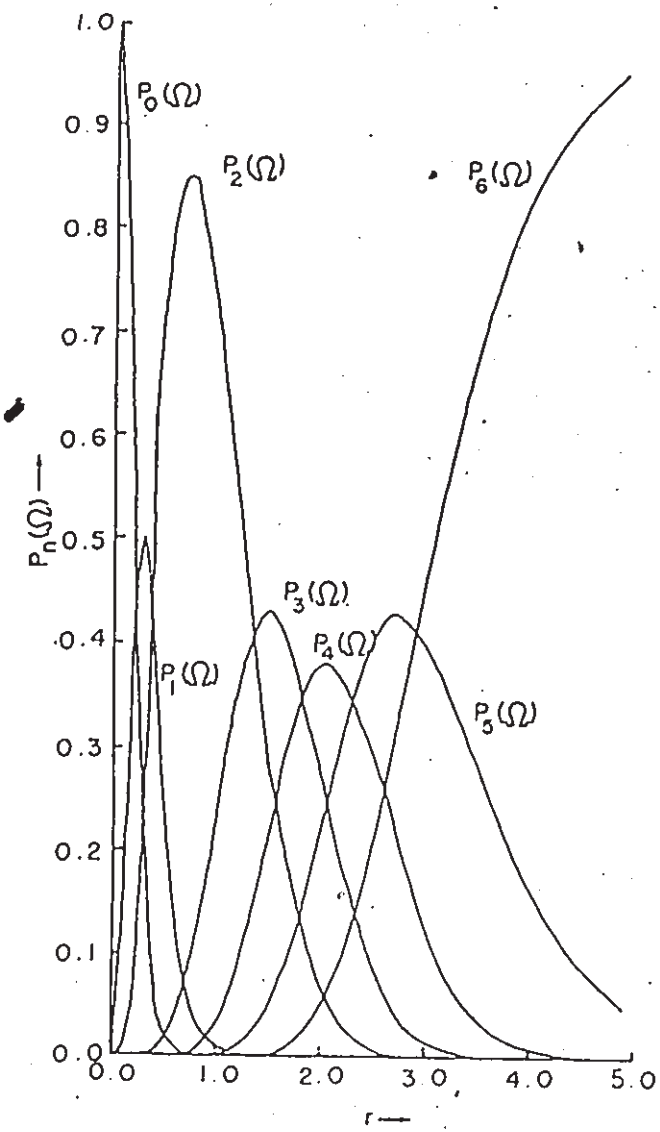
1.0
0.9
0.8
0.7
0.6
0.5
0.4
0.3
0.2
0.1
0.0
$P_n(\Omega)$ —
$P_0(\Omega)$
$P_2(\Omega)$
$P_6(\Omega)$
$P_3(\Omega)$
$P_4(\Omega)$
$P_1(\Omega)$
$P_5(\Omega)$
0.0
1.0
2.0
3.0
4.0
5.0
r —

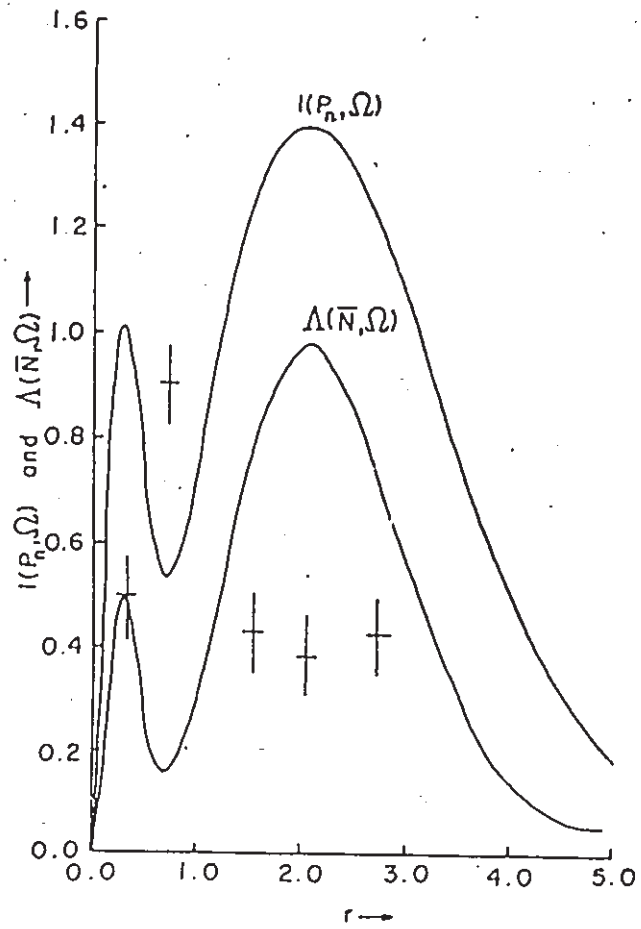
1.6
1.4
1.2
1.0
0.8
0.6
0.4
0.2
0.0
$I(P_n,\Omega)$ and $\Lambda(\bar{N},\Omega)$ —
$I(P_n,\Omega)$
$\Lambda(\bar{N},\Omega)$
0.0
1.0
2.0
3.0
4.0
5.0
r →

two equivalent bonding loges is only 33% compared to a value of 22% for each of two events which correspond to a pair of electrons in the core but one electron in one bonding loge and three electrons in the other bonding loge. This was interpreted as a significant overlap of the regions of space that the bonding pairs of electrons can be localized to (Daudel *et al.* 1974). However, the authors also pointed out that if the bond loges were separated by an annular region, defined by two conical surfaces forming an angle $\alpha = 85^0$ with each Be–H bond axis, that was added onto the core loge then the probability of the event localizing two electrons in each of the three loges more than doubles as it becomes 78%. The missing information function for this extended core partitioning is correspondingly reduced to half its value in the spherical core partitioning. Similarly, if the entire Li atom is treated as the core in LiH^+ and LiH, *i.e.* the zero–flux surface is used to partition the loges as well as the atoms, then lower $I(P,\Omega)$ values are obtained. It appears as though open cores may be the best choices in systems with no nonbonding loges, we will come back to this observation in the discussion of the shell structure exhibited by the Laplacian of the charge distrubution. Interestingly, it was also observed in the above work that the conical surfaces separating the bonding and nonbonding loges in BeH and BH closely approximate the zero–flux surfaces that partition these diatomic systems into atoms.

The loge theory of interpreting the electronic structure of a molecule provided a unification of the Lewis model with the quantum mechanical probability functions in the case of simple diatomic hydrides. However, this agreement between theory and the popular model does not turn out to be a general one, as we shall see later. The theory is also extremely difficult to apply to larger systems as the number of integrals necessary for a given $P_n(\Omega)$ increases as $N!N_\alpha!N_\beta!$, where N_α and N_β are the number of α and β electrons respectively. In addition the definition of loge boundaries can not be freely varied as this would be computationally horrendous. Instead the boundaries are described by surfaces defined by as few parameters as possible, such as r_c and α.

As the molecule became less symmetrical this difficulty would combine with the integral explosion to make the problem intractable.

Daudel *et al.* (1974) observed parallel behaviours of the missing information function $I(P_n,\Omega)$ defined in equation 2.6 and the fluctuation in the electron population of a loge, $\Lambda(N,\Omega)$. The population of a loge is just the integral of the charge density over the space of the loge. It is in general not an integer unless the probabilities of events localizing more electrons than the most probable event exactly balance the probabilities of events localizing less than the leading event. Figure 2.1 illustrates this empirical relationship for the two–loge partitioning of BH. The fluctuation in the population is defined in equation 2.7, it has been proposed as a measure of the extent of the localization of the electrons within a loge (Denis *et al.* 1973).

(2.7) $$\Lambda(N,\Omega) = N^2(\Omega) - [N(\Omega)]^2 = \sum_n n^2 P_n(\Omega) - [\sum_n n P_n(\Omega)]^2$$

Bader and Stephens (1974) have shown that $\Lambda(N,\Omega)$ can be expressed (equation 2.8) in terms of the diagonal elements of the first– and second–order density matrices, thereby reducing the complexity of the partitioning of a molecule into "best" loges and permitting the investigation of systems with greater numbers of electrons.

(2.8) $$\Lambda(N,\Omega) = \int_\Omega dr_1 \int_\Omega dr_2 D_2(r_1,r_2) + \int_\Omega dr_1 D_1(r_1) - [\int_\Omega dr_1 D_1(r_1)]^2$$

The reduced density matrices appearing above are defined and discussed in the following subsection, see equations 2.9 and 2.10. The methodology described below takes an approach to establishing the physical basis of electron pair models that is complimentary to the one described above in that the concept of loges is maintained, however, the extent and cause of localization of electrons into pairs is studied specifically.

FOCUSING ON THE PAIR DISTRIBUTION FUNCTION

The behaviour of pairs of electrons is completely described by a distribution function which is drastically less complex than the total state function and its

associated spinless N–particle density matrix. The information necessary to establish the physical basis of the Lewis model and predict the properties of molecules that are rationalized on the basis of this model, should at the most be contained in the pair distribution function (Löwdin 1955, McWeeny 1960). Just as quantum mechanics determines $\rho(\mathbf{r})$, the probability of finding an electron at a given point in space (equation 2.9), the probability of simultaneously finding an electron at each of two chosen points is the pair density, $D_2(r_1,r_2)$ (equation 2.10).

$$D_1(r_1) = \rho(r_1) = N\int ds_1 \int dx_2 \cdots \int dx_N \psi^*(x_1,x_2,\ldots,x_N)\psi(x_1,x_2,\ldots x_N) \tag{2.9}$$

$$D_2(r_1,r_2) = N(N-1)\int ds_1 \int ds_2 \int dx_3 \cdots \int dx_N \psi^*(x_1,x_2,\ldots,x_N)\psi(x_1,x_2,\ldots,x_N) \tag{2.10}$$

The prefactors in equations 2.9 and 2.10 simply ensure that the integral of these functions over their respective spaces would yield the correct number of electrons (equation 2.9) and the correct number of nondistinct pairs of electrons (equation 2.10), assuming the state functions are normalized. The pair density differs locally, *i.e.* at (r_1,r_1) in pair space, from the simple product of single particle densities at r_1 and r_2 by the relation 2.11 (McWeeny 1960). The correlation term $f(r_1,r_1)$ corrects for the counting of N self–pairs in the integration of $D_1(r_1)D_1(r_2)$ over all space as shown in equation 2.12. The local form of the correlation term depends on the types of electron correlation that are accounted for in the calculation of the state function. This property of the pair distribution function will be discussed in the next subsection.

$$D_2(r_1,r_2) = D_1(r_1)D_1(r_2)[1 + f(r_1,r_2)] \tag{2.11}$$

$$\int dr_1 \int dr_2 D_1(r_1)D_1(r_2)f(r_1,r_2) = -N \tag{2.12}$$

Bader and Stephens (1975) examined the properties of pair densities calculated from near Hartree–Fock state functions to: 1) determine whether or not one can generally partition a molecule into loges representing the maximum possible localization of electrons within each of the loges, 2) determine the average number of pairs withir these loges to estimate the absolute extent of pair–wise localization, 3)

provide quantitative insight into the mechanism that is responsible for pair–wise localization, namely Fermi correlation.

First, they attempted to partition the series LiH, BeH_2, BH_3, BH_4^-, CH_4, NH_3, OH_2, FH, Ne, N_2, F_2 and Ar into loges which minimized the fluctuations in the loge populations (equation 2.8) with respect to variations of the loge boundaries. Maximally localized spherical core loges centered on each of the nuclei other than hydrogen were found for all species studied. The radii of the loges decreased with increasing nuclear charge, and each loge had an average population in the neighbourhood of two electrons. Only Ar exhibited two minima in $\Lambda(N,\Omega)$ as a function of r. The sum of the fluctuations in the populations of the three concentric shells of charge density is also minimized by simultaneous variation of both r_1 and r_2. Attempts to partition the valence density of the above series into loges that exhibited a maximum degree of localization failed beyond BH_4^- (Bader and Stephens 1975). In LiH the localization of a core loge containing an average of two electrons automatically implies that the valence electrons are localized in a single bonding loge also containing two electrons on average. The valence charge density in the other ionic systems BeH_2, BH_3 and BH_4^- could be partitioned into nonoverlapping bonding loges which individually contained on average two electrons. When the bonding loges were equivalent and centered about the internuclear axes, the fluctuations in their populations were minimized. These observations are in accord with the Lewis model of a localized pair of electrons forming n A–H bonds in these AH_n systems. Methane was borderline in that the sum of the fluctuations of all the loges, including the core, could be minimized for a partitioning of the molecule into a core loge and four equivalent bonding loges centered about the C–H internuclear axes, each loge containing two electrons on average. However, this minimum is a only a result of the pronounced decrease in the fluctuation of the core loge at its optimum radius. The four equivalent bonding loges in CH_4 exhibit a plateau over which their individual $\Lambda(N,\Omega)$ values

remains relatively unchanged as the loges are made larger, smaller, unsymmetric etc..., there is no "best" partitioning of the valence density into localized loges. In the remaining molecules that were studied the valence region cannot be partitioned in any way that minimizes either the fluctuations in the individual loge populations or the sum of the loge fluctuations. The implications of this observation directly contradict the Lewis model of localized pairs of electrons in the valence region of a molecule. Further, the concept that each chemical bond is a result of the sharing of a localized pair of electrons is therefore generally not a true representation of the electronic structure of a molecule (Bader and Stephens 1975).

Once the question "Can the electronic structure of a molecule be described by spatially localized electron pairs that can be classified as bonding or nonbonding?" has been satisfactorily answered, two questions take its place. First, to what extent is the pair density localized and what are the factors governing this property of the pair distribution. Secondly, what then is the physical reason for the success of the Lewis model and those models that are derived from it, such as the VSEPR model of molecular geometry (Gillespie and Nyholm 1957, Gillespie 1963 and 1972).

The answer to the first question is summarized by tables 2.1, 2.2 and 2.3 (Bader and Stephens 1975). The data in these tables illustrate the extent of localization of the charge density into pairs for the core, bonding and nonbonding loges for the molecules in the above series. The definition of $F(\Omega,\Omega)$ and its significance will be discussed in the next subsection. It was reported earlier that there was no "best" loge decomposition of the valence region for the systems beyond BH_4^- in the series. To indicate the extent of pair–wise localization in the bonding and nonbonding regions, loges were chosen which contained average populations, $N(\Omega)$, as close as possible to two electrons and had the same basic shape as the "best" loges found for BH_4^-. The values for $D_2(\Omega,\Omega)$ indicate the average number of nondistinct electron pairs that are

Table 2.1. Properties of Core Loges.

Molecule	r,au	$\bar{N}(\Omega)$	$D_2(\Omega,\Omega)$	$F(\Omega,\Omega)$	$\lvert F(\Omega,\Omega)/\ \bar{N}(\Omega)\rvert \times 100$ percentage localization
LiH	1.42	1.999	2.088	-1.908	95.5
BeH_2	0.95	2.012	2.173	-1.875	93.2
BH_3	0.70	2.023	2.256	-1.836	90.8
BH_4^-	0.70	2.026	2.291	-1.814	89.5
CH_4	0.53	2.005	2.254	-1.766	88.1
NH_3	0.43	2.002	2.282	-1.726	86.2
OH_2	0.36	2.001	2.314	-1.691	84.5
FH	0.30	1.966	2.244	-1.621	82.5
N_2	0.43	2.001	2.271	-1.733	86.6
F_2	0.31	2.008	2.367	-1.667	83.0
Ne	0.26	1.963	2.348	-1.506	76.7
Ar	0.12	1.856	2.090	-1.355	73.0

Table 2.2. Properties of Bonded Loges.

Molecule	$\bar{N}(\Omega)$	$D_2(\Omega,\Omega)$	$F(\Omega,\Omega)$	$\lvert F(\Omega,\Omega)/\bar{N}(\Omega)\rvert \times 100$ percentage localization
LiH	2.001	2.094	−1.910	95.5
BeH_2	1.994	2.126	−1.850	92.8
BH_3	1.992	2.341	−1.623	81.8
BH_4^-	1.994	2.454	−1.522	76.3
CH_4	1.999	2.619	−1.377	68.9
NH_3	1.997	2.762	−1.226	61.4
OH_2	1.987	2.833	−1.117	56.2
FH	2.037	3.067	−1.081	53.1
$N_2(\sigma)$	1.995	3.420	−0.560	28.1
$N_2(\pi)$	1.966	3.296	−0.569	28.9
F_2	2.034	3.785	−0.353	17.4

Table 2.3. Properties of Nonbonded Loges.

Molecule	$\bar{N}(\Omega)$	$D_2(\Omega,\Omega)$	$F(\Omega,\Omega)$	$\lvert F(\Omega,\Omega)/\bar{N}(\Omega)\rvert \times 100$ percentage localization
NH_3	2.005	2.914	-1.106	55.2
OH_2	2.005	2.981	-1.037	51.7
FH	1.999	3.010	-0.988	49.4
Ne	2.009	3.070	-0.967	48.1
N_2	2.035	2.943	-1.199	58.9

contained in the corresponding loge; it is defined in equation 2.13.

(2.13) $$D_2(\Omega,\Omega) = \int_\Omega dr_1 \int_\Omega dr_2 D_2(r_1,r_2)$$

The reader may ask "How can a bonding loge of CH_4 have almost two and two–thirds pairs of electrons when its population is only two electrons?". First, because the integration of the pair density is over the coordinates of two electrons independent of one another, each pair in the integrated region is counted twice. Therefore the values of $D_2(\Omega,\Omega)$ in tables 2.1, 2.2, 2.3 should be divided by two to determine the number of distinct pairs. That still leaves one and one–third distinct pairs in a bonding loge of CH_4 which only has a population of two electrons. The concept of a pair population is certainly not as easily envisioned as that of an electron population. To clarify this concept and to put the pair populations in tables 2.1, 2.2 and 2.3 into perspective (they could actually be even higher!), consider the following hypothetical derivation of the number of distinct pairs of electrons in a bonding loge of CH_4 labelled Ω_{b1}. For the sake of simplicity we will assume that the core loge contains two electrons that are completely localized there. The probability that electron 1 is in Ω_{b1} is 1/4. If the motions of the electrons are completely independent of one another, then the probability that any one of the remaining seven electrons is in Ω_{b1} at the same time as electron 1 is equal to 1/4x(7x1/4). There is a 7/16 probability of there being a pair of electrons in Ω_{b1}, one of which is electron 1. Since there are eight valence electrons whose motions have been assumed to be uncorrelated, there are 8x7/16 or 3.5 nondistinct pairs of electrons in Ω_{b1}. Now one can better appreciate the pair populations given in tables 2.1, 2.2 and 2.3.

CORRELATION HOLES IN THE PAIR DISTRIBUTION

From the above discussion it is clear that the pair distribution of uncorrelated electrons is delocalized to a much greater extent than the pair distributions obtained

from near Hartree–Fock calculations. From equation 2.11 it is clear that the correlation term is accountable for the difference. The effect of the correlation term can be visualized best by considering the correlation hole it creates in the pair distribution when the coordinates of one of the electrons are held fixed at some point r_1. The pair distribution and the correlation term then become more interpretable three–dimensional functions that can be studied as a function of r_1, the coordinates of the reference electron. The probability of finding an electron anywhere in the r_2 portion of pair space is instantaneously modified by the correlation term when the coordinates of the reference electron are fixed. This is because the single particle density is premultiplied by N, yet there are only N–1 electrons remaining. The r_2 space of the pair density therefore has a hole in it, relative to the single particle density, that removes exactly one electron when integrated over all of r_2 (equation 2.14).

(2.14) $$\int dr_2 D_1(r_2) f(r_1,r_2) = -1 \quad \text{for any } r_1$$

The integrand in equation 2.14 is the correlation hole. The above discussion applies equally to the pair density in r_1 space if we hold r_2 fixed. Equation 2.15 expresses the fluctuation in a loge population in terms of the correlation hole. It is evident that the fluctuation in a loge population approaches zero when the correlation hole integrates, over the space of the loge, to its limiting value of –1 for every position of the reference electron within the loge (Bader and Stephens 1974).

(2.15) $$\Lambda(N,\Omega) = N(\Omega) + \int_\Omega dr_1 \int_\Omega dr_2 D_1(r_1) D_1(r_2) f(r_1,r_2) = N(\Omega) + F(\Omega,\Omega)$$

The quantity $F(\Omega,\Omega)$ is the total correlation in the motions of the electrons within Ω with each other. In the limit that $F(\Omega,\Omega) = -N(\Omega)$ the motions of the electrons within Ω are totally independent of the rest of the system, in this case the electrons are 100% localized within the region Ω. This is of course only satisfied when Ω refers to an isolated system. We can define the extent of localization as the percentage, of the

maximum correlation of the electrons in Ω, that is actually contained in Ω (equation 2.16).

(2.16) $$\mathcal{L}(\Omega) = |F(\Omega,\Omega)/N(\Omega)|(100\%)$$

For a pair distribution calculated from a state function described by simple Hartree product, *i.e.* the value of the state function when electron 1 is at r_1 is independent of the space and spin coordinates of electron 2, the correlation term is a constant, $f(r_1,r_2) = -1/N$. The correlation hole is therefore equal to $-D_1(r_2)/N$ and can not localize the pair density to any portion of a molecule. In this case the localization of any region is simply the fraction of the total electron population contained in the region, *i.e.* $\mathcal{L}(\Omega)=(N(\Omega)/N)(100\%)$. The correlation term in the expression of a Hartree pair density is strictly a statistical correction.

In Hartree–Fock calculations the pair density is further correlated by the requirement of the Pauli principle that the state function be antisymmetric, with respect to any permutation of the electrons. The effect of this constraint on the pair density is that two electrons of the same spin have a zero probability of being located at the same point in space at the same time. Thus for a closed shell system, when an α electron is at r_1, the correlation hole must decrease the probability of locating a second α electron at r_1, by exactly $D_1(r_1)/2$, while the correlation hole has no effect on the distribution of β electrons. The correlation holes that are calculated in Hartree–Fock theory thus alter the pair density over and above that required strictly for pair counting purposes. The correlation hole in Hartree–Fock theory is called the Fermi hole, since the fermion nature of electrons is properly accounted for (Wigner and Seitz 1934). Equation 2.17 is the orbital expression of the Fermi hole density, $h^{\alpha}(r_1,r_2)$, of an α electron when another α electron is at r_1.

(2.17) $$h^{\alpha}(r_1,r_2) = -\sum_i\sum_j \phi_i(r_1)\phi_j^*(r_1)\phi_i^*(r_2)\phi_j(r_2)/\sum_i \phi_i^*(r_1)\phi_i(r_1)$$

The Fermi hole is negative everywhere in all cases observed so far. The form of h^{α} is invariant to whether the ϕ_i's are the set of occupied orthogonal spin–orbitals

that are the eigenvectors of the Hartree–Fock operator or any orthogonal set resulting from a unitary transformation of them. The Fermi hole is not an orbital dependent function, it is a property of the total state function that can be conveniently written as a function of orthogonal spin–orbitals.

The pair density of an exact many–electron state function or of a multi–determinantal approximate state function exhibits two types of correlation holes, $h^{\alpha\alpha}$ and $h^{\alpha\beta}$, corresponding to the correlations between the motions of electrons with like and unlike spin respectively. These functions have the same integral properties as their Hartree–Fock counterparts, $h^{\alpha\alpha}$ and the Fermi hole integrate to –1, while $h^{\alpha\beta}$ integrates to zero (the Coulomb hole is nonexistent in a Hartree–Fock pair density). Locally, however, they differ by an amount that can be attributed purely to Coulomb correlation. The addition of Coulomb correlation can cause $h^{\alpha\alpha}$ and/or $h^{\alpha\beta}$ to become positive.

CORRELATION AND LOCALIZATION IN HARTREE–FOCK CHARGE DISTRIBUTIONS

Equation 2.16 relates the extent of electron localization within a loge to its contained correlation, relative to the limiting value. For Hartree–Fock calculations Fermi correlation is completely responsible for any pair–wise electron localization. The total amount of Fermi correlation contained in a given region of space is limited by equation 2.16 and is defined by equation 2.18.

(2.18) $$F(\Omega,\Omega) = -\sum_{i,j} S_{ij}^2(\Omega)$$

The S_{ij}'s are the overlaps of the occupied spin–orbitals ϕ_i and ϕ_j over the region Ω. In relation to the definition of the Fermi hole density, $F(\Omega,\Omega)$ is the integral of the numerator of equation 2.17 over the coordinates of both r_1 and r_2 within Ω. Tables 2.1, 2.2 and 2.3 report values of the total Fermi correlation (integrated over the coordinates of both electrons) for the previously discussed series of molecules. It can

be seen that the magnitude of $F(\Omega,\Omega)$ approaches the average population of the loge, $N(\Omega)$, only for those systems where electrons were found to be spatially localized into pairs (Bader and Stephens 1975). The percent localization of the electrons within a loge provides a bench mark for partitioning a molecule into loges that best describe the electronic structure of a molecule as a set of weakly coupled electron pairs. The loges determined by Bader and Stephens (1975) were determined variationally. The best loges extremized the fluctuation in the loge population. The bench mark for such a pair–wise partitioning appears to be that > 70% of the possible Fermi correlation must be contained within a given loge. Below this value the fluctuation in the loge population can not be minimized. The bonded loge in CH_4 is borderline. This bench mark parallels the observations of the relative importance of the interpair and intrapair correlation energies obtained from various "correlated pair" theories which tackle the electron correlation problem of molecular quantum mechanics by assuming at the onset separable electron pairs (Sinanoğlu 1962). Kutzelnigg (1973), Sinanoğlu and Skutnik (1968) have observed that the relative importance of interpair and intrapair correlation in methane, which is just below the borderline in its pair–wise localizability marked by the percent localization of the electrons in its bonding loges, also sits close to point where interpair and intrapair correlation energies contribute equally to the total correlation energy. The intrapair correlation energy constitutes 56% of the total electron correlation energy of methane. Whereas in the systems LiH, BeH_2, and BH_3 (which can be partitioned into loges with > 70% localization) the intrapair correlation energy accounts for 90%, 86% and 77% of the total correlation energy, repectively (Ebbing and Henderson 1965, Kutzelnigg 1973). In the majority of systems studied that would not be described as ionic, where localization is self–evident, the intrapair correlation is outweighed by the interpair correlation (Davidson 1972, Sinanoğlu and Skutnik 1968, Kutzelnigg 1973).

CALCULATIONS OF FERMI AND COULOMB HOLES IN ATOMS AND MOLECULES

Correlation holes are six–dimensional functions, they therefore require enormous amounts of computer time to explore in their entirety. There is an abundance of research directed at the generation and analysis of localized orbitals, yet the explicit details of the physical mechanism which is solely responsible for the localization of electrons has received a pittance of attention, relatively. Maslen (1956) and Sperber (1971) have reported some numerical calculations of Fermi holes in atoms. Maslen (1956) first pointed out that the Fermi hole is equivalent to Slater's exchange charge density that corrects for the self–pairing of electrons with parallel spin in the exchange repulsion term of the Hartree–Fock operator (Slater 1951, 1960). The Coulomb and Fermi holes of atoms have also been described in terms of the effect that electron correlation has on the distribution function of the interelectronic distance r_{12} (Benesch and Smith 1971, Boyd and Coulson 1973, 1974). Couper and Pounder (1980) have tabulated various numerical quantities associated with correlation holes. Only recently have plots of a Fermi hole density appeared in the literature (Luken and Beratan 1982, Luken 1982). Luken (1984) has noted that the shape of the Fermi hole for positions of the reference electron in the bonding region of a molecule resembles that of a localized bonding orbital. He proposes that the form of the Fermi hole be used as an alternate criterion for the definition of localized orbitals. As mentioned before the question of whether or not orbitals are localized is not germane to the description of the spatial properties of the charge or pair densities. Later in this thesis, the role that the form of the Fermi hole does play in relation to the physical basis for electron pair models will be discussed.

SUMMARY OF PAST RESEARCH INTO THE QUANTUM EXPRESSION OF LEWIS' MODEL

All of the work summarized so far in this chapter unanimously support the conclusion that, in general, the physics of a many–electron system is not dominated by the behaviour and properties of individual electron pairs. Earlier, two questions were generated in response to the above conclusion. The first question dealt with the *extent* and *mechanism* of electron pairing. The extent of electron pairing is effectively measured by the pair populations of loges (Bader and Stephens 1975). Although far from an exhaustive survey has been done on this property, it is found that as the molecule incorporates heavier elements and more electrons there is a strong trend to larger pair populations of the loges. The mechanism of electron pairing has been identified as the correlation of the motions of electrons of parallel spin, Fermi correlation in Hartree–Fock theory. This mechanism, however, has not yet received detailed study owing to the difficulty of studying a six–dimensional function. Later in this thesis a detailed investigation of the operation of this mechanism will be presented.

The second question that was generated by the conclusion above, "What do we base the success of the Lewis model on?", is an obligatory one. The electron pair model initiated by Lewis is probably the most widely used and certainly the most widely taught chemical concept born in this century. It is an integral part of the foundations of chemistry, it can not simply be taken away. Theoretical chemists are charged with the *onus probandi* of presenting a physical theory which can rationalize the observed valencies, geometries and reactivities of molecules as well or better than the Lewis model and other electron–pair based models. The remainder of this thesis is devoted to this responsibility. It will be proposed that the topological and energetic properties of the Laplacian of the electronic charge distribution provide the physical basis of the above models. This function assimilates many of the properties that are

ascribed to electron pairs. As such, it provides a foundation for the future construction of a predictive and physical theory of valency, geometry and reactivity that can assume the place of electron pair models of chemistry with minimal adjustment to the corresponding language and concepts of chemistry.

2.2 PROPERTIES OF THE LAPLACIAN OF THE ELECTRONIC CHARGE DISTRIBUTION

The Laplacian of a scalar function, such as the electronic charge distribution $\rho(r)$, measures its "lumpiness" (Morse and Feshbach 1953). For a one–dimensional function the Laplacian is simply the second derivative, or curvature of that function. An arbitrary function, f(x), is depicted in figure 2.2 along with its first derivative, $f'(x)$, and the negative of its second derivative, $-f''(x)$. The function was chosen so as to mimic the coarse features of the radial behaviour of the total charge density of a heavy atom, i.e. the function decreases monotonically away from the nucleus but can exhibit a shoulder in the valence region. For all values of x it can be seen that $f'(x) < 0$, indicating the lack of any maxima in the function other than the maximum at the origin. Between the points labelled x_1 and x_2 in figure 2.2 the second derivative changes sign, and there is an intervening inflection point. The sign of the second derivative of a function indicates whether the function is locally depleted there ($f''(x) > 0$) or locally concentrated there ($f''(x) < 0$). For a function to be locally concentrated at a point x, it is not necessary that f(x) be greater than $f(x + dx)$ and $f(x - dx)$, that implies a local maximum in the function. The term "locally concentrated" indicates that the value of f(x) is greater than the average of the values of $f(x + dx)$ and $f(x - dx)$. Conversely, the term "locally depleted" indicates that the value of the function at x is less than the average of the values of the function at neighbouring points. The point x_2 in figure 2.2 marks a local maximum in the extent that f(x) is locally concentrated, although it is not a maximum it represents the point

Figure 2.2

An arbitrary function, f(x), is expressed at the top of the figure. The function itself is plotted in the top figure, its gradient is plotted in the middle figure, and the negative of its second derivative is plotted in the lower figure. At the point x_1 the function is locally depleted, its gradient is increasing rapidly. At the point x_2 the function is maximally concentrated, its gradient is decreasing at the fastest rate. The constantly negative first derivative (middle figure) illustrates that, like all atomic charge distributions, this is a monotonically decreasing function.

$f(x) = 8\exp(-7x) + \exp(-10(x-0.5)^{**}2)$

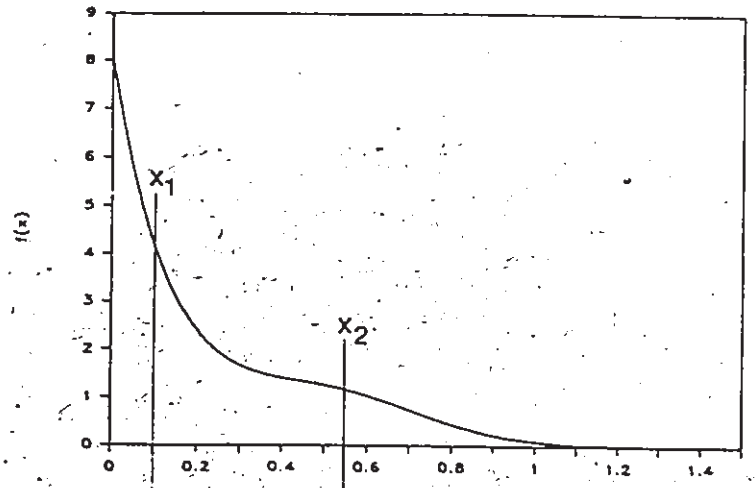

First derivative

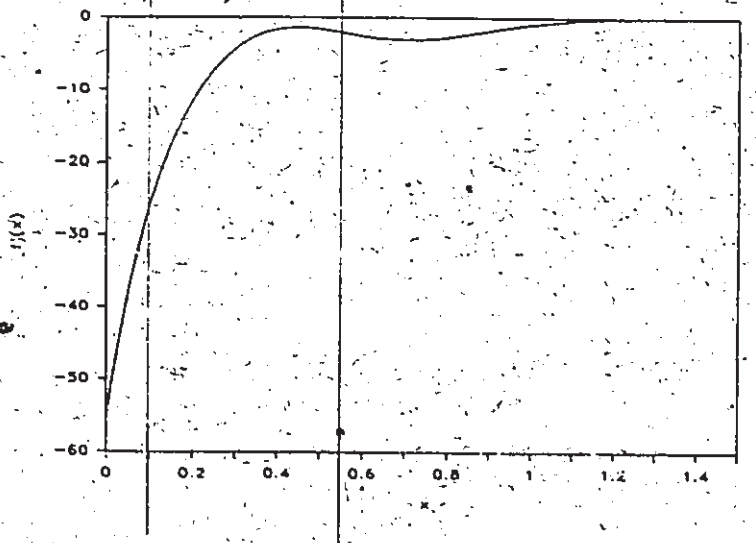

Second derivative

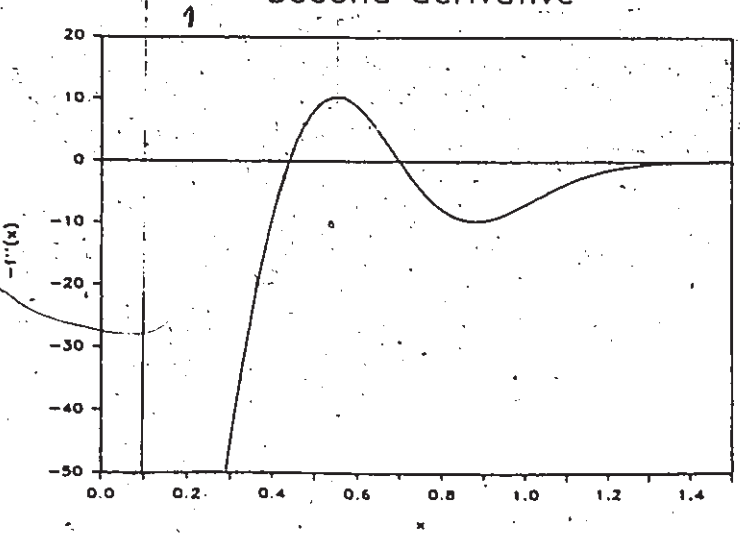

of the shoulder where the slope is changing most rapidly. Equation 2.19a defines the second derivative of a one–dimensional function in terms of the limiting differences of the slope at points bracketing the point x.

(2.19a) $$f''(x) = \{\{[f(x + \Delta x) - f(x)]/\Delta x - [f(x) - f(x-\Delta x)]/\Delta x\}/\Delta x\}_{\Delta x \to 0}$$

The Laplacian of a three–dimensional scalar function, such as $\rho(r)$, maps out regions in which the function is locally concentrated ($\nabla^2\rho(r) < 0$) and regions in which the function is locally depleted ($\nabla^2\rho(r) > 0$). Maxwell (1954) coined the term locally concentrated to indicate that the value of a function at r, in this case $\rho(r)$, is greater than $\bar{\rho}(r)$ which is the average value of ρ on the surface of an infinitesimal sphere centered at r with radius τ (equation 2.19b). The opposite applies to regions of local depletion. The Laplacian can also be expressed in terms of the local curvatures in the charge density (equation 1.4), in this context the Laplacian is the trace of the Hessian (equation 2.19c). For an isolated system or an atom in a molecule defined by surfaces of zero–flux in $\nabla\rho$, the integral of the Laplacian over these spaces is zero (equation 1.6).

(2.19b) $$\nabla^2\rho(r) = 10\{\rho(r) - \bar{\rho}(r)/\tau^2\}$$

(2.19c) $$\nabla^2\rho(r) = \mathrm{Tr}\{H(r)\}$$

ENERGY RELATED PROPERTIES OF THE LAPLACIAN

The function $L = -(\hbar^2/4m)\nabla^2\rho(r)$ is an energy density, it has the units energy/volume. It is the Lagrangian density of a many–particle quantum mechanical system (equation 1.9) that satisfies Schrödinger's time-dependent equations (equation 1.8) (Bader and Nguyen–Dang 1981). The total energy of a one–electron atomic system is proportional to the integrated magnitude of the Laplacian. Since the amount of local charge concentration must be exactly balanced by the amount of local charge depletion, equation 2.20 relates the overall curvature or lumpiness of the charge density to the total energy of a one–electron atom. There exists an approximate

relationship between the integrated magnitude of the Laplacian and the Hartree–Fock energy of first–row atoms (Bader and Essén 1984).

(2.20) $$-\frac{1}{4}\int_{\nabla^2\rho<0} \nabla^2\rho(\mathbf{r})d\tau = -\frac{1}{4}\int_{\nabla^2\rho>0} \nabla^2\rho(\mathbf{r})d\tau = (4e^{-2})E(Z)$$

Equation 1.3 noted the appearance of the energy density L(r) as a local measure of the difference between the Schrödinger–style kinetic energy density K(r) (equation 1.2a) and the positive definite kinetic energy density G(r) (equation 1.2b).

For a molecule in a stationary state, i.e. there are no external forces acting on the system and the molecule itself is in an equilibrium geometry, the total potential energy of the system is equal to the all–space integral of a local single–particle potential energy density that is completely determined by the near–diagonal elements of the spinless first–order density matrix $\Gamma^{(1)}(\mathbf{x},\mathbf{x}')$ (Bader 1980). This potential energy density, a scalar quantity denoted as $V(\mathbf{r})$ in equation 2.21, is the virial of the quantum force density $\mathbf{F}(\mathbf{r})$. The quantum force is a vector quantity that is in turn determined (equation 2.22) by the divergence of the quantum stress tensor, $\overleftrightarrow{\sigma}(\mathbf{r})$.

(2.21) $$V(\mathbf{r}) = -\mathbf{r}\cdot\nabla\cdot\overleftrightarrow{\sigma}(\mathbf{r}) + \nabla\cdot\{\mathbf{r}\cdot\overleftrightarrow{\sigma}(\mathbf{r})\}$$

(2.22) $$\mathbf{F}(\mathbf{r}) = -\nabla\cdot\overleftrightarrow{\sigma}(\mathbf{r})$$

Introduced into quantum mechanics by Pauli (1958), the stress tensor is fundamental in classical continuum mechanics, particularly in theorems of elasticity and stress–strain relationships (Malvern 1969). Bader (1980) has derived an expression of the quantum mechanical stress tensor for a many–electron system in terms of the gradients of the state function (only the gradients in the vicinity of the diagonal of the first–order density matrix are required) and the curvatures of the charge density (equation 2.23).

(2.23) $$\overleftrightarrow{\sigma}(\mathbf{r}) = -(\hbar^2/m)\{\nabla\nabla'\Gamma^{(1)}(\mathbf{r},\mathbf{r}')|_{\mathbf{r}=\mathbf{r}'}\} + (\hbar^2/4m)\nabla\nabla\rho(\mathbf{r})$$

The stress tensor is a 3 X 3 matrix that determines the pressures exerted on the surface elements of an infinitesimal volume element centered on r. The local pressure P(r) in equation 2.24 is the average force per unit area exerted on the infinitesimal volume

element centered at r (Bader 1980). Only positive pressures or compression of the volume element have thus far been observed (Bader and Essén 1984). The diagonal components correspond to "normal" compression while the off–diagonal components represent shear pressures (Arfken 1985). The stress tensor can be diagonalized such that in the principal axis system the shear pressures vanish.

(2.24) $$P(r) = -Tr\{\overleftrightarrow{\sigma}(r)\}/3$$

The second term on the right hand side of equation 2.23 contains the full Hessian matrix at r. This term can also be interpreted as a pressure tensor, although it can be either positive or negative. It represents how compressed or expanded the charge density is relative to a uniform distribution where the curvatures are zero everywhere. The integral over all space of this local pressure is zero when the general form of the virial theorem is obeyed (equation 2.26). Taking the trace of equation 2.23 gives the local expression of the virial theorem, equation 2.25a (Bader 1980, Bader and Nguyen–Dang 1981).

(2.25a) $$V(r) = Tr\{\overleftrightarrow{\sigma}(r)\} = -2G(r) + (\hbar^2/4m)\nabla^2\rho(r)$$

(2.25b) $$-P(r)/3 = -2G(r) + (\hbar^2/4m)\nabla^2\rho(r)$$

Equation (2.25b) relates the total pressure exerted on an element of charge to the local concentration or compression of that element of charge. The mediating term, the kinetic energy G(r), is always positive. Hence one could think of equation 2.25b as a comparison of the applied pressure P, and a residual pressure $\nabla^2\rho$. These pressures are related by the charge mobility, G(r), or in effect its ability to dissipate the applied pressure. The integration of equation 2.25a over the total system or a quantum subsystem, Ω, yields the usual statement of the virial theorem, equation 2.26.

(2.26) $$V(\Omega) = -2T(\Omega)$$

Alternatively, one can interpret equation 2.25a in terms of local imbalances in the ratio of the potential energy density $V(r)$ to the kinetic energy density G(r), relative to their overall or subspace average ratio of –2 to 1. In regions where charge is

locally concentrated, $\nabla^2\rho(r) < 0$, the potential energy density $V(r)$ makes a proportionately larger contribution to the total energy. Whereas in regions of local charge depletion, $\nabla^2\rho(r) > 0$, $V(r)$ makes a proportionately smaller contribution to the overall stability of the system (Bader and Essén 1984, Bader, MacDougall and Lau 1984, Bader and MacDougall 1985). In this interpretation one assumes a particular expression for the local energy density E(r), which is identically equal to K(r) defined earlier in equation 1.2a. The expression for the local energy density implied in the above interpretation is given in equation 2.27.

(2.27) $\quad E(r) = V(r) + G(r)$

SHELL STRUCTURE IN ATOMS

The total charge density of an atom in its ground state exhibits a maximum at the position of the nucleus and decays monotonically to infinity (Weinstein *et al.* 1975). Figure 2.3 illustrates $\rho(r)$ for a plane containing the nucleus of an argon atom in its ground state (Bader and Essén 1984). The plane shown is the yz plane, however $\rho(r)$ appears the same in any plane containing the nucleus because of its spherical symmetry. The density is cut off at an arbitrarily low value to emphasize that even in the valence region the density only exhibits a shoulder. In figure 2.3 the negative of the Laplacian of the argon atom is plotted as a positive elevation in order to focus attention on the local concentrations of electronic charge. A shell of local charge concentration followed by a shell of local charge depletion is observed for the three principal quantum shells of the argon atom. The innermost shell of charge concentration rises exponentially near the nucleus. The Laplacian is depicted for values ranging $-2.0 \geq \nabla^2\rho(r) \leq 2.0$ au for the purpose of emphasizing details in the valence region. The presence of alternating shells of charge concentration and charge depletion is a result of the radial curvature (usually positive) and the sum of the tangential curvatures (always negative) competing in the determination of the sign of

Figure 2.3

The charge density (top) and Laplacian distribution (bottom) of the argon atom, shown for a plane containing the nucleus. The charge density is cut off at an arbitrary value. The Laplacian is cut off at a value of ±2.0 au (1 au = 1 e/a_o^5). In this and all subsequent relief maps of the Laplacian, the function plotted is $-\nabla^2\rho$. This is so that maxima in charge concentration are seen as peaks in the relief maps.

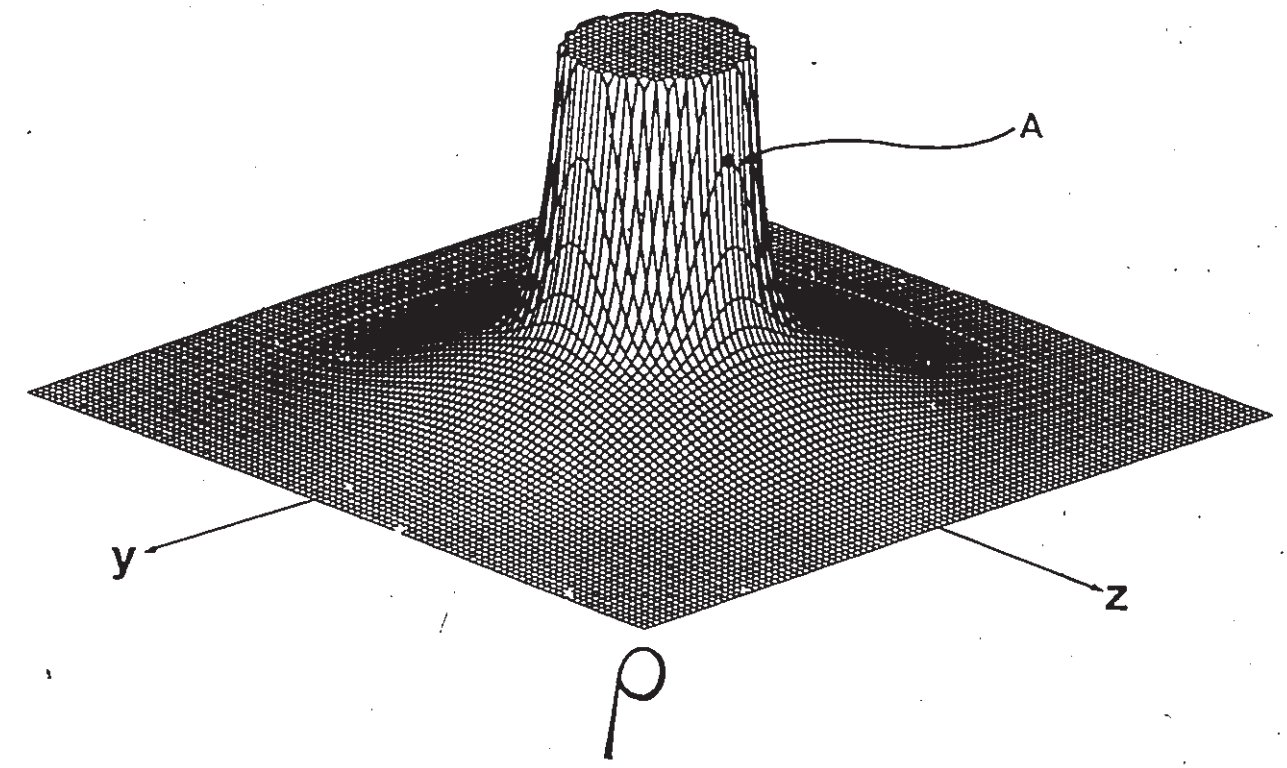

ρ

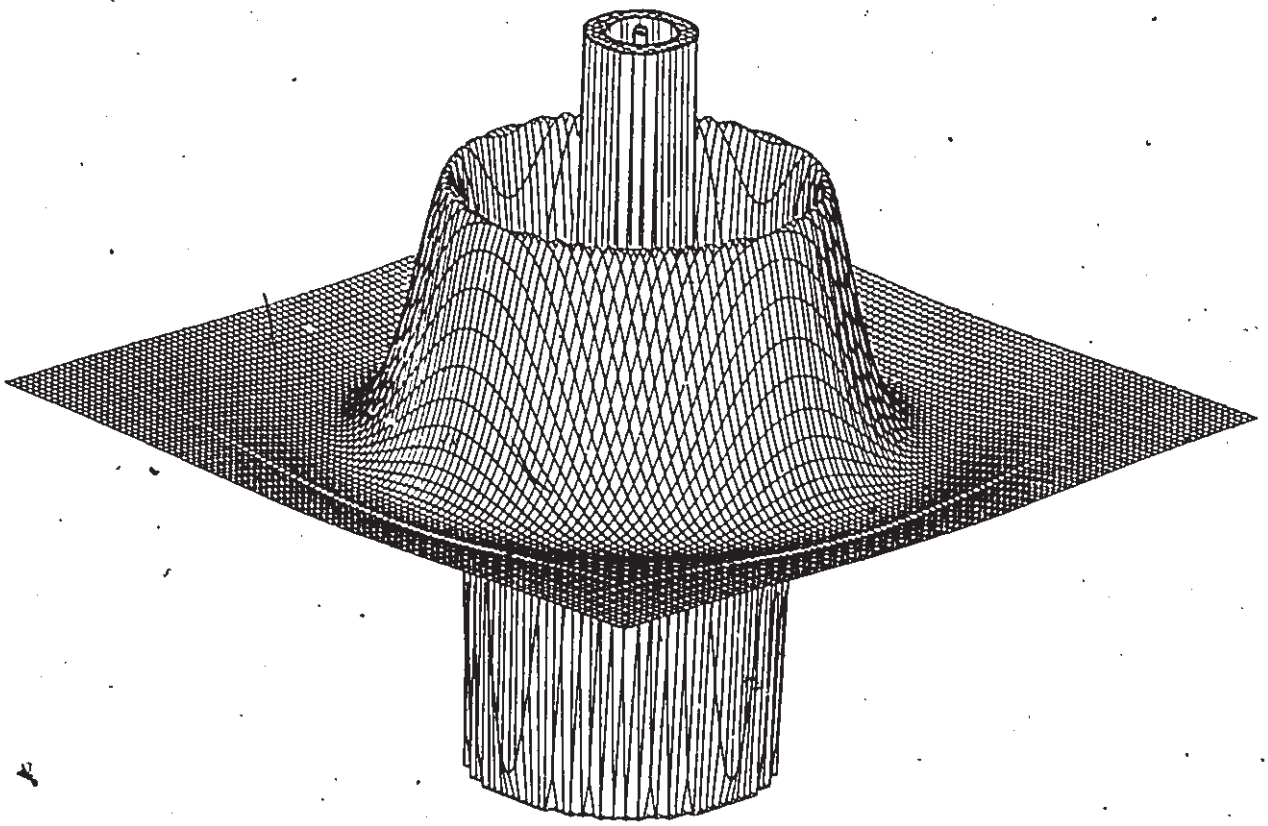

$-\nabla^2\rho$

$Tr\{H(r)\}$. At point a in figure 2.3 $\partial^2\rho/\partial z^2 < 0$, while $\partial^2\rho/\partial x^2 = \partial^2\rho/\partial y^2 > 0$. At this particular point the sum of the magnitudes of the tangential curvatures is greater than the radial curvature and the charge density is locally depleted. If the Laplace operator ∇^2 is expressed in spherical polar coordinates as opposed to the usual cartesian coordinate system, then the Laplacian for a spherically symmetric atom such as argon is given by equation 2.28 (Sagar *et. al.* 1988).

(2.28) $$\nabla^2\rho(r) = \partial^2\rho(r)/\partial r^2 + (2/r)\partial\rho(r)/\partial r$$

In this coordinate system the sign of the Laplacian is determined by the competition between the radial curvature (usually positive) and the radial slope (always negative for a monotonically decreasing atomic density). The value of the Laplacian is independent of the choice of coordinate system.

Studies of the shell structure of the Laplacian in atoms and singly–charged ions up to $Z = 92$ indicate that: 1) The maximum value of $-\nabla^2\rho(r)$ in each shell of charge concentration decreases with each succeeding shell. 2) The maximum extent of local concentration of the n'th shell increases with increasing nuclear charge. 3) The radius of the n'th shell decreases with increasing nuclear charge. 4) The outer quantum shells in atoms beyond krypton in the periodic table often do not possess a corresponding shell of local charge concentration, particularly if they occur early in a period. 5) The maximum number of shells of charge concentration is found to be five, only atoms with $Z > 80$ exhibit five shells (Sagar *et al.* 1988). Table 2.4 tabulates the radii and values of $-\nabla^2\rho(r)$ for the $n \geq 2$ shells of charge concentration for Li – Kr. Figure 2.4 illustrates the profile of $-\nabla^2\rho(r)$ for the krypton atom, the shells of charge concentration and charge depletion corresponding to the K, L, M and N quantum shells are all accounted for.

The radial distribution function for spherically averaged atomic charge densities, the quantity $D(r)$ in equation 2.29, also exhibits a shell structure.

(2.29) $$D(r) = 4\pi r^2\rho(r)$$

Table 2.4.[a]

2.4.1. Radii r_n of Spheres of Maximum Charge Concentration for Quantum Shells $n > 2$.

n	Li	Be	B	C	N	O	F	Ne
2	2.49	1.59	1.19	0.94	0.78	0.66	0.57	0.50
	Na	Mg	Al	Si	P	S	Cl	Ar
2	0.44	0.40	0.36	0.33	0.30	0.28	0.26	0.24
3	3.44	2.55	2.08	1.76	1.52	1.34	1.20	1.08
	K	Ca	Ga	Ge	As	Se	Br	Kr
2	0.23	0.21	0.13	0.12	0.12	0.12	0.11	0.11
3	0.98	0.90	0.49	0.47	0.45	0.43	0.41	0.39
4	4.94	3.77			2.18	1.83	1.65	1.50

2.4.2. Values of $-\nabla^2\rho$ at r_n Values above.

n	Li	Be	B	C	N	O	F	Ne
2	0.002	0.027	0.141	0.506	1.447	3.480	7.592	15.29
	Na	Mg	Al	Si	P	S	Cl	Ar
2	29.99	55.61	96.15	157.4	247.4	375.3	553.3	794.7
3	0.0002	0.002	0.009	0.038	0.115	0.273	0.592	1.196
	K	Ca	Ga	Ge	As	Se	Br	Kr
2	1115.	1544.	18494	22126	26303	31124	36615	42961
3	2.219	3.818	109.0	140.2	179.7	226.9	288.3	361.4
4	-3.1E-5	-1.2E-4			-0.026	-0.025	-0.010	0.052

[a]Unpublished results from V.H. Smith, Jr., see Sager *et al.* (1988) for details of calculation and discussion of results. Radii and values of $-\nabla^2\rho$ are in atomic units,
one au of length = a_o = 0.52918 Å. Units of Laplacian are e/a_o^5 = 24.100 $e/Å^5$.

Figure 2.4

The radial profile of the Laplacian is shown for the krypton atom, derived from a STO–3G RHF calculation. The Laplacian is cut off at ±1.0 au for the first three shells of charge concentration and charge depletion.

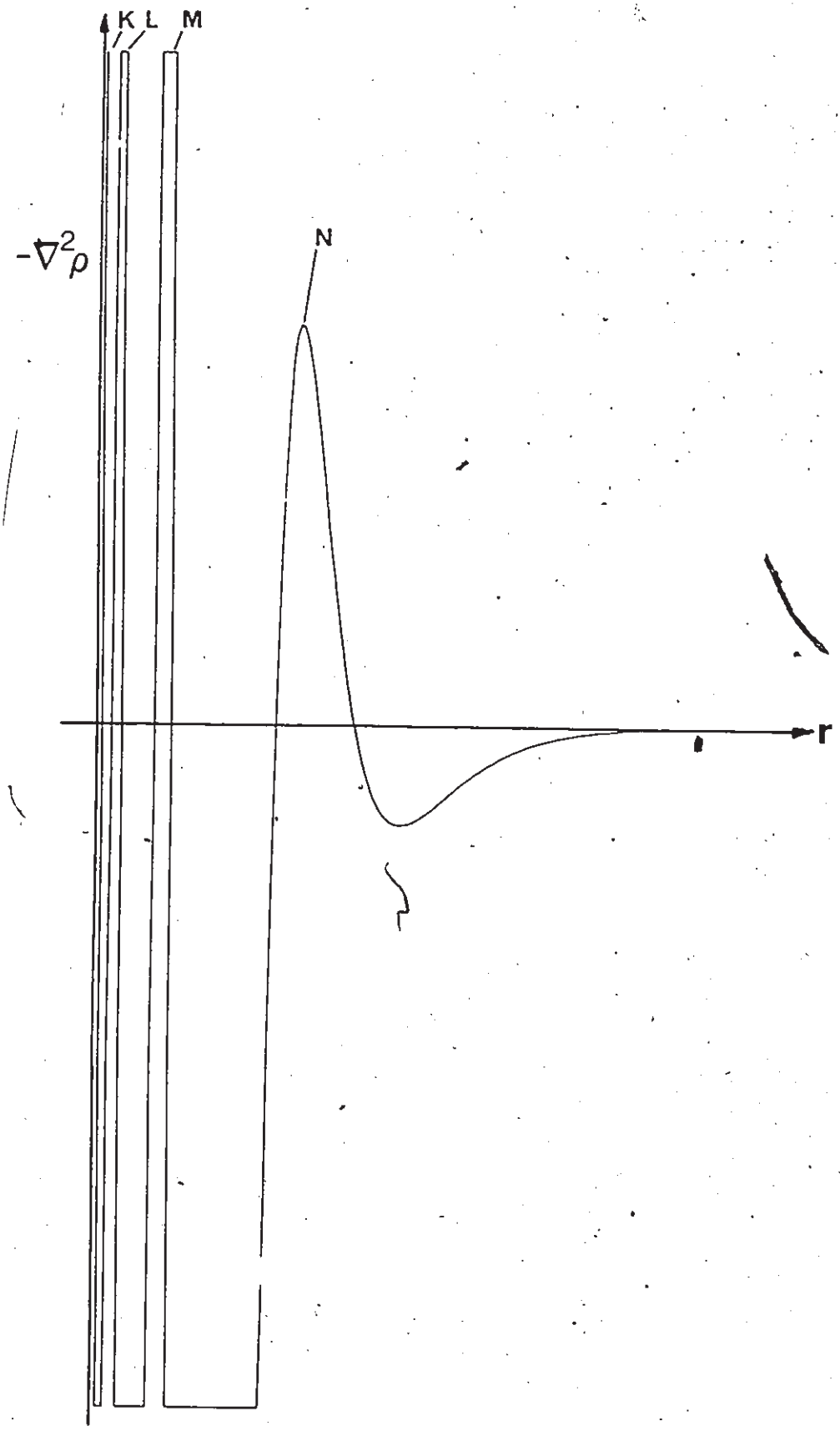
K
L
M
N
$-\nabla^2\rho$
r

The radial distribution function is a one–dimensional function that does not suggest the presence of shells of greater concentration of electrons in real space. The maxima in the radial distribution function for the first 92 atoms of the periodic table have been compared to the description of the shell structure of an atom in terms of the Laplacian (Sagar *et al.* 1988). The shell structure of $-\nabla^2\rho(\mathbf{r})$ for an atom persists when the atom is in chemical combination, while $D(\mathbf{r})$ is inapplicable in the molecular case.

2.3 THE VALENCE SHELL CHARGE CONCENTRATION OF ATOMS IN MOLECULES

The outermost shell of charge concentration of an isolated atom is termed the valence shell charge concentration (VSCC). An atom in a molecule generally possesses the same number of shells of charge concentration as it does in isolation. Exceptions to this are found in ionic molecules where one atom has lost most of its valence electrons to its bonding partner(s). In these cases the VSCC of the electropositive element is eliminated upon molecule formation. For instance the isolated Li atom has two shells of charge concentration, one at the nucleus and a very diffuse VSCC with its maxima in $-\nabla^2\rho$ at 1.320 Å. The Li fragment in LiH possesses only a single core–like shell of charge concentration at the Li nucleus, while the single region of charge concentration of the hydride fragment has been expanded relative to its radius of 1.0 au in an isolated H atom (Bader and Essén 1984).

In the general case where the VSCC of each atom persists after molecule formation, the VSCC's are no longer of uniform concentration and local maxima and minima are created in the VSCC of each atom. The quantitative description of these changes requires a study of the topology of the Laplacian distribution.

TOPOLOGICAL ANALYSIS OF THE VSCC

The Laplacian is a scalar field just like the charge density, therefore its topological features are identified and characterized by its gradient vector field, $\nabla\{\nabla^2\rho(r)\}$. Extrema in the Laplacian are classified by rank and signature in the same way as are critical points in the charge density. So that we can refer to maxima in local concentration as (3,–3) critical points we will study the topology of the function $-\nabla^2\rho(r)$. Critical points in the Laplacian are points where $\nabla\{-\nabla^2\rho(r)\} = 0$, the rank and signature of the critical point are determined by the eigenvalues of the Hessian matrix $\nabla\nabla\{-\nabla^2\rho(r)\}$. The VSCC of an isolated atom contains a spherical surface over which the charge density is maximally concentrated, each point on this surface is a degenerate (1,–1) critical point in $-\nabla^2\rho$. There is only one non–zero curvature, the radially directed one, and it is negative since the value of $-\nabla^2\rho$ is a maximum at the intersection of the critical point surface and any radial vector.

The distortion of the VSCC that accompanies the formation of chemical bonds is illustrated in the comparison of figures 2.3 and 2.5. The symmetry of the VSCC of a neutral argon atom (figure 2.3) is lowered from spherical symmetry to axial symmetry (figure 2.5) upon formation of the diatomic cation ArF^+ (MacDougall *et al.* 1989). Keeping in mind that the radial eigenvalue of any critical point in the VSCC is negative, the topological features of the resulting VSCC of the argon atom consist of: 1) A (3,–3) critical point along the Ar–F bond path (point b in figure 2.5), such a local concentration of charge will be refered to as a bonded charge concentration. 2) A torus of degenerate (2,–2) critical points encircling the extended Ar–F internuclear axis in the nonbonded region of the molecule (points n in figure 2.5), such a charge concentration, including those associated with nondegenerate critical points, will be called a nonbonded charge concentration. 3) A (3,+1) critical point opposite to the bonded charge concentration (point h in figure 2.5), when the Laplacian is positive at such a ring critical point it will be refered to as a hole in the VSCC. 4) A torus of

Figure 2.5

Relief maps of the Laplacian distribution for ArF^+, derived from a 4–31G* RHF calculation. Both figures display the Laplacian in a plane containing the Ar–F internuclear axis. The lower figure depicts the Laplacian from the opposite perspective as the top figure. The labels indicate the following: n = nonbonded torus, b = bonded maximum, s = saddle point and h = hole or point of maximum charge depletion in the VSCC.

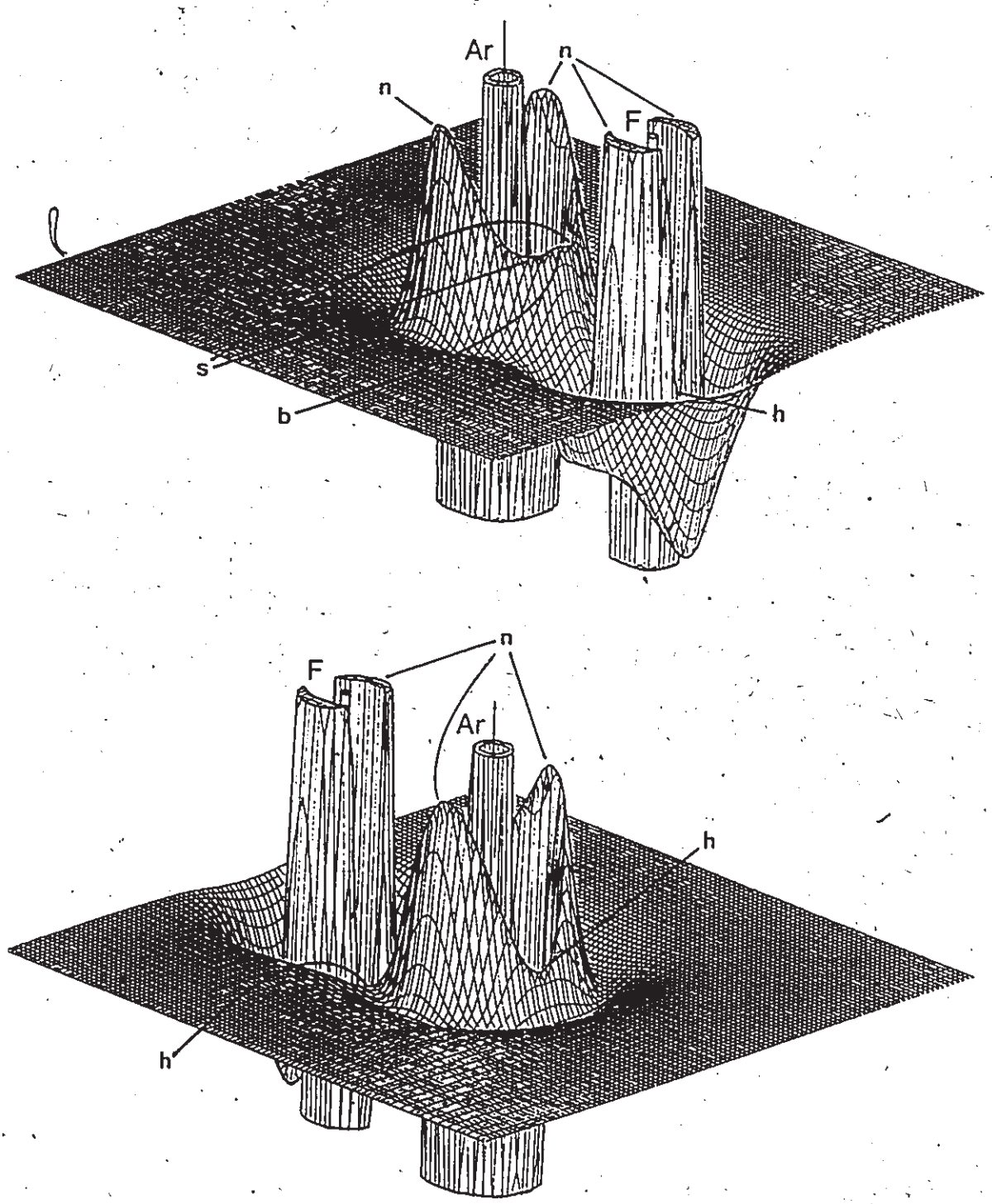
Ar
n
n
F
s
b
h
n
F
Ar
h
h

degenerate (2,0) critical points encircles the Ar–F bond path (points s in figure 2.5), the eigenvectors with the positive eigenvalue at each (2,0) critical point define an infinite set of pairs of gradient paths in $-\nabla^2\rho$ that link the bonded and nonbonded charge concentrations.

We have seen how the Laplacian extracts shell structure from the monotonically decaying charge density of an isolated atom (figure 2.3). We then examined the topological features created in the VSCC of an atom as a result of molecule formation (figure 2.5). Figure 2.6 illustrates the extraction of shell structure from the total density of a molecule (water in this case). The spatial characteristics of the topological features of the VSCC are further illustrated by this figure as well. The oxygen atom in H_2O possesses two shells of charge concentration, while each hydrogen atom has just one. The top–left plot in figure 2.6 depicts the total density in the symmetry plane containing the oxygen nucleus and orthogonal to the plane containing all three nuclei. The form of the charge density offers no suggestion of a build up of charge in the nonbonding region of the oxygen atom due to the surmised existence of nonbonding electrons or lone–pairs. The Laplacian, however, does indicate that within the VSCC of the oxygen atom there are two equivalent maxima in local charge concentration in the nonbonding region symmetrically positioned above and below the plane containing all three nuclei. The two (3,–3) critical points associated with these nonbonded charge concentrations, labelled n, are 0.335 Å from the oxygen nucleus and form an angle between them of 138.3° subtended at the oxygen nucleus. This type of geometrical characterization of the topological features of a VSCC will be discussed in detail in a later section. The Laplacian is a maximum at the positions of these critical points in any plane shown that contains them. There is a (3,–1) critical point hidden from view, labelled s, between the two nonbonded charge concentrations and behind the oxygen atom relative to the O–H bond axes. The last topological feature of the VSCC in this plane is the one labelled r. It appears to have the same topological properties of the

Figure 2.6

Relief maps of the total charge density and the Laplacian for the water molecule, derived from a 6–31G** RHF calculation. The plane shown in the top pair of figures is the symmetry plane perpendicular to the plane containing all three nuclei. In this plane the charge density exhibits a single peak at the position of the oxygen nucleus, while the Laplacian exhibits two shells of charge concentration. The VSCC contains two maxima in this plane, one above and one below the plane defined by the nuclei. In this plane there are also two points in the VSCC of oxygen at which the Laplacian appears as a saddle, they are labelled r and s (hidden). The lower pair of figures correspond to the charge density and the Laplacian in the plane of the nuclei. The charge density exhibits a peak at each nucleus. The Laplacian exhibits a peak at each nucleus, but in addition there is a peak labelled b corresponding to a bonded maximum along each bond. The saddles labelled r and s in the top–right appear as a minimum and a maximum in this plane, respectively.

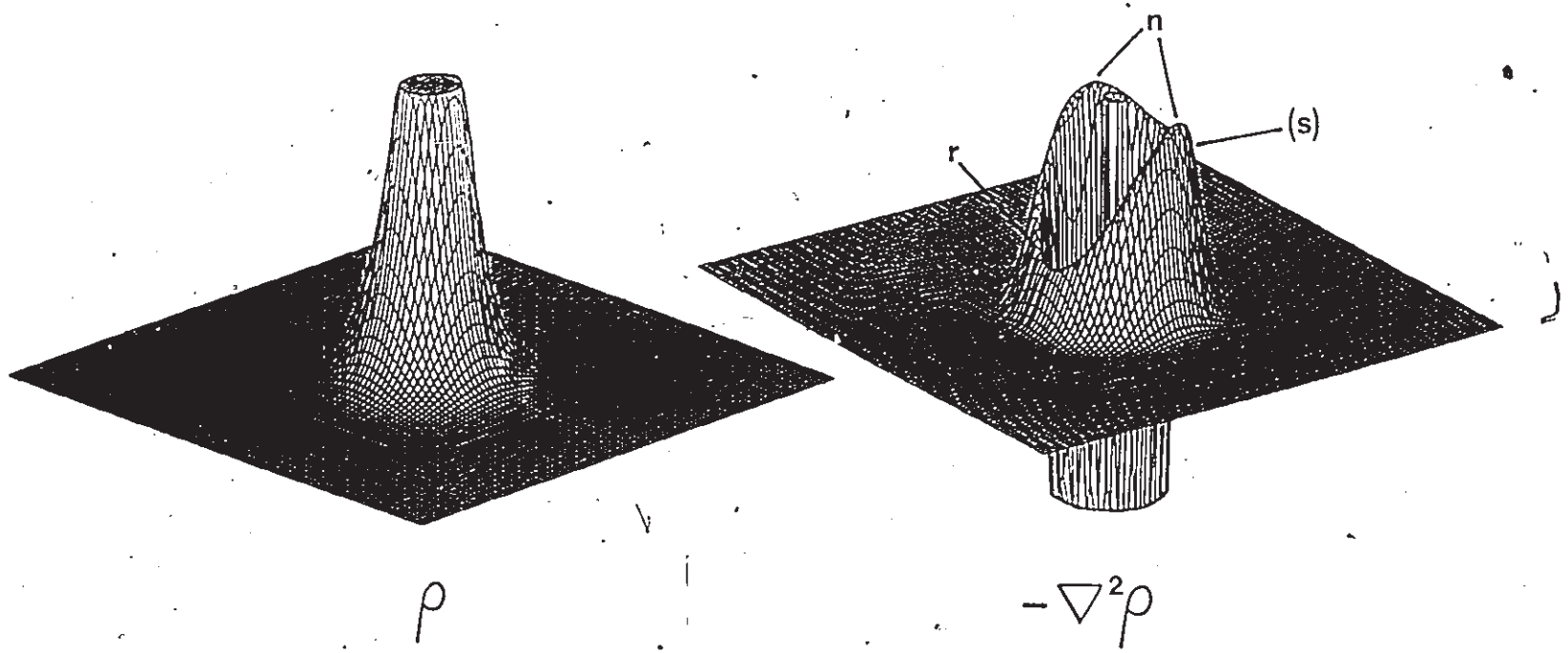

ρ $\quad -\nabla^2\rho$

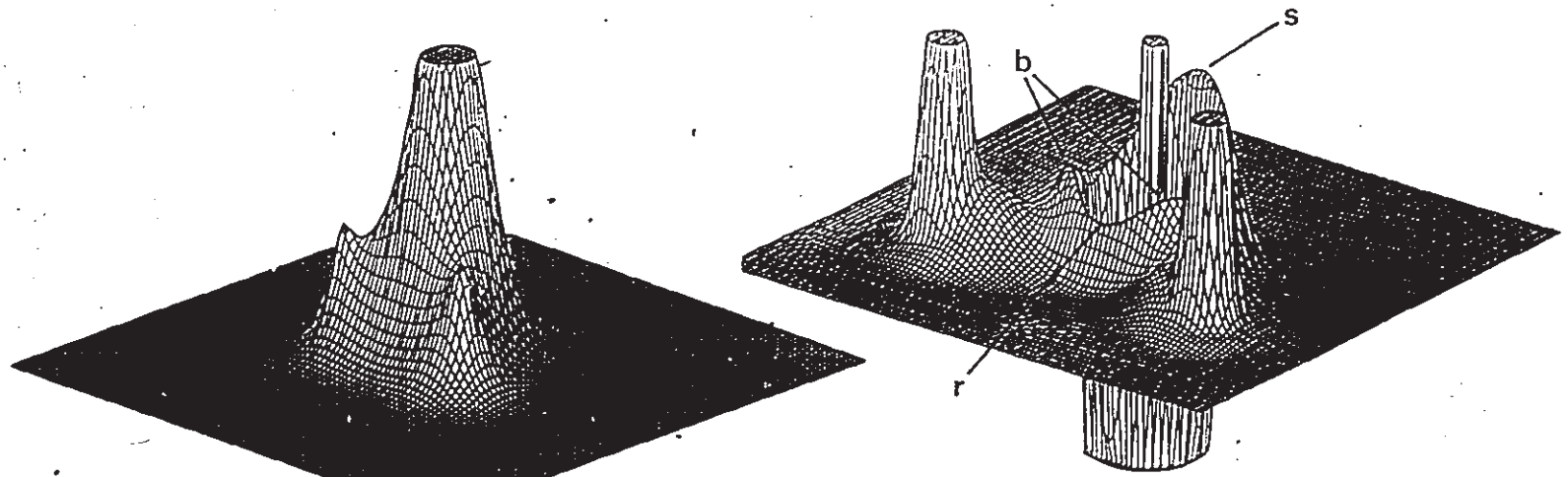

the (3,–1) or saddle critical point, however an infinitesimal displacement from these points perpendicular to the plane shown leads to a decrease in charge concentration for point s and an increase in charge concentration for point r. The lower pair of plots in figure 2.6 illustrates the two functions of interest in the plane containing all three nuclei. The charge density does exhibit a maximum for each nucleus and a bond path between the oxygen atom and each of the hydrogen atoms. In this figure the bond path is seen as a ridge joining the peaks at the oxygen and hydrogen nuclei. The internuclear ridges can be assigned with certainty to a particular bond, but the charge density does not indicate any kind of separability between the valence bonding density and the core density. The Laplacian does separate the valence region from the core region by the formation of a shell structure. It also reflects the existence of two O–H bonds by exhibiting two maxima in charge concentration, labelled b. The (3,–3) critical points associated with these bonded charge concentrations are 0.374 Å from the oxygen nucleus and approximately on the O–H bond paths defined by $\rho(\mathbf{r})$.

Further discussion of each of these topological features is essential to develop the concept of an atomic structure that summarizes the topology of a VSCC much like the molecular graph summarizes the topology of the total charge distribution. The number of nondegenerate critical points in the VSCC of a given atom must obey a relationship (equation 2.30) analogous to the Poincaré–Hopf relationship (equation 1.17). In equation 2.30 the following notation applies: b is the number of (3,–3) critical points associated with bonded charge concentrations, n is the number of (3,–3) critical points associated with nonbonded charge concentrations (the set of (2,–2) critical points n in figure 2.5 would coalesce into a finite number of (3,–3) critical points upon symmetry reduction), h is the number of (3,+1) critical points regardless of the value of $\nabla^2\rho$ at the critical point, s is the number of (3,–1) critical points that link maxima by a unique pair of gradient paths (the set of critical points s in figure 2.5 would coalesce to a finite number of (3,–1) critical points upon symmetry reduction).

(2.30) $\quad b + n - s + r = 2$

This relationship applies only when the VSCC is complete, *i.e.* there must be a surface that completely envelops the core of the atom, over which the value of $-\nabla^2\rho(r)$ is a maximum with respect to radial displacement. In this case all of the topological features of the Laplacian inside the VSCC can be replaced by a single (3,+3) critical point, this corresponds to c in the Poincaré–Hopf relationship being fixed at 1. The term n in the Poincaré–Hopf formula is simply broken up into two distinct types of (3,–3) critical points in equation 2.30. The terms s and r in equation 2.30 correspond to b and r in equation 1.17. The Laplacian exhibits topology beyond the VSCC, *i.e.* the minimum in figure 2.4, however equation 2.30 is invariant to details of this topology.

We can introduce the atomic graph to summarise the principal topological features of the Laplacian, in particular those in the VSCC's of a molecule's constituent atoms. We can further represent the essential topology of the Laplacian for an entire molecule as a set of connected atomic graphs. The atomic graph is analogous to the molecular graph in that only the connectivity of the maxima is shown, the positions of ring and cage critical points are omitted for clarity. Originating from each (3,–1) critical point in a VSCC is a pair of gradient paths which terminate at (3,–3) critical points within that same VSCC. The union of these paths links the maxima associated with two charge concentrations that share a surface, *i.e.* the portions of the VSCC associated with these maxima touch at more than a point. So that later we can relate the charge concentrations in the VSCC of a given atom to the valence shell electron pairs postulated by Lewis and assumed in the VSEPR model, we can refer to these pairs of gradient paths as lines of maximum charge concentration. The atomic graphs for the carbon and hydrogen atoms in methane are shown connected in figure 2.7. The atomic graph for a hydrogen atom is simply a point, since the maximum at the nucleus is the only topological feature of its VSCC. The carbon atom in methane is found to

Figure 2.7

This figure illustrates the atomic graph of the carbon atom in the methane molecule (derived from a 6–311G** RHF calculation) as well as the lines of maximum charge concentration (LOMCC) linking the hydrogen nuclei to the carbon VSCC. The large circles denote the positions of the nuclei and are labelled, they are also local maxima in charge concentration. The small solid circles denote the positions of (3,–1) saddle points in $-\nabla^2\rho$. The stars mark the positions of the bonded maxima in the VSCC of the carbon atom.

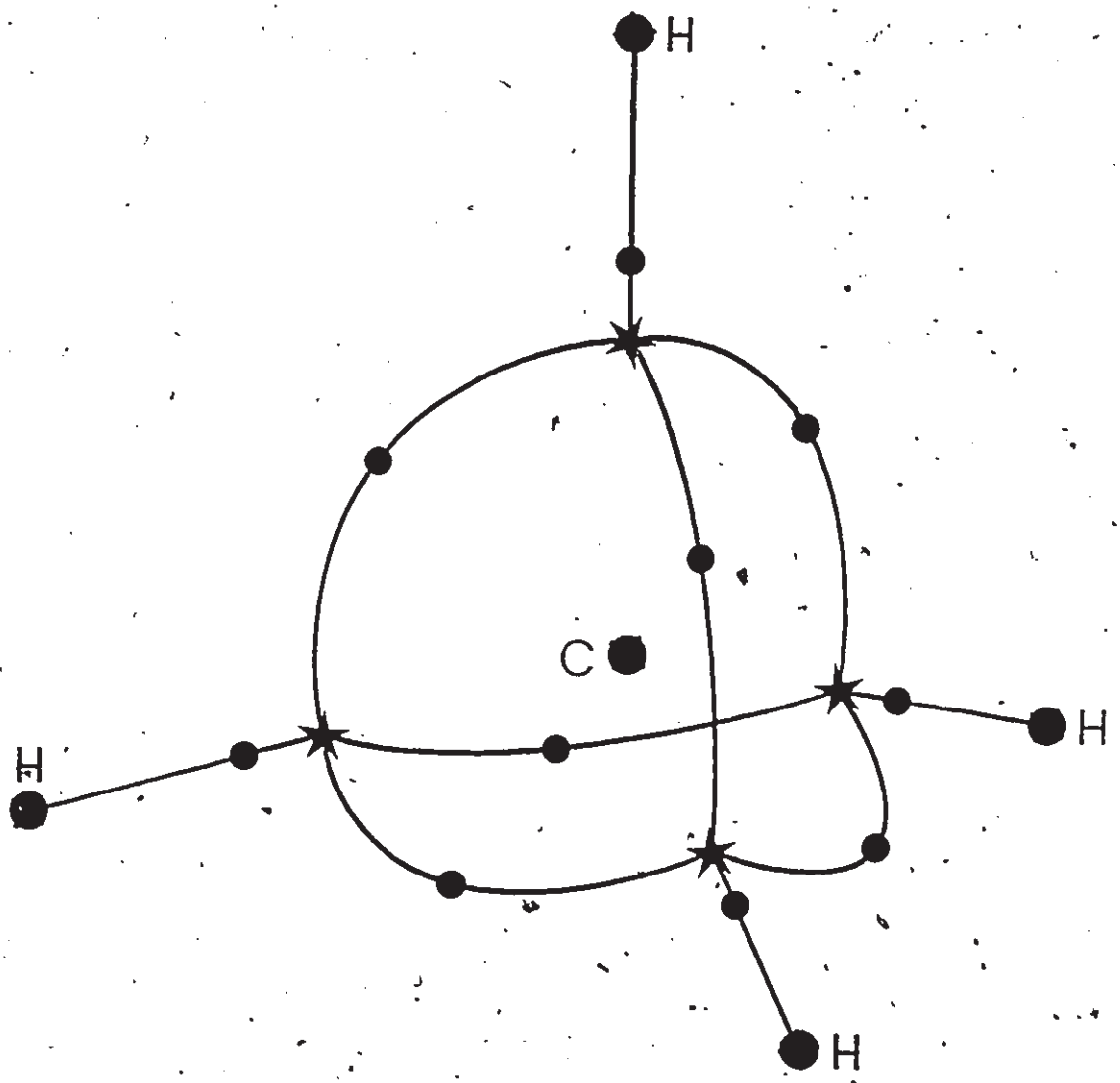
H
C
H
H
H

possess four equivalent bonded charge concentrations which necessarily are connected to one another by lines of maximum charge concentration. The VSCC of the carbon atom is connected to the trivial VSCC's of the hydrogen atoms by four equivalent interatomic lines of maximum charge concentration, or LOMCC. It should be noted that the interatomic LOMCC do not necessarily have to connect the atoms in the same way that the molecular graph does. For instance in the equilibrium geometry of the molecule $SiLi_4$, which is of C_{2v} symmetry (Schleyer and Reed 1989), there exist interatomic LOMCC linking the Li nuclei to one another while the topology of the charge density exhibits only four Si–Li bond paths. The topology of the Laplacian beyond the VSCC's of each of the atoms can exhibit complicated patterns. Because the network of interatomic LOMCC depends explicitly on these topological features we shall restrict our topological study of the Laplacian to the chemically more significant VSCC. The curved nature of the LOMCC reflects the nearly spherical nature of the VSCC.

The faces of the tetrahedron formed by the LOMCC in figure 2.6 are the ring surfaces defined by the four (3,+1) critical point opposite each of the C–H bonds. The extent of charge concentration at these ring critical points is a minimum with respect to displacement towards or away from the nucleus. While any infinitesimal lateral displacement from the radial axis passing though this point results in an increase in the extent of charge concentration. These topological features of a VSCC are analogous to those of a ring critical point in the charge distribution. The complete set of gradient paths (in $-\nabla^2\rho$) that originate at the ring critical points of a VSCC define the surface of maximum charge concentration within the VSCC. It is this surface which can be partially or entirely dissolved by extreme loss of valence charge density upon molecule formation or during a chemical reaction of a given molecule. Ring critical points locate the positions of holes in the VSCC when charge is locally depleted at the position of the ring critical point. In a following section this topological feature of the Laplacian

will be discussed in relation to a possible physical basis of the frontier orbital theory of chemical reactivity.

At least thirty studies reporting the topological properties of the VSCC's of atoms in molecules have already been accepted for publication or published in the chemistry, physics and biology literature. The author of this thesis and co–originator of the topological analysis of the Laplacian was involved in only ten of these studies. An incomplete sample of some of the investigations in which other researchers have utilized the topological analysis of the Laplacian follows. Boyd *et al.* (1984) studied the Laplacian distributions in the isoelectronic series benzene, s–triazine, borazine and boroxine. Cremer and Kraka (1984) studied the interactions between the charge concentrations of neighbouring atoms in substituted cyclopropanes. Ritchie *et al.* (1986) studied the topologies of the VSCC's of the carbon atoms in different C_4 isomers. Gatti *et al.* (1987) studied the topology of the Laplacian in clusters of Li atoms. Wiberg *et al.* (1987) studied the topologies of the VSCC's of carbon atoms in strained hydrocarbons. Carroll *et al.* (1987) predicted the structures of hydrogen–bonded complexes using the topology of the Laplacian. Koch *et al.* (1987) predicted the structures of cations containing helium with the aid of the topological analysis of the Laplacian. Bader and Chang (1989) rationalized substituent effects in electrophilic aromatic substitution reactions employing a topological analysis of the VSCC's of the carbon atoms. Carroll *et al.* (1989) have employed a topological analysis of the Laplacian in the prediction of relative reactivities of activated double bonds in Michael addition reactions.

It would not serve a useful purpose to present here in detail all of the author's results that have been obtained by analyses of the topological properties of Laplacian distributions. Instead, selected examples will be discussed in detail. In particular those which serve to illustrate the main theme of this dissertation, which is that properties of the Laplacian of the electronic charge distribution can be used to provide a physical basis for chosen electron–pair models.

THE ROLE OF THE LAPLACIAN IN CHARACTERIZING ATOMIC INTERACTIONS

The Laplacian in the internuclear regions shown in figures 2.5 and 2.6 are of opposite nature. Charge is locally concentrated over a region of space that envelops all three nuclei in the water molecule (figure 2.6). In contrast, the VSCC's of the argon atom and the fluorine atom are not contiguous. The bonds in water and ArF^+ individually belong to the two broad classes of atomic interactions that are classified on the basis of observable properties of a molecule (Bader and Essén 1984). The broad classes are shared interactions, to which the O–H bonds in water belong, and closed–shell interactions, to which the bond in ArF^+ belongs. The terms shared and closed–shell describe the characteristics of the charge and pair distributions found for the limits of these two classes. There exists a region of overlap where the charge distribution may exhibit the properties of a shared interaction while the pair distribution exhibits the characteristics of a closed–shell distribution. Since these distributions are equally important to the chemical properties of a molecule, no attempt should be made to draw a line dividing the two classes. Such a division has been proposed by Cremer and Kraka (1984) who claim that a covalent bond is a bond path (as defined in chapter 1) that exhibits a negative value of E(r) (equation 2.27) at the position of the bond critical point. This function had previously been discussed in connection with chemical bonding (Bader and Preston 1969) and in connection with the topology of the Laplacian (Bader and Essén 1984, Bader, MacDougall and Lau 1984). However, because of the non–uniqueness of this definition of an energy density no attempt was made to define properties of molecules on the basis of local properties of this function.

The sum of the three eigenvalues of the Hessian matrix at the position of a bond critical point, $\nabla^2\rho(r_c)$, indicates whether charge is locally concentrated or depleted in the interatomic surface (Bader and Essén 1984). By definition, there are two negative

eigenvalues and one positive eigenvalue at r_c. The sign of $\nabla^2\rho(r_c)$ is therefore determined by the competition between 1) the contraction of the charge density toward the nuclei and out of the interatomic surface (this leads to a larger positive eigenvalue), and 2) the contraction of the density that is in the interatomic surface toward r_c (this leads to larger magnitudes of the negative eigenvalues). Figure 2.8 illustrates the characteristics of the charge density, that are revealed more directly by its Laplacian, for examples of a limiting case of each type of interaction (N_2 and Ar_2) and an example of an average case of each type of interaction (NO and KF). Note how there is a contiguous region of charge concentration enveloping both nuclei in the shared interactions, while the corresponding VSCC's of the atoms in the closed–shell cases are not contiguous.

The properties of the pair density for these classes of atomic interaction are perfectly summarized by their names. In shared interactions the atoms are found to share pairs of electrons. Recall from section 2.1 that the localization of electron pairs paralleled the Fermi correlation contained within a given region (Bader and Stephens 1974). The reverse pattern is simply that electron pairs are delocalized when the Fermi correlation within a given region is low. Correspondingly atoms that are bonded to other atoms via shared interactions possess a relatively low percentage localization (equation 2.16). For instance hydrogen atoms in hydrocarbon molecules where $\nabla^2\rho(r_c)_{C-H} \approx -1.0$ au exhibit $\ell(H)$ values between 40 and 50%. Whereas bonds between hydrogen and silicon are of the closed–shell type $\nabla^2\rho(r_c)_{Si-H} \approx +0.30$ au and $\ell(H)$ values > 75%. This is due to a large amount of charge transfer to each hydrogen atom of approximately 0.75e. The greater the ionicity of a given bond the more closed–shell the atomic interaction is found to be. In the closed–shell limit $\ell(\Omega)$ values are commonly found to be > 98%, *e.g.* the electrons of the Li atom in triplet CLi_2 are 98% localized within the Li atom which has a net charge of +0.91e. The data in the above discussion are taken from MacDougall and Bader (1986). A hydrogen atom has

Figure 2.8

Relief maps of the Laplacian for N_2, NO, KF and Ar_2 derived from 6–21G* RHF calculations. In the figure for NO the nitrogen atom has the less pronounced VSCC. In the figure for KF the potassium atom has three shells. The Laplacian distributions of N_2 and NO are typical of shared interactions, while those of KF and Ar_2 are typical of closed–shell interactions. Note that the pattern of charge concentrations in the VSCC of the potassium atom in KF is identical to that of the argon atom in Ar_2, except that it is more contracted.

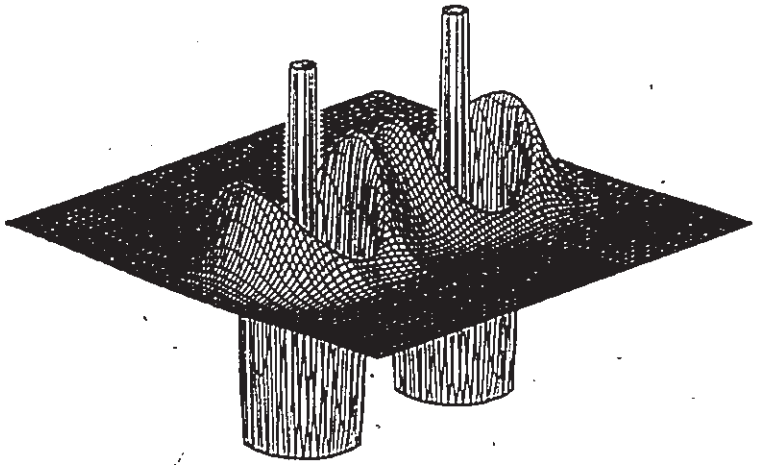

N_2

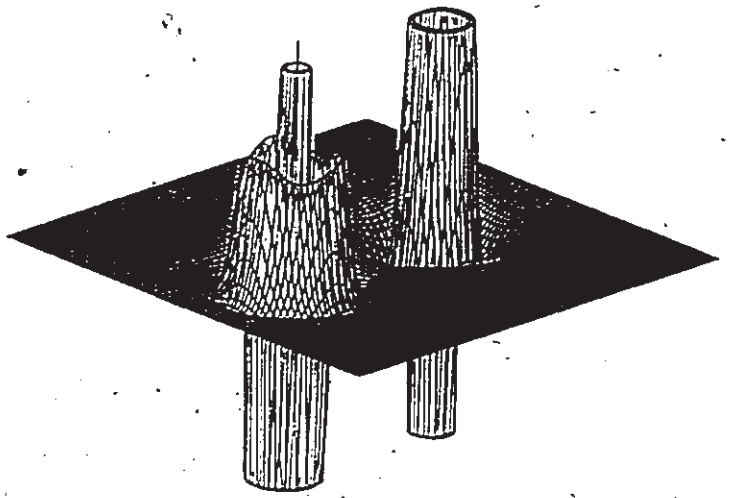

KF

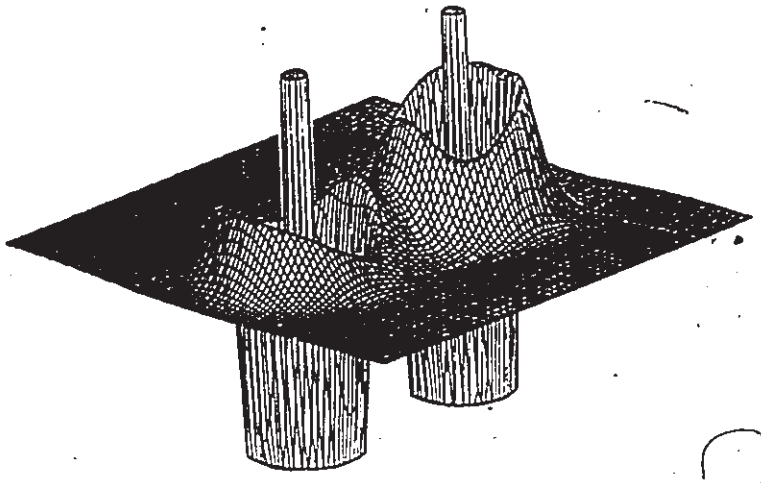

NO

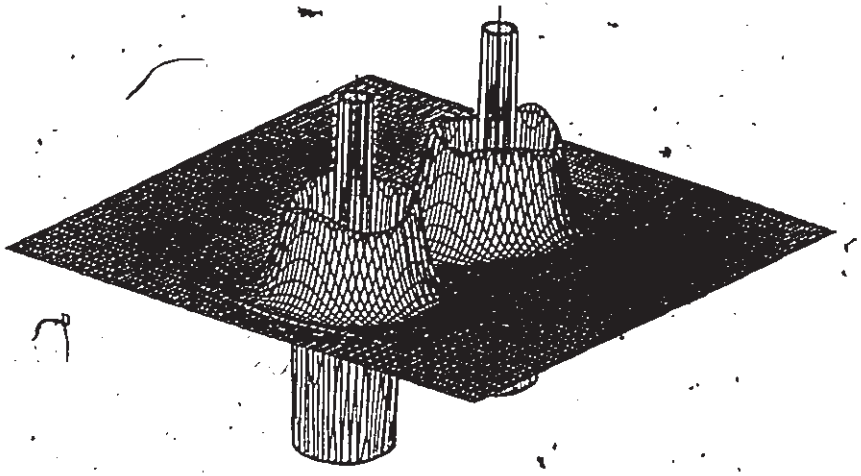

Ar_2

no core, thus on average its electrons have a tendency to be less localized than atoms with cores. Indeed, the value of $\ell(\Omega)$ for a given atom must be compared to the values of $\ell(\Omega)$ for atoms with the same number of core electrons if the localization of the valence density is to be judged in a meaningful way. Bader and Essén (1984) have reported $\ell(\Omega)$ values of 73, 78 and 93% for C_2, N_2 and F_2, respectively. The unbound closed–shell interaction of Ne_2 at R = 3.0 au localizes the ten electrons on each neon atom to an extent of > 99%.

The fluorine molecule is an excellent example of an intermediate atomic interaction, the majority of its characteristics belonging to the closed–shell domain. The VB and MO models of chemical bonding do not distinguish F_2 as a qualitatively different type of interaction than other "normal" singly bonded diatomic covalent molecules. Near the Hartree–Fock limit F_2 exhibits a local minimum in its potential energy surface, however this geometry is unbound with respect to two separated fluorine atoms. This result is attributed to the notoriously poor description of the open shell dissociation limit and not to any peculiarity of the F–F bond (Levine 1983). The Hartree–Fock charge distribution and its Laplacian, which have been shown to be minimally affected by the inclusion of coulomb correlation (Stephens and Becker 1983, Ritchie *et al.* 1986, Gatti *et al.* 1988), already indicate a qualitative difference in the bonding of F_2 relative to other singly bonded species (Bader and Essén 1984). The value of $\rho(r_c)$ for F_2 is 0.296 au (cf. for H_2 $\rho(r_c) = 0.273$ au), which is not unusual for a single covalent bond. However, the values of $\nabla^2\rho(r_c) = +0.233$ au and $\ell(F) = 93\%$ put the interaction in the closed–shell category. We have seen that the properties of the Laplacian of the charge distribution somehow bring out characteristics of the pair distribution function. The following section will explore the mechanism behind this observation.

2.4 FERMI CORRELATION AND THE TOPOLOGY OF THE VSCC

As mentioned in section 2.1, the analysis of the spatial properties of Fermi correlation is difficult in that it is a six–dimensional function. The problem of interpreting Fermi holes would be substantially reduced if there were a unique way of pin–pointing the "best" positions of the probe electron. As we have seen in section 2.3 the topology of the Laplacian indicates that there are identifiable points, (3,–3) critical points in $-\nabla^2\rho(\mathbf{r})$ to be precise, where the charge density is maximally concentrated. As we shall now see, when the probe electron is fixed at the coordinates of these (3,–3) critical points the Fermi hole behaves in a very instructive manner.

In section 2.1 it was stated that the antisymmetry requirement of the Pauli exclusion principle resulted in the creation of a Fermi hole in the pair density. It was also stated that this correlation was solely responsible for any pair–wise localization observed in Hartree–Fock calculations. Sinanoğlu has further argued (1962) that introduction of further correlation of the motions of the electrons, *i.e.* Coulomb correlation, would likely have a disrupting influence on any pair–wise localization predicted by Hartree–Fock theory. The mechanism by which this occurs has not yet been researched in detail. Calculations of Fermi holes have been performed for varied positions of the reference electron in several molecules. These results will be used to discuss in a more illustrative manner the general questions of how can localized pairs of electrons be formed and to what extent are electrons, particularly valence electrons, localized into pairs.

As an electron moves through space it is followed by a *doppelgänger*, its Fermi hole. If the probe electron is of α (or β) spin, then the Fermi hole represents the decreased probability of finding another α (or β) electron at a given point as a result of fixing the coordinates of the probe electron. Because an α (or β) electron can instantaneously exchange with any other α (or β) electron, electrons are quantum mechanically spread out as they move through space. When we computationally fix an

α (or β) electron at a point r, its *doppelgänger* collapses and we are left with a hole in the α (or β) total density, $\rho^{\alpha}(r)$, that is a mirror image of the spread out distribution of that electron the moment we fixed its position. The shape of the Fermi hole is determined by the probability of exchange with other like–spin electrons (see equation 2.17), it has several general characteristics: 1) It is generally deeper for positions near the reference coordinates, although it is not necessarily a maximum at r_1. 2) Its magnitude has upper and lower limits, $0 \leq |h^{\alpha}(r_1,r_2)| \leq \rho^{\alpha}(r_2)$. 2) The lower limit only applies to Hartree–Fock calculations, although it has not yet been demonstrated that the correlation hole for electrons of like spin, $h^{\alpha\alpha}$, takes on positive values. We will see in section 2.9 an indication that the addition of Coulomb correlation has minimal affect on the electron's *doppelgänger*. 3) The magnitude of the Fermi hole at the coordinates of an α (or β) reference electron must equal $\rho^{\alpha}(r_1)$, thereby ensuring a zero probability of finding two electrons of the same spin at the same point. 4) It commonly exhibits more than one maximum and one or more surfaces that are very nearly nodal surfaces, thus giving it the appearance of a hybrid or a localized orbital density (Luken and Beratan 1982, Luken 1984). 5) The Fermi hole integrates to -1 over all space, for any position of the probe electron.

One can achieve perfect localization of a pair of electrons in a given finite region Ω iff $h^{\alpha}(r_1,r_2) = -\rho^{\alpha}(r_2)$ for every position r_1 and r_2 within Ω and the same applies to the β hole. If this condition is met then $F(\Omega,\Omega) = -2$. The pair of electrons are completely contained within Ω and their motions are totally independent of the remaining electrons in the system. This limit is approached by the core regions of molecules and hydride fragments. Figure 2.9 depicts the Fermi hole of an electron for various positions (denoted by a star) in methane (Bader, Gillespie and MacDougall 1988, 1989), determined from a Hartree–Fock calculation using the extended 6–311G** basis set (Binkley *et al.* 1980, Chandrasekar *et al.* 1981). When the probe electron is moved anywhere within the core loge determined by Bader and Stephens (r_c=0.53 au)

Figure 2.9

Fermi holes for various positions of a probe electron in the methane molecule, derived from a.6–311G** RHF calculation. In each figure the contour values start at –0.002 au (outermost) and increase in magnitude inwards in the same manner as those in figure 1.1 (1 au = 1 e/a_0^3). This set of contour values is used in all subsequent plots of Fermi holes. The positions of the in–plane nuclei are marked by solid circles and are labelled in b. The projected positions of the out–of–plane hydrogen nuclei are marked by open circles. The position of the probe or reference, electron is denoted by a star. (a) The reference electron is 0.35 au from the carbon nucleus and situated on the C–H bond path. (b) The reference electron is located at the position of the bonded maximum in the VSCC of the carbon atom. It is 1.02 au from the carbon nucleus and is also on the C–H bond path. (c) The reference electron is 0.69 au from the carbon nucleus and on the C–H bond path. (d) The reference electron is at the position of the C–H bond critical point, 1.28 au from the carbon nucleus. The area within the innermost contour (–0.08 au) encircling the position of the probe electron is decreased relative to map b and the hole extends further into the core and nonbonded regions. (e) The reference electron is displaced from the C–H bond path by a 10^0 angle subtended at the carbon nucleus. It is 0.99 au from carbon nucleus and still in the vicinity of the bonded maximum. (f) The reference electron is the same distance from the carbon nucleus as in map e, but is now situated on a C_2 axis. It is on the boundary of two bonded regions.

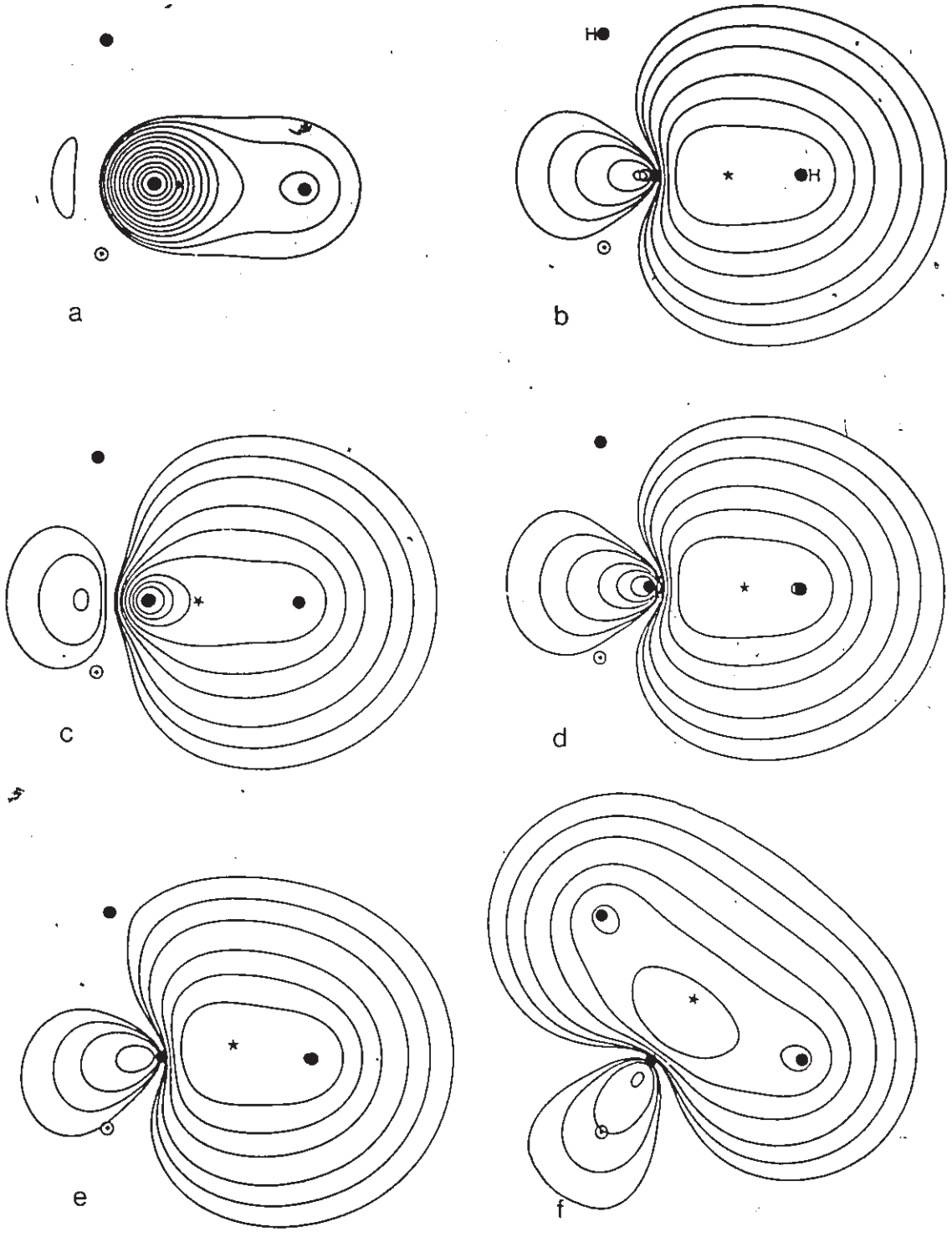
a
b
c
d
e
f

the electron's Fermi hole maintains a relatively constant shape, see figure 2.9b. The potential well of the carbon nucleus is so attractive that even when the probe electron is a distance of 0.35 au away from the nucleus, its *doppelgänger* prevents virtually all other electrons of the same spin from being at the carbon nucleus or any other position within roughly a 0.75 au radius of the carbon nucleus. The result of this extreme localization of an α (or β) electron's *doppelgänger* in the vicinity of such a strong potential field is that by excluding all other α (or β) electrons it attracts an electron of opposite spin. In turn, this second electron excludes the remaining electrons in the system. Thus Fermi correlation does not act directly to "pair up" electrons. Rather, since there is no Fermi correlation between electrons of opposite spin, an α,β pair is obtained as a result of all other electrons being excluded from a given region of space. Regions of space that are witness to this occurence must exert a strong enough attractive potential to overcome the Coulomb repulsive force that acts to keep all electrons apart.

As the probe electron samples positions in the valence region of a molecule (see figures 2.9b – 2.9f) its *doppelgänger* undergoes a significant delocalization in response to the weakening of the attractive force that the α,β pair feel. As the common attraction that an α,β pair experiences is diminished, the repulsive Coulomb force between them acts to delocalize the electrons. The expansion of their *doppelgängers* inevitably causes electrons in different regions of space to overlap significantly with more than one electron of opposite spin, thus the distinct pair population of a given region (with an average electron population of two) increases above one. It should be noted however that the electrons are most likely to be somewhere on the C–H bond path that the probe electron is nearest.

The formation of a molecule from isolated atoms results in the creation of potential wells in addition to the nuclear wells present in the isolated atoms, these are the internuclear potential wells. Although these are not capable of forming a localized

pair of electrons in a bonding loge (table 2.2) they do cause a greater extent of localization of the pair density than is observed outside of these wells. To judge the partial condensation of the pair density that can be attributed solely to the internuclear potential well, compare figures 2.9b and 2.9f. Figure 2.9f depicts the extent of delocalization of an electron located at the boundary of two bonding loges. Rather than partially localizing itself to a region in between two internuclear wells, the electron is spread over both of the neighbouring bonds. Figures 2.9b – 2.9e qualitatively examine the extent of leakage of an electron's *doppelgänger* outside the domain of the bonding loge as it is probed by the reference electron. In figure 2.9c the probe electron is just 0.16 au (0.08 Å) beyond the radius of the core loge yet it only has a magnitude of ≈ 1.0 au at the carbon nucleus, this is to be compared to a magnitude of > 20 au when the probe electron is anywhere within the core radius. This is a dramatic demonstration of the extent to which the Pauli exclusion principle, when assisted by a deep potential well, is capable of localizing electrons of the same spin to separate regions of space and forcibly keeping them there.

In figure 2.9d the probe electron is farther from the carbon nucleus than in either 2.9b or 2.9e, however there is a greater overlap of the probe electron's *doppelgänger* with the core loge in this more removed position. The maximum Fermi hole magnitude within the core loge is ≈ 0.2 au in figure 2.9d, while only ≈ 0.08 au in both 2.9b and 2.9e. This observation is a curious one, and is left as a puzzle for the reader. The *doppelgängers* in figure 2.9b and 2.9d both exhibit magnitudes < 0.002 au at every point along the C–H bond paths in the neighbouring bond loges. In this way they maximally avoid the other valence electrons of the same spin which are spread out in similar Fermi holes centered on their respective bond paths. The *doppelgänger* shown in figure 2.9e corresponds to a 10^0 displacement of the reference electron off of the C–H bond path, but at the same distance from the carbon nucleus as shown in figure 2.9b. The electrons *dappelgänger* still strongly avoids the neighbouring bond

path, exhibiting a maximum magnitude there of ≈ 0.004 au. Electrons have been shown to maximally avoid other electrons of the same spin, thereby minimizing their mutual repulsion, when they are located at a position such as the one marked by a star in figure 2.9b. There are four such positions, one along each C–H bond. In figure 2.9b the probe electron is located at the point of maximum charge concentration in the VSCC of the carbon atom! This suggests that local concentrations of charge are created in the valence shells of atoms in molecules at positions where the mutual repulsions between electrons of the same spin are minimized. This proposal is supported by the local expression of the virial theorem (equation 2.25) which relates maxima in local concentration to maximum lowering of the potential energy density relative to the local value of the kinetic energy density G(r).

It should be stressed that although it has been demonstrated that the pair density can condense to yield partially localized electron pairs in the valence region of methane, this only occurs when the electrons are near the bonding charge concentration in the VSCC of the carbon atom. In general the valence electrons are more delocalized and, on average, pair with 1.3 electrons of opposite spin (Bader and Stephens 1975).

The observations discussed above further illustrate the point that chemically important information can be learned from the Laplacian of the charge density. This includes information that reflects the most important features of the pair density, which completely determines the energy of a molecule. Since, in principle, the Laplacian is an experimentally measurable property of matter in the crystalline state, this is an exciting prospect.

The topological and energetic properties of the Laplacian have been introduced, illustrated and interrelated. We can now begin to interpret the physical basis of the Lewis electron pair model of the atom, and other successful models, in the light of the new understanding afforded by studies of the Laplacian and Fermi correlation.

2.5 VALENCE SHELL CHARGE CONCENTRATIONS: SUCCESSORS TO ELECTRON PAIRS?

The Lewis structure of the water molecule consists of two electrons in the "kernel" of the oxygen atom, one bonding pair of electrons in each of the two O–H bonds, two equivalent nonbonding pairs of electrons on the oxygen atom, each pair of valence electrons being situated at the vertices of a tetrahedron centered on the oxygen nucleus (Lewis 1916, p.777). The geometrical component of the Lewis model was not immediately applied to chemical problems. In fact Lewis barely mentions the implications of the tetrahedral arrangement of pairs in his paper. It was not until the VSEPR model was introduced that the geometrical component of Lewis' model was paid much attention (Gillespie and Nyholm 1957). The Lewis and VSEPR models are two of the first models taught to young, prospective chemists. One of the last models taught to a student before he/she is branded a chemist is that the electronic structure of the water molecule is $(1a_1)^2(2a_1)^2(1b_2)^2(3a_2)^2(1b_1)^2$. Within this model neither the bonding nor the nonbonding pairs of orbitals are equivalent. When the orbital model is misused by suggesting that the charge distribution of the five pairs of electrons in the water molecule are described by the densities of the five canonical molecular orbitals[7], then the student is unnecessarily confused about the most basic property of a molecule – its electron distribution. This section will further illustrate that the topological properties of the Laplacian faithfully recover the anticipated Lewis structure of a molecule. However, the valence shells of the atoms are observed to consist of bonded and nonbonded local concentrations of charge and not localized pairs of electrons.

In section 2.1 we saw that, in general, valence electrons are not localized into pairs that could be classified as bonding or nonbonding. In section 2.3 it was reported

[7] Indeed entire books are devoted to the depiction of the "electron densities of molecular orbitals" (van Wazer and Absar 1975, Hout *et al.* 1984).

that the VSCC of an atom is distorted upon chemical combination resulting in the formation of local concentrations and possible local depletions of charge. Figure 2.6 and the discussion of this figure demonstrated that the distortion of the VSCC of the oxygen atom upon the formation of the water molecule results in the creation of four charge concentrations. Two equivalent bonded charge concentrations and two equivalent nonbonded charge concentrations. The geometry of these local charge concentrations is basically that of a tetrahedron. At this point we are not concerned with distortions of molecular geometries from the simple predictions of; tetrahedra for atoms with four valence shell electron pairs (Lewis 1916), and trigonal bipyramids or octahedra for atoms with five or six valence shell electron pairs, respectively (Sidgwick and Powell 1940). This section will establish by multiple examples that the localized valence shell electron pairs predicted on the basis of the Lewis model are recovered in number and in kind as valence shell charge concentrations (Bader, MacDougall and Lau 1984).

CENTRAL ATOMS WITH FOUR VALENCE SHELL ELECTRON PAIRS

The following results were obtained from Hartree–Fock calculations, including geometry optimization, using the 6–21G** basis set (Binkley *et al.* 1980). The molecules CH_4, SiH_4, NH_3, PH_3, OH_2, SH_2, NF_3, PF_3, $ClCl_2^+$ and ClF_2^+ all possess four electron pairs in the respective valence shells of their central atoms, all except SiH_4 and PF_3 exhibit four local maxima in their VSCC's (see table 2.5). Those that exhibit the expected four charge concentrations in the VSCC of the central atom, faithfully exhibit the correct number of bonded versus nonbonded maxima. Furthermore, the positions of the bonded and nonbonded maxima (table 2.5) are in general agreement with the Lewis and VSEPR models, *i.e.* each bonded maximum (only one type observed for each molecule) was in the proximity of the A–X bond path and the nonbonded maxima were positioned with respect to the bonded maxima with

Table 2.5. Bonded and Nonbonded Charge Concentrations on A in AX_n[†].

AX_n	R(AX) A		∠XAX deg		Bonded Charge Concentrations						Nonbonded Charge Concentrations					net charge
					r_A	$-\nabla^2\rho$	∠bAb	Area	μ_3	∠nAb	r_A	$-\nabla^2\rho$	∠nAn	Area	μ_3	
	calc.	exp.	calc.	exp.	A	au	deg	A^2	au	deg.	A^2	au	deg	A^2	au	on X,e
CH_4	1.087	1.093	109.5	109.5	0.612	1.158	109.5	0.99	6.2							-0.04
SiH_4	1.477	1.480	109.5	109.5	charge transfer to hydrogen											-0.74
NH_3	1.007	1.015	105.7	106.6	0.510	1.685	104.4	0.71	19.5	114.2	0.388	2.299		0.83	100.0	+0.34
PH_3	1.408	1.42	95.4	93.5	0.945	0.638	96.1	1.61	2.5	120.8	0.775	0.325		2.49	7.8	-0.63
OH_2	0.947	0.96	103.8	104.5	0.441	2.057	101.0	0.38	51.4	104.4	0.339	4.138	134.0	0.50	210.1	+0.56
SH_2	1.330	1.323	94.3	92.1	0.841	0.806	95.4	1.17	4.4	105.4	0.696	0.554	133.7	2.20	17.3	-0.34
NF_3	1.337	1.371	102.5	102.9	0.473	0.990	97.6	0.45	28.2	119.6	0.358	4.450	119.6	0.70	294.7	-0.36
PF_3	1.548	1.535	97.5	100	charge transfer to fluorine						0.750	0.502	119.8	2.15	12.1	-0.90.
$ClCl_2^*$	2.002		106.3		0.653	0.717	104.3	1.48	25.3	101.9	0.615	1.148	140.9	1.88	48.9	
ClF_2^*	1.576		100.2		0.658	0.671	99.0	0.66	27.9	102.0	0.604	1.541	142.8	1.84	62.2	-0.18
S					charge transfer to oxygen						0.678	0.785		1.56	24.4	
SO_2	1.423	1.43	118.7	119.5			124.0	1.82		118.0						
O					0.426	1.769			54.1		0.346	3.697			182.0	-1.26

[†]All results calculated using the 6-21G** basis set. Experimental values are taken from Wells (1975).

varying distortions from a tetrahedral arrangement. In the case of SiH_4 the silicon atom has a net atomic charge[8] of +2.96e. Silicon has lost a full 75% of its valence density and as a result no longer possesses a valence shell of charge concentration. PF_3 similarly loses most of its valence density available for bonding to the fluorine atoms, q(P) = +2.70e, however its remaining valence electrons exhibit a single charge concentration in the nonbonding region of the molecule (see figure 2.10). Phosphine does exhibit four charge concentrations in the VSCC of phosphorus, however reference to figure 2.10, which has the interatomic surfaces overlayed on the contour maps of the Laplacian, indicates that the bonded maxima in the VSCC of the phosphorus atom are actually within the atomic domain of the hydrogen atoms. Phosphine is therefore an example near the point at which the Lewis model would cease to describe the bond in these AX_n systems as a shared electron pair bond, but rather as an ionic interaction between two closed–shell atoms. In order to avoid the misinterpretation that molecules which do not possess bonded charge concentrations represent failures of the Laplacian to recover the Lewis model, we further consider the original model.

AN ASIDE ON WHEN, AND WHEN NOT, TO EXPECT A BONDED CHARGE CONCENTRATION

Lewis emphasized the importance of a type of tautomerism between the ionic and shared descriptions of a given bond. Lewis' tautomerism was a precursor to the resonance model of Pauling (1960) and should not be confused with the more common usage of the word in organic chemistry. If the reader accepts the proposal that the charge concentrations in the VSCC of an atom are the authentic expression of the electron pairs of the Lewis model, then we can further propose that the topology of the VSCC's of the atoms involved in a chemical bond provides a physical basis for the discussion of the relative contributions of the "tautomeric" forms that Lewis also

[8]Throughout this thesis net atomic charge is defined as $q(\Omega) = Z(\Omega) - \int_\Omega \rho(r) d\tau$.

Figure 2.10

Contour diagrams of the Laplacian distributions of NH_3, NF_3, PH_3 and PF_3, derived from 6–21G** RHF calculations. All maps show the Laplacian in a σ_v plane of symmetry with the central atom closest to the center of the map. The corresponding A–X bond paths and interatomic surfaces are overlayed in each figure. The positions of the bonded and nonbonded maxima in the VSCC of the central atom are denoted by solid squares. The determination of the angle α is indicated for NH_3 and PH_3. It is subtended at the nucleus of the central atom by the (3,–1) saddle point in $-\nabla^2\rho$ (solid triangles) neighbouring the nonbonded maxima and a neighbouring (3,+1) ring critical point or the edge of the charge concentration as shown for PH_3. The contour values are ± 0.002 au increasing in magnitude in the same manner as in figure 1.1 (+0.002 is the outermost contour in each map). The contours in the inner shells of charge concentration and depletion are not seen because the contour values do not become large enough in magnitude. This set of contour values is used in all subsequent contour maps of the Laplacian distribution.

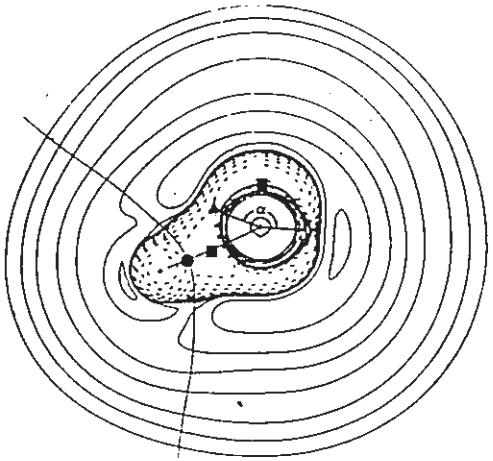

NH_3

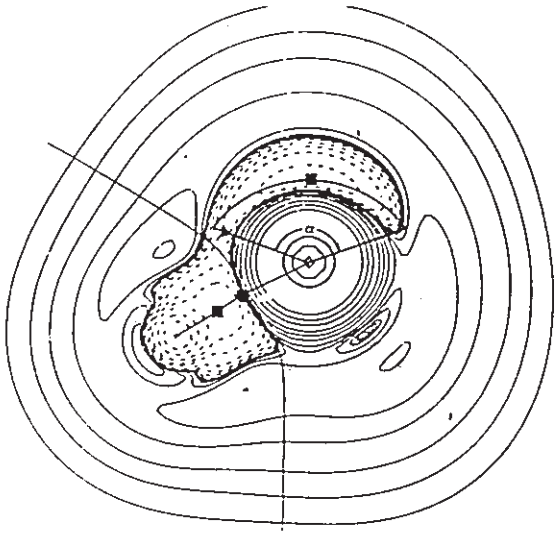

PH_3

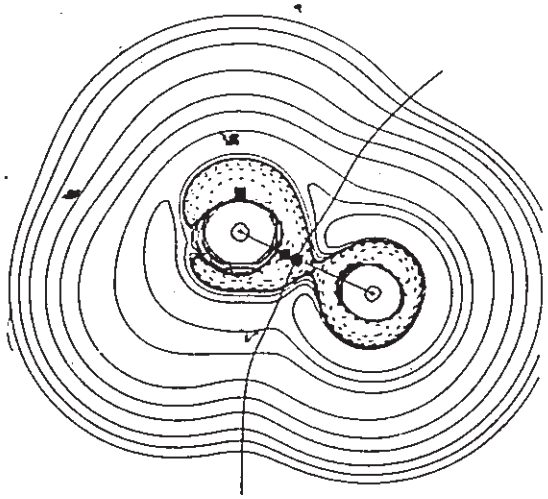

NF_3

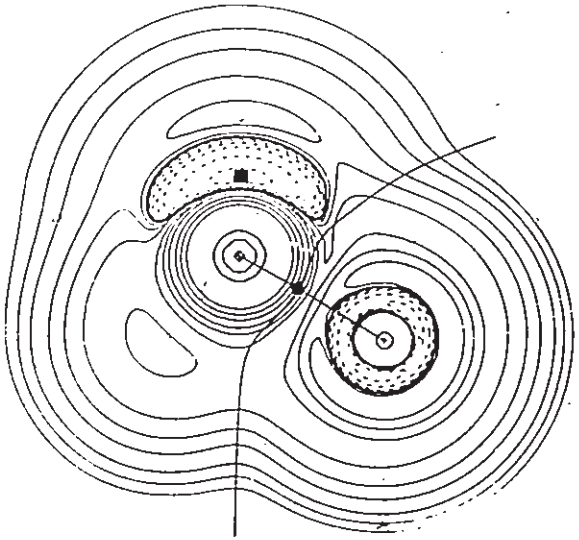

PF_3

postulated in his model. Figure 2.10 depicts a progression from the dominance of the shared form (NH_3) to the dominance of the closed–shell or ionic form (PF_3). The atomic charges of the ligands (table 2.5) indicate that the order of increasing ionicity of this series is $NH_3 < NF_3 < PH_3 < PF_3$. Correspondingly, beginning at the shared limit (NH_3) figure 2.10 illustrates a migration of the charge concentration on the central atom closer to the interatomic surface (NF_3), followed by crossing the interatomic surface but still within the shell of charge concentration encompassing the central atom (PH_3), and finally the vanishing of the bonded charge concentration (PF_3) at the ionic limit.

The reader may have noticed that the topology of the VSCC of a fluorine atom does not possess an obvious bonded maximum in either NF_3 or PF_3. In fact it does not. The VSCC of the fluorine atom in these molecules possesses a minimum, *i.e.* a (3,+1) critical point, at its intersection with the A–X bond path. Even more anomalous is the presence of a bonded hole [$\nabla^2\rho(r_c) > 0$] in the VSCC of the fluorine atom in ArF^+ (figure 2.5) and F_2 (figue 2.11). To date, the only known case where the VSCC of a fluorine atom possesses a bonded maximum is in the molecule FH. However, the bonded charge concentration is so small that it was initially undetected by Carroll *et al.* (1988). In most cases the electron withdrawing power of the fluorine atom is sufficient to "fill" the hole in its VSCC when it is covalently bonded, as in F_2 [q(F) = 0.0e] or ArF^+ [q(F) = +0.07e]. An increase in atomic population does not necessarily result in an increase in the extent of local concentration in the VSCC, since the atomic average of $\nabla^2\rho$ is always zero. However, if the approximate proportionality between the integrated magnitude of the Laplacian and the total energy of an atom (equation 2.20) holds for atoms in molecules, then we would expect "holes" in valence shells to be filled by charge transfer since an increase in atomic population generally leads to lowering of the energy of an atom. Hypothesizing aside, observations support the expectation of an increase in the extent of charge concentration in the VSCC of an atom resulting from charge transfer to that atom (figure 2.10).

No satisfactory rationale can be put forward at the moment to account for the almost universal lack of a bonded charge concentration in the VSCC's of fluorine atoms. The author suspects that extremely high amounts of interpair Fermi correlation between the valence electrons somehow disrupt the previously described mechanism of partial localization of valence electrons into pairs that results in a corresponding number of local maxima in charge concentration. The sizes of the bonded charge concentrations in table 2.5 (how this property is determined will be described in the next section) decrease in the series CH_4, NH_3, OH_2 and the previously mentioned FH in which the bonded charge concentration is barely noticeable. If one also looks back to tables 2.2 and 2.3, there is a concurrent decrease in the percent localization, $\ell(\Omega)$, of the electrons in each of the two–electron valence loges in these molecules. In particular, the average localization of the valence electrons to their respective loges in FH is 50.3%.

Perhaps it is a coincidence, but it is worth postulating that there is a requirement that more than half of the maximum Fermi correlation be contained within a given two–electron loge in order for it to possess a maximum in local charge concentration if it is a nonbonded loge, and two maxima if it is a bonded loge (one in the VSCC of each bonded atom). An alternative expression of this requirement is that: for the topology of the VSCC to have a one–to–one mapping onto the Lewis model there is a leeway of only one half of a pair in the distinct pair population of each two–electron loge from the perfect pair population of one[9]. This hypothesis is supported by the minute fraction of the maximum Fermi correlation contained in a two–electron σ–bonding loge of the fluorine molecule (Bader and Stephens 1975). For this loge $\ell(\Omega) = 17.4\%$ and $D_2(\Omega,\Omega) = 3.78$! Figure 2.11 demonstrates the pronounced failure of the Fermi correlation mechanism of electron pairing to create a bonded charge concentration in the VSCC of the fluorine atoms in F_2.

---

[9]This definition of the requirement is based on the equation $D_2(\Omega,\Omega) = N(\Omega)^2 - F(\Omega,\Omega)$. Thus, when $F(\Omega,\Omega) \leq \frac{1}{2} N(\Omega)$ and $N(\Omega) = 2.0$, then $D_2(\Omega,\Omega) \geq 3.0$.

Figure 2.11 (taken from Bader and Essén 1984)

Contour diagram of the Laplacian distribution in the fluorine molecule at the equilibrium geometry. There is actually a hole in the VSCC of the fluorine atoms in the bonded region, charge is locally depleted there to an extent of > 0.4 au as determined by the Laplacian. In the nonbonded torus of charge concentration, charge is locally concentrated < -8.0 au as determined by the Laplacian.

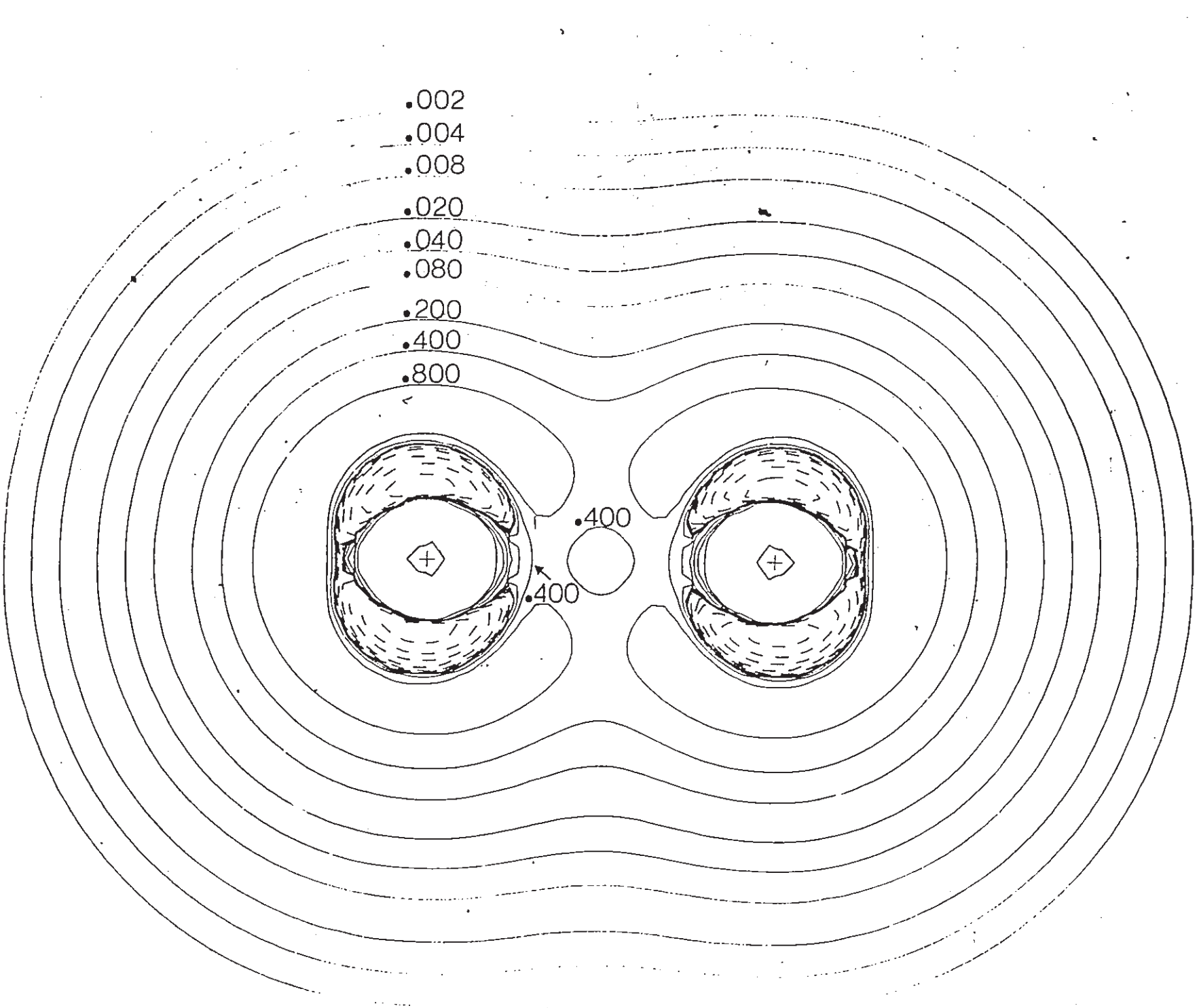
.002
.004
.008
.020
.040
.080
.200
.400
.800
.400
.400

In the context of molecular orbital models of chemical reactivity, the absence of a bonded maximum in the VSCC of fluorine atoms would be attributed to the extremely low energy of the 2s atomic orbital of a fluorine atom. This results in "poor overlap" with the central atom's bonding orbitals and a consequently "inert" 2s lone pair on each fluorine that is essentially spherical and could not directly create a local concentration of charge. This argument can also account for the decreasing sizes of the bonded charge concentrations in the series CH_4, NH_3, OH_2 and FH. However, as mentioned earlier, this argument is flawed in that the properties of individual orbitals do not determine physical properties of a many–electron atom or molecule.

The Laplacian does not exhibit a pair of bonded charge concentrations corresponding to Lewis' single bonding pair of electrons in the VSCC's of the fluorine atoms in F_2. Figure 2.8 illustrates that the VSCC's of the nitrogen atoms in N_2 exhibit only a single bonded maximum (on the bond axis) in addition to the anticipated single nonbonded charge concentration. Thus the reader may challenge "Why does the Laplacian not exhibit a bonded charge concentration for each bonded pair of electrons?". The translation of this expected behaviour into the topological possibilities of the VSCC's in N_2 (an axially symmetric system) is: why are there not two tori of charge concentration encircling the N–N bond path consisting of degenerate sets of (2,–2) crtitical points? Considering in unison the results of Bader and Stephens (1975) and the observed topologies of the VSCC's in N_2, further support is found for the requirement placed on the extent of intrapair Fermi correlation necessary for the creation of a bonded maximum in a two–electron loge. When the six bonding electrons in N_2 are partitioned into a σ and two π two–electron loges they each possess only 28% of the maximum Fermi correlation. Stephens (1975 p.185) also attempted a partitioning into three equivalent bonding loges with an unspecified but assumed lower extent of Fermi correlation containment (otherwise this value would have been tabulated with the other "best" loges). However, when all six bonding electrons are

treated as a single loge, the Fermi correlation containment rises to 72%. This extent of "intrahextuplet" Fermi correlation greatly exceeds the postulated requirement of 50%, and a single, very large bonded charge concentration is observed.

The description of the electronic structure of ethylene has been the subject of heated debates for some time (Messmer and Schultz 1986, Hay *et al.* 1972). The familiar Lewis structure of ethylene describes the double bond as the sharing of two equivalent pairs of electrons, each at the common corners of two tetrahedra sharing an edge. While the equally familiar molecular orbital picture of the double bond distinguishes between the two C–C bonding electron pairs, one pair occupies a σ–orbital and the second occupies a π–orbital. As in molecular nitrogen the topology of the Laplacian in the VSCC's of the carbon atoms does not exhibit one bonded maximum for each of the four electron pairs, rather, there is one bonded maximum for each bond. Recall that internuclear potential wells are a significant driving force in the formation of local concentrations of charge, via the mechanism described in section 2.4. Thus it would appear that the lowering of the potential energy that electrons can achieve by locally concentrating in regions of space where their *doppelgängers* can avoid one another, *i.e.* at the corners of a tetrahedron in this case, does not outweigh the cost in potential energy of locally concentrating outside of the single potential well between the carbon nuclei. Because of the additional pair of electrons in the C–C bonding region of ethylene, and their associated repulsive forces, the Fermi hole of the electrons are more delocalized than found in methane or ethane (figure 2.12). Figure 2.12 also depicts the appearance of an electron's *doppelgänger* when the probe electron is situated in the VSCC of the carbon atom, but displaced 45° above the C–C bond axis. This Fermi hole looks very much like a "banana bond" from a VB calculation, however the topological and energetic properties of the Laplacian suggest that this is not an optimum model of the spatial electronic structure of the ethylene molecule. In section 2.7 the additional topological features of the VSCC of the carbon atoms in

Figure 2.12

Fermi holes for various positions of the probe electron in the ethylene molecule, derived from a 6–311G** RHF calculation. The positions of the carbon nuclei, and the hydrogen nuclei in map b, are denoted by solid circles. The projected positions of the hydrogen nuclei in maps a, c and d are denoted by open circles. The position of the probe electron is marked by a star. (a) The Fermi hole when the reference electron is at the position of the bonded maximum associated with the C–C double bond is shown in the π plane. (b) The same Fermi hole as above is shown in the plane containing the C–H bonds. (c) The Fermi hole is shown in the π plane when the position vector of the reference electron is rotated above the plane of the nuclei by 45^0, but at the same distance from the carbon nucleus as in maps a and b. (d) The complementary Fermi hole to that shown in c, the position vector of the reference electron is rotated below the plane of the nuclei by 45^0. The maximum cross–sectional widths, as shown in a, are 4.56, 4.50, 4.31 and 4.31 au for a, b, c and d, repectively. Thus the *doppelgänger* associated with a double bond is "fatter" in the π plane than in the nuclear plane, and is also more delocalized than one arbitrarily associated with "banana bonds".

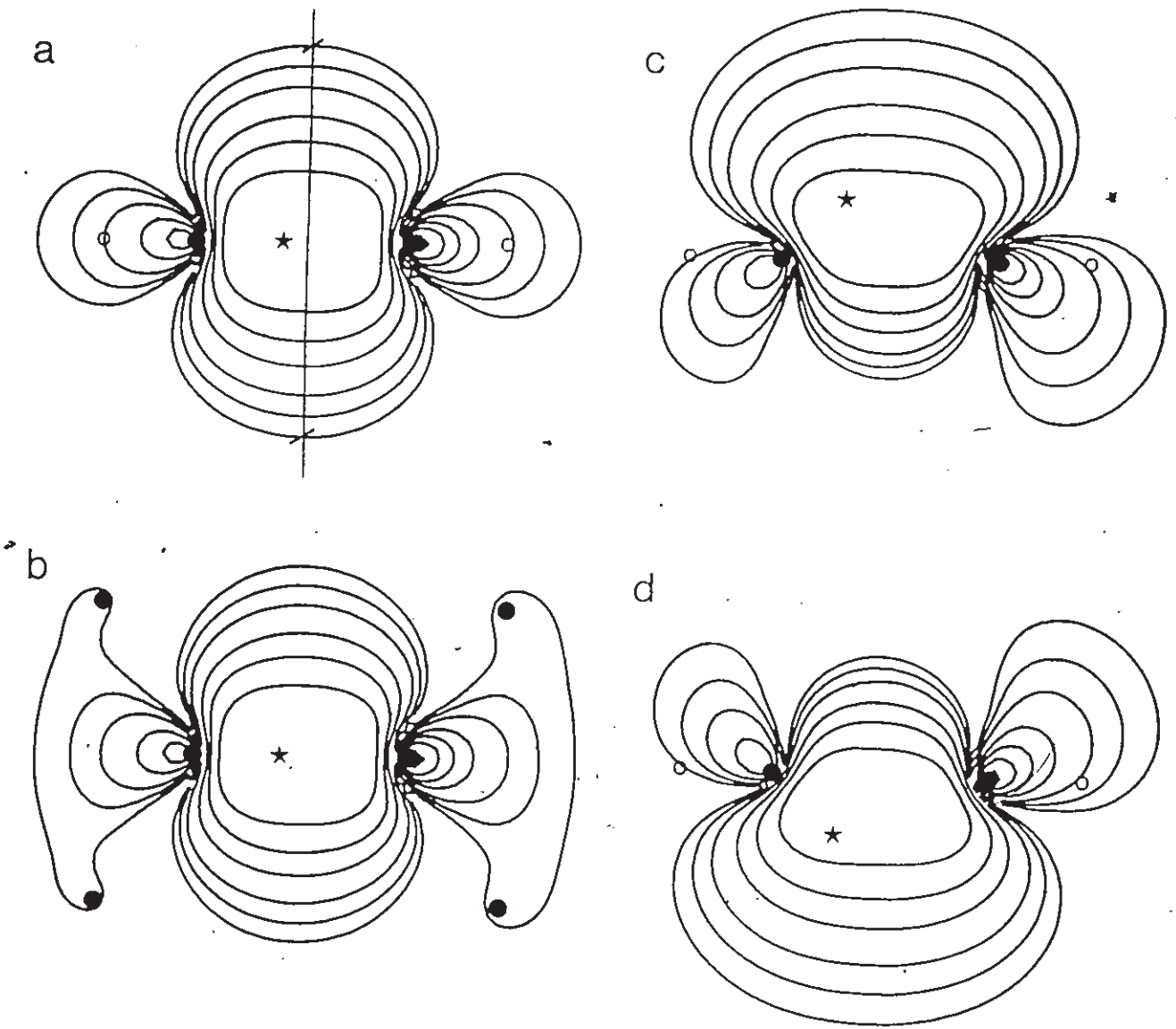
a
c
b
d

unsaturated molecules will be discussed in relation to the orbital model of chemical reactivity.

CENTRAL ATOMS WITH EXPANDED VALENCE SHELLS

In 1940 Sidgwick and Powell expanded Lewis' model of the electronic structure of molecules to include atoms with more than four pairs of electrons in their valence shell. They argued that the expanded size of the valence shell in third–row atoms could accomodate more than four electron pairs through the involvement of one or two d–orbitals. With this slight modification to the Lewis model a vast array of stable molecules with five or six electron pairs in the valence shell of the central atom, such as SF_4 and SF_6, were brought into the scope of this widely used model. They were not able to predict the geometries of molecules with lone pairs, this refinement was introduced by the VSEPR model. Sidgwick and Powell's model is still widely employed in the qualitative description of the bonding in so–called hypervalent molecules, notwithstanding molecular orbital based claims that d–orbital involvement is negligible in molecules such as SF_6 (Reed and Weinhold 1986).

The topologies of the VSCC's of the central atoms in SO_2, ClF_3, SF_4, SF_4O, ClF_5, and ClF_6^- have been examined. All of the calculations in this subsection were performed using the same basis set as in the subsection reporting on systems with four valence shell electron pairs. The data in table 2.6 (SO_2 is in table 2.5) summarize the types and positions of the maxima found in the valence shells of the central atoms as well as the net charges on the ligands. The data for two less stable geometries of ClF_3 are given below those for the T–shaped equilibrium geometry. The data for one less stable geometry of SF_4 are listed below the data for its equilibrium geometry. The relative properties of the equilibrium and less stable geometries will be discussed in the following section.

Table 2.6. Bonded and Nonbonded Charge Concentrations in ClF_3, SF_4, SF_4O and ClF_5.

Molecule & geometry	Bond	Bonded charge concentrations						Nonbonded charge concentrations					net charge on F or O
		r_A Å	$-\nabla^2\rho$ au	Area $Å^2$	μ_3 au	$\angle b_a A b_e$	$\angle nAb$	r_A Å	$-\nabla^2\rho$ au	Area $Å^2$	μ_3 au	$\angle nAn$	e
ClF_3	equatorial(e)	0.670	0.595	0.66	23.1	83.6°		0.605	1.58	1.52	61.9	147.8°	-0.30
	axial (a)	0.687	0.319	0.41	14.6		96.5°						-0.52
ClF_3	equatorial	0.661	0.374		21.2								-0.49
	axial				(b_eAb_e)	120.0°	90.0°	0.601	1.787		68.7	180.0°	
ClF_3	equatorial	0.663	0.428		20.9	73.1°	76.5°	0.607	1.529		59.5	134.2°	
	axial	0.672	0.526		19.7		139.3°	0.605	1.635		62.5		
SF_4	equatorial	0.707	0.342	0.94	21.5	84.5°	129.7°	0.666	0.999	1.90	30.7		-0.71
	axial	0.726	0.268	0.49	15.6		98.6°						-0.74
SF_4	equatorial	0.714	0.262		17.7	80.7°	99.3°						
	axial	0.713	0.410		19.6		180.0°	0.667	1.033		30.8		
SF_4O	equatorial	0.705	0.381	0.89	21.9	83.0°	101.7° (b_oSb_a)	double bond charge concentration on O: 0.463	1.175	2.06	30.8		-0.70
	axial	0.715	0.381	0.71	19.1								-0.72
ClF_5	single short Cl-F bond	0.653	0.866	0.78	29.4		180.0°	0.600	1.900	1.35	69.9		-0.30
	four long Cl-F bonds	0.662	0.619	0.64	23.8	82.8°	97.2°						-0.44

Figure 2.13 vividly illustrates that the topology of the VSCC of an atom in an expanded valence state maintains a one–to–one mapping onto the corresponding Lewis model of that atom. The chosen example is the ClF_3 molecule in its equilibrium geometry, where the VSCC of the chlorine atom exhibits two nonbonded maxima and a single bonded maximum in the equatorial plane in addition to one bonded maximum associated with each of the axial fluorine ligands. The molecules SF_4 and ClF_5 similarly display the anticipated number and types of charge concentrations in the VSCC's of the central atoms. The VSCC of the sulphur atom possesses two bonded charge concentrations and a single nonbonded charge concentration in the equatorial plane of SF_4 in its equilibrium geometry (figure 2.14), in addition to one bonded charge concentration associated with each of two axial fluorine ligands. There are therefore five charge concentrations in the VSCC of the central atom in accord with the five valence shell electron pairs invoked in the Sidgwick–Powell description of the bonding in this molecule. In the square–based pyramidal molecule ClF_5 there are six charge concentrations in the valence shell of the chlorine atom, one bonded charge concentration associated with each of the four Cl–F bonds and a single nonbonded charge concentration on the underside of the pyramid (see figure 2.16). Thus the VSCC of a chlorine atom can accommodate a charge concentration associated with up to six electron pairs. Whether or not there is d–orbital participation in the Cl–F or S–F bonding is a question that only has meaning within the VB or MO models, so no attempt is made here to discuss this question.

The Lewis model of SF_4O assigns six electron pairs to the valence shell of the sulphur atom, two are involved in the double bond to oxygen and the remaining four pairs each make up one of the four S–F bonds. Figure 2.14 illustrates that the topology of the sulphur atom's VSCC is only slightly changed from that in SF_4, where the S–O bonded charge concentration is replaced by a nonbonded one. Further, the S–O bonded charge concentration in SF_4O has migrated into the oxygen atom in

Figure 2.13

Relief maps of the Laplacian distribution in ClF_3, derived from a 6–21G* RHF calculation. The top figure shows the Laplacian in the equatorial plane, while the lower figure is of the axial plane. The chlorine atom is identified by the presence of three shells of charge concentration. The axial fluorines are on the far left and far right of the lower figure.

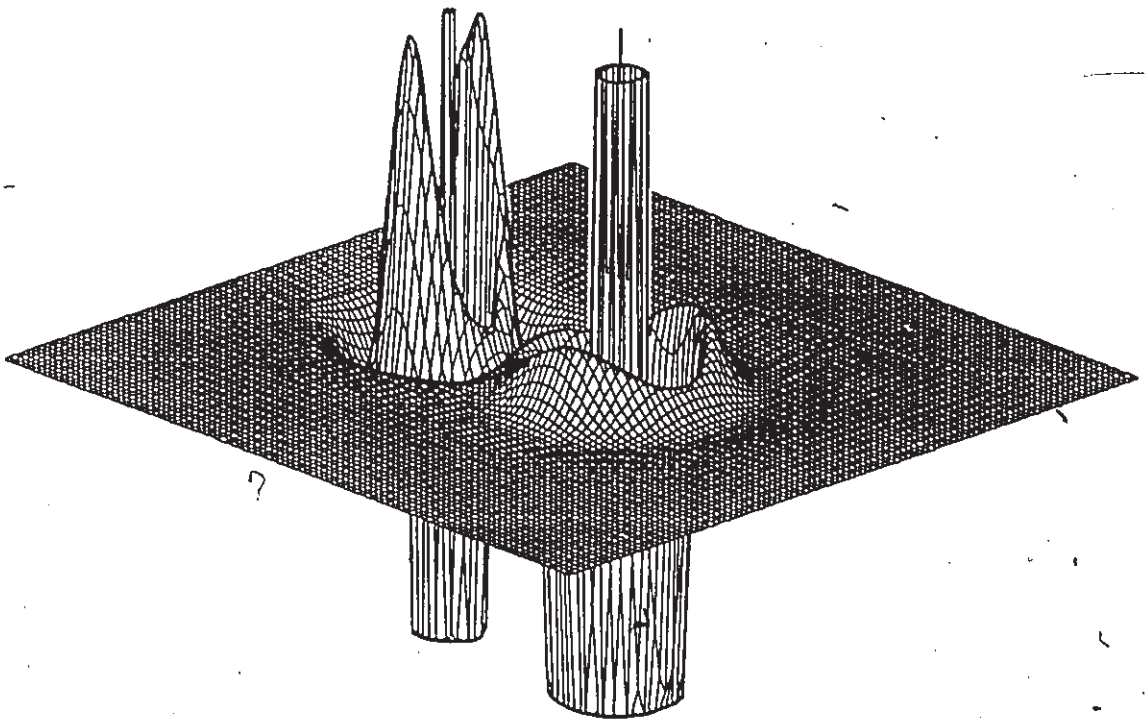

ClF_3

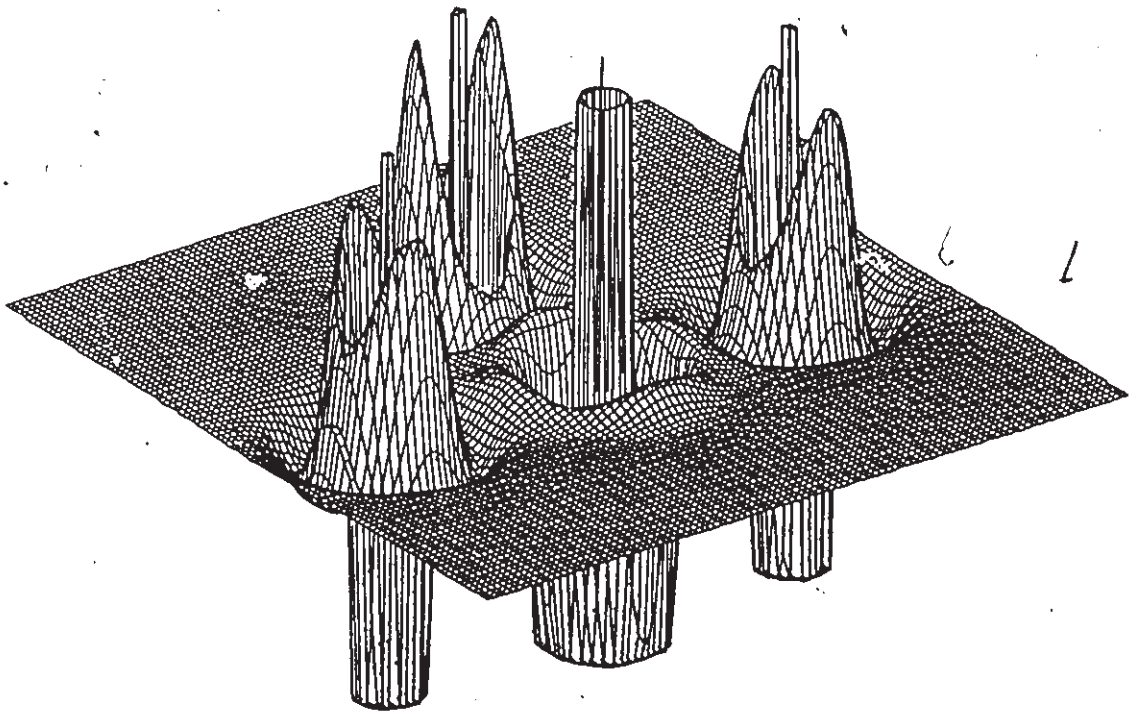

Figure 2.14

Contour diagrams of the Laplacian distributions in SF_4 and SF_4O, derived from 6–21G* RHF calculations. Both figures depict the Laplacian in the axial plane of the corresponding molecule. The bond paths and interatomic surfaces are overlayed as well. The positions of bond critical points are denoted by solid circles. The positions of maxima in the VSCC of the central atom are denoted by solid squares.

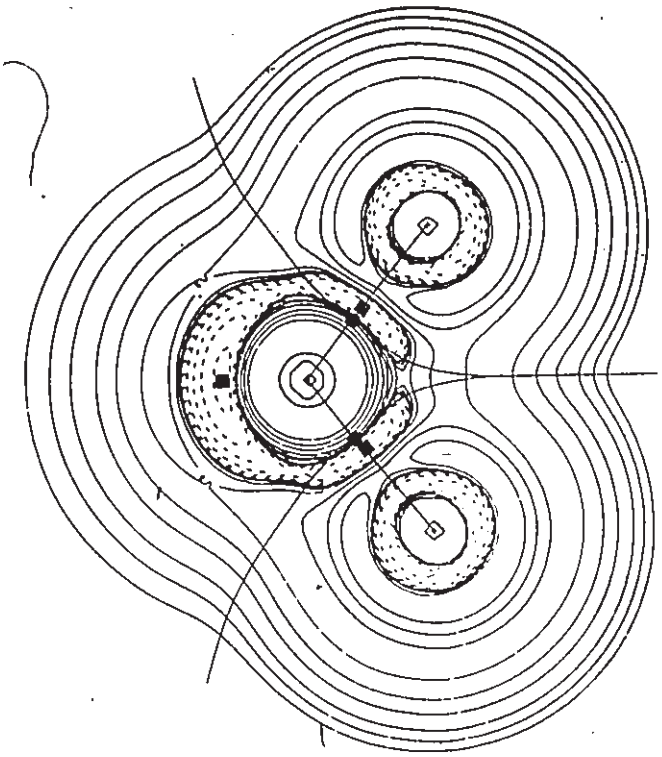

$:SF_4$

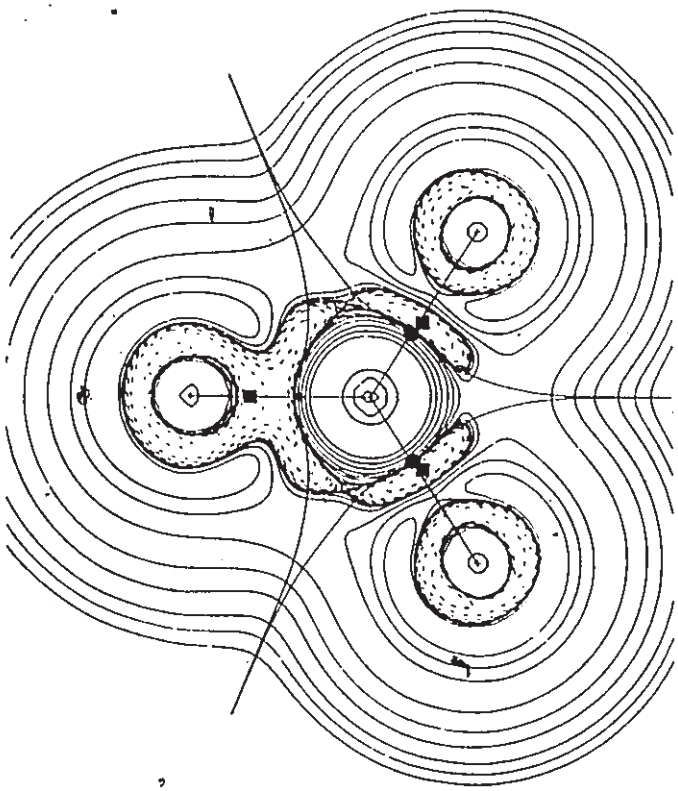

$O{=}SF_4$

Figure 2.15

A contour diagram of the Laplacian distribution in ClF_6^-, derived from a 6–21G* RHF calculation at the C_{3v} equilibrium geometry. The geometry is sketched in the top–right corner. The Laplacian is shown in a σ_v plane of symmetry. The fluorine forming one of the vertices of the expanded face of the distorted octahedron is on the left, the fluorine atom forming one of the vertices of the contracted face of the distorted octahedron is on the right. The maxima in the VSCC of the chlorine atom are denoted by solid circles. The projected positions of the out–of–plane fluorine nuclei are marked by open crosses.

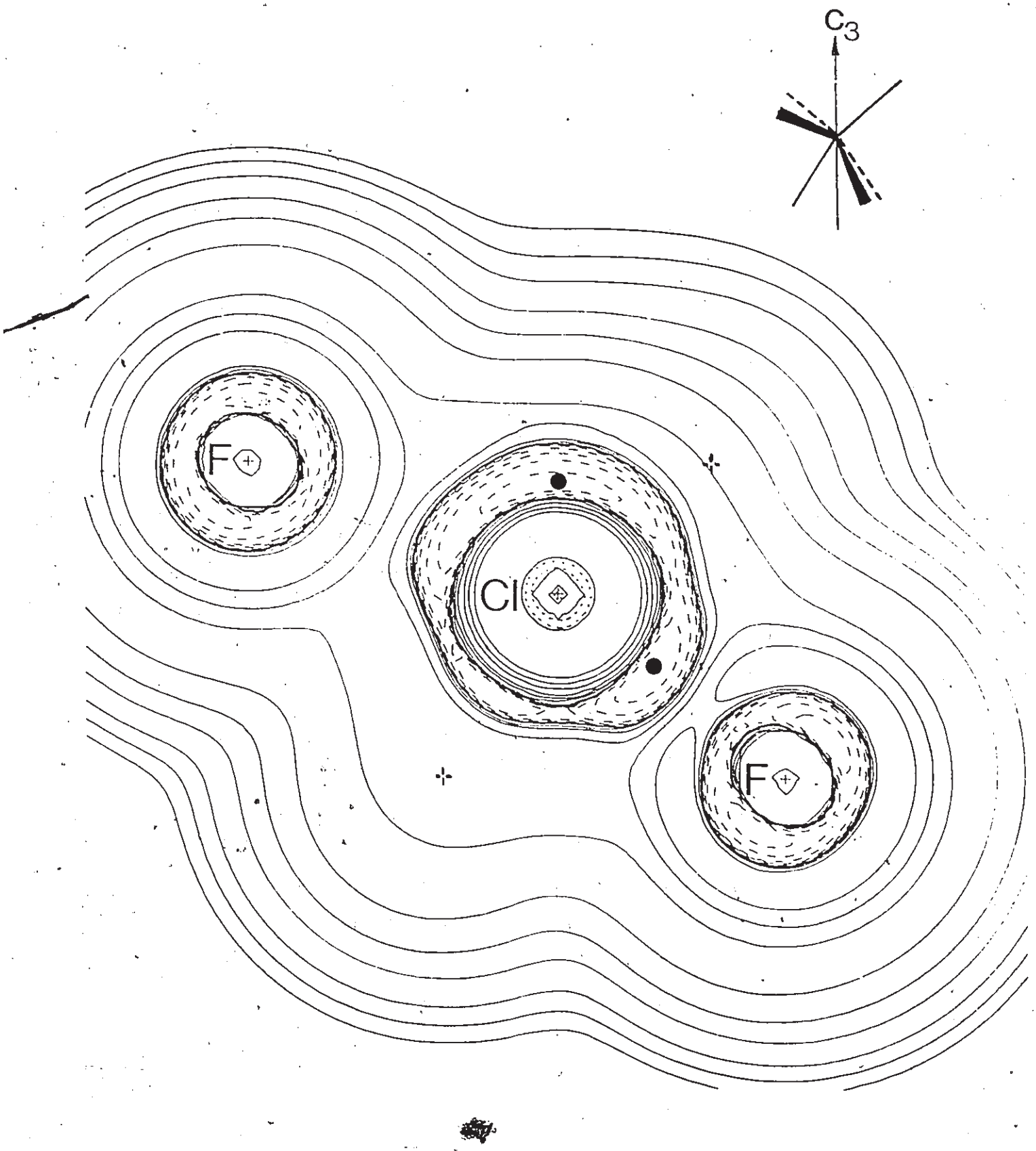
C3
F
Cl
F

Figure 2.16

Relief maps of the Laplacian distributions in SO_2 and ClF_5, derived from 6–21G* RHF calculations. The Laplacian is illustrated in the plane containing all three nuclei in SO_2, the axial plane is shown for ClF_5. The position of the shoulder on the bonded charge concentration associated with the S–O bond is indicated by an x. The position of the (3,–1) saddle point in the VSCC of the sulphur atom is marked by an s. The bonded maxima to the single axial fluorine in ClF_5 is opposite the nonbonded charge concentration and is noticeably larger in magnitude than the bonded maxima to the two equatorial fluorines shown in this plane.

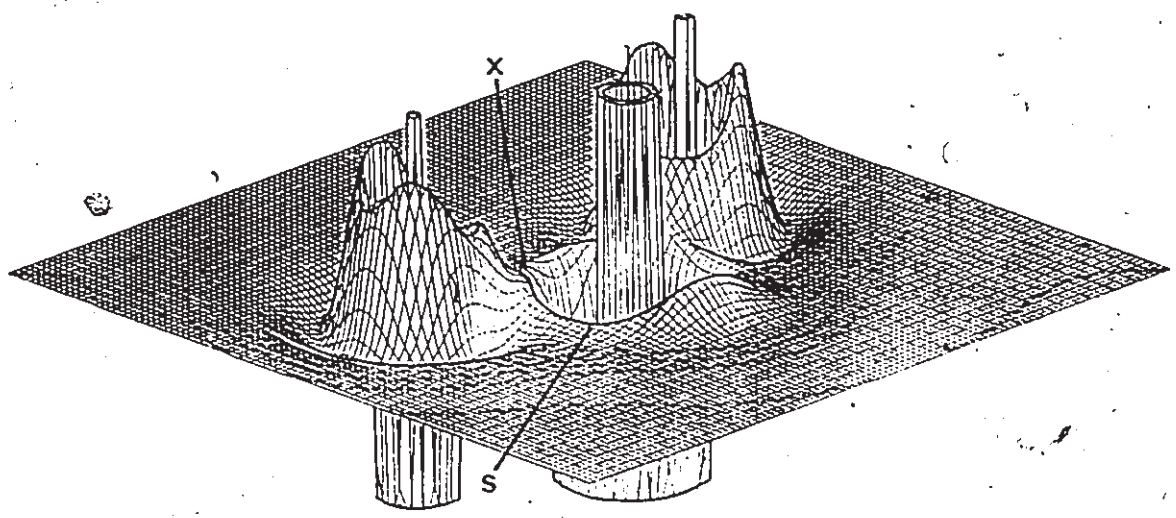

SO_2

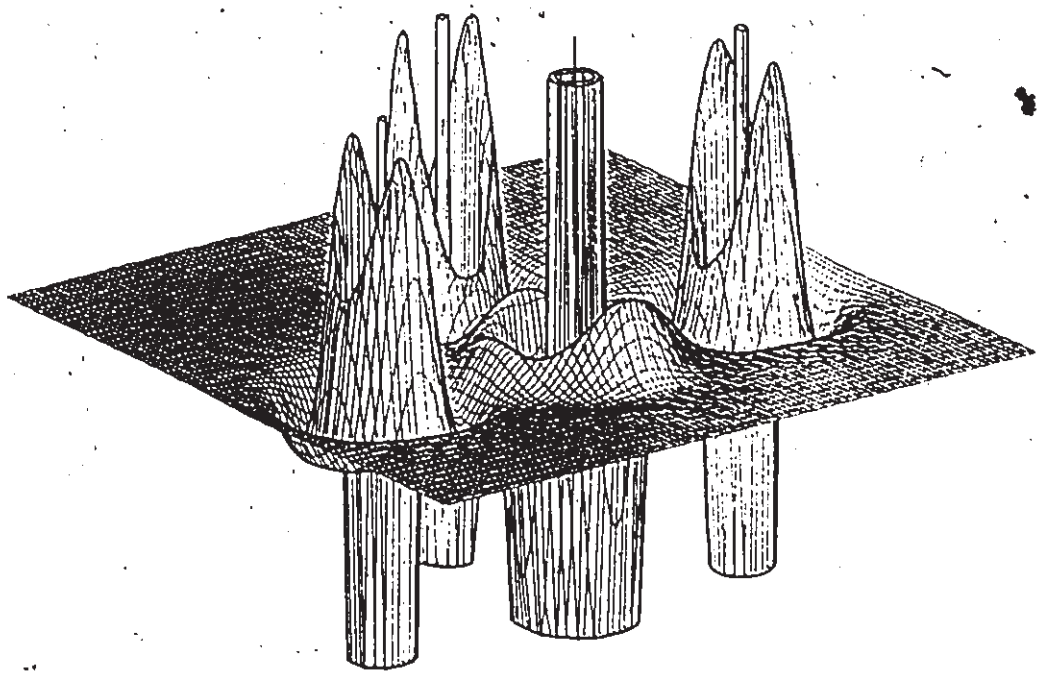

ClF_5

conjunction with sulphur's valence electrons (table 2.6). The S–O bond in this molecule is practically identical to the S–O bonds in sulphur dioxide, which will be discussed in a later subsection devoted to multiple bonds.

When the valency of the central atom is extended to seven pairs of electrons, such as in the anion ClF_6^- (MacDougall 1986), then the topology of the central atom's VSCC no longer concurs with the corresponding predictions of Sidgwick and Powell's extended version of the Lewis model. Figure 2.15 is a contour diagram of the Laplacian in a σ_v plane of symmetry of the anion in its equilibrium geometry. The geometry is that of a distorted octahedron with C_{3v} symmetry, see figure 2.15. One of the faces of the octahedron is expanded while the opposite face is contracted. This distortion is predicted by the VSEPR model of molecular geometry and will be discussed in the next section. Here we are concerned with the correlation between the topology of the VSCC and the Lewis model of atoms with expanded valence shells. As indicated in figure 2.15 the VSCC of the chlorine atom only exhibits a single nonbonded charge concentration in the expanded face of the octahedron, as well as one bonded charge concentration at each of the vertices of the contracted face of the octahedron. Thus the topology of the VSCC of the chlorine atom in ClF_6^- is homeomorphic with that of the nitrogen atom in NF_3. Opposite each of the three fluorine atoms that form the expanded face of the octahedron there is only a shoulder on the nonbonded charge concentration of the chlorine VSCC. The topologies summarized above indicate that the VSCC of a chlorine atom can accommodate up to six charge concentrations, but apparently there is not room for a seventh.

THE TOPOLOGY OF THE VSCC VERSUS THE LEWIS MODEL OF MULTIPLE BONDS

As do nitrogen and ethylene, sulphur dioxide only exhibits one bonded charge concentration per bond. In fact, not a single example of multiple bonded charge

concentrations for a given bond path has yet been observed. The VSCC of the sulphur atom also possesses a nonbonded charge concentration in accord with the Lewis model. As shown in figure 2.16, the bonded charge concentration that unites the VSCC's of the sulphur and oxygen atoms only exhibits a shoulder near the average radius of the VSCC of the sulphur atom. Since there is not a bonded (3,–3) critical point in the VSCC of the sulphur atom, the LOMCC that passes through the saddle point shown in figure 2.16 links the nonbonded charge concentration on sulphur to the bonded charge concentration on oxygen. Thus the surfaces of maximum charge concentration corresponding to the VSCC's of the oxygen and sulphur atoms are in direct contact with each other at the position of the bonded charge concentration that is common to the two atoms. Further migration of the VSCC surrounding the sulphur atom towards the oxygen will lead to vanishing of the saddle points, such as the one shown in the diagram, and an effective collapse of the VSCC of the sulphur atom to just the nonbonded charge concentration. This unequal sharing of the bonded charge concentration is indirectly related to the unequal sharing of the valence electrons (table 2.5). The observation of such a pronounced shoulder, it is just shy of being a local maximum, suggests that the within the context of the Lewis model the shared and ionic descriptions of the S–O bond strike a nearly perfect balance. Figure 2.16 also illustrates, in the σ_h plane, the two nonbonded maxima that are found in the VSCC of each oxygen atom.

ATOMS WITH UNPAIRED ELECTRONS

Lewis refered to atoms with unpaired electrons as being in an odd state. A study of the topological properties of the VSCC's of the carbon atoms in several substituted methylene systems, in both their singlet and triplet states, has been reported (MacDougall and Bader 1986). It is observed that singlet methylenes possess two bonded maxima and a single nonbonded maximum in the central carbon atom's.

VSCC forming a trigonal planar arrangement. Triplet methylenes possess two bonded maxima and a pair of nonbonded maxima in an approximately tetrahedral arrangement. Figure 2.17 illustrates these topological features of the different electronic states of the divalent carbon atom in difluoromethylene. Interestingly, the magnitude of charge concentration at each of the nonbonded charge concentrations in the triplet state of CF_2 is approximately half (54%) of the magnitude of the single nonbonded charge concentration in the singlet state.

SUMMARY OF THE CORRESPONDENCE BETWEEN THE VSCC AND THE LEWIS MODEL

We have seen that in nonpolar, saturated molecules the pattern of localized electron pairs anticipated on the basis of the Lewis model and the Sidgwick–Powell extended model, is duplicated by the pattern of charge concentrations in the VSCC's of a molecule's constituent atoms. As the polarity of a bond is increased, the migration of the bonded charge concentration on the electropositive atom towards its bonding partner is observed until it is completely absorbed into the VSCC of the more electronegative atom. The VSCC topologies of atoms forming bonds typical of the polar limit are mapped equally well onto the corresponding "tautomer" of the Lewis model, *i.e.* they exhibit incomplete valence shells. In molecules where the electrons in a suitably defined bonding loge are correlated with the remainder of the system to a greater extent than they are with each other, i.e. $\ell(\Omega) < 50\%$, then it appears that the Lewis model is not assimilated by the VSCC topology. Below this threshold of localization, the electron pair concept is unrecoverable in terms of a local concentration of charge. In unsaturated molecules the observed topological features of the VSCC's do not imitate the popular Lewis model. The topological properties of the VSCC's of atoms involved in multiple bonding, as well as analysis of the Fermi correlation in various definitions of the bonding loges, caution against any attempt to partition a multiple bond into bent bond or σ,π components.

Figure 2.17

Relief maps of the Laplacian distributions of the triplet (first excited) state of difluoromethylene and the singlet (ground) state of difluoromethylene, derived from single–determinantal UHF (triplet) and RHF (singlet) calculations using the 6–31G* basis set. The top figures illustrate the Laplacian in the σ_v planes of symmetry, the lower figures depict the Laplacian in the planes containing the fluorine nuclei as well as the carbon nucleus. The cut–off value in all of these figures is ±2.0 au. In the triplet state the (3,–1) saddle point along the line of maximum charge concentration (LOMCC) linking the two nonbonded maxima appears as a saddle in the σ_v plane, and as a maximum in the nuclear plane (labelled **a**). In the σ_v plane of the singlet state there is a pair of holes (labelled **h**) in the VSCC of the carbon atom forming an angle of approximately 120^0 with the single nonbonded maximum, subtended at the carbon nucleus. Since there is no lip to cross over between the outer regions and the core region of charge depletion along the direction indicated by the arrow, the VSCC of the carbon atom is not closed. The VSCC of the carbon atom in the triplet state is closed, there is no access to the core region from the outer regions that does not pass over a lip.

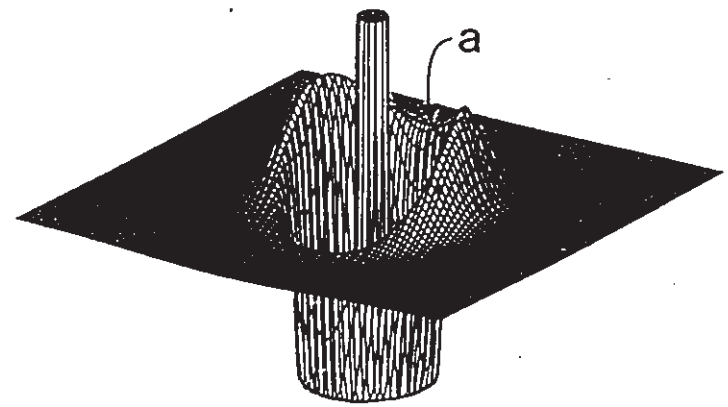

$^{3}CF_{2}$

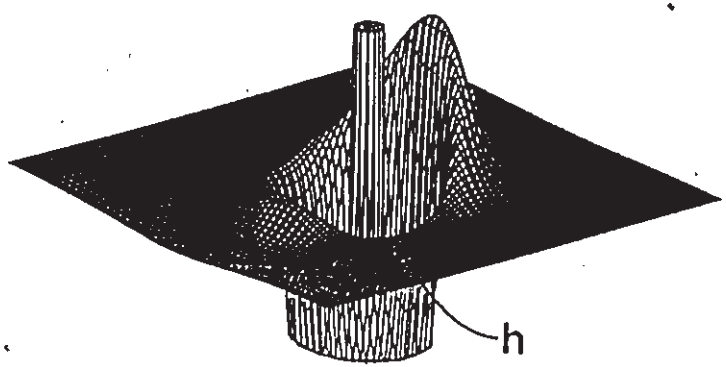

$^{1}CF_{2}$

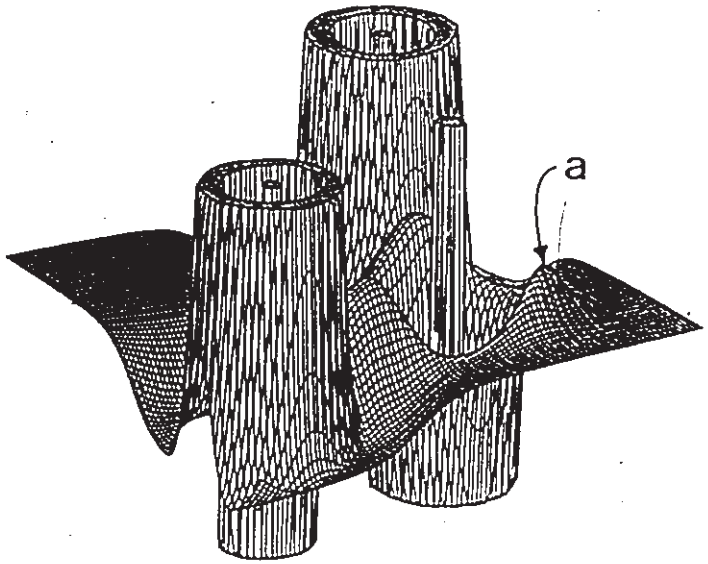

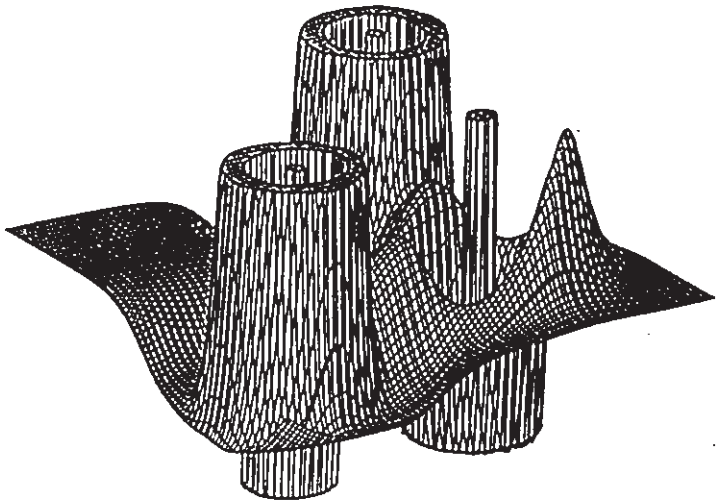

2.6 A PHYSICAL BASIS FOR THE VSEPR MODEL OF MOLECULAR GEOMETRY

In 1957 Gillespie and Nyholm extended and refined the Lewis and Sidgwick–Powell models of the valence shell electron pair arrangements into what has now become widely known as the *V*alence *S*hell *E*lectron *P*air *R*epulsion or VSEPR model of molecular geometry (Gillespie 1963, 1972). This model is finding its way into chemistry curricula because of its nonpareil ability to provide qualitatively correct predictions as well as simple explanations of many features of molecular geometry. The basic assumption of the model is that valence electrons are localized into pairs described as more or less inpenetrable charge clouds, and these pairs adopt an arrangement that maximizes the interpair separations. The principle factor governing the predicted molecular geometry is the number of electron pairs. The subsidiary postulates of the VSEPR model factor–in when the electron pairs are not equivalent. These postulates ascribe relative sizes to the valence shell electron pairs. In particular the lateral diffuseness of an electron pair determines how strongly it interacts with its neighbouring pairs. The region of space occupied by a pair of electrons is termed its domain. The first subsidiary postulate of the VSEPR model is that nonbonding or lone pairs have larger domains in the valence shell of a central atom than do bonding pairs in the same valence shell. Secondly, bonding pair domains in the valence shell of a central atom decrease in size with increasing electronegativity of the ligand, and increase in size with increasing electronegativity of the central atom. Lastly, triple bond domains are larger than double bond domains, which in turn are larger than single bond domains. The subsidiary postulates above serve to establish the relative sizes of the electron pair domains in a given molecule or a series of molecules. The geometries of the molecules are then determined by requiring maximum separation of the domains, or minimum overlap of their mostly inpenetrable charge clouds. This results in a hierarchy of interpair interactions that decrease in importance in the order

lone pair – lone pair > lone pair – bond pair > bond pair – bond pair. The physical basis for each of these postulates will be presented in the following subsections. However, we have already shown that valence electrons are not separately localized into pairs and that the operation of the Pauli exclusion principle in conjunction with the ligand field only leads to partial localization of the valence density into pairs. This partial localization is related to the formation of local concentrations of charge in an atoms VSCC. It is these charge concentrations that are postulated here to be the physical expression of the Lewis model and thus are the entities with which we will test the tenets of the VSEPR model.

TEST OF THE RELATIVE DOMAIN SIZES OF BONDED AND NONBONDED PAIRS

In the following discussions we are concerned with whether or not the spatial properties ascribed to the electron pair domains accurately describe the observed sizes and shapes of the bonded and nonbonded charge concentrations, which are the physical entities which simulate the role of the electron pairs of the Lewis and VSEPR models. The molecules ClF_3 and SF_4 contain five charge concentrations in the valence shells of their respective central atoms. In both cases there are both bonded and nonbonded types. Five pairs are maximally separated in a valence shell when they are arranged in a trigonal bipyramid fashion, which contains nonequivalent equatorial (three) and axial (two) sites. Thus different relative arrangements of the bonded and nonbonded charge concentrations lead to different geometries in these molecules.

In ClF_3 there are three possible arrangements of the charge concentrations that maintain the basic trigonal bipyramidal shape. They are: 1) both nonbonded charge concentrations in the equatorial plane 2) both nonbonded charge concentrations in axial positions 3) one nonbonded charge concentration in an axial position and one in the equatorial plane (table 2.6). In agreement with experiment (Smith 1953),

employment of the VSEPR model leads one to predict that arrangement #1 will be the most stable because it minimizes the number of 90° lone pair – lone pair interactions (zero) as well as the number of 90° lone pair – bond pair interactions (four). The second most stable arrangement is predicted to be #2 above because it possesses zero lone pair – lone pair interactions but six 90° lone pair – bond pair interactions. The least stable arrangement above is predicted to be #3 since it contains a 90° lone pair – lone pair interaction, which is postulated to be the most repulsive. We will now test this predicted ordering of the stability of the possible arrangements.

Further supporting the claim that the charge concentrations in the VSCC of the central atom are the physical entities which simulate the role of the localized electron pairs central to the VSEPR model, the three anticipated arrangements of the charge concentrations in the VSCC of the chlorine atom described above are indeed found when the geometry of the molecule is optimized to conform to that dictated by each assumed arrangement of electron pairs. The calculations discussed here are the same as reported in the previous section. Table 2.6 schematically illustrates the geometries of ClF_3 that were studied as well as the topological properties of the chlorine VSCC in each geometry. The equilibrium T–shaped geometry (experimental parameters in parentheses) was completely optimized and found to possess axial and equatorial bond lengths of 1.682 (1.70) and 1.607 Å (1.60), respectively. The FClF bond angle was found to be slightly acute at 85.36° (87.5°). The Hartree–Fock energy at this geometry is –757.03423 hartrees. This geometry corresponds within the VSEPR model to placing both of the lone pairs in the equatorial plane. As discussed in section 2.5 and illustrated in figure 2.13, the topology of the chlorine VSCC is in complete accord with the model. The geometry that corresponds to placing both lone pairs in axial positions was generated by optimizing the Cl–F bond lengths while constraining the molecule to D_{3h} symmetry. The calculated bond length is 1.709 Å and this geometry is 45.7 kcal/mole less stable than the T–shaped one. The locations of the charge

concentrations in the VSCC of the chlorine atom are precisely as anticipated in the second possibility listed above. The geometry that corresponds to placing the lone pairs in one axial and one equatorial position was found to be a local minimum on the C_s symmetry restricted potential energy surface of ClF_3 with the additional constraint that one FClF bond angle was constrained to be 120^0, this corresponds to the angle subtended at the Cl atom by the two equatorial Cl–F bonds. This tripod–like geometry (table 2.6) possesses axial and equatorial bond lengths of 1.678 and 1.718 Å, respectively. The unconstrained axial–equatorial bond angle is 80.6^0. This geometry is 63.0 kcal/mole less stable than the equilibrium geometry. The locations of the two nonbonded charge concentrations in the VSCC of chlorine are now considerably displaced from their anticipated "axial" and "equatorial" positions because of the obtuse angle (134.2^0) formed between them. The calculated energies of these stereoisomers are in agreement with the resultant prediction of the VSEPR model. We will now discuss in detail the sizes of the charge concentrations in relation to their postulated effect on the molecular geometry.

One could integrate the volume of a VSCC associated with a given (3,–3) critical point[10] and define this as the size of the charge concentration. This would be a very time consuming task. Instead we characterize the size of the charge concentration by two parameters, a surface area and a "thickness". The first parameter is defined as the portion of the surface of a sphere with a radius (r_A) equal to the distance from the maximum to the nucleus and bounded by a cone subtending an angle α at the nucleus (see diagrams for NH_3 and PH_3 in figure 2.10). This area is given by the expression $2\pi r_A{}^2[1 - \cos(\alpha/2)]$. The angle α is the average angle swept across a charge concentration from edge to edge. The edges are determined by neighbouring (3,–1) or (3,+1) critical points in the VSCC or points where $\nabla^2\rho = 0$ if charge is locally depleted

[10]Just as a nucleus is an attractor in the field $\nabla\rho(r)$, the (3,–3) critical points in a VSCC are attractors in the field $\nabla(-\nabla^2\rho(r))$. The portion of a VSCC that is associated with a given maximum is defined as that part of the VSCC that is traversed by gradient paths in the function $-\nabla^2\rho(r)$ which terminate at that maximum.

at the neighbouring critical point. The second parameter, λ_3, is the radial curvature in $\nabla^2\rho(r)$ at the maximum, *i.e.* $\lambda_3 \approx \partial^2(-\nabla^2\rho)/\partial r_A^2$. It is a measure of the radial thickness of the charge concentration, a high radial curvature indicates a thin, contracted shell, and a low radial curvature indicates a thick, expanded shell. Examination of both size parameters (tables 2.5 and 2.6) of the charge concentrations of a given VSCC indicates that in every case a nonbonded charge concentration is broader and more radially contracted than a bonded charge concentration. This is in complete consonance with the VSEPR postulate that bonded pairs possess smaller domains in the valence shell of a given atom than do nonbonded ones because bonded pairs are shared between two atoms.

The intermaxima angles listed in table 2.6 for each of the geometries of ClF_3 suggest that the relative sizes of the charge concentrations do indeed have a dominant effect in the determination of molecular geometry. For instance, the tripod–like geometry attempts to force the nonbonded charge concentrations into a proximate interaction. However, the apparent inpenetrability of the charge concentrations keeps the nonbonded charge concentrations 134.2^0 apart, only 14^0 closer together than in the unconstrained geometry yet the energy is less stable by 63.0 kcal/mole. The sizes of the nonbonded charge concentrations also has a direct effect on the Cl–F bond lengths. The smallest nClb angles in each of the three geometries are 96.5^0, 90.0^0 and 76.5^0, ordered according to decreasing stability of the corresponding molecular geometry. These correspond, respectively, to the longest Cl–F bonds in each molecule 1.682, 1.709 and 1.718 Å. This relationship between charge concentration size and molecular geometry parallels the VSEPR model's predication of molecular geometry on electron pair domain sizes.

The influence of charge concentration size on molecular geometry was examined for the SF_4 molecule to further establish that the properties of a central atom's VSCC provide the physical basis of the VSEPR model. There are only two possible electron

pair arrangements based on the Lewis model of SF_4, one placing the lone pair in an axial position and the other placing the lone pair in the equatorial position. The VSEPR model predicts the latter geometry to be the most stable because the larger lone pair is in a less crowded equatorial site. This is the experimentally determined geometry (Tolles and Gwinn 1962). The calculated equilibrium geometry (experimental parameters in parentheses) of SF_4 is found to possess axial and equatorial S–F bond lengths of 1.623 (1.646) and 1.556 Å (1.545), respectively. The FSF bond angle in the equatorial plane is 102.6° (101.5°), the FSF bond angle in the axial plane is 169.2° (173.1°) where the axial ligands are displaced away from the nonbonded side of the molecule. The Hartree–Fock energy of SF_4 at its equilibrium geometry is found to be –794.56437 hartrees. The less stable geometry was obtained by a C_{3v} symmetry constrained geometry optimization. The sole axial bond length is shortened to 1.587 Å while the three equatorial bond lengths are now longer than the axial one at 1.616 Å. The FSF bond angle in the axial plane, 83.1°, indicates a stronger distortion from trigonal bipyramidal shape than did the equilibrium geometry. This geometry exhibits a more crowded arrangement of the charge concentrations in the VSCC of the sulphur atom, there are three 99° dominant nSb angles compared to two 99° nSb angles in the equilibrium geometry (table 2.6). This results, however, in a considerably lower loss of stability than calculated for ClF3 when its VSCC was rearranged.

The difference in energy between the most and least stable trigonal bipyramidal arrangements of the charge concentrations in SF_4 is 32.9 kcal/mole, half of the corresponding value for ClF_3. We can interpret this as a more "penetrable" nature of the charge concentrations in the VSCC of the sulphur atom, particularly the nonbonded one. The sulphur atom in SF_4 has a larger valence shell than the chlorine atom in ClF_3 ($r_S \approx 0.71$ Å vs. $r_{Cl} \approx 0.67$ Å), hence the single nonbonded charge concentration is considerably expanded relative to the size of the corresponding pair of

charge concentrations in ClF_3. If we refer back to the discussion of the local expression of the virial theorem (equation 2.25) and the interpretation of the value of $-\nabla^2\rho(\mathbf{r})$ as a measure of some local residual pressure, then the relative extents of local charge concentration at the positions of the (3,–3) critical points associated with these nonbonded maxima (table 2.6) similarly describe those in the VSCC of the sulphur atom as more expanded.

Focusing on the values of $-\nabla^2\rho$ at the critical points associated with bonded and nonbonded charge concentrations indicates an interestingly opposite behaviour of these two features in reaction to increased crowding. When a nonbonded charge concentration is found in a more crowded position, such as the axial positions in both the D_{3h} and the tripod–like geometries of ClF_3, then it exhibits a higher value of $-\nabla^2\rho(r_c)$ indicating a more compressed state. Within the VSCC of the chlorine atom in the tripod–like geometry there are two different nonbonded maxima. Table 2.6 verifies that the axial nonbonded charge concentration is more compressed than the less crowded equatorial one. Similarly, in SF_4 the nonbonded charge concentration is observed to be slightly more compressed when it is in the axial position. In terms of size, the intermaxima angles suggest that only small changes occur. In fact the thickness parameter, λ_3, indicates that nonbonded charge concentrations are thicker in more crowded positions. The converse behaviour is observed for bonded charge concentrations. Whenever a bonded charge concentration is in a more crowded position it is observed to be expanded in the local pressure sense. This observation can be interpreted as the physical basis for the VSEPR argument that as a bonded pair domain is "squeezed" by neighbouring pairs in the valence shell of the central atom the domain merely "inflates" at the other end, which is in the valence shell of the ligand. Thus the VSEPR model predicts that ligands which share bonding pairs that are more crowded in the valence shell of the central atom should exhibit a charge gain relative to the ligands bonded via less crowded pairs. The net atomic charges on the axial and

equatorial fluorine atoms in ClF_3, SF_4, SF_4O and ClF_5 substantiate this prediction (table 2.6). Since nonbonded charge concentrations are not shared by other atoms, when they are found in more crowded positions they exhibit signs of compression. However, when bonded charge concentrations are found in more crowded positions they exhibit signs of expansion. Ligands that are associated with bonded charge concentrations that are relatively crowded in the VSCC of the central atom possess more negative atomic charges. Again, these observations are in perfect consonance with the reasoning of the VSEPR model.

The logical inversion of the mechanism that causes a given ligand to exhibit a larger or smaller net atomic charge is that the electronegativity of a ligand influences the size of the bonding pair domain within the valence shell of the central atom. This is the second subsidiary postulate of the VSEPR model. We will now investigate whether this aspect of the model has a physical basis in the properties of the Laplacian as well.

TEST OF THE POSTULATED BOND IONICITY – DOMAIN SIZE RELATIONSHIP

The behaviour of bonded charge concentrations that is observed as the bond ionicity is increased from A–X to $A^+ X^-$ was discussed in section 2.5. It was observed that a charge concentration for a shared interaction, *i.e.* one in which there exists a contiguous region of charge concentration adjoining the VSCC's of the bonded atoms, exhibits two maxima one in the VSCC of each bonded atom. As the ionic character of the bond is increased the charge concentration becomes asymmetric and the maxima in the VSCC of the electropositive atom is observed to migrate towards the more electronegative atom, see figure 2.10. The progression of the bond ionicity reaches a point at which the two bonded maxima coalesce to create a single maximum in the VSCC of the more electronegative atom, *i.e.* the S–O bonds in SO_2 and SF_4O are just

beyond such a "catastrophe point"[11]. Beyond this point it is no longer possible to talk about the properties of the bonded charge concentration on A, let alone the electron pair domain. Thus the second postulate of the VSEPR model corresponds to Lewis' discussion (1916) of the relative importance of the possible limiting descriptions of a given bond. The VSEPR model, however, further predicts that this effect will in turn have geometrical consequences. Correspondingly, we can quantitatively examine the sizes of bonded charge concentrations of differing ionicity.

Table 2.5 contains data that illustrate the effect on molecular geometry and bonded charge concentration size of substituting both A and X for more and less electronegative elements. The net charges on X are tabulated to scale the extent to which the bond ionicity has been altered. The effect on the size of the bonded charge concentration on the central atom is easiest to see for changes of X. Substituting fluorine for hydrogen in NX_3 leads to a decrease of 36% in the size of the bonded charge concentration on nitrogen. The XNX bond angle correspondingly narrows from 105.7^0 to 102.5^0. It appears that the electrostatic repulsion between the negatively charged fluorine ligands dampens the full effect of the reduction in size of the bonded charge concentrations, since the bonded charge concentrations on nitrogen form a bNb angle of 97.6^0 in NF_3 compared to 104.4^0 in NH_3 (virtually equal to the HNH bond angle). Similarly, when fluorine replaces chlorine in ClX_2^+ the bonded charge concentration on the central chlorine is reduced in size by 55% and the XClX bond angle narrows from 106.3^0 to 100.2^0. The bClb angle is essentially equal to the FClF angle in this case, but the fluorine atoms possess a net charge of only –0.18e. The VSEPR model assumes that interactions between the ligands are of minor importance in determining molecular geometry. The success of the VSEPR model seen so far and

[11]The topology of the Laplacian can exhibit stable and unstable structures in complete analogy with the charge distribution. The dynamics of the topology of the Laplacian have not yet been explored.

documented in the literature. (Gillespie 1963, 1972) supports this assumption. However, when fluorine replaces hydrogen in PX_3, the interaction between the ligands determines the resulting geometric change. The VSEPR model predicts that the XPX bond angle should decrease, in fact the bond angle widens from 95.4° in PH_3 to 97.5° in PF_3. Since a bonded charge concentration no longer exists in the VSCC of the phosphorus atom (figure 2.10), this bond angle widening can not be rationalized on the basis of the properties of the VSCC of the central atom. The net charges on the ligands have increased from q(H) = –0.63e in PH_3 to q(F) = –0.90e in PF_3. Thus to maintain the postulate that molecular geometries are in fact governed by the interactions between local charge concentrations, we may argue that in the case of PF_3 the dominant interaction between charge concentrations is between the nonbonded charge concentrations on the ligands.

To estimate the effect on the size of the bonded charge concentration on a central atom when its own electronegativity changes is more difficult to model. Consider the change in the HAH bond angle in AH_2 when sulphur replaces oxygen as the central atom, HOH = 103.8° and HSH = 94.3°. The relative sizes of the bonded charge concentrations on oxygen and sulphur do not directly agree with the observed change in geometry, the bonded charge concentration on sulphur is nearly three times as large as that on oxygen. One must also take into account that the nonbonded charge concentrations are simultaneously expanding when the central atom is replaced by one from a lower position in the periodic table. Thus if we compare the relative fractions of the central atom's VSCC associated with the bonded maxima to each hydrogen ligand we find that the fraction does decrease from 15% to 13% when sulphur replaces oxygen. Similarly, the HAH bond angle in AH_3 decreases from 105.7° to 95.4° when nitrogen is replaced by phosphorus as the central atom. While the bonded charge concentration on phosphorus is more than twice as large as that on nitrogen, the relative fractions of the VSCC are 14% and 22%, respectively.

TEST OF THE POSTULATED SIZES OF SINGLE, DOUBLE AND TRIPLE BOND DOMAINS

The VSEPR model's third subsidiary postulate is that the bonding domain sizes of single, double and triple bonds increase in that order. Again, to test whether or not there is a physical basis for this postulate we will examine the properties of the bonded charge concentrations of single, double and triple bonds. Currently, the only type of bond for which all of these sizes are available is the C–C bond for which the single, double and triple bonded charge concentration sizes are 0.62, 1.24 and 1.97 $Å^2$ in ethane, ethylene and acetylene, respectively[12]. These sizes deviate from a perfect ratio of 1 : 2 : 3 by a maximum of 4%. The size of the nonbonded charge concentration in the VSCC of the carbon atom in the singlet state of methylene is 0.94 $Å^2$, which according to the linear relationship noted above is as big as 1.5 bonding pairs. This ordering of size is not limited to hydrocarbons, although the linear relationship is not expected to be a general one. Tables 2.5 and 2.6 indicate that the sizes of single (S–F) bonded charge concentrations are a fraction of the sizes of the double (S–O) bonded charge concentrations, and that the nonbonded charge concentration in the VSCC of sulphur in SO_2 is intermediate.

The bond angle in sulphur dioxide is calculated to be 118.7°, close to the experimental value of 119.5° (Kivelson 1954). Thus the two larger double bonded charge concentrations, at first glance, appear to have a stereochemical effect slightly in reverse to that expected. However, the size of a double bonded charge concentration reflects its overall size, the OSO bond angle is determined primarily by the size of the double bonded charge concentration in the plane of the bonds. The double bonded charge concentrations in SO_2 exhibit an elliptical distortion in a direction

[12]These sizes are determined in the same manner as those reported in tables 2.5 and 2.6. However, the 6–31G** basis set was used in the RHF calculations of ethane, ethylene and acetylene. This basis set yields properties of the charge concentrations that differ from those determined using the 6–21G** basis set by a small amount (Bader, MacDougall and Lau 1984)

perpendicular to the plane of the nuclei, thus they do not take up as much room in the plane of the nuclei as if they were axially symmetric. The angle α describing the size of the S–O bonded charge concentration is only 90^0 in the plane of the nuclei and 140^0 in the "π plane". The double bonded charge concentration in SF_4O is elliptically distorted also. It subtends an angle, $\alpha = 150^0$, at the sulphur nucleus in the equatorial plane, while the corresponding angle in the axial plane is only 114^0. Thus, as predicted by the VSEPR model the π plane is on its side in the equatorial plane.

THE REMAINING POSTULATE OF A MODIFIED VSEPR MODEL

Within the VSEPR model the hierarchy of interpair interactions is predicated on the relative sizes of the electron pair domains. We have shown that there is a physical basis for all of the postulates concerning the relative sizes of the electron pair domains. The charge concentrations that were demonstrated to be the physical expression of the Lewis model in section 2.5, have been shown in this section to assimilate all of the characteristics that are ascribed to electron pairs within the VSEPR model as well. Thus we can restate the VSEPR model by replacing the assumed localized electron pairs with the observable local charge concentrations. In fact a more accurate model could be developed by banking accumulated data regarding the sizes, shapes and energetic properties of the charge concentrations. However, there still remains a single postulate in this modified VSEPR model. This postulate is that the most stable geometry of a molecule is that which minimizes the interactions between the local concentrations of charge. As shown in section 2.4 the local maxima in charge concentration represent points in space where the pair distribution function partially localizes pairs of electrons to minimally overlapping regions of space. This was demonstrated for the methane molecule, where core and bonding electrons were demonstrated to be "fully" and partially localized, respectively. Figure 2.18 illustrates the Fermi holes of electrons in the ClF_3 molecule. The probe electron is located at one

of the nonbonded maxima on chlorine (a), the equatorial bonded maximum (b and d) and at one of the axial bonded maxima (c). When the probe electron is situated at a nonbonded maximum its *doppelgänger* is found to be maximally localized relative to neighbouring reference coordinates and clearly avoids the core, equatorial bonding and second nonbonding regions. The Fermi hole of a nonbonded electron is seen to be laterally spread out while the Fermi hole of a bonding electron is seen to be extended over the ligands. The relative characteristics of the bonded and nonbonded Fermi holes parallel those of the bonded and nonbonded charge concentrations. Comparison of maps b and d in figure 2.18 illustrates that the partially localized α,β pair corresponding to the equatorial Cl–F bond is axially symmetric, in contrast to the partially localized quartet of electrons corresponding to the double bond in ethylene (figure 2.12).

We will now investigate the corresponding degrees of partial localization of electrons and the overlap of their respective *doppelgängers* for molecules in geometries not representing optimum separation of the charge concentrations. First, figure 2.19a illustrates that an electron at the position of a nonbonded (3,–3) critical point in the VSCC of the nitrogen atom in ammonia is partially localized to a region of space that maximally avoids the core and bonding regions, but it is less localized than the *doppelgänger* of an electron positioned at the (3,–3) critical point of a bonded maximum (figure 2.19b). Figures c and d in 2.19 illustrate that in the planar geometry of ammonia, the *doppelgänger* of an electron situated one of the two equivalent (3,–3) nonbonded critical points is unable to avoid significant overlap with the Fermi holes of the bonding electrons. Thus the energy of repulsion between electrons of the same spin is minimized when their respective coordinates in the 3N–dimensional space of the total state function are equal to those of the (3,–3) critical points in the Laplacian. This observation is in complete consonance with Linnett's model (1964) and the essence of the VSEPR model (Gillespie 1963, 1972) except that it was arrived at via a

Figure 2.18

Fermi holes for various positions of the reference electron (marked by a star) in ClF_3, derived from a 6–21G* RHF calculation. (a) The reference electron is located at the position of one of the two nonbonded maxima. Its Fermi hole is shown in the equatorial plane of the molecule, the nuclei are labelled. (b) The reference electron is situated at the position of the bonded maximum to the equatorial fluorine. The Fermi hole is shown in the equatorial plane, and the nuclei are oriented as in a. (c) The reference electron is located at the position of a bonded maximum to an axial fluorine. Its Fermi hole is shown in the axial plane, the nuclei are labelled. (d) This is a view of the Fermi hole in b shown in the axial plane. The nuclei are arranged as in c. The Fermi hole associated with this Cl–F bond appears to be nearly axially symmetric.

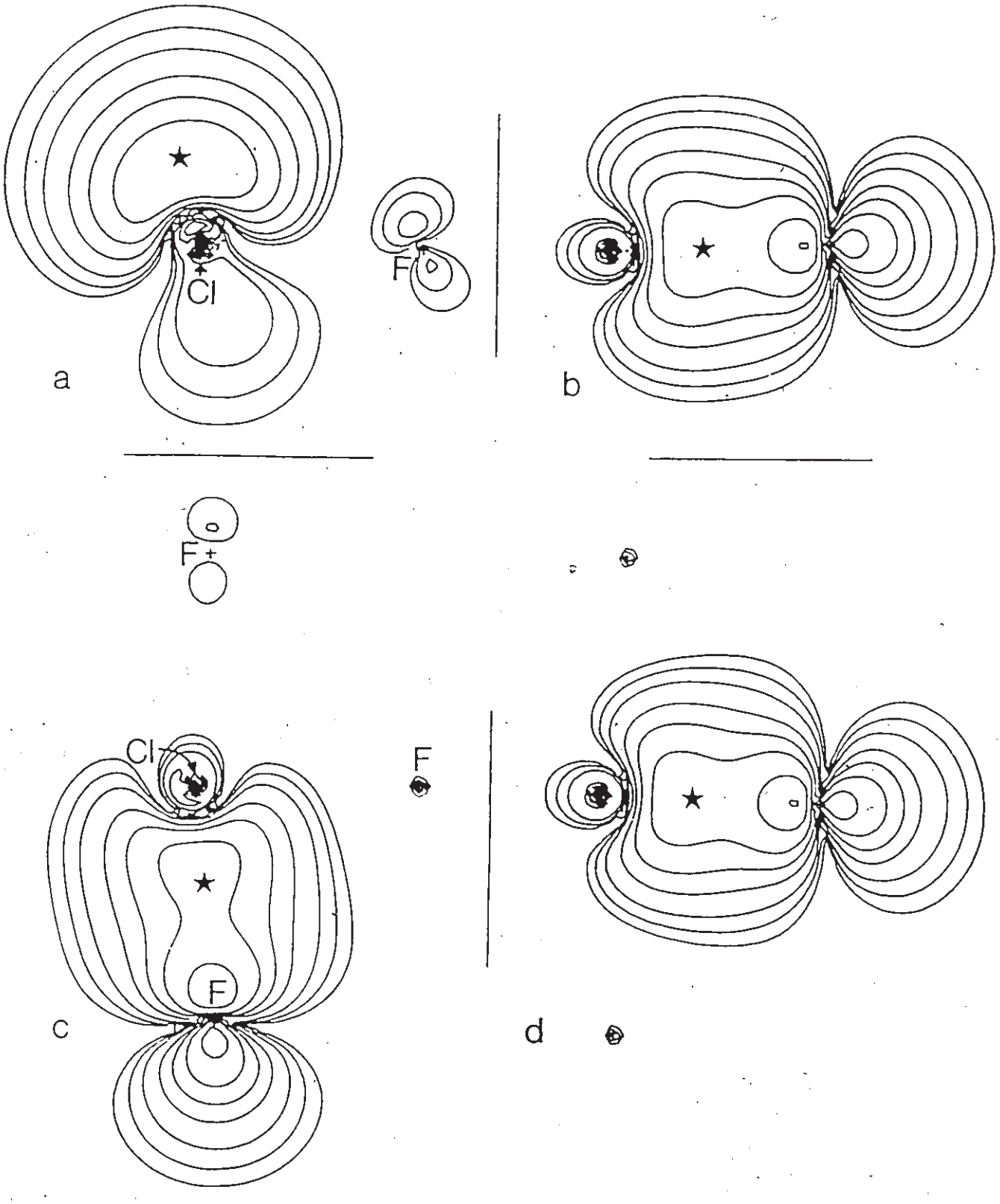
Cl
F
a
b
F
c
Cl
F
F
d

Figure 2.19

Fermi holes in pyramidal and planar ammonia, derived from a 6–31G** RHF calculation. The positions of the nitrogen nucleus and the in–plane hydrogen nucleus are denoted by solid circles. The projected positions of the out–of–plane hydrogen nuclei are marked by open circles. The nuclei are labelled in a. All figures depict the Fermi holes in a σ_v plane of symmetry. (a) The reference electron is situated at the nonbonded maximum in the optimized pyramidal geometry. (b) For the same geometry as in a, the reference electron is at the position of a bonded maximum. (c) The reference electron is situated at the position of the nonbonded maximum, while the molecule is in the planar geometry with an optimized N–H bond length. (d) For the same geometry as in c, the reference electron is placed at the position of a bonded maximum.

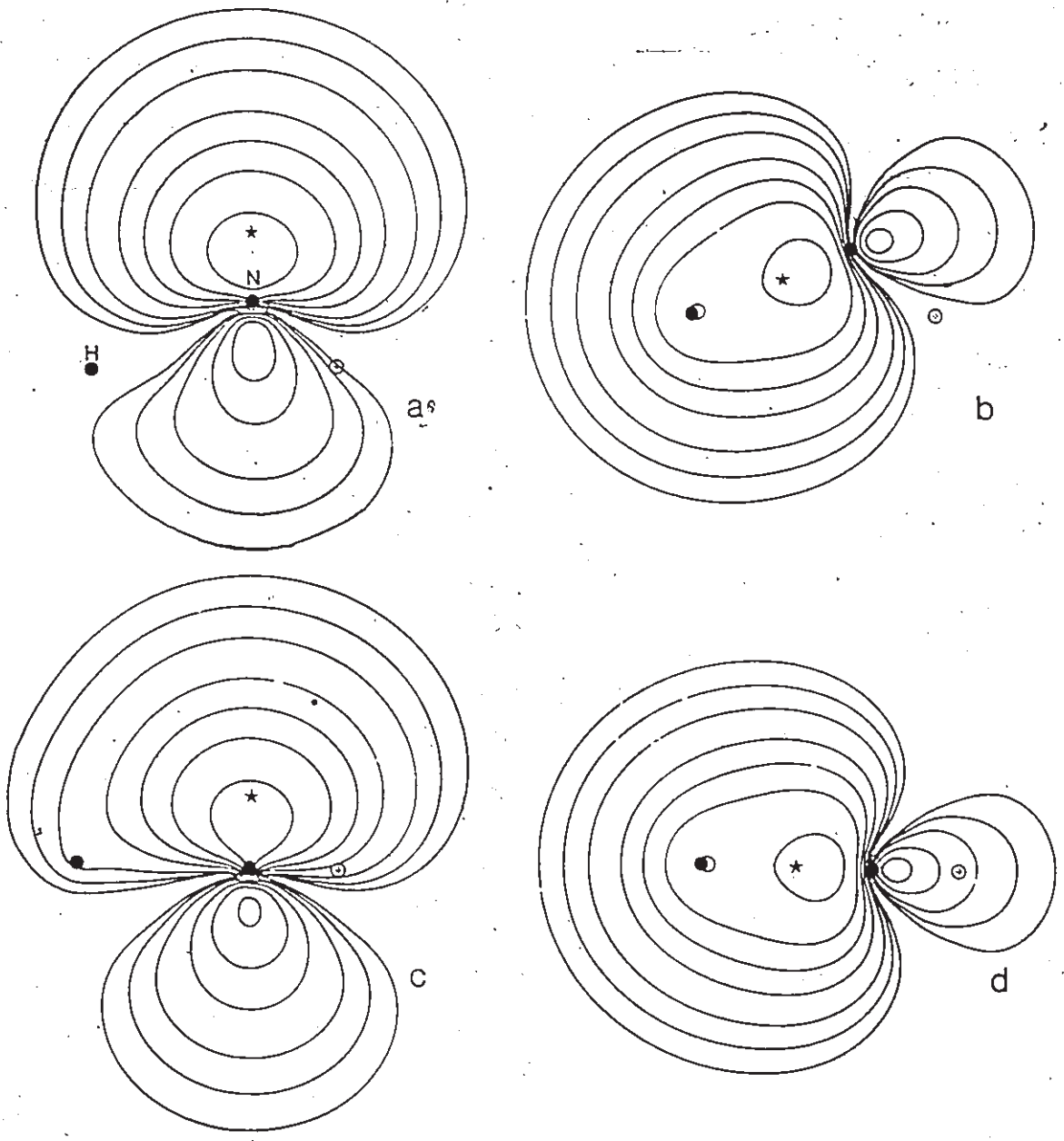
N
H
a
b
c
d

study of the observable Laplacian of the charge density and a very limited study of the pair density. The *caveat* that accompanies this observation, as well as Linnett's model, is that it does not describe average conditions. However, earlier we saw that the Fermi hole of an electron was relatively insensitive to motion of the electron in the vicinity of a charge concentration (figure 2.9), thus the diminished repulsion between electrons of like spin in the equilibrium geometry of a molecule applies to a finite region of the 3N–dimensional space spanned by the total state function. Furthermore, the property of the charge density used to identify the optimum set of coordinates of the electrons suggests that the above finite region does possibly describe average conditions. We can therefore postulate, with some physical justification, that the most stable geometry of a molecule corresponds to an optimum arrangement of the charge concentrations because a significant amount of the electron repulsion is minimized.

A CASE STUDY: THE MOLECULAR GEOMETRY OF ClF_3O

Single–determinant SCF calculations using the 6–21G* basis set (Binkley *et al.* 1983)[13] were carried out for the ClF_3O system. Within the modified VSEPR model the geometry is determined by the prefered arrangement of three Cl–F bonded charge concentrations, one Cl–O bonded charge concentration and one nonbonded charge concentration, all within the VSCC of the chlorine atom. There are four distinct arrangements of these five charge concentrations that are derived from a trigonal bipyramid. The modified VSEPR model orders these charge concentrations according to size as Cl–O (double) > nonbonded > Cl–F bonded. The order of the largest and second largest is based on observations of relative charge concentration sizes in SO_2

[13]The 6–21G* basis set used in these calculations is that contained in GAUSSIAN82. It differs from the basis set used in the earlier calculations only in that d–functions are included in the basis of second and third row atoms, while in the previous calculations using GAUSSIAN80, d–functions are not included in the atomic basis of second row atoms.

(table 2.5) and may be inappropriate for ClF_3O. An advantage of the modified VSEPR model is that observations continually add to the data base. Thus the predicted geometry of greatest stability, for reasons described above, is that which places the nonbonded and Cl–O bonded charge concentrations in the equatorial plane. This geometry has C_s symmetry. The three less stable arrangements of the charge concentrations place either or both the nonbonded and the Cl–O bonded charge concentrations in axial positions. The only one of these arrangements that we can reproduce in a calculation using symmetry constraints is that with the nonbonded and Cl–O bonded charge concentrations in axial positions, this geometry has C_{3v} symmetry. The optimized geometrical parameters and total energies of these geometries are listed in table 2.7 (the subscripts a and e refer to axial and equatorial). As predicted, the C_s geometry is the most stable. It is more stable by 48.0 kcal/mole. The original VSEPR model makes the same prediction. Now, however, we can observe the properties of the charge concentrations to check that each of our assumptions was correct.

Figure 2.20 depicts the Laplacian in the corresponding symmetry planes of ClF_3O in both the C_s and C_{3v} geometries. In each geometry there are indeed five charge concentrations, one bonded charge concentration associated with each Cl–F bond, one charge concentration associated with the Cl–O bond and a nonbonded charge concentration in the equatorial plane in the C_s geometry and in an axial position in the C_{3v} geometry. The data in table 2.7 indicate that our initial ordering of the relative sizes of the nonbonded and the Cl–O bonded charge concentrations based on data from SO_2 and SF_4O are not transferable to chlorine systems. The nonbonded charge concentration is found to be larger in size than the Cl–O bonded charge concentration in both geometries. This is reflected in the $OClF_e$ bond angle in the C_s geometry which is less than 120°. However in the C_{3v} geometry the equatorial fluorines are displaced from the equatorial plane away from the oxygen atom, opposite

Table 2.7. Bonded and Nonbonded Charge Concentrations on Cl in ClF_3O.

Geometry[a]	net atomic charges, e	type	properties of charge concentrations of VSCC of Cl[b] r_{Cl}, Å	$\nabla^2\rho(r_c)$	size, Å^2	intermaxima angles, deg.
C_s 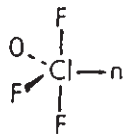	Cl, +2.859	n	0.600	1.832	1.48	$nClb_o$=138.6, $nClb_a$=89.5
	O, -1.118	b_o	0.648	1.060	1.33	$nClb_e$=116.5, b_oClb_a=97.0
	F_e, -0.547	b_e	0.668	0.646	0.70	b_oClb_e=104.9, b_eClb_a=81.2
	F_a, -0.597	b_a	0,682	0.414	0.41	
C_{3v} 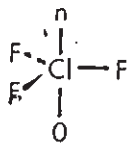	Cl, +2.790	n	0.602	1.633	1.59	$nClb_e$=80.9, b_eClb_e=117.5
	O, -1.134	b_o	0.655	1.066	1.46	b_oClb_e=99.1, $nClb_o$=180.0
	F_e, -0.552	b_e	0.650	0.420	0.50	

[a] C_s geometry: R(Cl-O) = 1.4184, $R(Cl-F_a)$ = 1.6372, $R(Cl-F_e)$ = 1.5591, $\alpha(OClF_e)$ = 110.13, $\alpha(OClF_a)$ = 95.15, $\alpha(F_eClF_a)$ = 84.72, all in Å and degrees, E(HF) = -831.774983 hatrees. C_{3v} geometry: R(Cl-O) = 1.4024, $R(Cl-F_e)$ = 1.6604, $\alpha(F_eClO)$ = 93.78, all in Å and degrees, E(HF) = -831.698421 hartrees.

[b] The first column gives the radial distance of the maximum of charge concentration from the Cl nucleus. The next column gives the value of $-\nabla^2\rho$ (in au) at this maximum, or (3,-3) critical point.

to the distortion expected from the relative sizes of the Cl–O bonded and the nonbonded charge concentrations. As found to occur in PF_3, when ligands with nonbonded charge concentrations within their own VSCC's are in close proximity, the interaction between these charge concentrations can compete with the interactions between the charge concentrations in the VSCC of the central atom. The sizes of the fluorine bonded charge concentrations are found to reflect their crowding. The most crowded fluorine bonded charge concentration is that corresponding to the axial fluorines in the C_s geometry, it has three $\approx 90^0$ interactions. Correspondingly, this charge concentration is the smallest in size. The net atomic charge on these two axial fluorines is the most negative of the three types of fluorine atoms, and the Cl–F_a bond length is the longest (table 2.7). The Cl–F bonded charge concentration that is the least crowded is the equatorial one in the C_s geometry, it has two $\approx 90^0$ interactions but only with axial fluorine bonded charge concentrations. Correspondingly, this bonded charge concentration is the largest in size, its associated fluorine atom has the least negative atomic charge, and the Cl–F_e bond length in the C_s geometry is the shortest of the Cl–F bonds. The equatorial Cl–F bonded charge concentrations in the C_{3v} geometry are intermediate in their degree of crowding, and correspondingly all of the parameters disussed above are intermediate in value.

The Fermi holes of electrons positioned at the coordinates of the maxima in the VSCC of the chlorine atom for the C_s and C_{3v} geometries are shown in figure 2.21 and 2.22, respectively. It may be of interest to note that the Fermi holes in these figures lack any significant density on the side of the chlorine nucleus opposite to the position of the probe electron, compared to the Fermi holes in figures 2.9 (methane) and 2.19 (ammonia) which exhibit density there in analogy with the minor lobe of a sp hybrid orbital. The density of a spd^2 hybrid orbital exhibits a significant diminishing of the minor lobe (Pauling 1960, p128). As in ClF_3, the Fermi holes associated with bonded maxima are most concentrated in the region of the ligand's VSCC. The shaded regions

in figures 2.21 and 2.22 illustrate the extent to which the Fermi holes of electrons situated at adjacent (3,–3) critical points overlap one another. Comparison of the figures supports the postulate that the optimum molecular geometry is that which maximally separates the local concentrations in the VSCC of the central atom. Figure 2.22b indicates that decreased separation of the charge concentrations results in a simultaneous increase in the overlap of the Fermi holes corresponding to adjacent charge concentrations, and an increase in delocalization of the most crowded charge concentration.

Figure 2.23 further demonstrates the general observation that an electron's *doppelgänger* is most localized and minimally overlapping other electrons of like spin when the reference coordinates of the electron are set to be the coordinates of (3,–3) critical points in $-\nabla^2\rho(r)$. The star indicates the coordinates of the probe electron, while the position of the nonbonded charge concentration is marked by a solid triangle. Again, the Fermi hole of an electron becomes maximally delocalized when the probe electron is situated at the boundaries of charge concentrations. The behaviour of the Fermi hole of an electron as it is moved slightly to either side of the nonbonded charge concentration on chlorine leads to an interesting observation. When the probe electron is situated off the nonbonded maximum towards the Cl–O bonded maximum, its *doppelgänger* spreads further towards the Cl–F_e bonded maximum. Similarly, when the probe electron is situated just off the nonbonded maximum towards the Cl–F_e bonded maximum its *doppelgänger* is spread further towards the Cl–O bonded maximum. This behaviour is analogous to the observations from figure 2.9, where it is seen that placing the probe electron at a slightly larger distance from the carbon nucleus in methane results in its *doppelgänger* spreading further into the core loge. We present here, for thought provoking purposes only, a possible explanation for these observations that makes use of the energetic properties of the Laplacian.

Figure 2.20

Contour diagrams and relief maps of the Laplacian distribution of ClF_3O in the equilibrium C_s (top pair of figures) and the C_{3v} geometry (lower pair of figures), derived from 6–21G* RHF calculations. The cut–off value of the relief maps is ±7.0 au. The projected positions of the out–of–plane fluorine nuclei are marked by open circles. The positions of (3,–3) critical points in $-\nabla^2\rho$ are denoted by solid circles.

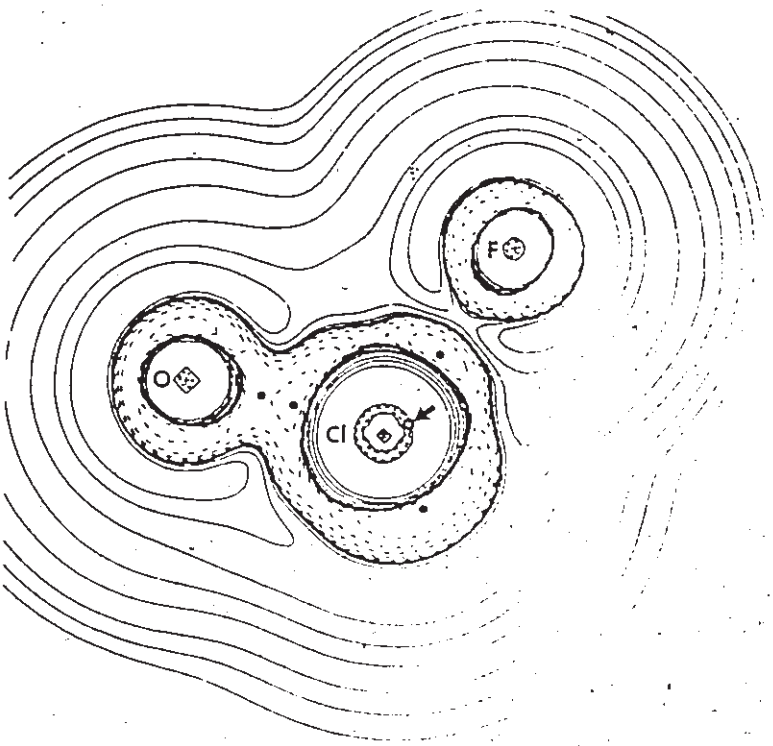
F
O
Cl

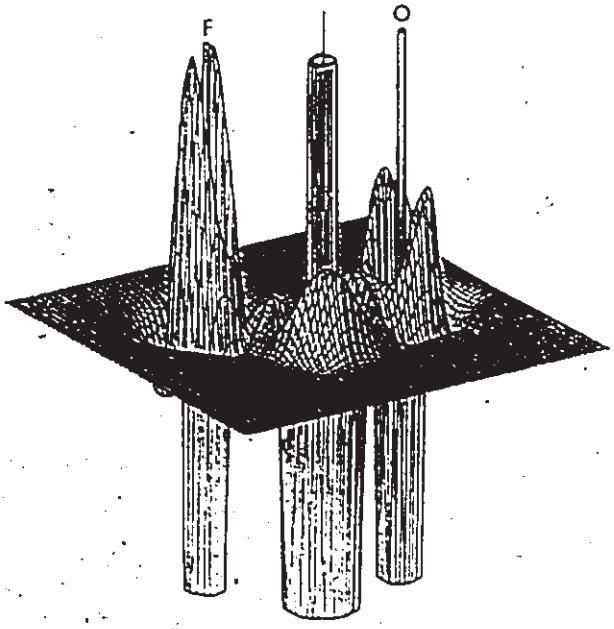
F
O

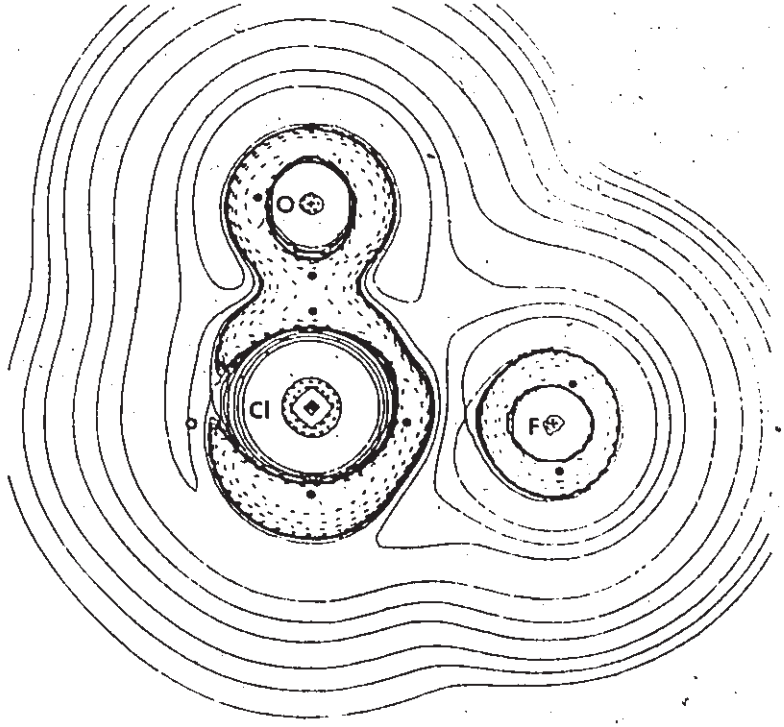
O
Cl
F

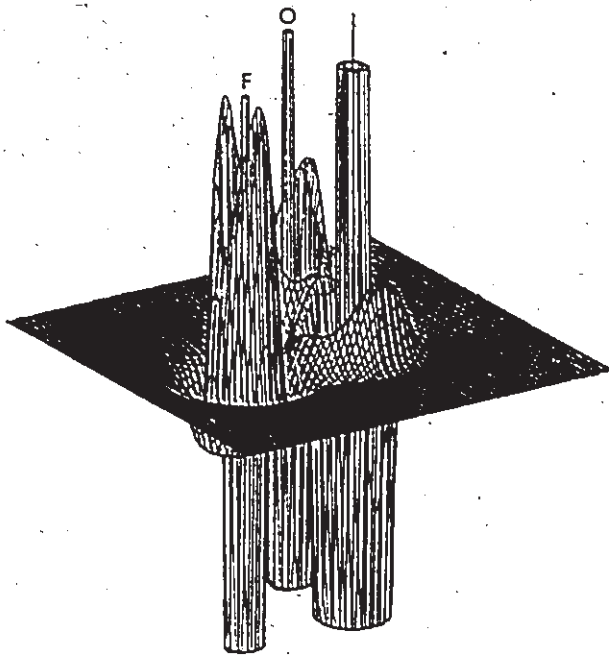
O
F

Figure 2.21

Fermi holes for various positions of the reference electron in the C_s geometry of ClF_3O. The position of the reference electron is denoted by a star. The positions of the in–plane nuclei are marked by solid circles, and the projected positions of the out–of–plane nuclei are shown by open circles. The position of the nonbonded maximum is marked by a solid triangle in maps a, c and d. The reference electron is at the bonded maximum to F_e in a, at the nonbonded maximum in b, at the bonded maximum to O in c, and at the bonded maximum to F_a in d. Maps a, b and c show the corresponding Fermi holes in the equatorial plane, the nuclei are labelled in a and shown in the same configuration in b and c. The plane shown in map d contains the chlorine nucleus, the bonded maximum to F_a and the nonbonded maximum on chlorine. The axial fluorine labelled is only slightly out of this plane. The stippled areas in each map show the regions of overlap with neighbouring Fermi holes, bounded by the –0.02 au contour. For example, the stippled areas in map a show the overlapping region of the Fermi hole in a with the Fermi holes in b and c. The stippled area in map d shows the overlap of the Fermi hole associated with the bonded maximum to F_a with the Fermi hole of the nonbonded maximum on chlorine (not shown in this plane but similar to that in map b).

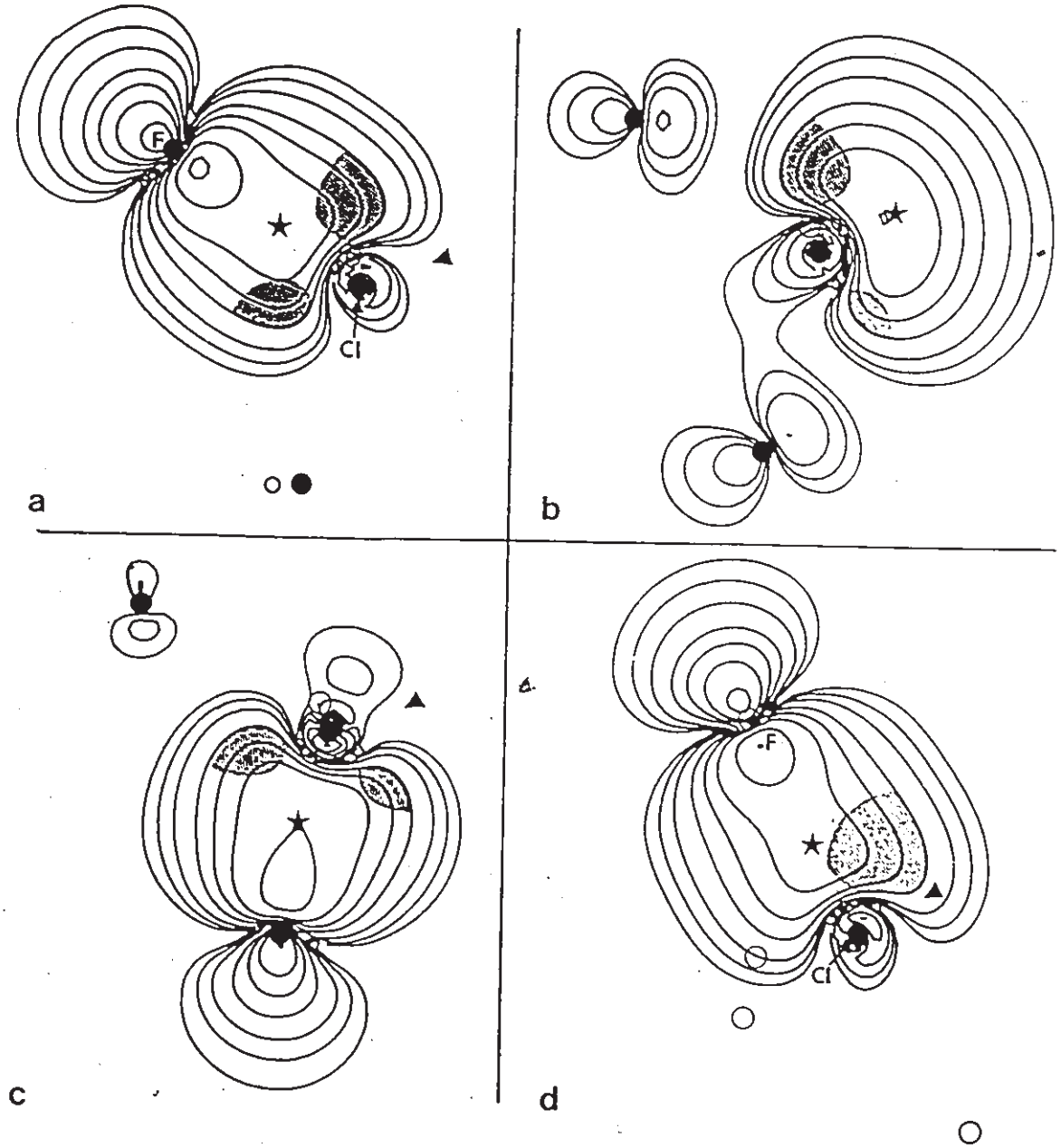
F
Cl
a
b
c
F
Cl
d

Figure 2.22

Fermi holes for various positions of the reference electron, marked by a star, for the C_{3v} geometry of ClF_3O. The maps show the Fermi hole density in the axial plane. The symbols and stippling represent the same features as in figure 2.21. The reference electron is at the nonbonded maximum on chlorine in a, the bonded maximum to F_e in b, and the bonded maximum to O in c. The overlap of the nonbonded Fermi hole with the Fermi hole associated with the bonded maxima to F_e is the largest overlap in this and the preceeding figure.

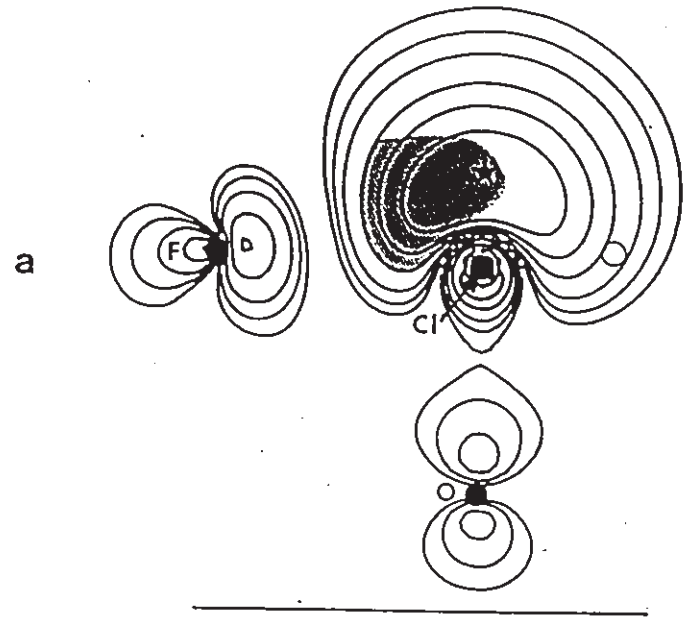
a
F
D
Cl

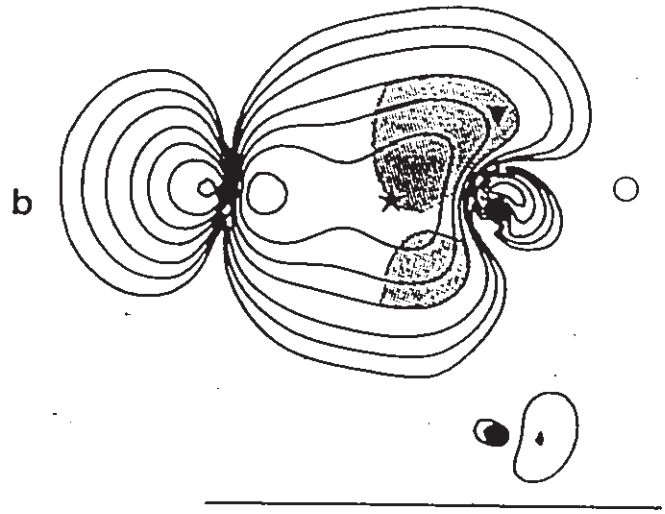
b

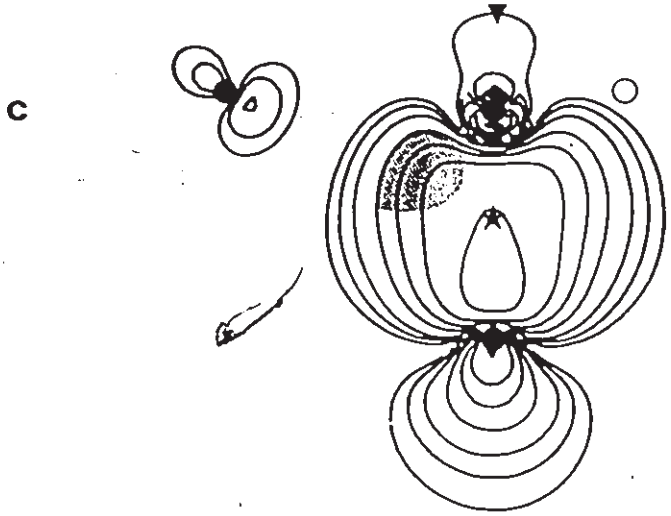
c

Figure 2.23

Fermi holes for positions of the reference electron at positions near the nonbonded maximum on chlorine in the equilibrium geometry of ClF_3O. All maps show the Fermi hole densities in the equatorial plane. The positions of the nuclei are labelled in a and held in the same configuration in b, c and d. The symbols represent the same features as in the previous two figures. The reference electron is moved 0.2 au away from the nonbonded maximum towards F_e in a, it is moved 0.2 au towards O in b. The reference electron is situated at the saddle point along the LOMCC linking the nonbonded maximum and the bonded maximum to F_e in c, and the corresponding saddle point linking the nonbonded charge concentration and the bonded charge concentration to O in d.

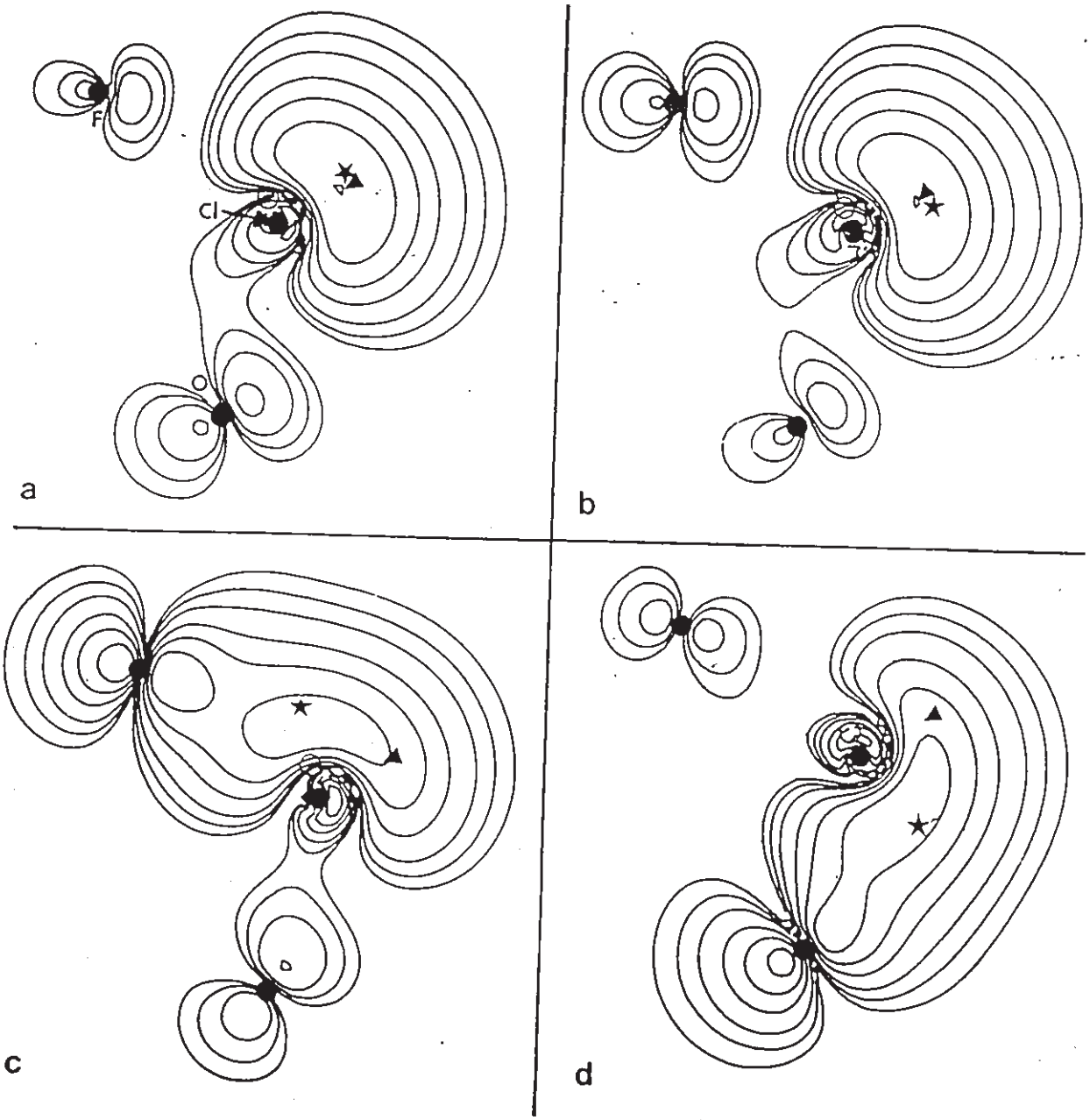
F
Cl
a
b
c
d

Recall that the Laplacian was interpreted as a measure of some residual pressure experienced by the charge density (equations 2.25a, 2.25b and related discussion). The gradient of the Laplacian, therefore, is related to the lines of force corresponding to this pressure. When a probe electron is situated just off the position of a (3,–3) critical point in $-\nabla^2\rho(\mathbf{r})$, this force is directed towards the maximum in opposition to the electron's displacement. Thus the observed spreading of an electron's Fermi hole in a direction opposite to its displacement from a nearby maximum is parallel to the direction of a force on the charge density. It is the nature of this force that is the key to the remaining postulate of the modified VSEPR model. Investigations of the relationship between the total force acting on an element of electronic charge, $-\nabla\cdot\overleftrightarrow{\sigma}(\mathbf{r})$, and the residual force, $(\hbar^2/4m)\nabla\nabla^2\rho(\mathbf{r})$, may provide insight into the physical basis of the only remaining postulate of the modified VSEPR model. An understanding of the nature of this effective force appears to be the last requirement for the development of a quantum mechanical theory of moleular geometry.

2.7 THE TOPOLOGY OF THE VSCC AND MODELS OF CHEMICAL REACTIVITY

The electron pair concept is central to models of chemical reactivity as well as models of molecular geometry. This chapter will conclude with brief discussions of observed correlations between the topological properties of the Laplacian and two models of chemical reactivity; Lewis acid–base reactions (Lewis 1923) and Fukui's frontier orbital theory (Fukui 1971). The relationship between the Laplacian and models of chemical reactivity is not as thoroughly developed as what we have seen so far in this chapter. The key observations that suggest there is a physical basis for these reactivity models will be presented; as well we shall identify the missing components of a quantum mechanical theory of chemical reactivity.

THE LEWIS MODEL OF ACID–BASE REACTIONS

Lewis (1923) postulated that an acid is an electron pair acceptor and that a base is an electron pair donor. In terms of the topological properties of the Laplacian, this definition translates into: an acid either has a region of local charge depletion in the VSCC of the reactive atom or the reactive atom has an incomplete VSCC, and a base has a nonbonded charge concentration in the VSCC of the reactive atom (Bader, MacDougall and Lau 1984, Bader and MacDougall 1985, MacDougall and Bader 1986). The reaction pathway of an acid–base reaction is determined by the mutual alignment of the nonbonded charge concentration of the base with the hole in the acid. Figure 2.24 illustrates the alignment of the nonbonded charge concentration in the VSCC of the carbon atom in carbon monoxide with the shell of charge depletion in the core region of the boron atom in borane. As an aside it is interesting to note that systems with incomplete VSCC's, *e.g.* LiH, BeH_2 and BH_3, which expose the core regions of charge depletion to approaching nucleophiles, were also found by Bader and Stephens (1975) to possess open regions with greater core electron localization than the best spherical loge.

FUKUI'S FRONTIER ORBITAL THEORY OF CHEMICAL REACTIVITY

The frontier orbital theory of chemical reactivity will be referred to here as "Fukui's model" for sake of brevity and consistency. Fukui and coworkers originally argued (Fukui *et al.* 1952) that the reactive site of a polyaromatic hydrocarbon towards an electrophile was the carbon atom with the largest coefficient in the LCAO expansion of the *H*ighest *O*ccupied *M*olecular *O*rbital (HOMO). Subsequently, the reactive site towards a nucleophile was identified as the carbon atom with the largest coefficient in the LCAO expansion of the *L*owest *U*noccupied *M*olecular *O*rbital (LUMO). This model has subsequently been developed by several researchers and generalized to a large variety of chemical reactions (see for example Fleming 1976).

The primary postulate of Fukui's model is that the relative orientations of the reactants in an "orbital controlled" reaction is that which maximally overlaps the HOMO of the base with the LUMO of the acid. It was observed that several organic molecules exhibited (3,+1) critical points (ring critical points) in the VSCC of the atom which possesses the highest coefficient in the LCAO expansion of the LUMO (Bader, MacDougall and Lau 1984). Furthermore, the value of $\nabla^2\rho(r)$ at the position of the ring critical point in the VSCC of the reactive atom is commonly found to be more positive than the corresponding values at other ring critical points in the VSCC's of other, less reactive, atoms in the molecule. Consider the molecules formaldehyde and acrolein, the LUMO in both these molecules is a π^* orbital with the largest coefficient on the carbonyl carbon. Each of the carbon and oxygen atoms in these molecules exhibits a pair of ring critical points in their VSCC's, one above and one below the plane of the nuclei (figure 2.25). However, the ring critical points with the greatest degree of local charge depletion are the pairs in the VSCC's of the carbonyl carbons in both formaldehyde and acrolein. Interestingly, the β–carbon in acrolein exhibits a much greater degree of local charge depletion at the (3,+1) critical points in its VSCC than the α–carbon does, in accord with the LUMO in acrolein having the second largest coefficient at the β–carbon. Correspondingly, a nucleophile is found to exhibit a nonbonded charge concentration in the VSCC's of those atoms which contribute significantly to the LCAO expansion of the HOMO. Formamide, for instance, exhibits two nonbonded charge concentrations in the VSCC of the oxygen atom (figure 2.26) which is found to make the largest contribution to one of the nearly degenerate pair of HOMOs. The formamide molecule is correspondingly found to protonate at the oxygen atom (Birchall and Gillespie 1963).

The translation of the principle postulate of Fukui's model into terms of the topology of the Laplacian is seen to be exactly the same as the translation of Lewis' model of an acid–base reaction. Thus it is likely that the two models of chemical

Figure 2.24

The zero–envelopes of the Laplacian distribution for CO and BH_3, derived from 6–311G** RHF calculations. The value of $\nabla^2\rho = 0.0$ at every point of the surfaces shown. The hole exposing the core of the boron atom is evident, as are the nonbonded charge concentration and the torus of charge depletion of the carbon atom. The carbon and boron nuclei are 6.0 au apart.

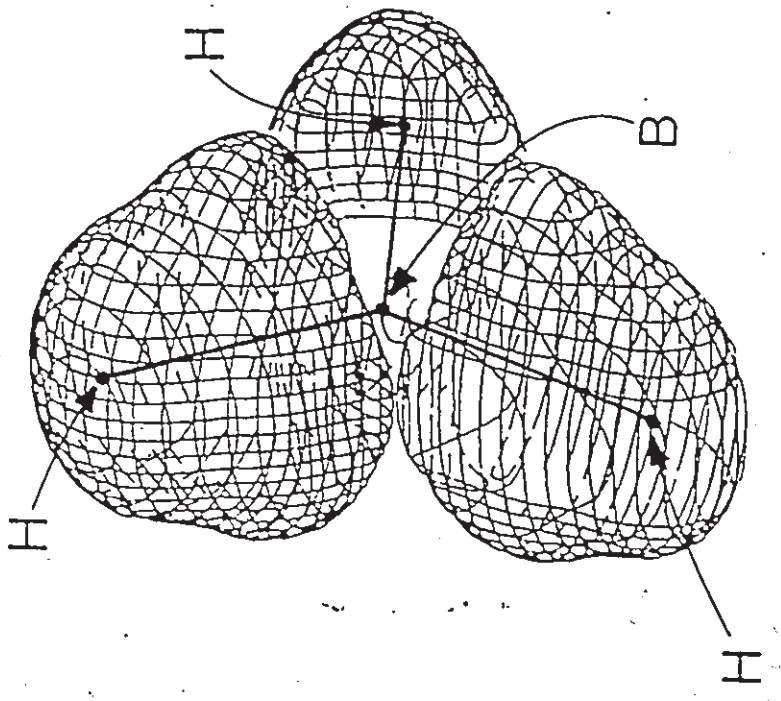
H
B
H
H

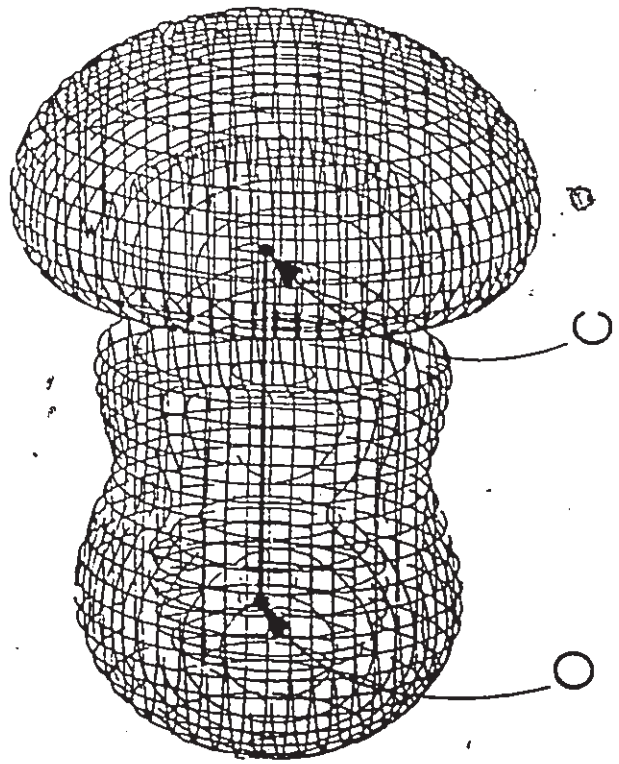
C
O

Figure 2.25

Contour diagrams of the Laplacian distribution in formaldehyde and acrolein, derived from 6–31G** and 4–31G* RHF calculations, respectively. The bond paths and interatomic surfaces are overlayed on the maps for formaldehyde. The solid squares denote the positions of maxima in charge concentration. The solid triangles denote the primary sites of nucleophilic attack, determined by the positions of the ring critical points associated with the largest holes in the VSCC's of the carbon atoms. The top–left map shows the Laplacian in the plane containing all the nuclei in formaldehyde, while the bottom–left map illustrates the Laplacian in the π plane of this molecule. The top–right map displays the Laplacian in the π plane of the α,β double bond, the β–carbon is on the left and the α–carbon is on the right. The lower–right map displays the Laplacian in the π plane of the carbonyl fragment. The carbonyl carbon is on the left, it possesses the largest region of charge depletion in the molecule.

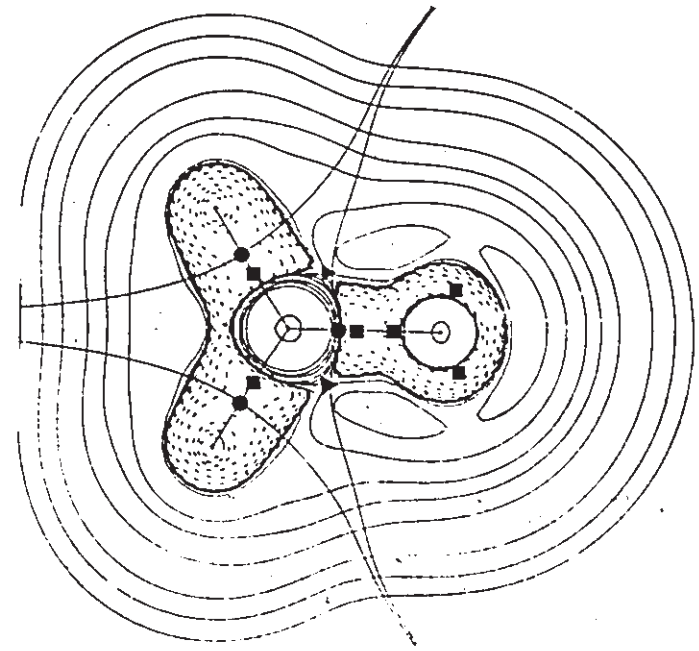

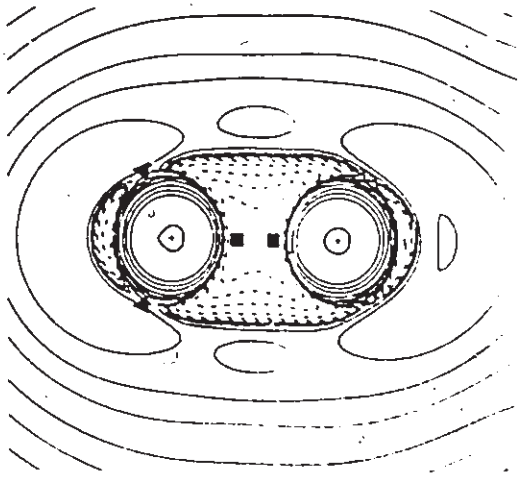

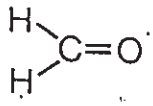
H
C=O
H

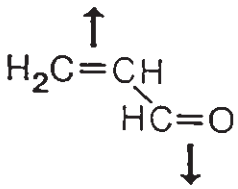
H2C=CH
HC=O

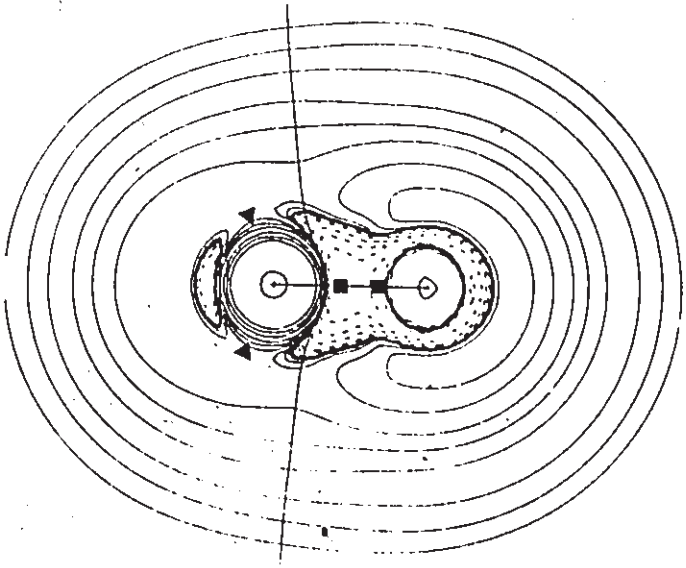

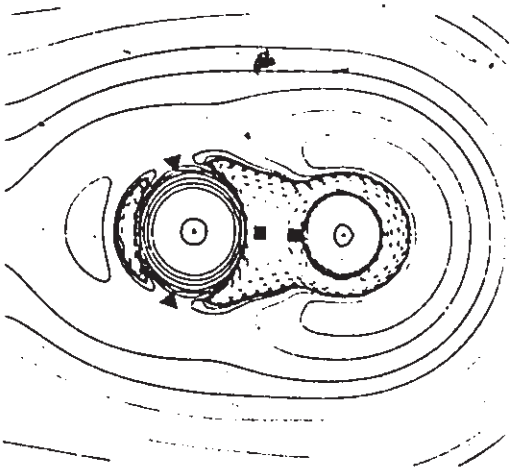

Figure 2.26

Relief maps of the Laplacian in formamide. The top figure illustrates the Laplacian in the plane containing the nuclear framework, while the lower figure shows the Laplacian in the π plane of the N–C bond. The value of $\nabla^2\rho$ at the largest of the two nonbonded maxima in the VSCC of the oxygen atom is shown in the top figure. The value of $\nabla^2\rho$ at one of the two equivalent nonbonded maxima in the VSCC of the nitrogen atom is shown in the lower figure. The cut–off value is ± 7.0 au in both figures.

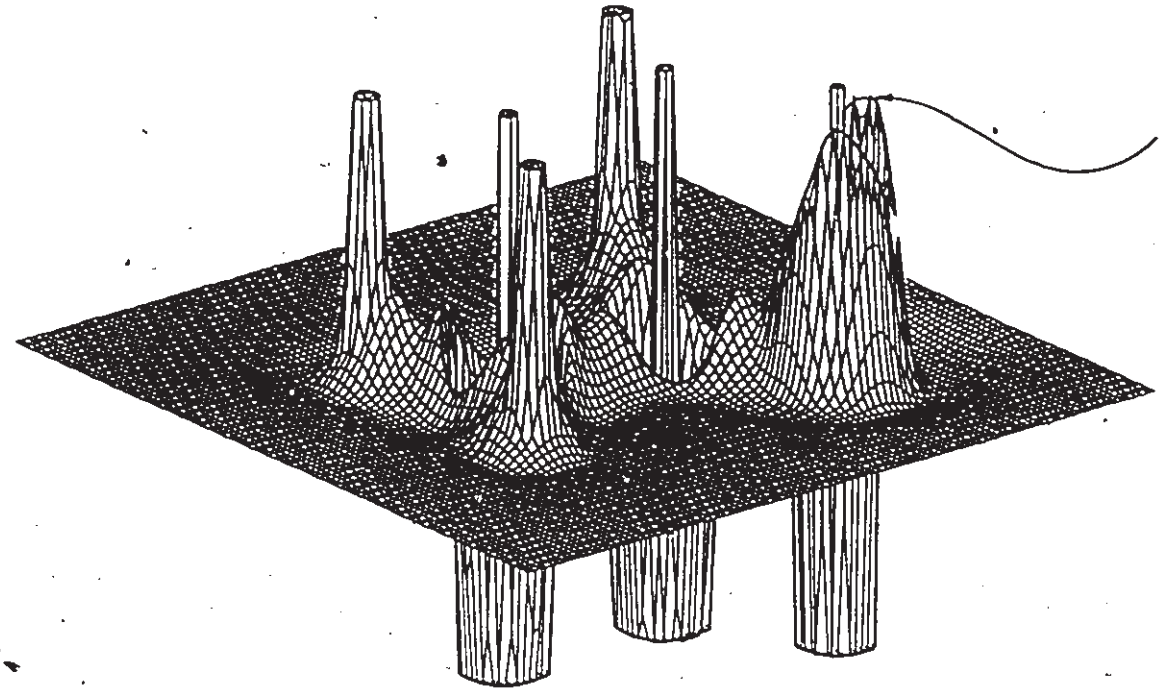
-6.25

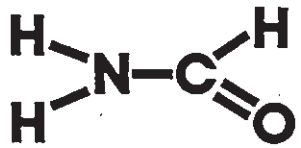
H
H
N
C
H
O

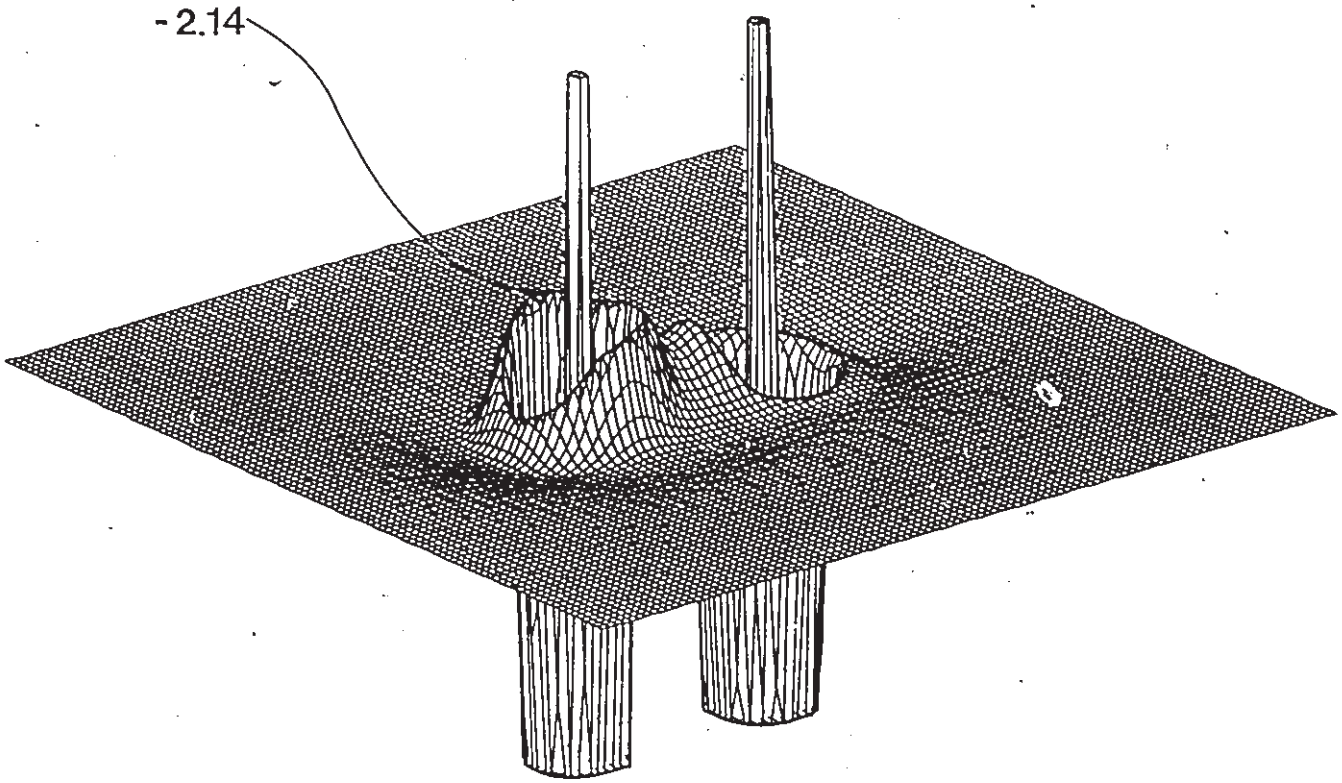
-2.14

Figure 2.27

A relief map of the Laplacian in the dication S_4^{2+}, derived from a 6–21G* RHF calculation. The cut–off value is ±5.0 au. The arrows indicate the sites of nucleophilic attack determined by the ring critical points in the VSCC of the sulphur atoms.

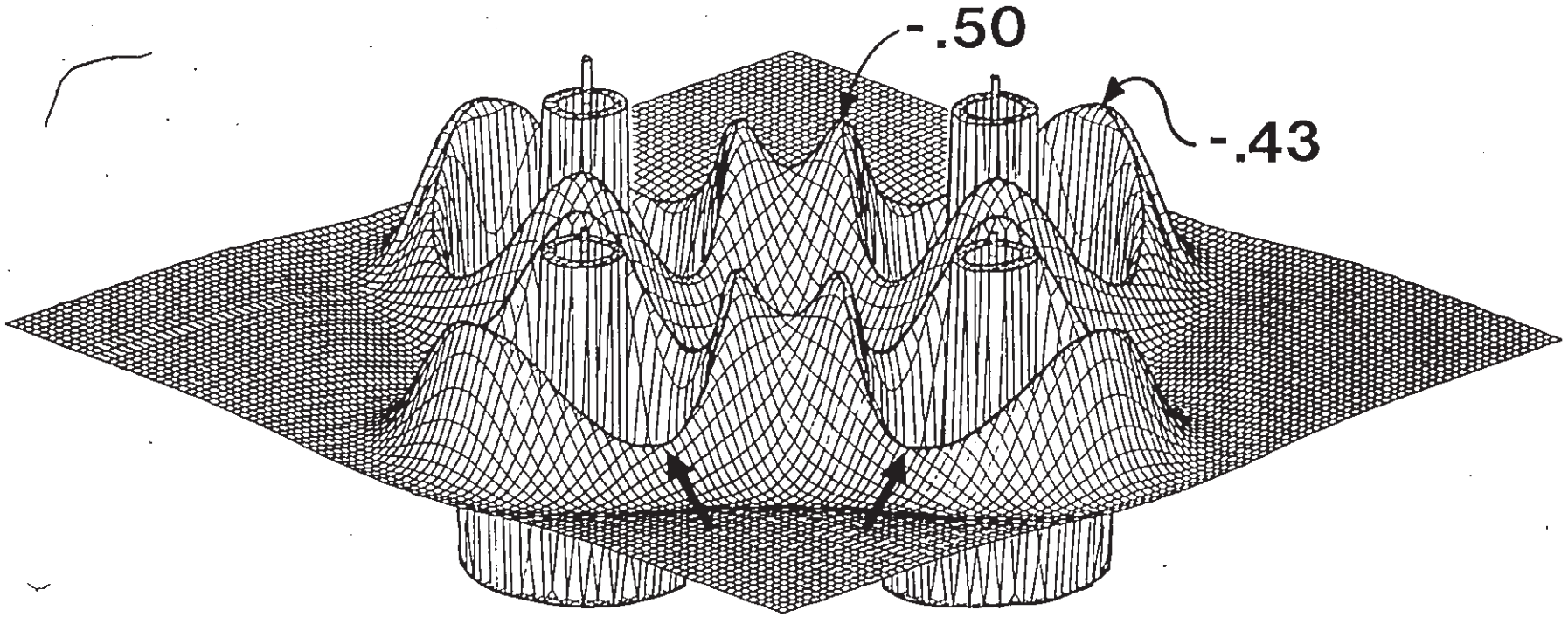
-.50
-.43

reactivity share a common physical basis. The development of a unifying quantum mechanical theory of chemical reactivity would be advanced by further investigations into the energetic consequences of postulating that a reaction pathway is initially determined by mutual alignment of the holes in the acid with the charge concentrations on the base. We can now discuss some of the energetic consequences of this postulate.

THE ENERGETICS OF ALIGNING THE CHARGE CONCENTRATIONS WITH THE HOLES

A local charge concentration is identified by the local expression of the virial theorem (equation 2.25a) to be a region wherein the potential energy experienced by the charge density is more stabilizing than that required to locally satisfy the overall potential:kinetic energy ratio, $V/G = -2$. Correspondingly, a hole in the VSCC of an atom is identified as a region wherein the potential energy experienced by charge density is less stabilizing than that required to locally satisfy the overall ratio $V/G = -2$. The energetic consequence of aligning a nonbonded charge concentration on a base with a hole in the VSCC of an acid is that this geometry maximally exposes charge density that is "overstabilized" to charge density that is "understabilized". The mechanism that transforms this situation into a lower total energy is not understood.

COMPARISON OF THE PROPOSED MODEL WITH EXPERIMENTALLY DETERMINED ORIENTATIONS OF ATTACK

The (3,+1) critical points in the VSCC of a carbonyl carbon form an angle of $\approx 110^0$ with the C–O bond axis (figure 2.25), this angle varies between narrow limits for a large number of molecules with carbonyl groups. Burgi and Dunitz in the "structure correlation" method have examined the orientations of nitrogen atoms in amino groups relative to the carbon atoms in carbonyl groups for a large number of crystal structures

containing both groups. They found that as the N···C–O distance reached its lower limit, the NCO angles in the different crystals converged at 110° (Burgi and Dunitz 1983). Another example of holes in the VSCC of an atom predicting the orientation of nucleophilic attack is provided by the crystal structure of $(S_4^{2+})(AsF_6^-)_2 \cdot 0.6SO_2$ (Passmore *et al.* 1980). In this crystal structure the shortest contacts between the sulphur atoms of the square–shaped dication and the nucleophilic fluorine atoms of the counter–ions, by a significant margin, were found in the plane of the sulphur nuclei and forming acute angles with the S–S bonds averaging 68°. The holes in the VSCC's of the sulphur atoms were also found to lie in the plane of the sulphur nuclei and forming an acute angle with the S–S bonds of 60° (figure 2.27). The predicted angle is considerably smaller than the observed angle, however, the observed position of the fluorine atoms permits the interaction of one fluorine atom with two holes simultaneously (Tang, Bader and MacDougall 1985). This prediction is of particular interest since the LUMO of the S_4^{2+} dication is a π^* orbital and calls for nucleophilic attack from above or below the plane of the sulphur nuclei.

2.8 THE EFFECT OF COULOMB CORRELATION ON THE TOPOLOGY OF THE LAPLACIAN

The observations upon which the physical bases of the Lewis and VSEPR models are based are derived from single–determinantal state functions. The correlation of the motions of electrons with opposite spin are completely unaccounted for. Especially since the topological properties of the Laplacian have been shown to be directly related to the correlation of the motions of electrons of like spin, the effect of Coulomb correlation must be examined if the arguments presented in this thesis are to be accepted. The effect of Coulomb correlation on the topological properties of the charge density has been investigated by Stephens and Becker (1983), Ritchie *et al.* (1986), Gatti *et al.* (1987) and Cao *et al.* (1987). In each case the conclusion was that

the topology of the charge density is unaffected by the addition of Coulomb correlation. The quantitative properties of the topological features were shown to be more sensitive to choice of basis set than to the addition of Coulomb correlation (Gatti *et al.* 1987, Cao *et al.* 1987).

The inclusion of Coulomb correlation has been shown to be essential to correct for the unbalanced Hartree–Fock description of the singlet–triplet energy difference in carbenes (Shavitt 1985 and references therein). The topology of the Laplacian in substituted methylenes has been presented in this thesis as one of the demonstrations of the claim that the bonded and nonbonded charge concentrations are the physical entities that are responsible for the success of electron pair models. The effect of Coulomb correlation on the topological properties of the Laplacian in the correlation sensitive divalent species CH_2, CF_2 and SiH_2 can arguably be regarded as a worst case scenario.

State functions which do take into account the correlated motions of electrons of opposite spin may be obtained by the configuration interaction (CI) method which expresses the state function as a sum of Slater determinants. Each of these determinants represents an electron configuration excited from the "ground state" configuration, of which the Slater determinant represents the Hartree–Fock state function (McWeeny and Sutcliffe 1969). In rare cases where the ground state configuration accounts for 90% or less of the determinantal expansion of the CI state function, the description of the correlated state function is better described as a sum of determinants derived from multiple reference configurations. For instance, when the state function of singlet CH_2 is described as a minimal two configuration expansion using the 6–31G** basis set, the normalized coefficients of the configurations that correspond to the unshared pair of electrons on carbon being in a p_σ or a p_π atomic orbital are 0.8515 and 0.1485, respectively (MacDougall and Bader 1986). Topological

analyses have been performed on the Laplacian distributions of charge densities derived from correlated state functions for the singlet and triplet states of CH_2, CF_2 and SiH_2.

COMPUTATIONAL DETAILS OF THE INCLUSION OF COULOMB CORRELATION

Large basis sets were used in the present calculations in order to minimize overestimating the effect of Coulomb correlation, since for minimal basis sets the correlation energy has been said to be nine parts basis set improvement to one part Coulomb correlation (Shavitt 1985). The details of the basis sets are given by Gatti *et al.* (1988), we list here the basic construction of the basis sets which illustrates their adequacy for the above stated purpose. The hydrogen basis used is a (5s2p/3s2p) set, where this notation implies that five s functions are contracted to three s functions and two p functions are uncontracted. The carbon basis is (10s6p2d/5s3p2d) in methylene while the carbon and fluorine basis sets in difluoromethylene are (9s5p2d/3s2p2d). The silicon basis set is (11s7p2d/6s4p2d). As in all the basis sets employed thoughout this thesis, the six cartesian components of the d functions are kept. The optimized geometries from the restricted Hartree–Fock (RHF) and restricted open–shell Hartree–Fock (ROHF) calculations are given in table 2.8, the effect of Coulomb correlation on the molecular geometries is not considered. The electronic configuration from the ROHF calculations of the triplet states were used as the single reference configuration in the CI expansions of these states. The two configurations corresponding to those described above for methylene were used as reference configurations in the CI expansion of the singlet states. The effect of using a single reference configuration is examined for methylene only. Single and double excitations of the reference configurations (CI–SD) were allowed from all but the single (five) core orbital(s) to any virtual orbital for both states of methylene (silylene). The effect of releasing this constraint was determined for methylene only. In difluoromethylene,

Table 2.8. Geometries, Energies and Singlet-Triplet Separation Energies (ΔE) for XY_2 Molecules (X=C,Si;Y=H,F) Evaluated at Different Theoretical Levels[a]

System	Method	n.c.[b]	r_{XY}[c]	θ_{YXY}[c]	-E[d]	ΔE[d]
$CH_2(S)$	RHF		1.095(1.11)[e]	103.6(102.4)[e]	38.89323	25.0
	1R-SDCI	4052	-	-	39.05455	14.4
	2R-SDCI[f]	19107	-	-	39.05746	12.6
	2R-SDCI	7050	-	-	39.04105	11.7 (9.01)[g]
$CH_2(T)$	ROHF		1.069(1.078)[h]	129.5(133.8)[i]	38.93307	
	1R-SDCI[f]	27774	-	-	39.07748	
	1R-SDCI	9950	-	-	39.05976	
$SiH_2(S)$	RHF		1.515(1.516)[l]	93.3(92.5)[l]	290.00778	-5.5
	2R-SDCI	7050	-	-	290.12921	-18.6
$SiH_2(T)$	ROHF		1.476	117.5	289.99899	
	1R-SDCI	9950	-	-	290.09956	
$CF_2(S)$	RHF		1.280(1.30)[m]	104.8(104.9)[m]	236.72752	-33.7
	2R-SDCI	10420[n]	-	-	236.88273	-60.4
$CF_2(T)$	ROHF		1.302	117.9	236.67378	
	1R-SDCI	29310[n]	-	-	236.78653	

[a] Experimental data are reported in parentheses. The CI calculations were performed on the SCF optimized geometries. (S) denotes the singlet state, (T) denotes the triplet state.

[b] Total number of configurations included in the CI expansion.

[c] Bond distances(r_{XN}) in A and YXY angles (θ_{YXY}) in degrees.

[d] Total electronic energies (E) in au: the singlet-triplet separation energies, ΔE = E(singlet) - E(triplet), are expressed in kcal/mol and refer to computations at corresponding theoretical levels.

[e] G.Herzberg, and J.W.C. Johns, *Proc. R. Soc. (London), Ser.A*, 295,107 (1966).

[f] Core double occupancy constraint released.

[g] A.R.W.McKellar, P.R. Bunker, T.J. Sears, K.M. Evenson, R.J. Saykally, S.R. Langhoff, *J. Chem. Phys.* 79,5251 (1983)

[h] G.Herzberg, and J.W.C. Johns, *J. Chem. Phys.* 54, 2276 (1971).

[i] P.R.Bunker, and P. Jensen, *J. Chem. Phys.* 79, 1224 (1983)

[l] I.Dubois, *Can. J. Phys.* 46,2485 (1968).

[m] C.W.Matthews, *J. Chem. Phys.* 45,1068 (1967).

[n] The non-interacting doubly excited configurations,i.e. the configurations which have a zero Hamiltonian matrix element with the reference configuration, were excluded from the CI expansion.

[o] B.R. Brooks, W.D. Laidig, P. Saxe, N.C. Handy, and H.F. Schaefer III, *Physica Scripta* 21,312 (1980).

Table 2.9. $-\nabla^2\rho$ Critical Point Data for Carbenes.[a]

XY_2	Method	Crit.point type[b]	r_x[c]	$\nabla^2\rho$	ρ[d]	δG[e]	δV[e]
$CH_2(S)$	RHF	n.b.	0.87	-1.523	0.329		
		b.	0.97	-1.502	0.314		
	1R-SDCI[f]	n.b.	0.87	-1.413	0.321	0.016	-0.004
		b.	0.96	-1.474	0.315	0.019	-0.031
	2R-SDCI[f]	n.b.	0.87	-1.358	0.315	0.016	0.009
		b.	0.96	-1.466	0.314	0.019	-0.029
$CH_2(T)$	ROHF	n.b.	0.97	-0.462	0.186		
		b.	0.99	-1.353	0.311		
	1R-SDCI[f]	n.b.	0.97	-0.441	0.185		
		b.	0.99	-1.330	0.310	0.012	-0.019
$SiH_2(S)$	RHF	n.b.	1.68	-0.138	0.076		
	2R-SDCI	n.b.	1.69	-0.117	0.071	0.002	0.002
$SiH_2(T)$	ROHF	n.b.	1.77	-0.087	0.052		
	1R-SDCI	n.b.	1.77	-0.078	0.051		
$CF_2(S)$	RHF	n.b.	0.83	-1.815	0.368		
		b.	0.96	-0.865	0.323		
	2R-SDCI	n.b.	0.84	-1.641	0.351	0.000	0.044
		b.	0.96	-0.819	0.327	0.009	-0.007
$CF_2(T)$	ROHF	n.b.	0.89	-0.929	0.256		
		b.	0.99	-0.663	0.305		
	1R-SDCI	n.b.	0.90	-0.914	0.256		
		b.	0.99	-0.648	0.304	0.003	-0.002

[a] All quantities in au.
[b] n.b. = nonbonded maximum. There are two such n.b. maximum in the triplet states of all systems, while only one in the singlet states; b = bonded maximum between X and Y.
[c] Critical point distance to X nucleus.
[d] Charge density value at the $-\nabla^2\rho$ critical point.
[e] $\delta G = G(CI) - G(SCF)$ where G is the kinetic energy density at the critical point as defined earlier.
$\delta V = V(CI) - V(SCF)$ where V is the potential energy density at the critical point as defined earlier.
[f] Core double occupancy constraint released.

Figure 2.28

Relief maps of the Laplacian distribution in the σ_v symmetry planes of singlet (a) and triplet (b) states of difluoromethylene, derived from CI–SD calculations employing a similar basis set as that used in figure 2.17. The cut–off value is ±2.0 au.

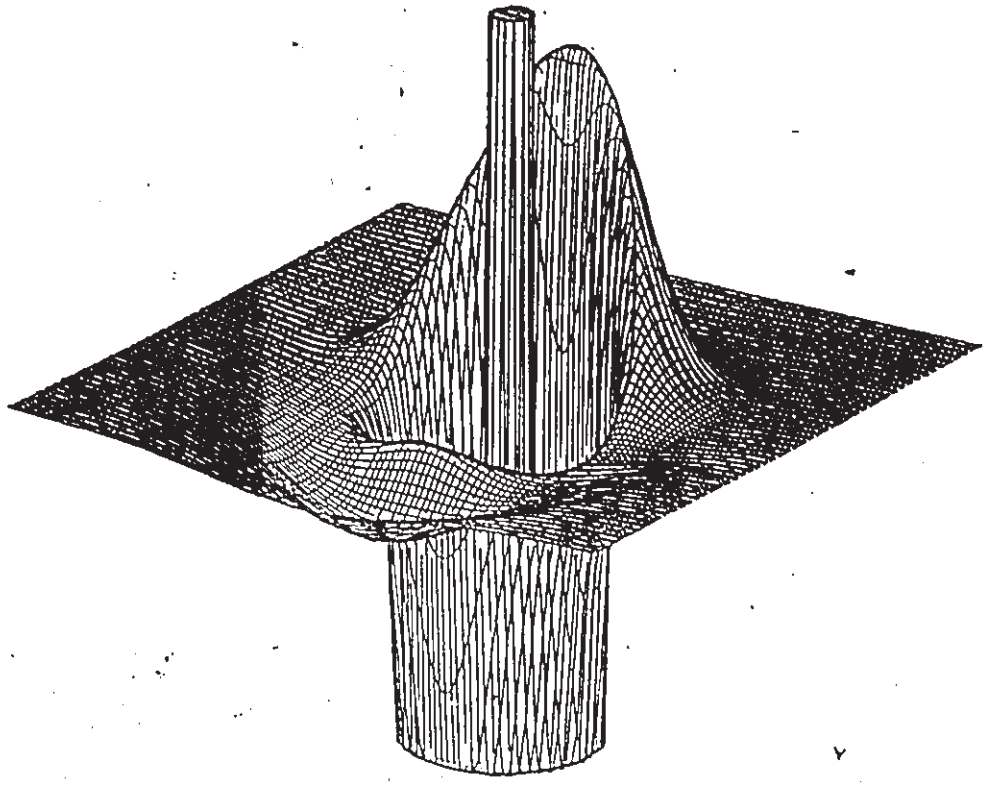

a

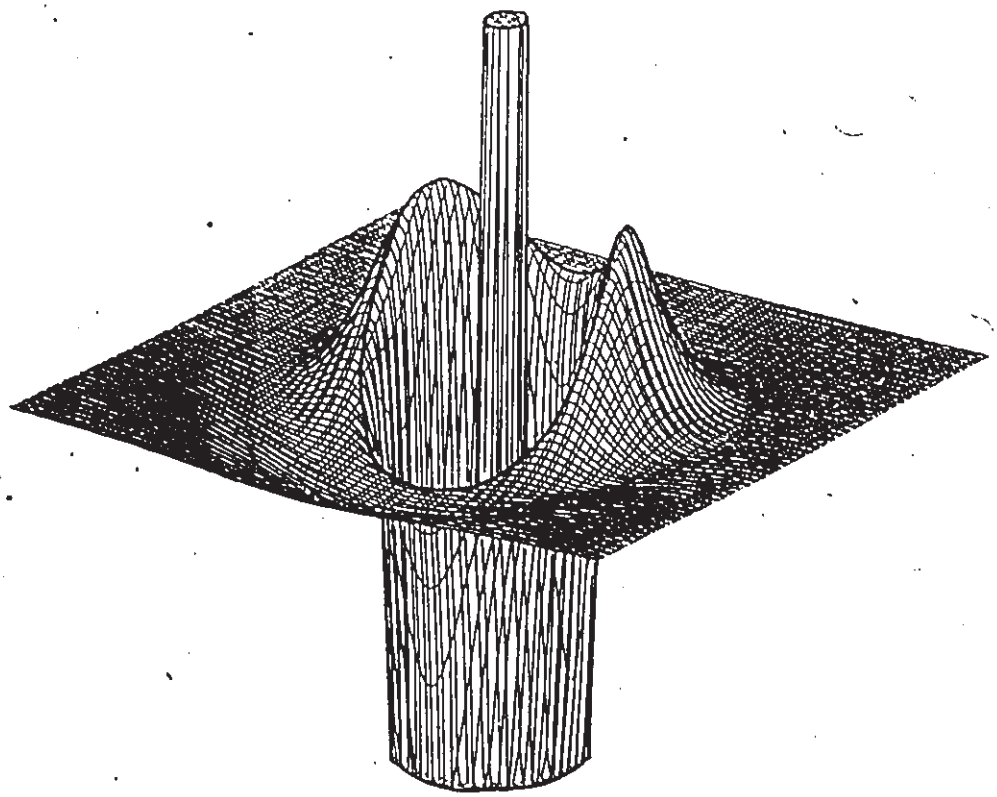

b

single and double excitations of the ground state configurations were allowed from all but eight of the lowest energy orbitals in the three configurations of interest here, to any virtual orbital. The effect of Coulomb correlation on the singlet–triplet energy gap is evident in table 2.8. The shift in the ΔE values is large on the chemical scale of energy differences.

THE WORST CASE SCENARIO LEAVES THE TOPOLOGY OF THE VSCC UNALTERED

The divalent atoms in the systems studied possess the same atomic graph when the charge density is derived from an "exact" state function as they do when described by a single–determinantal state function. The singlet states of CH_2 and CF_2 exhibit two bonded charge concentrations and one nonbonded charge concentration, while the corresponding triplet states exhibit two bonded charge concentrations and two nonbonded charge concentrations of smaller size. In both the CI–SD and Hartree–Fock descriptions the singlet and triplet states of silylene exhibit only one and two nonbonded charge concentrations, respectively, due to migration of the bonded charge concentrations to the hydrogen atoms. The data in table 2.9 indicate that the lack of qualitative changes to the Laplacian in the VSCC's of the divalent atoms is nearly equaled by the minor quantitative changes to several properties of these critical points. Figure 2.28 illustrates the form of the Laplacian in the σ_v plane of singlet and triplet difluoromethylene. This figure can be compared to the corresponding diagrams shown in figure 2.17 calculated at the Hartree–Fock level of theory.

2.9 THE EFFECT OF COULOMB CORRELATION ON AN ELECTRON'S *DOPPELGÄNGER*

The addition of Coulomb correlation must alter the form of the pair distribution function, otherwise the correlation energy would be zero. What is not obvious is the

extent that the pair distribution function will be altered in the half of its total space that corresponds to pairs of like–spin electrons relative to the other half corresponding to pairs with opposite spin. One can further differentiate between the relative importance of Coulomb correlation and changes to the Fermi correlation in the alteration of the pair density in the former half above. We will not attempt to fully answer these questions here, since the proposal that electron pair models can be given a physical basis in terms of the topological and energetic properties of the Laplacian does not invoke correlation between electrons of opposite spin in any way. Furthermore, only the correlation between electrons with parallel spin that is due to exchange is utilized in the revision of the Lewis and VSEPR models. What is crucial for the acceptance of those conclusions drawn so far in this chapter concerning the role of Fermi correlation, is that the spatial distribution of an electron's *doppelgänger* is not affected in such a way as to disprove the proposed mechanisms. The density of the Fermi hole given in equation 2.17 correctly describes the "spreading out" of an electron at r_1 for a single–determinantal state function expressed in terms of orthogonal spin–orbitals. The expression of the Fermi hole density for Coulomb correlated state functions has been shown by Luken (1982) to be identical in form to equation 2.17 except that the orthogonal spin–orbitals are not singly occupied in the natural orbital expansion of a many–determinantal state function. However, only for a single determinantal state function does the Fermi hole completely account for the total correlation hole in the pair density of electrons with parallel spin as defined in equation 2.14 (McWeeny and Sutcliffe 1969).

To determine the effect of Coulomb correlation on the essential property of Fermi correlation employed in this thesis, that it leads to partial condensation of the valence electrons into pairs when the probe electron is near a maximum in local charge concentration, RHF and CI–SD calculations of carbon monoxide have been performed. The basis set of the carbon and oxygen atoms is (6s3p/3s2p) from Williamson and Hall

(1987). All single and double excitations of valence electrons were included in the CI expansion. The C–O bond length was optimized at both levels of theory. This inclusion of electron correlation leads to a bond lengthening of 0.025 Å. The respective values of r_c and $\nabla^2\rho(r)$ at the position of the nonbonded maximum on carbon are 0.897 au and –1.270 au for the RHF state function compared to 0.906 au and –1.136 au for the CI–SD state function. The inclusion of Coulomb correlation leads to a lowering of the total energy by 125.5 kcal/mole. Figure 2.29 illustrates the *doppelgänger* of an electron situated at the nonbonded maximum in the VSCC of the carbon atom in carbon monoxide, without Coulomb correlation (top) and with Coulomb correlation (bottom). The difference between the two distributions is practically undetectable. The inclusion of Coulomb correlation does not appear to affect the Fermi hole of an electron located at a (3,–3) critical point in $-\nabla^2\rho$, thus the proposed mechanisms by which maxima in charge concentration are formed and interact with one another, are operative at higher levels of theory.

Figure 2.29

The Fermi holes of a reference electron at the position of the nonbonded charge concentration on carbon is shown for a RHF calculation (top, R(CO) = 1.1285 Å) and a CI–SD calculation (bottom, R(CO) = 1.1535 Å), both using a 3–21G basis set.

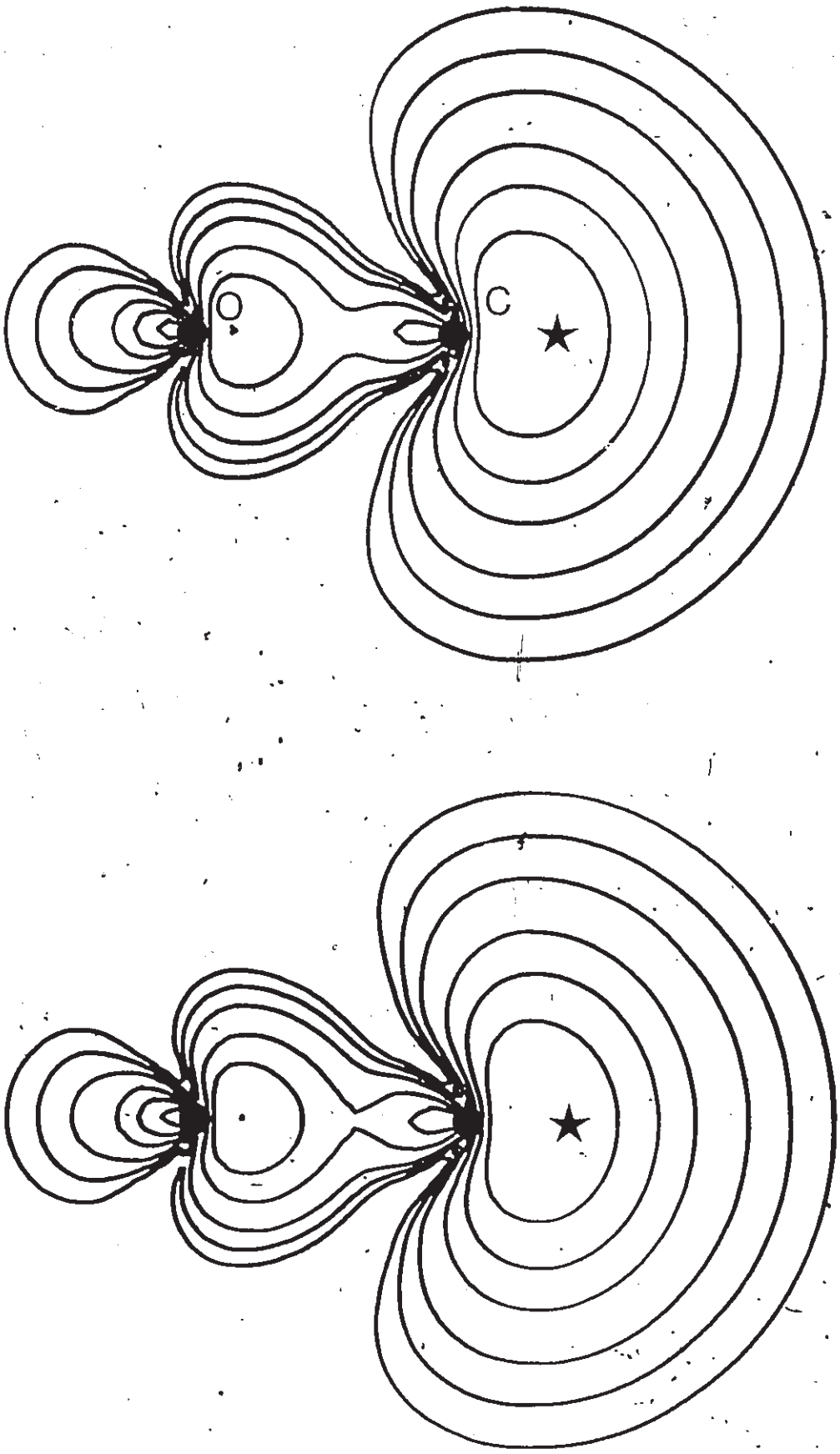
O
C

CHAPTER 3

CONCLUSIONS AND ADDITIONAL WORK

3.1 CONCLUSIONS

The stated goal of this thesis was to integrate the electron pair concept of Lewis with the predictions of quantum mechanics. Although we have not synthesized a quantum mechanical theory that rationalizes and predicts the behaviour of electron pairs, by linking the electron pair concept to a physical property we have elevated the understanding of the electron pair above that afforded by orbital models.

From the observations presented in chapter 2 we can draw several conclusions regarding the physical bases of the Lewis electron pair model and Gillespie's VSEPR model of molecular geometry. These conclusions are summarized below.

1. Except in core regions and the hydrogen atoms of ionic hydrides, electrons are not separately localized into pairs. In general, one can not even define regions of space containing on average two electrons in which the fluctuation in the average number of electrons is minimized (Bader and Stephens 1975).

2. We do find that the number and types of charge concentrations in the valence shell charge concentration of an atom in a molecule parallel the anticipated Lewis structure of the atom.

3. The one–to–one mapping of the topology of the VSCC onto the Lewis structure of an atom is carried over onto the Sidgwick–Powell model of the electronic structure of molecules that do not obey the octet rule.

4. Lewis' prediction of the tetrahedral arrangement of the electron pairs in the valence shell of a carbon atom, and Gillespie's model of the spatial arrangement of

valence shell electron pairs, are found to apply to the spatial arrangements of maxima in the VSCC of a central atom with remarkable accuracy.

5. The bonded and nonbonded charge concentrations in the VSCC of an atom are found to exhibit all of the spatial characteristics attributed to the valence shell electron pairs within the VSEPR model of molecular geometry. In particular, the relative sizes of singly bonded, doubly bonded, triply bonded and nonbonded charge concentrations are found to agree with the assumed sizes of the corresponding electron pair domains. In addition, the effect that bond ionicity is assumed to have on the size of the bonded pair domains (within the VSEPR model) is found to correlate with observed trends in the properties of bonded charge concentrations.

6. Bonded charge concentrations in the VSCC of a central atom are found to exhibit the behaviour that the VSEPR model ascribes to bonded pairs of electrons in crowded positions, there is migration of the charge concentration towards the ligand.

7. In analogy with the main postulate of the VSEPR model, the energy of a molecule in a given geometry is found to be lower if the charge concentrations in the VSCC of the central atom are maximally separated, according to their size. This conclusion is a consequence of the perfect translation of the subsidiary postulates of the VSEPR model into observed properties of the charge concentrations.

8. The Fermi hole of an electron, its *doppelgänger*, determines an electron's delocalization due to quantum mechanical exchange. It represents the manifestation of the Pauli exclusion principle on the pair distribution function. Localization of their Fermi holes is the only mechanism by which a pair of electrons can be physically localized. We find that the concerted action of the Pauli exclusion principle and the ligand field causes a partial condensation of the Fermi hole when the probe electron is near the core, in an internuclear position, and sometimes in a nonbonded position. When the probe electron is situated exactly at a position of maximum charge concentration, the Fermi hole is maximally localized and minimally overlapping other regions of space where partial localization of the Fermi hole is also observed.

9. Capturing the essence of the physical connotations of Gillespie's VSEPR model, the Fermi holes associated with the charge concentrations in the VSCC of a central atom are found to overlap one another to a greater extent when the charge concentrations are not maximally separated within the VSCC, according to their size. It is argued that greater overlap of the Fermi holes when the probe electrons are located at positions of maximum charge concentration, leads to greater repulsion between electrons of the same spin.

10. It has been observed that the Lewis model of acid–base reactions and the Fukui model of orbital controlled reactions are translated into a common model of chemical reactivity based on the topology of the Laplacian. This model predicts that a reaction pathway is initially determined by the alignment of a nonbonded charge concentration in the VSCC of the basic atom with a hole in the VSCC of the acidic atom. Energetically, this corresponds to aligning a region with excess potential energy (the basic atom) with a region with excess of the kinetic energy density G(r) (the acidic atom).

11. Investigation of the Laplacian of charge distributions derived from correlated state functions suggest that all of the conclusions above, that concern the topological properties of the Laplacian, can be expected to hold at higher levels of theory.

12. The inclusion of Coulomb correlation does not noticeably affect the spatial properties of Fermi holes. Thus, the mechanism involved in the creation and interaction of charge concentrations, summarized in conclusions #8 and 9, is valid at higher levels of theory.

3.2 ADDITIONAL WORK: THE TOPOLOGY OF THE LAPLACIAN AND LIGAND FIELD THEORY

Hartree–Fock state functions for the metal carbonyl complexes $Cr(CO)_6$, $Fe(CO)_5$ and $Ni(CO)_4$ have been obtained from Williamson and Hall (1987). The

optimized geometries of the complexes were found to be in good agreement with experiment, the error in the M–C distance averages ±0.03 Å (Williamson and Hall 1987). We present here preliminary studies of the topological properties of the Laplacian in these systems. Bethe (1929) and van Vleck's (1932) crystal field theory makes simple and useful predictions of the one–electron d–orbital energies of transition metal complexes by replacing the metal–ligand interaction with a variable electrostatic field which represents the ligands as point charges. The ligand field theory (see Ballhausen 1962) seeks to model the spectral and magnetic properties of these complexes through a similar employment of a pure d–orbital basis set, but it replaces the Coulomb operator of atomic theory and the classical crystal field operator of its predecessor with either nonphysical effective operators or more commonly a set of parameters determined from a spectroscopic data base.

The topologies of the Laplacian in the third shell of charge concentration of the metal atoms in $Cr(CO)_6$, $Fe(CO)_5$ and $Ni(CO)_4$ are found to exhibit very pronounced features. Contour diagrams of the Laplacian distribution, determined from the above mentioned state functions, are illustrated in figure 3.1. First, one should note that in accord with the VB model of the bonding in these systems the metal atoms only exhibit three shells of charge concentration corresponding to a "promoted" atomic state. Similarly to the VSCC's of the isolated metal atoms (Sagar *et al.* 1988), the average radius of the VSCC decreases and the maximum magnitude of $\nabla^2\rho$ in the VSCC increases, as the nuclear charge on the metal atom increases. Secondly, the VSCC's of the metal atoms exhibit ring critical points where the unoccupied d–orbitals, predicted using either crystal field (CF) or ligand field (LF) theory, are maximally concentrated. For instance, the atomic graph of the chromium atom in $Cr(CO)_6$ possesses a ring critical point along each of the Cr–C bond paths. Within the models of the electronic structure of this molecule the empty d–orbitals are most concentrated at these positions; the e_g orbitals in MO and LF theory, or the d_{z2} and d_{x2-y2}

Figure 3.1

Contour maps of the Laplacian distributions for first row transition metal carbonyls and isolated carbon monoxide (inset), derived from RHF calculations using a double–zeta basis set. The nuclei are labelled in each figure as are principal topological features of the Laplacian and the value of $\nabla^2\rho$ at these positions. A star denotes a maximum in charge concentration, a solid circle denotes a saddle point on a LOMCC linking two maxima, and a solid triangle marks the position of a ring critical point in a VSCC. On the left, the Laplacian of $Cr(CO)_6$ is shown in a σ_d symmetry plane. The Laplacian is negative over the entire third shell, or valence shell of the chromium atom. The first and second shells of charge concentration of the metal atoms are not clearly portrayed at the level of resolution used to generate these plots. The map in the centre displays the Laplacian in a σ_v symmetry plane of $Fe(CO)_5$. There are two holes of charge depletion in the VSCC of the iron atom opposite the axial carbonyl groups. The map on the right displays the Laplacian in a σ_v symmetry plane of $Ni(CO)_4$. The VSCC of the nickel atom is noticeably more spherically symmetric than the metal atom VSCC's in the other carbonyls.

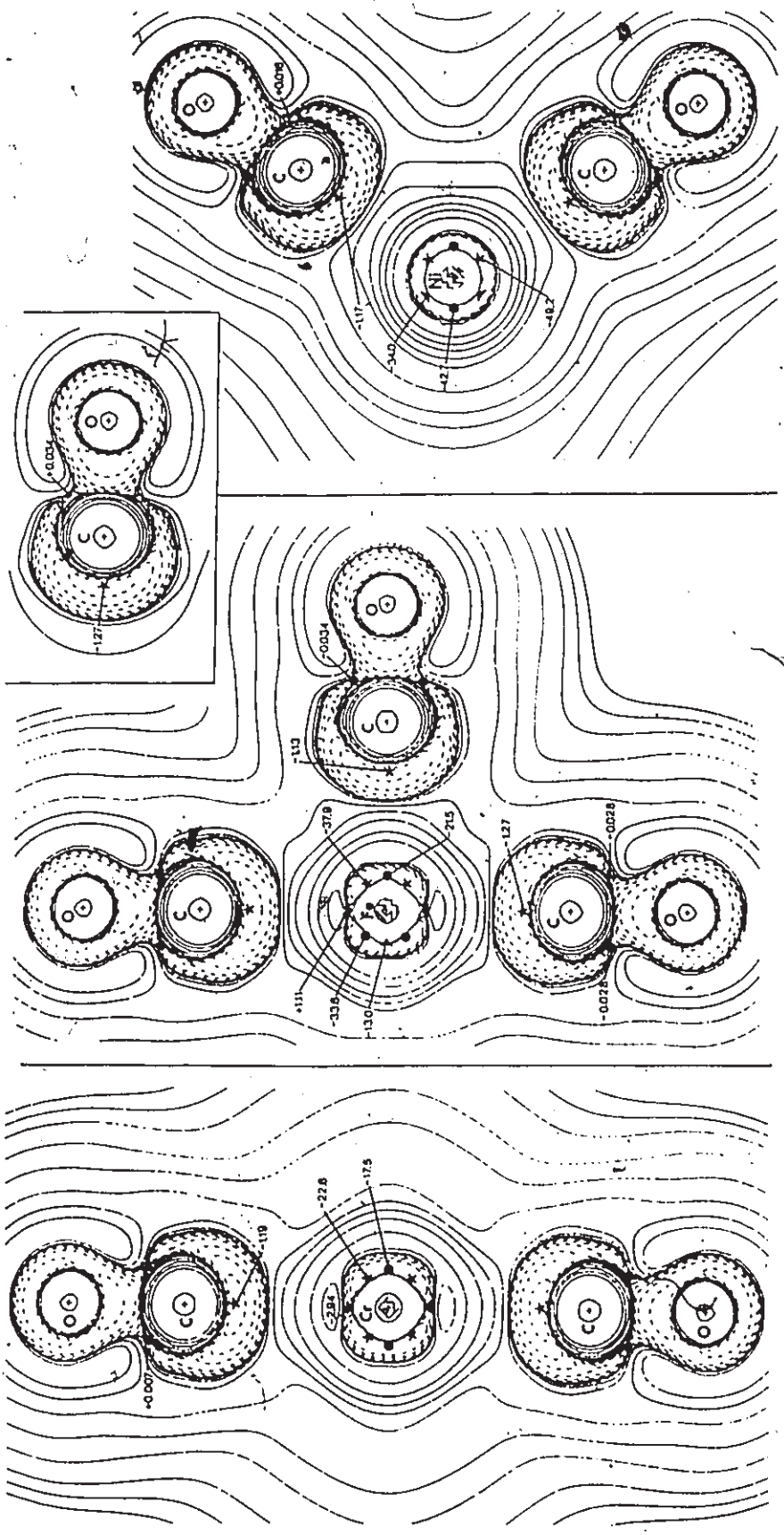
+0.006
-117
-340
-42
-48.2
-0.031
-127
-0.0034
113
-37.9
21.5
127
-0.028
+111
-33.6
-130
-0.0228
-119
-22.8
-17.5
-234
+0.007

orbitals in VB and CF theory. The extent of charge concentration at these ring critical points is a pronounced reduction compared to the eight maxima in the VSCC, one in each face of the octahedron formed by the six Cr–C bonds (see figure 3.1). One does not necessarily expect charge depletion at these points since the third quantum shell also contains the eight 3s and 3p electrons. In $Fe(CO)_5$ the a_1' orbital in MO and CF theory, or the d_{z2} orbital in VB and CF theory, is predicted to be unoccupied. Correspondingly, the VSCC of the iron atom exhibits a hole along the axial Fe–C bonds where the unoccupied orbital is most concentrated. Unlike $Cr(CO)_6$ wherein the maxima in the chromium VSCC maximally avoid the ligands by being located in the centres of the octahedral faces, the six maxima in the VSCC of the iron atom are located on the axial edges of the trigonal bipyramid. Interestingly, within the MO and LF theories of the Fe–CO interaction the locations of the maxima in the VSCC of the iron atom coincide with the positions where the stabilized e'' orbitals are maximally concentrated. In $Ni(CO)_4$, where the d–shell is complete, the VSCC of the nickel atom does not exhibit any pronounced (relative to the VSCC's of iron and chromium) ring critical points. In fact, the topology of the VSCC of the nickel atom perfectly maps onto the Lewis structure that one would draw for this molecule.

Figure 3.1 also displays the Laplacian distribution in the isolated carbon monoxide molecule. The qualitative features of the Laplacian in the isolated and bonded states of carbon monoxide are unchanged. The key quantitative properties (those shown in figure 3.1) are unusually unperturbed by M–C bond formation. This observation rekindles the controversy between MO and LF theory proponents over the nature of metal–ligand bonding. Within MO theory the metal carbonyl bond is described as a synergistic mechanism involving σ donation to the metal and π back–donation to the ligand (Dewar 1951, Chatt and Duncanson 1953). Within LF theory the d–electrons are considered almost totally localized on the metal and only indirectly interacting with the ligands via M–L bonding orbitals made up from ligand

orbitals (such as 5σ in carbon monoxide) primarily overlapping the vacant metal 4s,4p orbitals (Gerloch and Woolley 1983). A small amount of overlap of the metal d–orbitals is allowed with the ligand orbitals, but this only so that the d–d′ transitions observed in the electronic spectrum of metal complexes have nonzero intensities. The intensity of a pure d–d′ transition is zero as a result of the electric dipole transition rule ($\Delta\ell = \pm 1$), thus the transition is modelled as $(d + b\chi) - (d' + b'\chi')$ where χ is the M–L bonding orbital. The M–L bonding orbitals are illustrated schematically below (Gerloch 1988), they are never actually calculated because the ligand field parameters used in the calculations of the spectra are determined empirically. However, the effective Hamiltonian is consistent with the physical picture of mostly metal–localized d–electrons.

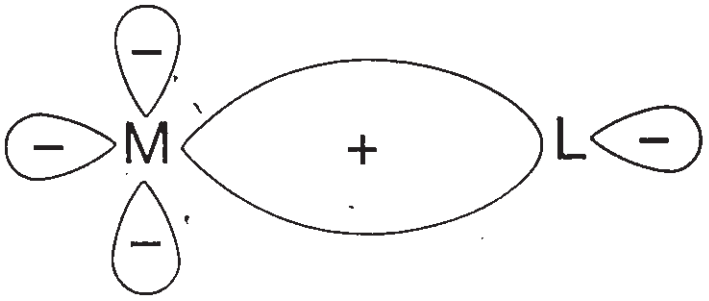

$\chi(M\text{–}L)$

The Fermi holes when the probe electron is located at a d–shell maximum in the VSCC of the metal atoms and at the carbon nonbonded maximum are shown in figure 3.2 for the systems $Cr(CO)_6$, $Fe(CO)_5$ and $Ni(CO)_4$.

When an electron is at the nonbonded maximum in carbon monoxide, one can see from a comparison of figures 2.29 and 3.2 that its *doppelgänger* is only slightly perturbed by the presence of the metal atom. Furthermore, the shape of the Fermi hole when the probe electron is at the bonded charge concentration (to the metal) on carbon, resembles the M–L bonding orbital proposed by Gerloch. The Fermi holes in figure 3.2 are all plotted to the same scale and the nuclei are oriented as in figure 3.1.

Figure 3.2

Fermi holes of electrons located at bonded maxima (to metal) on carbon and VSCC maxima of the metals for the same metal carbonyl systems shown in figure 3.1. The scale and nuclear configurations are the same as in figure 3.1. In the top–left map the reference electron is at the bonded maximum (to chromium) in the VSCC of the carbon atom shown in a σ_d symmetry plane. In the bottom–left map the probe electron is at the coordinates of the maximum in the VSCC of the chromium atom that is pointed to in figure 3.1. In the top–middle map the probe electron is at the bonded maximum (to iron) in the VSCC of the equatorial carbon. The Fermi hole of the corresponding maximum of the axial carbon is not shown, but is nearly superimposable on the map for the equatorial carbon. In the lower–middle map the reference electron is at the maximum in the VSCC of the iron atom pointed to in figure 3.1. The maps on the right are for corresponding positions of the reference electron in $Ni(CO)_4$.

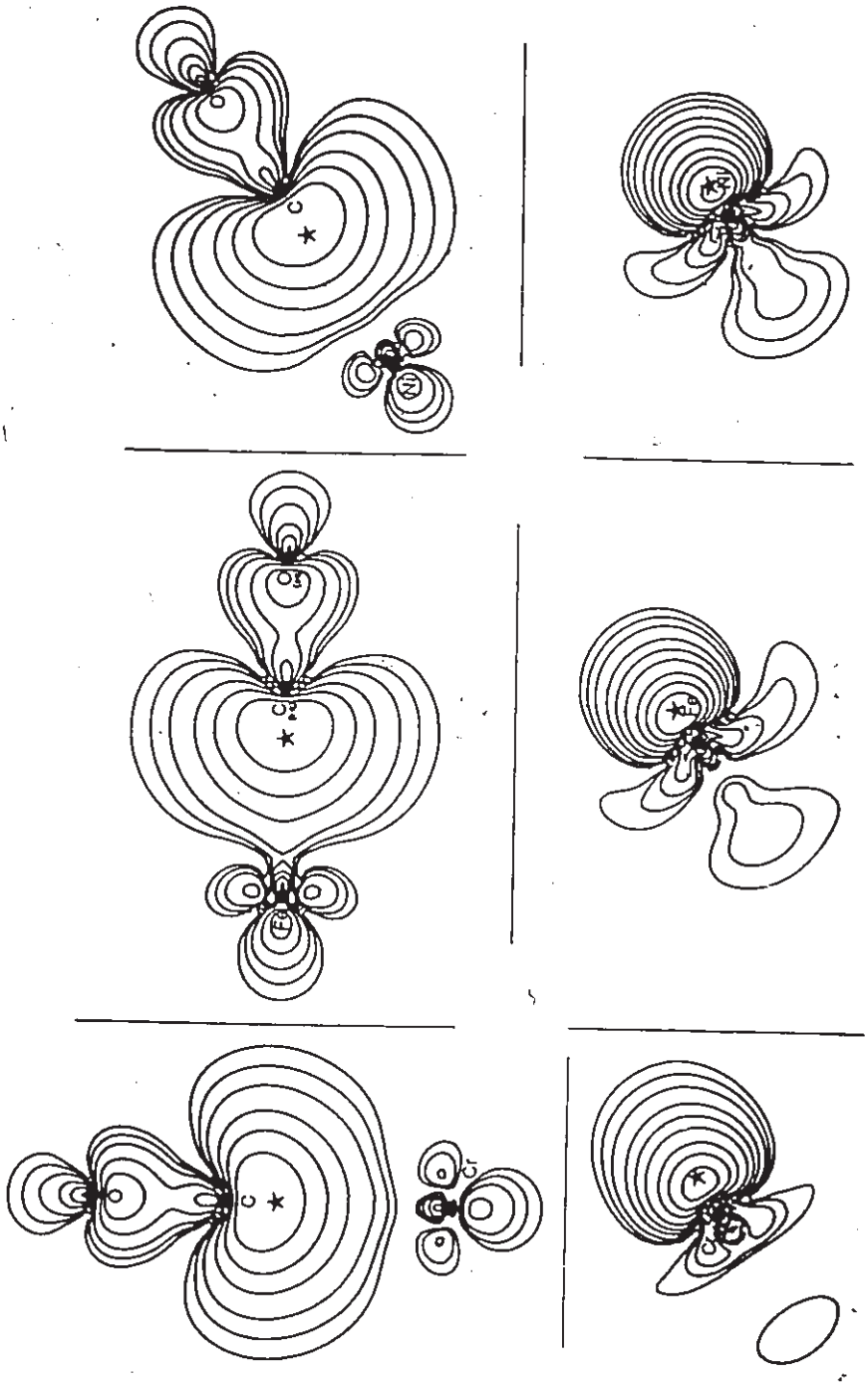

Thus one can see that the *doppelgänger* of an electron situated at a d–shell maximum is highly localized within the metal atom (figure 3.2). Again, the spatial properties of the Fermi holes parallel those of the charge concentrations they are associated with, they become more contracted as the nuclear charge increases. Interestingly, the Fermi hole at the carbon nonbonded maximum is most delocalized onto the metal atom for the equatorial CO in $Fe(CO)_5$ and this is the most tightly bound carbonyl of the series. The properties of the Laplacian of the electronic charge distribution as well as the Fermi correlation in the metal carbonyls studied here support the physical picture implied by the ligand field model.

Clearly, a more detailed study of the state functions, charge distributions and their corresponding Laplacians, will add to our understanding of the properties of the atoms and bonds in transition metal complexes. In particular, the quantum theory of atoms in molecules enables one to calculate the atomic electron–electron repulsion energies for a molecule in a stationary state. Thus one can investigate the nature of the nephelauxetic effect, the effective decrease in the d–d electron repulsion upon metal complexation (Jörgenson 1957). Proinov *et al.* (1988) have attempted to apply the quantum theory of atoms in molecules to the study of this phenomenon. They approximate Bader *et al.*'s quantum atom as a sphere with radius equal to the bonded radius of the metal atom in the complex. They then compare the change in the d–d electron repulsion of the metal atom to the overall reduction in electron repulsion. They find that the atomic contribution to the nephelauxetic effect exhibits a reciprocal dependence on the radius of the "atom".

Predictions made on the basis of LFT are of central importance to the study of heterogeneous and homogeneous catalysis by transition metal complexes or surfaces, respectively. Future investigations of the atomic, structural and charge concentration properties of transition metal coordination compounds will be aimed at providing greater resolution to the study of reaction mechanisms in these processes.

3.3 ADDITIONAL WORK: NATURE OF METAL–METAL BONDS IN TRANSITION METAL CLUSTERS

Using the Discrete–Variational–Method (Baerends *et al.* 1973) of approximating the exchange+correlation energy in Hartree–Fock–Slater SCF electronic structure calculations, Ellis, Guo and Cheng (1987 and 1988) have reported the topological properties of the charge distributions in Ni_3 and Ni_4 as well as H_2 and C_2H_2 absorbed on Ni_4. The author of this thesis interfaced the programs necessary for the topological analysis of the total charge density, to the DVM–HFS SCF electronic structure programs employed by Ellis *et al.* Calibration of their preliminary results with corresponding results obtained by Hartree–Fock methods is currently underway. Future work will involve studies of the bonding of adsorbates on metal surfaces and partitioning the total binding energy into atomic contributions.

Hartree–Fock state functions of slightly better quality than those used in the metal carbonyl systems above have been obtained for some binuclear metal carbonyl systems. Williamson and Hall (1987) have supplied the author with the state function for $Mn_2(CO)_{10}$ in its equilibrium geometry. Kunze and Hall (1987) have communicated the state functions for $Fe_2(CO)_9$ and $Co_2(CO)_8$ in their equilibrium geometries. In all three systems the basis sets for the metal atoms are (10s7p5d/4s3p2d), while the basis sets of the carbon and oxygen atoms are (7s4p/3s2p). On the basis of Sidgwick's effective atomic number (EAN) rule (1927) and the short M–M internuclear distances, these binuclear systems are thought to contain a M–M bond (Braterman 1972). Several researchers have questioned the existence of M–M bonds in the bridged binuclear species on the basis of qualitative molecular orbital analyses (Lauher *et al.* 1976, Heijser *et al.* 1980, Bauschlicher 1986, Thorn and Hoffmann 1976, Summerville and Hoffmann 1979). But, if the existence of a M–M bond is based on a positive $\Delta\rho$ in the density difference maps at the midpoint of the M–M bond, then theory (Heijser *et al.* 1980) and experiment (Leung and

Coppens 1983) predict the existence of a Co–Co bond in $Co_2(CO)_8$. In agreement with the conclusion of a Co–Co bond on the basis of $\Delta\rho$ maps, using the Hartree–Fock state function described above, Kunze and Hall (1989) have argued that a localized molecular orbital analysis supports the existence of a Co–Co bond. They also present an argument based on delocalized molecular orbital analysis, qualitatively similar to that by Thorn and Hoffmann (1976) in all respects except that the conclusion is in diametrical opposition. Such contradictions are not uncommon within the molecular orbital model of chemical bonding which becomes severely obfuscated when the number of valence orbitals becomes large.

The results from a topological analysis of the total charge density provide definitive answers to the question of the existence of M–M bonds in these systems. As universally anticipated, the manganese atoms are joined by a bond path in the D_{4d} optimized geometry of $Mn_2(CO)_{10}$. The values of $\rho(r_c)$ and $\nabla^2\rho(r_c)$ at the Mn–Mn bond critical point are 0.031 au and –0.006 au, respectively. These values are comparable to the corresponding values at the non–nuclear maxima in lithium and sodium clusters. The partitioning of the molecule into its atomic fragments by the field $\nabla\rho(r)$ is illustrated in figure 3.3. The very cubic nature of the metal atoms is noteworthy. For interest's sake the *doppelgänger* of an electron in a metal–metal bond is shown in figure 3.4. The delocalized nature of an electron in the outer valence (fourth) shell of a transition metal atom is in distinct contrast to the very localized nature of an electron in the inner valence (third) shell.

The partitioning of the iron and cobalt binuclear systems into their constituent atoms is illustrated in figure 3.5 (same scale as figure 3.3). The metal atoms appear to share an interatomic surface in both $Fe_2(CO)_9$ and $Co_2(CO)_8$ in the σ_v planes shown. In fact, there is a cage critical point in the centre of the iron dimer and a ring critical point roughly at the centre of the cobalt dimer. The dashed lines in both these maps indicate the intersections of the four–membered $\overline{M–C–M–C}$ ring surfaces with the σ_v

Figure 3.3

The gradient vector field of the charge density in a σ_v symmetry plane of $Mn_2(CO)_{10}$. The positions of in–plane nuclei are denoted by solid circles and labelled. The projected positions of out–of–plane nuclei are marked by open circles. The bold gradient paths are the bond paths and intersections of the interatomic surfaces with the plane shown. The positions of bond critical points are denoted by small solid circles.

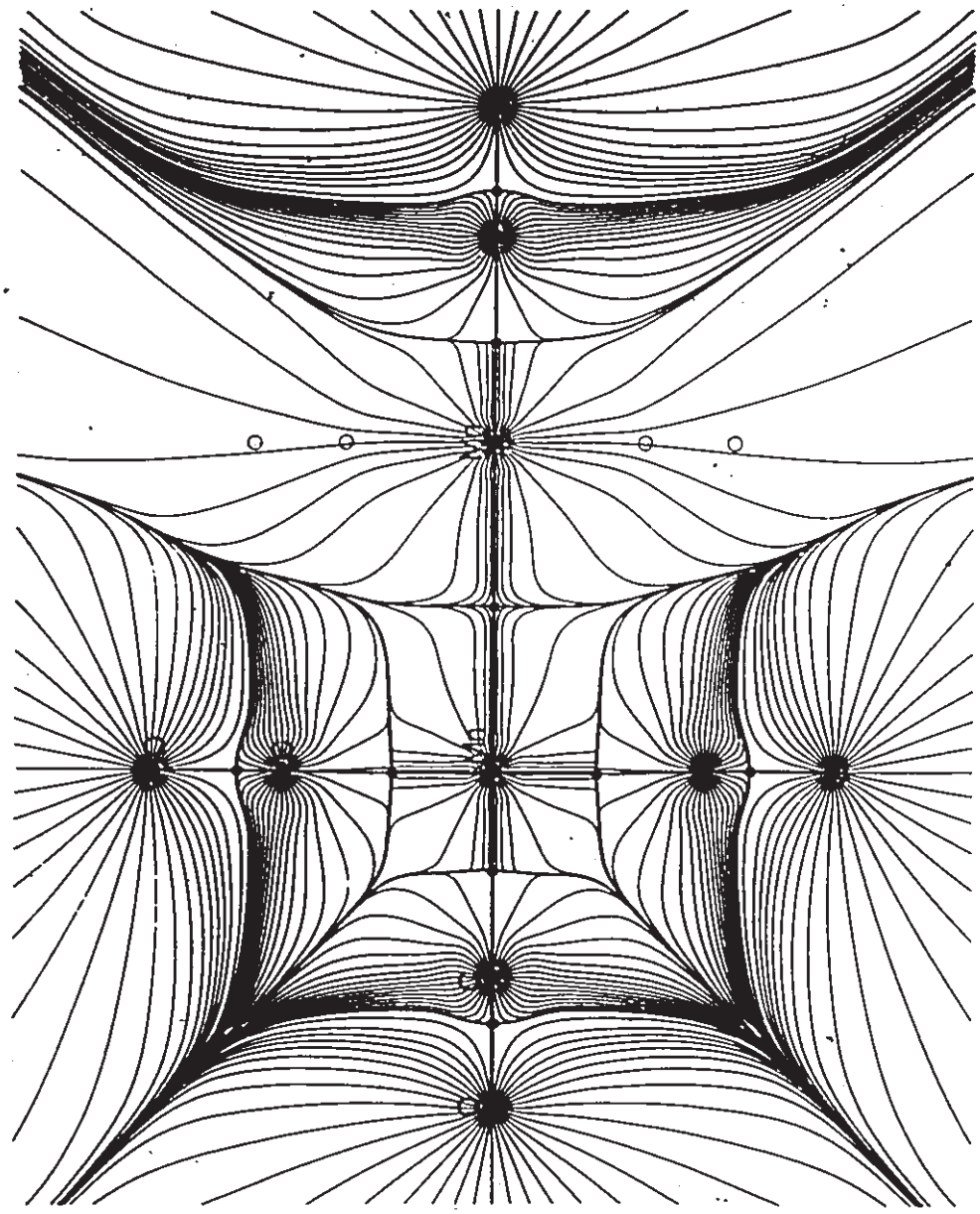

Figure 3.4

This figure illustrates the Fermi hole of an electron situated at the position of the single maximum of charge concentration in what remains of the fourth shell of charge concentration of both of the manganese atoms. This point is also the position of the Mn–Mn bond critical point.

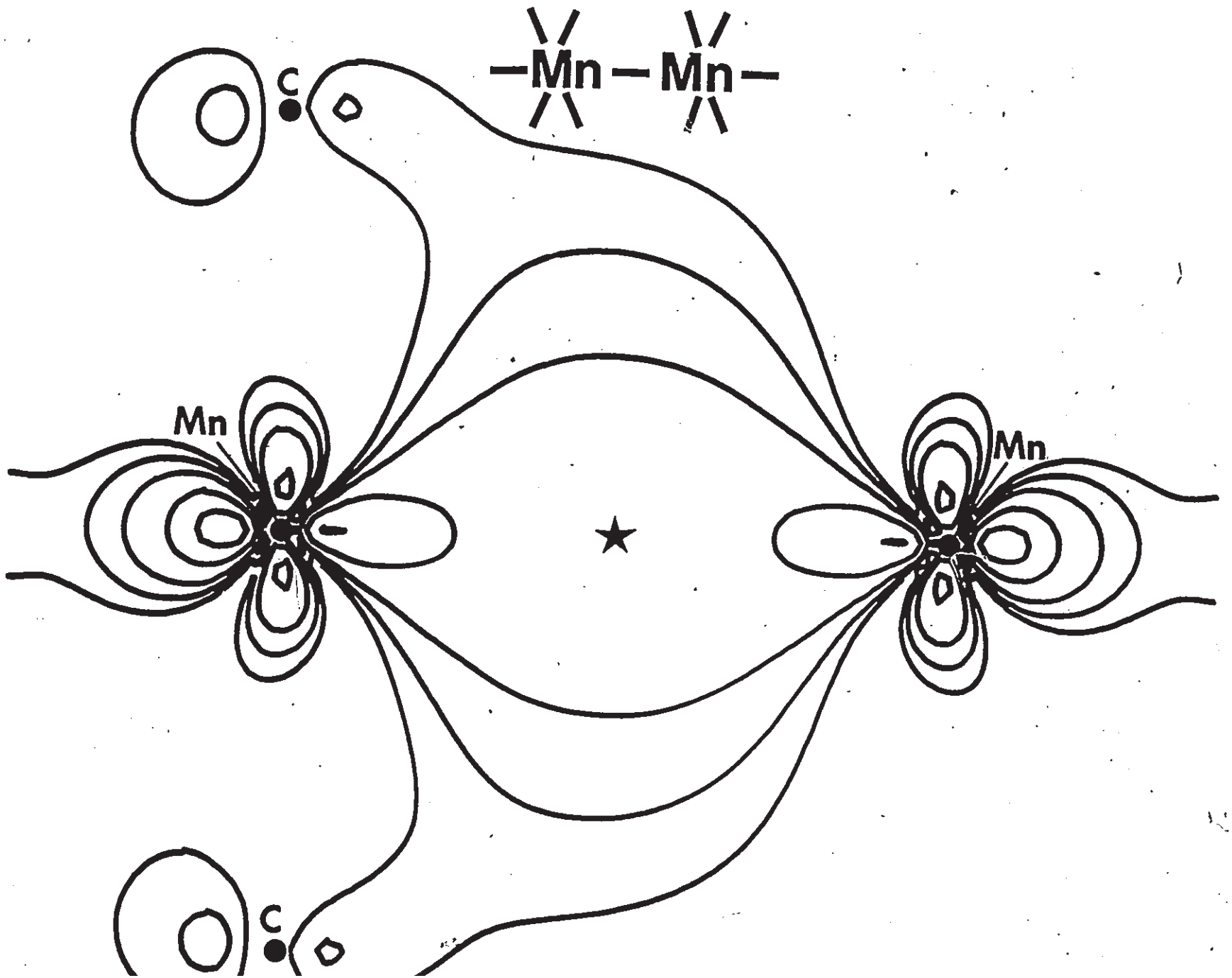
Mn
Mn
Mn
Mn
C
C

Figure 3.5

These gradient vector fields are drawn to the same scale as figure 3.3, and the symbols represent the same features. (a) The gradient vector field of the charge density displayed in a σ_v symmetry plane of $Fe_2(CO)_9$. The star indicates the position of the cage critical point, however there is one ring critical point immediately below it in this plane and two other ring critical points equally close, above and below the plane plotted. The dashed line represents the intersection of the $\overline{Fe–C–Fe–C}$ ring surface with the plane shown. (b) The gradient vector field of the charge density is shown for the σ_v symmetry plane in $Co_2(CO)_8$. The solid triangle marks the position of the $\overline{Co–C–Co–C}$ ring critical point. The intersection of the ring surface with the plane that is plotted is shown as a dashed line. It is considerably more bent away from the Co–Co internuclear axis than is seen in the iron dimer.

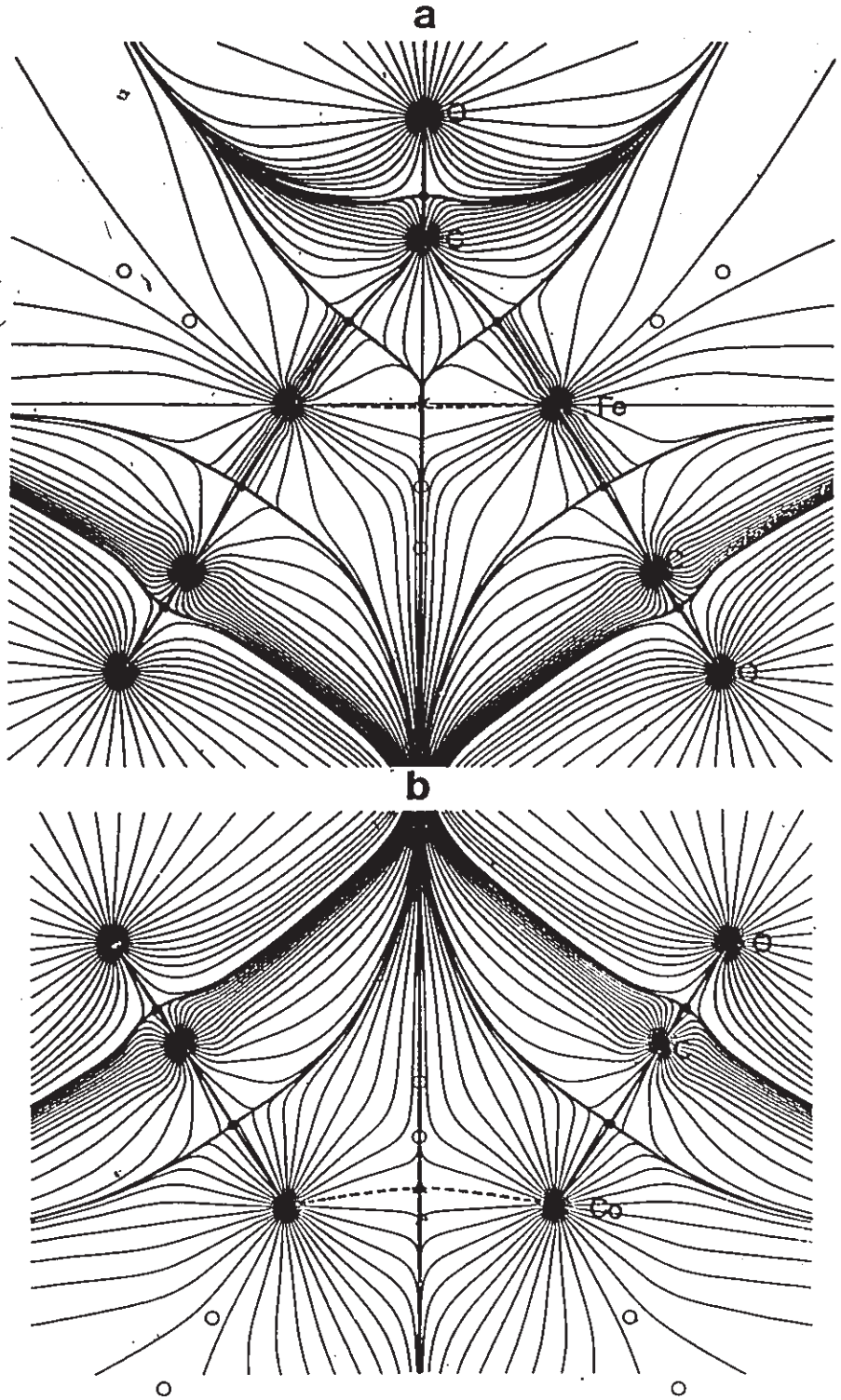
a
Fe
b

plane shown. There is only one such surface in the cobalt dimer, while there are three such four–membered rings in the iron dimer. In chapter 1 we foreshadowed that the molecular structure of one of these binuclear systems was near a catastrophe point. The molecular structure of $Fe_2(CO)_9$ possesses a cage critical point surrounded by three ring critical points, each only 0.064 au away. It is likely that some small perturbation in the molecular geometry and/or the change density could cause the three ring critical points to symmetrically migrate and coalesce with the cage critical point to form a singularity in the charge distribution of rank 1. Further change in this direction would result in a change in structure. The resulting structure would possess an Fe–Fe bond path and three three–membered rings. The author plans to investigate whether or not the inclusion of Coulomb correlation will induce such a change in structure. In covalent systems, however, the inclusion of Coulomb correlation reduces the charge density maximally at the position of the bond critical point (Gatti, MacDougall and Bader 1988). If the same effect holds for metal–metal bonding regions, then Coulomb correlation will cause the ring critical points to migrate away from the cage critical point making the structure more stable, in the topological sense. Further investigation of the state functions, charge densities and Laplacian distributions in these and other transition metal clusters is currently in progress.

3.4 IN DEFENCE OF: "WE ALREADY KNEW THAT"

This thesis has reiterated the conclusion that in general the charge density and the pair density of a molecular system do not support the model of pairs of electrons localized to separate regions of space. Instead, we have shown that the success of the models can be attributed to the extent to which the properties attributed to electron pairs describe the physical properties of the Laplacian distribution which reflect the effect of Fermi correlation. Quantum mechanical theories can be built on the observations presented here. Irving Langmuir coined the term "pathological science"

to describe "scientific studies based on non–existent phenomena" (1953). About such studies, he said "there is no dishonesty involved but ... people are tricked into false results by lack of understanding about what human beings can do to themselves in the way of being led astray by subjective effects, wishful thinking or threshold interactions". Theoretical chemistry is not immune to the symptoms of pathological science. The quantum theory of atoms in molecules, the topological theory of molecular structure and the conclusions concerning the physical basis of electron pair models, all pass the Langmuir litmus test.

REFERENCES

Arfken, G. (1985) "Mathematical Methods for Physicists", 3rd ed., (New York: Academic Press).

Aslangul, C. (1971) *Compt. Rend. Acad. Sci. (Paris)* 272B, 1.

Aslangul, C.; Constanciel, R.; Daudel, R. and Kottis, P. (1972) *Adv. Quantum Chem.* 6, 93.

Bader, R. F. W. (1975) *Int. Rev. Sci., Phys. Chem. Ser. 2, vol* 1 *Theor. Chem.* (ed.) Buckingham, A. D. and Coulson, C. A. (London: Butterworths) p 43.

Bader, R. F. W. (1985) *Acc. Chem. Res.* 18, 9.

Bader, R. F. W.; Anderson, S. G. and Duke, A. J. (1979a) *J. Amer. Chem. Soc.* 101, 1389.

Bader, R. F. W. and Beddall, P. M. (1971a) *Chem. Phys. Lett.* 8, 29.

Bader, R. F. W. and Beddall, P. M. (1972) *J. Chem. Phys.* 56, 3320.

Bader, R. F. W. and Beddall, P. M. (1973a) *J. Amer. Chem. Soc.* 95, 305.

Bader, R. F. W.; Beddall, P. M. and Cade, P. E. (1971b) *J. Amer. Chem. Soc.* 93, 3095.

Bader, R. F. W.; Beddall, P. M. and Peslak, J., Jr. (1973b) *J. Chem. Phys.* 58, 557.

Bader, R. F. W.; Carroll, M. T.; Cheeseman, J. R. and Chang, C. (1987a) *J. Amer. Chem. Soc.* 109, 7968.

Bader, R. F. W. and Chang, C. (1989) *J. Amer. Chem. Soc.* 111, 0000.

Bader, R. F. W. and Essén, H. (1984) *J. Chem. Phys.* 80, 1943.

Bader, R. F. W.; Gillespie, R. J. and MacDougall, P. J. (1988) *J. Amer. Chem. Soc.* 110, 7329.

Bader, R. F. W.; Gillespie, R. J. and MacDougall, P. J. (1989) *Molecular Structure and Energetics, vol II, chapt. 1* (eds.) Liebman, J. F. and Greenberg, A. (New York: VCH Publ.)

Bader, R. F. W.; Larouche, A.; Gatti, C.; Carroll, M. T.; MacDougall, P. J. and Wiberg, K. B. (1987b) *J. Chem. Phys.* **87**, 1142.

Bader, R. F. W. and MacDougall, P. J. (1985) *J. Amer. Chem. Soc.* **107**, 6788.

Bader, R. F. W.; MacDougall, P. J. and Lau, C. D. H. (1984) *J. Amer. Chem. Soc.* **106**, 1594.

Bader, R. F. W. and Nguyen–Dang, T. T. (1981a) *Adv. Quantum Chem.* **14**, 63.

Bader, R. F. W.; Nguyen–Dang, T. T. and Tal, Y. (1979b) *J. Chem. Phys.* **70**, 4316.

Bader, R. F. W.; Nguyen–Dang, T. T. and Tal, Y. (1981b) *Rep. Prog. Phys.* **44**, 893.

Bader, R. F. W. and Preston, H. J. T. (1969) *Int. J. Quantum Chem.* **3**, 327.

Bader, R. F. W.; Slee, T. S.; Cremer, D. and Kraka, E. (1983) *J. Amer. Chem. Soc.* **105**, 5061.

Bader, R. F. W.; Srebrenik, S. and Nguyen–Dang, T. T. (1978) *J. Chem. Phys.* **68**, 3680.

Bader, R. F. W. and Stephens, M. E. *Chem. Phys. Lett.* **26**, 445.

Bader, R. F. W. and Stephens, M. E. (1975) *J. Amer. Chem. Soc.* **97**, 7391.

Bader, R. F. W.; Tal, Y.; Anderson, S. G. and Nguyen–Dang, T. T. (1980) *Isr. J. Chem.* **19**, 8.

Bader, R. F. W.; Tang, T.–H. and Biegler–König, F. W. (1982) *J. Amer. Chem. Soc.* **104**, 946.

Bader, R. F. W. and Wiberg, K. B. (1987) in "Density Matrices and Density Functionals" (eds.) Erdahl, R. and Smith, V. H., Jr. (Dordrecht: D. Riedel Publ.) p 677.

Baerends, E. J.; Ellis, D. E. and Ros, P. (1973) *Chem. Phys.* **2**, 41.

Baeyer, A. (1885) *Ber.* **18**, 2269.

Ballhausen, C. J. (1962) "Introduction to Ligand Field Theory" (New York: McGraw–Hill).

Bauschlicher, C. W., Jr. (1986) *J. Chem. Phys.* **84**, 872.

Benesch, R. and Smith, V. H., Jr. (1971) *J. Chem. Phys.* **55**, 482.

Bethe, H. (1929) *Ann. Physik* **3**, 735.

Binkley, J. S.; Whiteside, R. A.; Krishnan, R.; Seeger, R.; DeFrees, D. J.; Schlegel, H. B.; Topiol, S.; Kahn, L. R. and Pople, J. A. (1980) *GAUSSIAN80* (Pittsburg: Carnegie–Mellon Univ. Publ. Unit).

Binkley, J. S.; Frisch, M. J.; DeFrees, D. J.; Ragavachari, K.; Whiteside, R. A.; Schlegel, H. B.; Fluder, E. M. and Pople, J. A. (1983) *GAUSSIAN82* (Pittsburg: Carnegie–Mellon Univ. Publ. Unit)

Birchall, T. and Gillespie, R. J. Can. *J. Chem.* **41**, 2642.

Boyd, R. J.; Choi, S. C. and Hale, C. C. (1984) *Chem. Phys. Lett.* **112**, 136.

Boyd, R. J. and Coulson, C. A. (1973) *J. Phys. B* **6**, 782.

Boyd, R. J. and Coulson, C. A. (1974) *J. Phys. B* **7**, 1805.

Boys, S. F. and Foster, J. *Rev. Mod. Phys.* **32**, 305.

Bragg, W. L. (1914) *Proc. Roy. Soc. London* **A89**, 468.

Braterman, P. S. (1972) *Structure and Bonding* **10**, 57.

Brecht, B. (1940) "Leben des Galiles": Translation by Brenton, H. (1980), "The Life of Galileo" (London: Eyre Methuen).

Burgi, H. B. and Dunitz, J. D. (1983) *Acc. Chem. Res.* **16**, 153.

Butlerov, A. M. (1861) *Z. Chem. Pharm.* **4**, 549.

Carroll, M. T.; Chang, C. and Bader, R. F. W. (1988) *Mol. Phys.* **63**, 387.

Carroll, M.T.; Cheeseman, J.R.; Osaman, R. and Weinstein, H. (1989) *J. Phys. Chem.* **93**, 0000.

Cao, W. L.; Gatti, C.; MacDougall, P. J. and Bader, R. F. W. (1987) *Chem. Phys. Lett.* **141**, 380.

Chandrasekar, J.; Andrade, J. G. and Schleyer, P. v. R. (1981) *J. Amer. Chem. Soc.* **103**, 5609.

Chatt, J. and Duncanson, L. A. (1953) *J. Chem. Soc.* 2939.

Collard, K. and Hall, G. G. (1977) *Int. J. Quantum Chem.* **12**, 623.

Coppens, P. (1967) *Science* **158**, 1577.

Couper, A. S. (1858) *Compt. Rend.* **46**, 1157.

Couper, I. L and Pounder, C. N. M. (1980) *Int. J. Quantum Chem.* **17**, 759.

Cremer, D. and Kraka, E. (1984) *Croat. Chem. Acta* **57**, 1259.

Cremer, D. and Kraka, E. (1985) *J. Amer. Chem. Soc.* **107**, 3800.

Cremer, D.; Kraka, E.; Slee, T. S.; Bader, R. F. W.; Lau, C. D. H.; Nguyen–Dang, T. T. and MacDougall, P. J. (1983) *J. Amer. Chem. Soc.* **105**, 5069.

Dalton, J. (1808) "A New System of Chemical Philosophy" (Manchester).

Daudel, R. (1953) *Compt. Rend. Acad. Sci. (Paris)* **237**, 601.

Daudel, R.; Brion, H. and Odiot, S. (1955) *J. Chem. Phys.* **23**, 2080.

Davidson, E. R. (1972) *Rev. Mod. Phys.* **44**, 451.

Denis, A.; Longlet, J. and Malrieu, J. P (1973) *Theoret. Chim. Acta* **29**, 117.

Dewar, M. J. S. (1951) *Bull. Soc. Chim. Fr.* **C79**, 18.

Dirac, P. A. M. (1928), *Roy. Soc., Proc.* **117**, 610.

Ebbing, D. D. and Henderson, R. C. (1965) *J. Chem. Phys.* **42**, 2225.

Edmiston, C. and Ruedenberg, K. (1963) *Rev. Mod. Phys.* **35**, 457.

Ehrenfest, P. (1927) *Z. Phys.* **45**, 455.

Ellis, D. E.; Guo, J. and Cheng, H.–P. (1987) *6th Amer. Conf. Theoret. Chem.* Gull Lake, Minnesota.

Ellis, D. E.; Guo, J. and Cheng, H. –P. (1988) *J. Phys. Chem.* **92**, 3024.

Epstein, S. T. (1974) *J. Chem. Phys.* **60**, 3351.

Fieser, L. F. and Fieser, M. (1959) "Steroids" pp.15–21 (London: Reinhold).

Fleming, I. (1976) "Frontier Orbitals and Organic Chemical Reactions" (London: Wiley).

Frankland, E. (1852) *Phil. Trans. Roy. Soc. London* **142**, 417.

Franklin, J. L. (1949) *Ind. Eng. Chem.* **41**, 1070.

Fukui, K. (1971) *Acc. Chem. Res.* 4, 57.

Fukui, K.; Yonezawa T. and Shingu, H. (1952) *J. Chem. Phys.* 20, 722.

Gatti, C.; Barzaghi, M. and Simonetta, M. (1985) *J. Amer. Chem. Soc.* 107, 878.

Gatti, C.; Fantucci, P. and Pacchioni, G. (1987) *Theoret. Chim. Acta* 72, 433.

Gerloch, M. (1988) Chemistry Departmental Seminar, University of Toronto, April 22.

Gerloch, M. and Woolley, R. G. (1983) *Prog. Inorg. Chem.* (ed.) Lippard, S. J. 31, 371.

Gillespie, R. J. (1963) *J. Chem. Ed.* 40, 295.

Gillespie, R. J. (1972) "Molecular Geometry" (London: Van Nostrand–Reinhold)

Gillespie, R. J. and Nyholm, R. S. (1957) *Quart. Rev. Chem. Soc.* 11, 239.

Goldstein, H. (1951) "Classical Mechanics" (Cambridge, Mass.: Addison–Wesley).

Hay, P. J.; Hunt, W. J. and Goddard, W. A., III (1972) *J. Amer. Chem. Soc.* 94, 8293.

Heijser, W.; Baerends, E. J. and Ros, P. (1980) *Disc. Faraday Soc.* (*Symp.*) 14, 211.

Heisenberg, W. (1925) *Zeit. Physik* 33, 879.

Heitler, W. and London, F. (1927) *Zeit. Physik* 44, 455.

Herzberg, G. (1945) "Molecular Spectra and Molecular Structure II. Infrared and Raman Spectra of Polyatomic Molecules" (New York: Van Nostrand–Reinhold).

Hoffmann, R. (1963) *J. Chem. Phys.* 39, 1397.

Hohenberg, P. and Kohn, W. (1964) *Phys. Rev. B* 136, 864.

Hout, R. F.; Pietro, W. J. and Hehre, W. J. (1984) "A Pictorial Approach to Molecular Structure and Reactivity" (New York: Wiley–Interscience).

Hund, F. (1928) *Zeit. Physik* 51, 759. (1931) *ibid* 73, 1. (1932) *ibid* 74, 429.

Hund, F. (1933) *Physik* 1, 163. (1937) *ibid* 5, 1.

Jackman, L. M. and Cotton. F. A. (1975) "Dynamic Nuclear Magnetic Resonance Spectroscopy" (New York: Academic Press).

Kato, W. A. (1957) *Commun. Pure Appl. Math.* 10, 151.

Kekulé, F. A. (1857) *Ann. Chem.* 104, 129.

Kivelson, D. (1954) *J. Chem. Phys.* 22, 904.

Kopp, H. (1855) as reported in: Glasstone, S. (1946) "Textbook of Physical Chemistry", 2nd ed. p.525 (London: Van Nostrand)

Kunze, K. L. and Hall, M. B. (1986) *J. Amer. Chem. Soc.* 108, 5122.

Kunze, K. L. and Hall, M. B. (1987) personal communication.

Kunze, K. L. and Hall, M. B. (1989) *J. Amer. Chem. Soc.* III, 0000.

Kutzelnigg, W. (1973) *Fortshr. Chem. Forsch.* 41, 31.

Ladner, R. C. and Goddard, W. A., III (1969) *J. Chem. Phys.* 51, 1073.

Langmuir, I. (1953) as transcribed in: Hall, R. N. (1985) *Spec. Sci. Tech.* 8, 77.

Lau, C. D. H.; Bader, R. F. W.; Hermansson, K. and Berkovitch–Yellin, Z. (1986) *Chem. Scripta*, 26, 476.

Lauher, J. W.; Elian, M.; Summerville, R. H. and Hoffmann. R. (1976) *J. Amer. Chem. Soc.* 98, 3219.

Le Bel, J. A. (1874) *Bull. Soc. Chim. Fr.* 22, 337.

Lennard–Jones, J. E. (1949) *Proc. Roy. Soc. London* A198, 1, 14.

Leung, P. C. and Coppens, P. (1983) *Acta. Crystallogr.* B39, 535.

Levine, I. N. (1983) "Quantum Chemistry" 3rd ed. (Newton, Mass.: Allyn and Bacon).

Lewis, G. N. (1916) *J. Amer. Chem. Soc.* 38, 762.

Lewis, G. N. (1923) "Valence and Structure of Atoms and Molecules" (New York: American Chemical Society Monograph, The Chemical Catalog Co.).

Linnett, J. W. (1964) "The Electronic Structure of Molecules – A New Approach" (New York: Wiley).

Linnett, J. W. and Pöe, A. J. (1951) *Trans. Far. Soc.* 47, 1033.

Löwdin, P.–O. (1955) *Phys. Rev.* 97, 1474.

Luken, W. L. (1982) *Int. J. Quantum Chem.* 22, 889.

Luken, W. L. (1984) *Croat. Chem. Acta* 57, 1283.

Luken, W. L. and Beratan, D. N. (1982) *Theoret. Chim. Acta, Berlin* 61, 265.

MacDougall, P. J. (1986) *Inorg. Chem.* **25**, 4400.

MacDougall, P. J. and Bader, R. F. W. (1986) *Can. J. Chem.* **64**, 1496.

MacDougall, P. J.; Bader, R. F. W. and Hall, M. B. (1987) *6th Amer. Conf. Theoret. Chem.*, Gull Lake, Minnesota.

MacDougall, P. J.; Schrobilgen, G. J. and Bader, R. F. W. (1989) *Inorg. Chem.* **28**, 0000.

Malvern, L. E. (1969) "Introduction to the Mechanics of a Continuous Medium" (New Jersey: Prentice–Hall).

Maslen, V. W. (1956) *Proc. Phys. Soc.* A69, 734.

Maxwell, J. C. (1954) "Treatise on Electricity and Magnetism" vol. 1, p.31 (New York: Dover).

McWeeny, R. (1960) *Rev. Mod. Phys.* **32**, 335.

McWeeny, R. and Del Re, G. (1968) *Theoret. Chim. Acta* **10**, 13.

McWeeny, R. and Sutcliffe, B. T. (1969) "Methods of Molecular Quantum Mechanics" (London: Academic Press).

Messmer, R. P. and Schultz, P. A. (1986) *Phys. Rev. Lett.* **57**, 2653.

Meyer, V. (1894) *Ber.* **27**, 510, 1584.

Morse, P. and Feshbach, H. (1953) "Methods of Theoretical Physics", Part I (New York: McGraw–Hill).

Mulliken, R. S. (1928) *Phys. Rev.* **32**, 186, 761, (1929) *ibid* **33**, 730. (1932a) *ibid* **40**, 55. (1932b) *ibid* **41**, 49.

Mulliken, R. S. (1932c) *Rev. Mod. Phys.* **4**, 1.

Mulliken, R. S. (1935) *J. Chem. Phys.* **3**, 375.

Mulliken, R. S. (1939) *Phys. Rev.* **56**, 778.

Palis, J. and Smale, S. (1970) *Pure Math.* **14**, 223.

Passmore, J.; Sutherland, G. and White, P. S. (1980) *J. Chem. Soc. Chem. Commun.* 330.

Pasteur, L. (1848) *Compt. Rend.* **26**, 535.

Pauli, W. (1958) "Encyclopedia of Physics", vol. 5, part 1, (ed.) Lügge, S. F. (Berlin: Springer).

Pauling. L. P. *J. Amer. Chem. Soc.* **53**, 1367, 3225. (1932) *ibid* **54**, 988.

Pauling, L. P. (1960) "The Nature of the Chemical Bond", 3rd ed. (Ithaca, New York: Cornell University Press).

Pople, J. A.; Schneider, W. G. and Bernstein, H. J. (1959) "High Resolution Nuclear Magnetic Resonance" (New York: McGraw–Hill).

Proiniv, E.; Neshey, N. and Andreev. A. (1988) *Int. J. Quantum Chem.* **34**, 1.

Prosen, E. J.; Johnson, W. H. and Rossini, F. D. (1946) *J. Res. Natl. Bur. Stand.* **37**, 51.

Proust, J. L. (1799) *Ann. Chim.* **32**, 26.

Ransil, B. J. and Sinai, J. J. (1967) *J. Chem. Phys.* **46**, 4050.

Reed, A. E. and Weinhold, F. (1986) *J. Amer. Chem. Soc.* **106**, 3586.

Ritchie, J. P.; King, H. F. and Young, W. S. (1986) *J. Chem. Phys.* **85**, 5175.

Roothaan, C. C. J. (1951) *Phys. Rev.* **23**, 69.

Roux, M.; Besnainou, S. and Daudel, R. (1956) *J. Chim. Phys.* **54**, 218. (1958) *ibid* **55**, 754.

Runtz, G. R.; Bader, R. F. W. and Messer, R. R. (1977) *Can. J. Chem.* **55**, 3040.

Sagar, R. P.; Ku, A. C. T.; Smith, V. H., Jr. and Simas, A. M. (1988) *J. Chem. Phys.* **88**, 4367.

Schleyer, P. v. R. and Reed, A. E. (1989) *J. Amer. Chem. Soc.* **111**, 0000.

Schrödinger, E. (1929) *Ann. Physik* **79**, 361, 489.

Schwinger, J. (1951) *Phys. Rev.* **82**, 914.

Shannon, E. (1948) *Bell Sys. Tech. J.* **27**, 379.

Sidgwick, N. V. (1927) "The Electronic Theory of Valence" (Ithaca, New York: Cornell University Press).

Sidgwick, N. V. and Powell, H. E. (1940) *Proc. Roy. Soc. London* A176, 153.

Sinanoglu, O. (1962) *J. Chem. Phys.* 36, 706.

Sinanoglu, O. and Skutnik, B. (1968) *Chem. Phys. Lett.* 1, 699.

Slater, J. C. (1930) *Phys. Rev.* 35, 514. (1951) *ibid* 81, 385.

Slater, J. C. (1960) "Quantum Theory of Atomic Structure", vol. 2, pp.8–15, (New York, McGraw–Hill).

Slee, T. S. (1986a) *J. Amer. Chem. Soc.* 108, 7541.

Slee, T. S. (1986b) Ph.D. Thesis, McMaster University, Hamilton, Ontario.

Slee, T. S. and MacDougall, P. J. (1988) *Can. J. Chem.* 66, 2961.

Smith, D. F. (1953) *J. Chem. Phys.* 21, 609.

Smith, V. H., Jr.; Price, P. F. and Absar, I. (1977) *Isr. J. Chem.* 16, 187.

Sperber, G. (1971) *Int. J. Quantum Chem.* 5, 189.

Srebrenik, S. and Bader, R. F. W. (1974) *J. Chem. Phys.* 61, 2536.

Srebrenik, S.; Bader, R. F. W. and Nguyen–Dang, T. T. (1978) *J. Chem. Phys.* 68, 3667.

Stephens, M. E. (1975) Ph.D. Thesis, McMaster University, Hamilton, Ontario.

Stephens, M. E. and Becker, P. J. (1983) *Mol. Phys.* 49, 65.

Summerville, R. H. and Hoffmann, R. (1979) *J. Amer. Chem. Soc.* 101, 3821.

Tal, Y.; Bader, R.F.W.; Nguyen–Dang, T.T.; Ojha, M. and Anderson, S.G. (1981) *J. Chem. Phys.* 74, 5162.

Tang, T.–H.; Bader, R. F. W. and MacDougall, P. J. (1985) *Inorg. Chem.* 24, 2047.

Thom, R. (1975) "Structural Stability and Morphogenesis" (Reading, Mass.: W. A. Benjamin).

Thorn, D. L. and Hoffmann, R. (1978) *Inorg. Chem.* 17, 126.

Tolles, W. M. and Gwinn, W. D. (1962) *J. Chem. Phys.* 36, 1119.

Townes, C. H. and Schawlow, A. L. (1955) "Microwave Spectroscopy" (New York: McGraw–Hill).

Van't Hoff, J. H. (1874) *Arch. Neerland. Sci.* 9, 445.

Van Vleck, J. H. (1932) *Phys. Rev.* **41**, 208.

Van Wazer, J. R. and Absar, I. (1975) "Electron Densities in Molecules and Molecular Orbitals" (New York: Academic Press).

Weinstein, H.; Politzer, P. and Srebrenik, S. (1975) *Theoret. Chim. Acta* **38**, 159.

Wells, A.F. (1975) "Structural Inorganic Chemistry", 4th ed. (Oxford: Clarendon Press).

Werner, A. (1893) *Z. Anorg. Chem.* **3**, 267.

Wiberg, K. B.; Bader, R. F. W. and Lau, C. D. H. (1987) *J. Amer. Chem. Soc.* **109**, 985, 1001.

Wierl, R. (1931) *Ann. Physik* **8**, 521.

Wigner, E. P. and Seitz, F. (1934) *Phys. Rev.* **46**, 509.

Williamson, R. L. and Hall, M. B. (1987) *Int. J. Quantum Chem.* **21**, 503.

Williamson, R. L. and Hall, M. B. (1987) personal communication.

Wolfsberg, M. and Helmholz, L. (1952) *J. Chem. Phys.* **20**, 837.

Woodward, R. B. (1952) *J. Amer. Chem. Soc.* **64**, 72.

Woolley, R. G. (1977) *Int. J. Quantum Chem.* **12**, 307.